



UNIVERSIDAD NACIONAL DE COLOMBIA

NNLO Vacuum Stability Analysis in the SM and the Higgs Bosons of the MSSM at Three-Loop Accuracy

Edilson Alfonso Reyes Rojas

Universidad Nacional de Colombia
Facultad de Ciencias, Departamento de Física
Bogotá, Colombia
2020

NNLO Vacuum Stability Analysis in the SM and the Higgs Bosons of the MSSM at Three-Loop Accuracy

Edilson Alfonso Reyes Rojas

Trabajo de grado presentado como requisito para optar al título de:
Doctor en Ciencias Física

Director:
Ph.D. Angelo Raffaele Fazio

Grupo de Campos y Partículas

Universidad Nacional de Colombia
Facultad de Ciencias, Departamento de Física
Bogotá, Colombia
2020

This thesis is based on the author's work conducted at the Universidad Nacional de Colombia in Bogotá. Main results of this work have already been published in the articles:

- [1] E. A. Reyes R., A. R. Fazio,
EPJ Web Conf. **192**, 00033 (2018).
DOI: 10.1051/epjconf/201819200033
- [2] A. R. Fazio and E. A. Reyes R.,
Nucl. Phys. B **942**, 164-183 (2019). [arXiv:1901.03651 [hep-ph]].
DOI: 10.1016/j.nuclphysb.2019.03.008
- [3] E.A. Reyes R., A.R. Fazio,
Phys. Rev. D **100**, no.11, 115017 (2019). [arXiv:1908.00693 [hep-ph]].
DOI: 10.1103/PhysRevD.100.115017

The author have presented and discussed the results of this thesis in different events:

- The Higgs Boson Masses of the MSSM at Three-Loop Accuracy
Katharsis of Ultimate Theory Standards 7 (KUTS7)
Karlsruhe - Karlsruhe Institute of Thechnology (KIT) (2017).
- The Higgs Boson Masses of the MSSM at Three-Loop Accuracy
XXVII Congreso Nacional de Física
Cartagena - Colombia (2017).
- The Lightest Higgs Boson Mass of the MSSM at Three-Loop Accuracy
2nd Colombian Meeting on High Energy Physics
Bogotá, D.C. - Universidad Nacional de Colombia (UNAL) (2017).
- The Lightest Higgs Boson Mass of the MSSM at Three-Loop Accuracy
MASS2018: Origin of Mass at the High Energy and Intensity Frontier
Odense - University of Southern Denmark (SDU) (2018).
- The light CP-even Higgs boson mass of the MSSM at three-loop accuracy
International Workshop on Quantum Chromodynamics Theory and Experiment
QCD@Work 2018. Matera - Italy (2018).

Acknowledgements

Empiezo agradeciendo al profesor A. Raffaele Fazio quien fue mi director de esta tesis doctoral, pero mas importante aun un valioso amigo que me ha acompañado en mi proceso de formación como investigador en el área de la física de partículas. Agradezco su apoyo continuo en medio del complejo camino que decidimos seguir en este proyecto, las valiosas discusiones que hemos tenido, sus consejos para poder realizar exitosamente el doctorado y sobretodo su paciencia y confianza en medio de los problemas que se nos han presentado. Espero sinceramente haber contribuido a su vida personal y profesional de la misma manera que el contribuyo a la mía.

Por otra parte quiero agradecer a varias personas que han formado parte a lo largo de este proceso. Al Prof. Dr. Bernd A. Kniehl, quien me presto su hospitalidad y apoyo incondicional en mi estancia realizada con su grupo en DESY en el año 2017. A la doctora Sophia C. Borowka, quien estuvo en la Universidad Nacional de Colombia con nuestro grupo en el año 2016 como profesora invitada y con quien iniciamos este camino. Su amable disponibilidad para discutir acerca de los detalles técnicos de nuestro cálculo hicieron realizable este proyecto. Al profesor Alexis Irlande por ayudarnos con la instalación de nuestro propio servidor en la UNAL y por su apoyo técnico todos estos años. Al profesor Sven Heinemeyer por las diferentes discusiones en el evento KUTS y via e-mail. Al equipo de KUTS por permitirme exponer mis resultados y por todas las discusiones llevadas a cabo en su evento. Al profesor Ayres Freitas por sus discusiones acerca del código TVID que es una pieza importante en nuestro cálculo. Al profesor Mikhail Kalmykov por sus discusiones acerca del estado de arte de las integrales master a tres-loop. Al profesor German Rodrigo y al profesor William Torres, quien es también un antiguo amigo, por su amable invitación a presentar un seminario en su grupo de investigación en el IFIC de la universidad de Valencia - España, por las discusiones llevadas a cabo y por incluirme como miembro de COST. A la profesora Heidi Rzehak por su colaboración y apoyo financiero para participar en el evento MASS2018 realizado en Odense – Dinamarca. Al profesor C. Coriano y en general a los organizadores del seminario QCD@Work 2018 por su apoyo financiero, por permitirme presentar un poster y por las discusiones en su evento.

Quiero agradecer a las instituciones que han financiado este proyecto. La Universidad Nacional de Colombia a través de la beca: CONVOCATORIA NACIONAL DE PROYECTOS PARA EL FORTALECIMIENTO DE LA INVESTIGACIÓN, CREACIÓN E INNOVACIÓN DE LA UNIVERSIDAD NACIONAL DE COLOMBIA 2016-2018 con el proyecto N. 34729, Minimal Supersymmetric Standard Model Higgs Boson to High Accuracy. Colciencias a través de la beca: CONVOCATORIA 727 DE COLCIENCIAS PARA DOCTORADOS NACIONALES 2015 con el Proyecto N. 39844, NNLO Vacuum Stability Analysis in the SM and the Higgs Bosons of the MSSM at Three-Loop Accuracy.

Finalmente, quiero agradecer el apoyo de mi familia, necesario para hacer mas fácil el camino que escogí. Este documento esta dedicado a ellos: Celia, Alfonso, Diego, Freddy, Cristian, Susana y en especial a Paola por su paciencia y apoyo en estos ultimos años. Amorem nostrae memoriam spero sempiternam fore.

Resumen

En esta tesis proporcionamos un cálculo diagramático a orden fijo de las correcciones cuánticas a la masa del boson de Higgs liviano en el modelo super-simétrico minimal con parámetros reales. Hemos calculado las contribuciones provenientes del sector de la QCD super-simétrica con una precisión de tres-loops al orden $O(\alpha_t\alpha_s^2)$. El procedimiento de regularización adoptado esta basado en el esquema de reducción dimensional con el fin de preservar la super-simetría en todos los ordenes perturbativos. El cálculo extiende la región de validez de estudios previos al espacio completo de parámetros super-simétricos. Las correcciones a la masa del Higgs son expresadas en términos de un conjunto de integrales del vacío a tres-loops las cuales han sido calculadas explotando las técnicas del método de dispersión que permite realizar su evaluación numérica para una jerarquía arbitraria de las escalas de masa involucradas. Por otro lado, hemos realizado una comparación numérica de nuestros resultados con las demás predicciones teóricas encontradas en la literatura. En particular, el código FeynHiggs combina cálculos a orden fijo con los cálculos provenientes de la teoría efectiva de campos cuánticos dando una predicción confiable para la masa del boson de Higgs hasta el orden de tres-loops. Las dos predicciones numéricas son compatibles en el escenario donde solo hay una escala de la super-simetría que toma valores menores a 10 TeV y donde el parámetro de mezcla del quark stop se anula. Para escalas mayores a 10 TeV observamos diferencias numéricas significativas. La diferencia crece sin acotarse al aumentar la escala de la super-simetría debido a los efectos de los términos con logaritmos grandes en el cálculo a orden fijo que dañan la perturbatividad de las correcciones cuánticas. Por lo tanto, hemos realizado un análisis numérico adicional donde buscamos restricciones al valor que puede tomar la escala super-simétrica. El valor experimental combinado para la masa del boson de Higgs obtenido por los laboratorios CMS y ATLAS y el problema de la estabilidad del vacío en el modelo estándar son usados para derivar cotas superiores sobre esta escala. En el escenario considerado en este trabajo, para un valor grande de la razón entre los valores esperados en el vacío de los dos campos de Higgs pares bajo CP ($\tan\beta \geq 10$), hemos encontrado que valores de la escala super-simétrica superiores a 12.5 ± 1.2 TeV están excluidos. Para valores pequeños de $\tan\beta \approx 1$, una cota superior muy grande de alrededor de 10^{11} GeV fue encontrada.

Abstract

In this thesis we provide a fixed-order Feynman diagrammatic computation of the quantum corrections to the lightest CP-even Higgs Boson mass in the real version of the Minimal Supersymmetric Standard Model. We have computed the contributions coming from the SUSY-QCD sector with a precision of three-loops at order $O(\alpha_t\alpha_s^2)$. The adopted re-

gularization procedure is based on the dimensional reduction scheme in order to preserve supersymmetry to all perturbative orders. The calculation extends the region of validity of previous studies to the whole supersymmetric parameter space. The Higgs mass corrections are expressed in terms of a set of three-loop vacuum integrals which have been computed by exploiting dispersion relation techniques which allows their numerical evaluation for an arbitrary hierarchy of the involved mass scales. A numerical comparison of our results with the other predictions found in literature has been done. In particular, the code FeynHiggs combines one- and two-loop fixed-order with the effective-field-theory calculations and gives a reliable prediction for the same Higgs mass at three-loop level. The two numerical predictions agree considering the scenario of only one SUSY-scale and vanishing stop mixing parameter below 10 TeV. For large scales above 10 TeV we have observed sizeable numerical differences between the two predictions. The difference grows monotonically with the SUSY scale due to the effects of large logarithmic terms in the fixed-order computation which spoil the perturbativity of the corrections. Therefore, we have developed an additional numerical analysis where we look for constraints on the supersymmetric scale. The combined CMS/ATLAS Higgs mass value and the vacuum stability problem of the SM are used to derive an upper bound on the needed SUSY scale. In the considered scenario, for a large size of the ratio between the vacuum expectation values of the two CP-even Higgs boson fields ($\tan\beta \geq 10$), values above the SUSY scale 12.5 ± 1.2 TeV are excluded. For small values of $\tan\beta \approx 1$, a higher upper bound of about 10^{11} GeV was found.

Keywords: Higgs boson mass, Supersymmetry, rMSSM, SQCD, Self-energy, Tadpole, Vacuum integral, Dispersion method.

Contents

| | |
|--|-------------|
| Acknowledgements | VII |
| Abstract | IX |
| List of Figures | XIII |
| List of Tables | XV |
| 1. Introduction | 2 |
| 2. The Higgs Bosons of the real MSSM (rMSSM) | 7 |
| 2.1. The rMSSM Higgs sector at tree-level | 7 |
| 2.2. Renormalization of the rMSSM Higgs boson masses | 12 |
| 2.3. The SQCD sector of the rMSSM | 19 |
| 2.3.1. The squark masses and mixing angles | 20 |
| 2.3.2. Renormalization of the fermion masses | 24 |
| 2.3.3. Role of the top quark mass | 25 |
| 2.4. State of art of the higher-order corrections to M_h | 28 |
| 3. The Lightest MSSM Higgs Boson Mass (M_h) at Three-Loop Accuracy | 33 |
| 3.1. Renormalization of the CP-even Higgs boson masses | 33 |
| 3.2. Three-loop fixed-order calculation of M_h | 36 |
| 3.2.1. Three-loop counter-term diagrams | 46 |
| 3.2.2. Three-loop M_h -corrections in the heavy SUSY limit | 49 |
| 3.3. Numerical M_h -predictions in the diagrammatic approach | 50 |
| 4. M_{SUSY} Constraints and Vacuum Stability Analysis in the SM | 54 |
| 4.1. EFT and hybrid calculation of M_h | 54 |
| 4.2. Comparison of the EFT hybrid and three-loop fixed-order calculations of M_h | 57 |
| 4.3. Phenomenological bounds on the SUSY scale | 62 |
| 4.4. Vacuum stability problem | 64 |
| 4.4.1. Vacuum stability constraints on the SUSY scale | 67 |
| 5. Conclusions and Perspectives | 73 |

| | |
|--|------------|
| A. DRED: Notation and Technical Setup | 76 |
| B. DRED Renormalization Constants | 78 |
| C. Feynman Rules in the SQCD Sector | 81 |
| D. Three-loop 1PI Topologies | 86 |
| E. Generation of Amplitudes at $O(\alpha_t\alpha_s^2)$ | 92 |
| E.1. Three-loop Higgs self-energies at $O(\alpha_t\alpha_s^2)$ | 92 |
| E.2. Selection rules for Higgs tadpole topologies | 97 |
| E.3. Selection rules for counter-term diagrams | 98 |
| F. Regularization of Three-Loop Integrals in DRED | 100 |
| G. Scalar Integrals in Reduze | 111 |
| H. Amplitudes of the Three-Loop Diagrams | 113 |
| I. Divergent Parts of the Three-loop Master Integrals | 119 |
| J. Known Analytical Expressions of Master Integrals | 121 |
| K. Amplitudes of the Counter-term Diagrams | 125 |
| L. EFT loop functions | 133 |

List of Figures

| | | |
|-------------|---|----|
| 2-1. | Left: Generic three-loop Higgs tadpole topology with $\phi = \phi_{1,2}^0$, A . There is no momentum dependence. Right: Generic three-loop Higgs self-energy diagram where p is the external momentum and $\phi = \phi_{1,2}^0$, A | 18 |
| 2-2. | Renormalization of the vev. The sum of the topologies in red color vanishes. . . . | 28 |
| 2-3. | One-loop predictions of the Higgs boson masses M_h (solid), M_H (dashed) and m_{\pm} (dotted) as a function of the CP-odd Higgs boson mass m_A . We have considered $\tan\beta = 3$ (blue) and 30 (black) in a scenario where $M_{SUSY} = 1$ TeV, $\mu = 200$ GeV and the stop mixing parameter X_t vanishes. | 30 |
| 2-4. | Left: Predictions of the lightest Higgs boson mass, M_h , at tree (dot-dashed), one-loop (dashed) and two-loop (black solid) level as a function of the CP-odd Higgs boson mass m_A . We have considered the m_h^{max} scenario ($X_t/M_{SUSY} \approx 2.4$) at the kinematical point $\tan\beta = 30$, $M_{SUSY} = 1$ TeV, $\mu = 200$ GeV and $M_{\tilde{g}} = 1.5$ TeV. Right: The three-loop M_h -predictions (red solid line) are included for large m_A in the maximal stop mixing scenario. | 31 |
| 3-1. | Generic three-loop topology. An external vertex is a vertex joined to an external line. An internal vertex is a vertex joined only to internal lines (propagators). . . | 37 |
| 3-2. | Basis of three-loop vacuum integrals obtained from the IBP reduction with Reduze. . . . | 42 |
| 3-3. | Basis of three-loop Master Integrals. The dashed line represents a massless propagator. The solid lines are massive propagators, each color represent an independent mass scale. | 43 |
| 3-4. | Basis of one and two -loop master integrals obtained from the Tarasov method. The dot over the internal line j represents a partial derivative of the propagator regarding the squared mass m_j^2 | 47 |
| 3-5. | Basis of three-loop Master Integrals in the heavy SUSY limit. The dashed line represents a massless propagator. The thin solid line is the propagator with a mass at the electroweak scale M_t and the thick solid line depicts the propagator involving the SUSY scale M_{SUSY} | 48 |
| 3-6. | Dependence of M_h on (a) A_t and (b) $\tan\beta$. The dot-dashed and dashed lines are the one and two -loop predictions of FeynHiggs. The dotted line is the three-loop prediction of H3m and the red solid line depicts our three-loop predictions. | 51 |

- 3-7.** Dependence of M_h on μ_r . (a) The evolution for three different values of $\tan\beta$ is studied. We consider $\tan\beta = 3, 10$ and 20 . (b) M_h is plotted for the scenarios with $A_t = 0.3$ TeV, 1 TeV and 1.7 TeV. The inclusion of three-loop corrections reduces the scale dependence by a factor between $1.5 - 2.0$. The scale dependence is improved when we consider lower values of $\tan\beta$ and A_t . To draw these plots we have used the same conventions as in the Figure **3-6**. 51
- 3-8.** The lightest Higgs boson mass M_h as a function of M_A in (a) the m_h^{max} limit for $\tan\beta = 3, 10$ and (b) in the m_h^{mod+} scenario. Our three-loop corrections are, within theoretical uncertainties, in agreement with the predictions of H3m. The difference can amount a size of about 0.2 GeV in m_h^{max} and 0.05 GeV in m_h^{mod+} . These plots follow the same conventions as in the Figure **3-6**. 53
- 4-1.** Comparison of the M_h predictions of FeynHiggs with the three-loop fixed-order computation of M_h at $O(\alpha_t\alpha_s^2)$ in the heavy SUSY limit. The dot-dashed and the dashed lines are the fixed-order results of FeynHiggs at one and two -loop level respectively. The blue dotted line contains the NNLL resummation of the large logarithms in FeynHiggs. The blue band corresponds to the uncertainty in the NNLL prediction taken from FeynHiggs. The brown band is the CMS/ATLAS Higgs boson mass, $M_h^{exp} = 125.09 \pm 0.24$ GeV. The red solid line represents our three-loop fixed-order predictions. **Left:** Dependence of M_h on the super-symmetric scale M_{SUSY} for a vanishing stop mixing, $X_t/M_{SUSY} = 0$. **Right:** Numerical differences between the FeynHiggs predictions and the three-loop fixed-order predictions of M_h 58
- 4-2.** Numerical comparison of the M_h predictions in a scenario where $M_{\tilde{g}} = 1.5$ TeV and $X_t/M_{SUSY} = 0$. These plots follow the same conventions as in the Figure **4-1**. **Left:** Evolution of M_h as a function of M_{SUSY} . **Right:** Differences between the three-loop fixed-order and the FeynHiggs predictions. 59
- 4-3.** Numerical comparison of the M_h predictions for a non-vanishing stop mixing in the heavy SUSY limit. The blue dashed lines are the NNLL predictions of FeynHiggs and the red solid lines represent our three-loop fixed-order predictions. The brown band is the CMS/ATLAS Higgs boson mass, $M_h^{exp} = 125.09 \pm 0.24$ GeV. **Left:** M_h as a function of M_{SUSY} for different stop mixing values, $X_t/M_{SUSY} = 0.2, 0.5, 0.7, 1.0, 1.5$ and 2.4 . **Right:** Absolute numerical differences between the three-loop fixed-order predictions and the NNLO results of FeynHiggs plotted in the left figure. 60
- 4-4.** Dependence of M_h on X_t/M_{SUSY} in the heavy SUSY limit evaluated at the same kinematic point considered in Figure **4-3** with $\tan\beta = 10$ and $M_{SUSY} = 1$ TeV, 5 TeV and 20 TeV. The blue lines represent the NNLL predictions coming from FeynHiggs and the blue bands are their corresponding theoretical uncertainties. 61

- 4-5.** Dependence of M_h on M_{SUSY} and X_t in the heavy SUSY limit. We have used $\tan\beta = 10$. The gray lines represent the values of M_{SUSY} and X_t which produce the same Higgs boson mass. The predicted value of M_h increases monotonically with M_{SUSY} 62
- 4-6.** Region of rMSSM parameters in the heavy SUSY limit which is compatible with the central value and the combined uncertainty of the CMS/ATLAS Higgs boson mass, $M_h^{exp} = 125.09 \pm 0.24$ GeV. **Left:** Gray lines represent the points $(M_{SUSY}, \tan\beta)$ compatible with a 125.09 GeV Higgs mass for different values of the stop mixing parameter, $X_t/M_{SUSY} = 0, 0.8, 1.2, 1.5, 2.4$. The purple line represents the combined uncertainty for the case of zero stop mixing. **Right:** Gray lines are the 125.09 GeV contours as a function of M_{SUSY} and X_t/M_{SUSY} for different values of the parameter $\tan\beta$, $\tan\beta = 4, 5, 10, 30$. The purple lines are the points compatible with the combined uncertainty for the lowest value of $\tan\beta$ considered. 63
- 4-7.** **Left:** Evolution of the Higgs quartic self-coupling λ as a function of the renormalization scale Q . **Right:** Beta function of the Higgs self-coupling. We have included the uncertainties in M_t and M_h as is indicated. The plots were drawn with the help of the program SMDR. 66
- 4-8.** SM vacuum stability phase diagram in terms of the Higgs and top quark masses. The region plotted shows the dominant experimental range of M_h and M_t 67
- 4-9.** Higgs boson mass predictions as a function of the SUSY scale and the stop mixing parameter in the \overline{DR} scheme. The light blue regions correspond to the points compatible with $M_h^{exp} = 125.09 \pm 5.0$ GeV for $\tan\beta = 1, 4, 10$ and 30. The gray lines are the contours for the central value of the CMS/ATLAS Higgs mass. The red regions represent the values of X_t and M_{SUSY} where $\lambda(M_{SUSY})$ becomes negative while the red lines display the parameter space which have $\lambda(M_{SUSY}) = 0$ 70
- F-1.** Generic three-loop Higgs self-energy diagram. The field h stands for the lightest higgs boson, t is the top quark field, \tilde{t} is the stop and \tilde{g} represents the gluino field. 103

List of Tables

| | |
|---|----|
| 2-1. MSSM spectrum fields and their $SU(3) \times SU(2) \times U(1)$ quantum numbers. In this table only one generation of leptons and quarks is exhibited. For each lepton and quark super-multiplet there is associated a corresponding multiplet of scalar superpartners, while for the Higgs super-multiplet an anti-particle multiplet of charge-conjugated fermions is associated. | 8 |
| 3-1. Input parameters for the m_h^{max} and m_h^{mod+} scenarios. | 52 |
| C-1. Index labels and ranges included in the Feynman rules of the vertex diagrams. | 81 |

1. Introduction

The discovery of the Higgs boson particle by the ATLAS and CMS experiments at the CERN Large Hadron Collider (LHC) [4, 5] and the rather precise knowledge of its mass, $M_h^{exp} = 125.09 \pm 0.24$ GeV [6–8], and of its couplings [6] to the other Standard Model (SM) particles represent a significant progress in our understanding of the electroweak symmetry breaking mechanism. The SM extrapolated up to the Planck scale ($\Lambda_P = \sqrt{\hbar c/G} = 1.22 \times 10^{19}$ GeV) is theoretically consistent with the inclusion of the ATLAS/CMS Higgs boson in the sense that no Landau pole [9] emerges. However, the metastable nature of the electroweak vacuum [10–15] as well as the unsolved hierarchy problem [16–18], which leads to an unnatural high amount of fine-tuning (10^{34}) for the prediction of the Higgs boson mass at the electroweak scale ($\Lambda_{EW} \approx 10^2$ GeV), arises the question whether the LHC Higgs boson is actually the SM Higgs or a new dynamics with additional degrees of freedom beyond the Standard Model (BSM) regulate the Higgs sector. In this thesis we focused our analysis on two working hypotheses. The first one is the so called desert scenario [19] in which the SM is valid up to Λ_P and the Higgs boson is considered as an elementary weakly coupled particle. In this approach a precise running of the SM parameters in a well defined renormalization scheme is mandatory. Using the LHC measured value of the Higgs mass and the combination of the three-loop beta functions and two-loop matching conditions, the running of the relevant SM parameters (the three gauge couplings, the top Yukawa coupling and the Higgs self-coupling) are found to remain perturbative up to the Planck scale [20]. The Landau pole is located at a scale much larger than Λ_P and therefore we can reasonably assume that no new physics appears up to the scale where the gravitational interactions are not suppressed. The vacuum stability analysis imposes more stringent constraints about the behaviour of the SM at large energy scales close to Λ_P . Due to the borderline behaviour of the SM which lies in a near-critical position between the absolute stability and the metastability phases, the current status of the studies of the vacuum stability problem urges a precise definition and computation of the Higgs boson mass, the top quark mass and their corresponding uncertainties. In this analysis the near-criticality of the Higgs boson self-coupling and its beta-function is used as guideline to go beyond the SM [21]. These arguments assume the existence of a multiverse ruled by anthropic selection rules where the Higgs parameters found in our universe are not at all special, in fact, they correspond to the most likely occurrence in the multiverse. In the desert scenario, however, there are still several puzzles that remain unsolved by the SM dynamics. The neutrino oscillation, the identification of the dark matter, the baryon asymmetry, among others, are all left unanswered and require new BSM physics. Besides, if

one insists that naturalness would represent a real problem of the theory, then one has to conclude that the new physics has to appear about the TeV scale in the coming experiments at the LHC and future colliders, like the International Linear Collider (ILC) [22] and Future Circular Collider (FCC) [23]. The above are strong physical arguments to believe that the SM is actually a low energy effective field theory (EFT) coming from a more fundamental model which includes new physical degrees of freedom. In this second approach deviations from the SM in the dynamics of the Higgs are expected and can be used to obtain indirect information about the nature of the completion of the SM at higher energy scales. The best motivated and the most intensively studied framework of new physics, providing a widely amount of precise predictions for experimental phenomena at the TeV scale, is formulated as a supersymmetric extension of the SM, the Minimal Supersymmetric Standard Model (MSSM) [24–31]. The supersymmetry (SUSY) is the only symmetry that correlates bosonic and fermionic degrees of freedom. One of the main motivations to introduce it is the possibility to provide a solution to the hierarchy problem which emerges in the Standard Model when there is a large hierarchy between the energy scale that characterizes electroweak symmetry breaking and the scale of new physics [32–35]. Due to the introduction of the Higgs scalar sector into the Lagrangian of the Standard Model, the quantum corrections to the Higgs boson mass contain quadratic divergences. In the scenario where new physics appears only up to the Planck scale, it is necessary an unnatural fine-tuning of 32 significant digits in order to get the prediction of the Higgs mass at Λ_{EW} , where the Higgs boson particle was found, from the mass evaluated at Λ_P . In the minimal supersymmetric extension to the SM the radiative corrections to the Higgs boson mass with SM gauge boson loops are also quadratically divergent. However, the contributions coming from a new kind of particles, the supersymmetric partners of the gauge bosons (the gauginos), have the same dependence on the cut-off scale but with opposite sign and cancel in this way the unwanted quadratic divergences. Moreover, the inclusion of additional supersymmetric particles make the effective potential stable, thus the MSSM can also cure the vacuum stability problem. It is worth to mention that MSSM also provides a dark matter candidate, a mechanism to explain the neutrino oscillations and a framework to include gravitational interactions since supersymmetry is a fermionic extension of the Poincare space-time symmetry.

In the MSSM the Higgs sector contains two $SU(2)$ doublets of scalar fields whose interactions with gauge bosons and matter fermions can recover the SM-like couplings in a decoupling limit where the 125 GeV LHC signal is associated to the lightest CP-even Higgs boson with a mass M_h which is not a free input parameter but a prediction coming from the parameters of the theory. The upper bound on its predicted mass at leading order (LO) is given by the Z^0 gauge boson mass, $M_{Z^0} = 91.2$ GeV, leading to the exclusion of the MSSM at current collider experiments. Nevertheless, higher order quantum corrections to M_h lead to a large shift in the upper limit ($\Delta M_h \approx 40$ GeV), where the bulk of the corrections comes from the supersymmetric quantum chromo-dynamics (SQCD) sector of the Lagrangian, and makes the MSSM Higgs whose interactions with sector compatible with the mass and the

detected production rates of the LHC Higgs-like signal over a wide range of the parameter space of the relevant phenomenology scenarios [36–39]. The determination of the theoretical uncertainty associated to the M_h -prediction requires a very precise calculation. Based on the missing higher order contributions to the Higgs self-energies, to the running of the gauge and Yukawa couplings, and also on the renormalization scheme dependence, the theoretical combined uncertainty associated to the determination of M_h has been estimated to be about 1 to 5 GeV [40,41]. However, the experimental uncertainty is expected to reach a value of the order of 100-200 MeV at the LHC [42] and this can go even down at future colliders, estimated to roughly 50 MeV at ILC [43]. Thus, an accuracy computation of M_h is mandatory in order to lead the theoretical uncertainty to the same order as the expected experimental one.

Our contribution follows this guideline. In this thesis we provide an alternative calculation of the lightest Higgs boson mass in the SQCD sector of the real version of the MSSM with a precision of three-loops at order $\alpha_t\alpha_s^2$. We have followed the Feynman diagrammatic (FD) procedure to obtain a renormalized correction in the \overline{DR} scheme [44–47]. The regularization procedure adopted is based on the dimensional reduction scheme in order to preserve supersymmetry to all perturbative orders. Taking in mind that in the MSSM is no clear a priori what are the hierarchies of the masses, we have avoided the application of asymptotic expansions at the integral level and we have obtained the quantum corrections in terms of a set of three-loop master integrals whose numerical evaluation is possible for an arbitrary mass hierarchy thanks to the development of new calculation techniques based on the dispersion method [48–54]. Thus, our calculation extends the region of validity of previous studies to the whole supersymmetric parameter space. The basis of three-loop master integrals contain logarithmic terms of the form $\ln^n(M_{SUSY}/\Lambda_{EW})$ for $n \leq 3$ which can spoil the good perturbative behavior of the quantum corrections when the supersymmetric scale (M_{SUSY}) is significantly larger than Λ_{EW} (which we identify in this work with the top mass M_t). Therefore, a fixed-order computation of M_h could become inadequate and the calculation of the Higgs mass has to be reorganized in an effective field theory approach. In order to study the effects of the large logarithmic terms we have done a numerical comparison of our three-loop fixed-order predictions with the other fixed-order and EFT results found in literature. We have decided to use the fixed-order and EFT hybrid calculations currently included in the codes H3m [55] and FeynHiggs [56], which seems to give a reliable three-loop predictions of the Higgs boson mass up to large SUSY scales, to make a cross check with our results. In the EFT considered in FeynHiggs, the heavy SUSY particles are integrated out at the scale M_{SUSY} in the decoupling limit where $M_{SUSY} \gg M_t$, while the SM renormalization group equations (RGEs) are used to evolve the couplings between the SUSY scale and the EW scale in such a way that the M_h -corrections are free of large logarithmic terms. We have assumed the same decoupling limit for the SUSY scale over our three-loop M_h predictions in order to size the numerical effect of the logarithmic terms for large M_{SUSY} values. Having in mind that the fixed-order corrections to M_h contain the effects of large logarithms, it is

natural to ask how large the SUSY scale can be in order not to spoil the convergence of the perturbative expansion. Thus, we also include in this work a phenomenological analysis about the compatibility of the experimental observations at the LHC for the Higgs boson mass and its combined uncertainty with the region of parameters in a specific MSSM benchmark scenario in order to find upper and lower bounds on the needed supersymmetric scale. However, the bounds obtained are valid just for large values of the ratio between the vacuum expectation values of the two CP-even Higgs bosons ($\tan\beta$). For small values of $\tan\beta$ we will show that the vacuum stability analysis in the Standard Model can give additional upper bounds on M_{SUSY} as a function of M_h . The constraints on the SUSY scale can be derived by studying the absolute stability condition of the Higgs effective potential in an approach where the SM is a low-energy EFT of the real MSSM and the Higgs quartic self-coupling correlates the high SUSY scale with the low scale Λ_{EW} through the renormalization group equations.

The plan of the thesis is the following. Chapter 2 contains a description of the Higgs sector and SQCD sector of the MSSM with real parameters at tree-level. In particular, we derive the expressions of the mass matrices for the neutral and charged MSSM Higgs bosons and we study the electroweak symmetry breaking on the MSSM Higgs potential. The tree-level mass matrices are used to derive a prescription for the renormalization of the neutral Higgs boson masses. Thus, this chapter also contains a complete description of the regularization scheme and the necessary renormalization conditions to obtain the quantum corrections to M_h at three-loop level in the gaugeless limit. We lastly review the state of art of the fixed-order and EFT calculations of the lightest Higgs boson mass.

Chapter 3 and Chapter 4 contain the main results of our project. In Chapter 3 a detailed description of our three-loop computation of M_h is presented. We discuss the technical details to the renormalization procedure adopted and in particular to the evaluation of the three-loop Feynman integrals involved. The three-loop corrections contain non-local divergences that must be removed with an additional subrenormalization procedure that will be discussed in this chapter. A numerical analysis, where the effects of the three-loop corrections on the pole mass M_h evaluated at some kinematic limits and the study of the dependence of M_h on the SUSY parameters, is included. This comprises a comparison with the other higher order predictions coming from the fixed-order computations implemented in the public codes FeynHiggs and H3m.

The basis of three-loop master integrals obtained in our calculation can spoil the convergence of the perturbative corrections to M_h when the SUSY scale grows up to an arbitrary large energy. We therefore provide in Chapter 4 a discussion about the effects of the large logarithms involved in the fixed-order calculation at large SUSY scales and a phenomenological analysis where some constraints on the needed SUSY scale coming from two sources

are determined. First, we study the compatibility of the region of parameters in a realistic MSSM benchmark scenario with the LHC Higgs boson mass value and its corresponding experimental uncertainty and we derived lower and upper bounds on the SUSY scale. We further explore the SUSY scale constraints from the vacuum stability analysis. We review the vacuum stability problem in the SM and we use the absolute stability condition derived from the Higgs effective potential in a low-energy EFT of the real MSSM to derive additional upper bounds on the SUSY scale.

Finally, we give our conclusions and perspectives in Chapter 5.

2. The Higgs Bosons of the real MSSM (rMSSM)

In this chapter we are going to review the structure of the Higgs sector of the MSSM with real parameters (rMSSM). We review the rMSSM classical Higgs potential and discuss the electroweak and SUSY breaking mechanisms. We also derive the expressions for the Higgs bosons mass matrices at tree-level and we use them to formulate a prescription to renormalize the quantum corrections to the physical Higgs boson masses in the EW gaugeless limit up to three-loop level. Besides, we go over the supersymmetric extension of the quantum chromodynamics (SQCD sector) and we describe the renormalization of the squark masses and mixing angles up to two-loop level, which will be important when quantum corrections to the Higgs boson masses beyond one-loop order be incorporated since two- and three-loop diagrams contain non-local UV divergences. We have also included a discussion of the renormalization of the gluino and the top quark masses. Finally, the current status of the higher-order quantum corrections to the Higgs boson masses are reviewed.

2.1. The rMSSM Higgs sector at tree-level

Supersymmetry is the only fermionic generalization of the Poincaré symmetry of the space-time which transforms fermions into bosons and vice versa. The existence of such a non-trivial extension of the Poincaré symmetry is highly constrained by theoretical principles [57, 58]. The minimal supersymmetric extension of the Standard Model consists of the fields contained in the two-Higgs-doublet extension of the SM (2HDM) and their corresponding superpartners. The field content of the MSSM is summarized in Table **2-1** [59]. The MSSM spectrum contains three gauge supermultiplets which consist of the gluons and their gluino fermionic superpartners and the EW gauge bosons and their gaugino superpartners. The matter supermultiplets consist of three generations of left-handed quarks and their scalar superpartners, the squarks. Three generations of left-handed leptons and their associated sleptons, and the corresponding antiparticles of all the fermions. The Higgs supermultiplets consists of two complex Higgs doublets, their higgsino fermionic superpartners and the corresponding antiparticles. In order to guarantee the cancellation of anomalies coming from the introduction of the higgsino superpartners and preserve supersymmetry and gauge invariance, the Higgs

| Super-Multiplet | Super-field | Bosons | Fermions | SU(3) | SU(2) | U(1) |
|-----------------|-----------------|--|--|-----------|-------|------|
| gauge/ino | \widehat{V}_8 | g | \widetilde{g} | 8 | 1 | 0 |
| | \widehat{V} | W^\pm, W^0 | $\widetilde{W}^\pm, \widetilde{W}^0$ | 1 | 3 | 0 |
| | \widehat{V}' | B | \widetilde{B} | 1 | 1 | 0 |
| s/lepton | \widehat{L} | $(\widetilde{v}_L, \widetilde{e}_L^-)$ | $(v, e^-)_L$ | 1 | 2 | -1 |
| | \widehat{E}^c | \widetilde{e}_R^+ | e_L^c | 1 | 1 | 2 |
| s/quark | \widehat{Q} | $(\widetilde{u}_L, \widetilde{d}_L)$ | $(u, d)_L$ | 3 | 2 | 1/3 |
| | \widehat{U}^c | \widetilde{u}_R^* | u_L^c | $\bar{3}$ | 1 | -4/3 |
| | \widehat{D}^c | \widetilde{d}_R^* | d_L^c | $\bar{3}$ | 1 | 2/3 |
| Higgs/ino | \widehat{H}_1 | (H_1^0, H_1^-) | $(\widetilde{H}_1^0, \widetilde{H}_1^-)$ | 1 | 2 | -1 |
| | \widehat{H}_2 | (H_2^+, H_2^0) | $(\widetilde{H}_2^+, \widetilde{H}_2^0)$ | 1 | 2 | 1 |

Table 2-1.: MSSM spectrum fields and their $SU(3) \times SU(2) \times U(1)$ quantum numbers. In this table only one generation of leptons and quarks is exhibited. For each lepton and quark super-multiplet there is associated a corresponding multiplet of scalar superpartners, while for the Higgs super-multiplet an anti-particle multiplet of charge-conjugated fermions is associated.

sector of the real MSSM Lagrangian [24–31] requires the definition of at least two doublets

$$H_1 = \begin{pmatrix} H_1^0 + \frac{1}{\sqrt{2}}v_1 \\ H_1^- \end{pmatrix} \quad \text{and} \quad H_2 = \begin{pmatrix} H_2^+ \\ H_2^0 + \frac{1}{\sqrt{2}}v_2 \end{pmatrix}, \quad (2-1)$$

with an associated hypercharge $Y_1 = -1$ and $Y_2 = +1$, respectively. The second Higgs doublet is necessary, moreover, to generate mass for both up- and down-type quarks as well as charged leptons. The complex fields H_j^0 have neutral components which are vevless scalar fields, $H_j^0 = \phi_j^0 + i\chi_j^0$, coming from the expansion around the minima of the Higgs effective potential, $v_{1,2}$. The components $H_{1,2}^\pm$ are charged scalar fields with vanishing vacuum expectation values (vevs) to ensure that the $U(1)_{em}$ symmetry will not be spontaneously broken. The Higgs sector comes from the bare Lagrangian

$$\mathcal{L}_{V-H} = \mathcal{D}_\sigma H_1^\dagger \mathcal{D}^\sigma H_1 + \mathcal{D}_\sigma H_2^\dagger \mathcal{D}^\sigma H_2 - V(H_1, H_2). \quad (2-2)$$

The kinetic term contains the covariant derivative

$$\mathcal{D}_\sigma = \partial_\sigma + ig \frac{\tau^a}{2} W_\sigma^a + ig' \frac{Y}{2} B_\sigma + ig_s \frac{\lambda^\alpha}{2} G_\sigma^\alpha, \quad (2-3)$$

where g' , g and g_s are the $U(1)_Y$, $SU(2)_L$ and $SU(3)$ gauge couplings respectively. The $SU(2)$ Pauli matrices is represented with τ^a while λ^α stands for the $SU(3)$ Gell-Mann matrices. The electroweak (EW) gauge bosons are defined as

$$W_\mu^\pm = \frac{W_\mu^1 \mp i W_\mu^2}{\sqrt{2}}; \quad \begin{pmatrix} Z_\mu^0 \\ A_\mu \end{pmatrix} = \begin{pmatrix} \cos\theta_W & -\sin\theta_W \\ \sin\theta_W & \cos\theta_W \end{pmatrix} \begin{pmatrix} W_\mu^3 \\ B_\mu \end{pmatrix}, \quad (2-4)$$

where the EW mixing angle, θ_W , is related to the coupling constants g and g' and the electric charge, e , by

$$g = \frac{e}{\sin\theta_W}; \quad g' = \frac{e}{\cos\theta_W}. \quad (2-5)$$

The classical Higgs potential, $V(H_1, H_2)$, is given by

$$\begin{aligned} V(H_1, H_2) = & (|\mu|^2 + m_{H_1}^2) |H_1|^2 + (|\mu|^2 + m_{H_2}^2) |H_2|^2 + b (\epsilon_{ab} H_1^a H_2^b + h.c.) \\ & + \frac{1}{2} g^2 |H_1^\dagger H_2|^2 + \frac{1}{8} (g^2 + g'^2) (|H_2|^2 - |H_1|^2)^2. \end{aligned} \quad (2-6)$$

The quadratic terms proportional to the higgsino mass parameter $|\mu|^2$ in eq. (2-6) come from the F -contribution to the SUSY Lagrangian, while the terms with the EW gauge couplings (g, g') come from the D -contribution; thus, from the D -terms, one obtains the four scalar vertices, which include the quartic Higgs self-interaction terms in the Higgs potential. In contrast to the SM, the Higgs quartic self-coupling is not a free parameter but is determined by the coupling $(g^2 + g'^2)/8$. From the F -terms, one obtains also another four scalar vertices, but they do not contribute to the Higgs potential since contain always at least two sfermions. The F and D fields are auxiliary fields that do not propagate in space-time and can be eliminated by applying the equations of motion. As supersymmetric particles have not been observed at the electroweak scale, supersymmetry is manifestly not an exact symmetry of the nature and therefore must be broken. Several SUSY breaking mechanisms have been considered [60–62] but in fact there is no consensus on how to break SUSY. In phenomenological application, one must introduce new terms that explicitly breaks supersymmetry and represent the low-energy effects of the unknown breaking mechanism. In eq. (2-6) the parameters $m_{H_1}^2, m_{H_2}^2$ and b parameterize the SUSY breaking. The SUSY-invariant Lagrangian cannot accommodate electroweak symmetry breaking since the terms proportional to $|\mu|^2$ are positive. Thus, the SUSY-violating parameters $m_{H_1}^2$ and $m_{H_2}^2$, which can of course have either sign, are needed in order to break the EW symmetry. The b -term is the only that depends on the phases of the fields. The parameter b is real and positive and the fields H_1^0 and H_2^0 have equal and opposite phases which can be reduce both to zero through a $U(1)_Y$ gauge transformation since these fields have equal and opposite hypercharges. The vevs, $v_{1,2}$, as well as the couplings are therefore all real, which means that CP invariance is not spontaneously broken by the classical Higgs potential of the rMSSM.

It is vital to point out that such phenomenological terms containing those SUSY breaking parameters must be 'soft', that is, the SUSY breaking terms must be super-renormalizable, with mass dimension less than four, and therefore their coefficients must have positive mass dimension. The reason is that a soft breaking term will not introduce additional divergences into the dimensionless coupling constants which guarantee the stability of the mass hierarchy, the cancellation of quadratically divergent corrections to scalar masses are maintained to all perturbative orders. Besides, it is important to emphasize that the mass terms which break SUSY and therefore the masses of the undiscovered SUSY particles do respect the SM gauge

symmetries. The masses of the known SM particles all arise from the spontaneous breaking of the EW symmetry.

From eq. (2-6) we can derive the linear part of the Higgs potential in the basis $(\phi_j^0, \chi_j^0, H_j^\pm)$ where $j = 1, 2$. For the fields χ_j^0 and H_j^\pm there are no contributions since the rMSSM Higgs potential is invariant under CP-transformation. Thus, the linear terms read: $T_1\phi_1^0 + T_2\phi_2^0$, where the coefficients T_j , better-known as Higgs tadpoles, have the expressions

$$\begin{aligned} \frac{T_1}{\sqrt{2}v_1} &= (|\mu|^2 + m_{H_1}^2) - b\frac{v_2}{v_1} + \frac{1}{8}(g^2 + g'^2)[v_1^2 - v_2^2], \\ \frac{T_2}{\sqrt{2}v_2} &= (|\mu|^2 + m_{H_2}^2) - b\frac{v_1}{v_2} + \frac{1}{8}(g^2 + g'^2)[v_2^2 - v_1^2]. \end{aligned} \quad (2-7)$$

As the vevs v_1 and v_2 minimize the Higgs potential, the following stationary conditions are satisfied:

$$\left. \frac{\partial V}{\partial |H_j^0|} \right|_{\langle H_j^0 \rangle=0; \langle H_j^\pm \rangle=0} = T_j = 0; \quad j = 1, 2. \quad (2-8)$$

From eq. (2-8) one can identify the conditions required for the stable minimum of V . First note that along the direction $|H_1^0| = |H_2^0|$ the potential will be unbounded from below and therefore it does not have a minimum unless

$$2|\mu|^2 + m_{H_1}^2 + m_{H_2}^2 > 2b. \quad (2-9)$$

Thus $(|\mu|^2 + m_{H_1}^2)$ and $(|\mu|^2 + m_{H_2}^2)$ cannot simultaneously take negative values. This implies that the point $|H_1^0| = |H_2^0| = 0$ cannot be a maximum of V . If instead both mass terms are positive, then the origin is not a minimum but a saddle point, and the minimum occur at non-zero vevs of H_j^0 , when

$$(|\mu|^2 + m_{H_1}^2)(|\mu|^2 + m_{H_2}^2) < b^2. \quad (2-10)$$

The rMSSM Higgs potential develops a stable minimum if the conditions of equations (2-9) and (2-10) are met.

Turning to the bilinear part of the kinetic terms in the Lagrangian \mathcal{L}_{V-H} (eq. 2-2) the masses of the EW gauge bosons can be derived, producing the expressions

$$M_W^2 = \frac{1}{4}g^2(v_1^2 + v_2^2); \quad M_{Z^0}^2 = \frac{1}{4}(g^2 + g'^2)(v_1^2 + v_2^2); \quad M_A^2 = 0. \quad (2-11)$$

The mass matrices of the rMSSM Higgs bosons can be identified from the bilinear part of the classical potential,

$$\begin{pmatrix} \phi_1^0 & \phi_2^0 \end{pmatrix} M^{\phi^0} \begin{pmatrix} \phi_1^0 \\ \phi_2^0 \end{pmatrix} + \begin{pmatrix} \chi_1^0 & \chi_2^0 \end{pmatrix} M^{\chi^0} \begin{pmatrix} \chi_1^0 \\ \chi_2^0 \end{pmatrix} + \begin{pmatrix} H_1^+ & H_2^+ \end{pmatrix} M^{H^\pm} \begin{pmatrix} H_1^- \\ H_2^- \end{pmatrix}, \quad (2-12)$$

To derive the M^{ϕ^0} -matrix the relations from eqs. (2-7) and (2-8) and the definitions

$$M_A^2 = b(\cot\beta + \tan\beta), \quad \tan\beta = \frac{v_2}{v_1}; \quad 0 \leq \beta \leq \frac{\pi}{2}, \quad (2-13)$$

are required. The tree-level mass matrix of the neutral $\phi_{1,2}^0$ -bosons reads

$$M^{\phi^0} = \begin{pmatrix} M_{Z^0}^2 c_\beta^2 + M_A^2 s_\beta^2 + \frac{T_1}{\sqrt{2}v_1} & -(M_A^2 + M_{Z^0}^2) s_\beta c_\beta \\ -(M_A^2 + M_{Z^0}^2) s_\beta c_\beta & M_{Z^0}^2 s_\beta^2 + M_A^2 c_\beta^2 + \frac{T_2}{\sqrt{2}v_2} \end{pmatrix}. \quad (2-14)$$

We have used the short notation $s_\beta = \sin(\beta)$ and $c_\beta = \cos(\beta)$ and we have written explicitly the contributions of the Higgs tadpoles, which vanish at tree-level according to eq. (2-8), because they will receive non-zero loop contributions when renormalization of the Higgs masses will be considered. Because both v_1 and v_2 are real and positive, the upper and lower bound on the angle β lies on the interval shown in eq. (2-13). By other side, the tree-level mass matrices of the $\chi_{1,2}^0$ and $H_{1,2}^\pm$ components are given by

$$M^{\chi^0} = \begin{pmatrix} M_A^2 s_\beta^2 + \frac{T_1}{\sqrt{2}v_1} & -M_A^2 s_\beta c_\beta \\ -M_A^2 s_\beta c_\beta & M_A^2 c_\beta^2 + \frac{T_2}{\sqrt{2}v_2} \end{pmatrix} \quad (2-15)$$

and

$$M^{H^\pm} = \begin{pmatrix} M_A^2 s_\beta^2 + \frac{T_1}{\sqrt{2}v_1} + \frac{1}{2}g^2 v_2^2 & M_A^2 s_\beta c_\beta + \frac{1}{2}g^2 v_1 v_2 \\ M_A^2 s_\beta c_\beta + \frac{1}{2}g^2 v_1 v_2 & M_A^2 c_\beta^2 + \frac{T_2}{\sqrt{2}v_2} + \frac{1}{2}g^2 v_1^2 \end{pmatrix}. \quad (2-16)$$

The potential can be brought into the physical basis, where the quadratic terms in the components of H_j are diagonalized, through the rotations

$$\begin{pmatrix} \phi_1^0 \\ \phi_2^0 \end{pmatrix} = D^\dagger(\alpha) \begin{pmatrix} H \\ h \end{pmatrix}, \quad \begin{pmatrix} \chi_1^0 \\ \chi_2^0 \end{pmatrix} = D^\dagger(\beta) \begin{pmatrix} G^0 \\ A \end{pmatrix}, \quad \begin{pmatrix} H_1^\pm \\ H_2^\pm \end{pmatrix} = D^\dagger(\beta) \begin{pmatrix} G^\pm \\ H^\pm \end{pmatrix}, \quad (2-17)$$

via the orthogonal transformation

$$D(\theta) = \begin{pmatrix} c_\theta & s_\theta \\ -s_\theta & c_\theta \end{pmatrix}. \quad (2-18)$$

In this basis the Higgs sector has five physical Higgs bosons, three of them are neutral: the lightest (h) and heavy (H) CP-even Higgs bosons and the CP-odd Higgs boson (A). The other two, H^\pm , are charged and vevless. There are also three unphysical massless Goldstone bosons, G^0 and G^\pm , which are absorbed by the EW gauge fields to build up their longitudinal components just as in the SM. The angle β is linked to the vevs through eq. (2-13) while α can be determined from the rotation of eq. (2-14) in terms of the MSSM parameters,

$$\tan(2\alpha) = \tan(2\beta) \frac{M_A^2 + M_{Z^0}^2}{M_A^2 - M_{Z^0}^2} \quad ; \quad -\frac{\pi}{2} < \alpha < 0. \quad (2-19)$$

Besides of the EW boson masses of eq. (2-11), after diagonalization the rMSSM Higgs sector is parametrized in terms of two additional parameters: $\tan\beta$ and the mass of the CP-odd Higgs boson m_A . The masses of the charged Higgs bosons, m_{\pm} , are linearly dependent on m_A , they are usually used in the complex version of the MSSM. Throughout this work we use m_A as input parameter. At tree-level we have:

$$m_A^2 = M_A^2 + \frac{T_1}{\sqrt{2}v_1}s_\beta^2 + \frac{T_2}{\sqrt{2}v_2}c_\beta^2 \quad ; \quad m_{\pm}^2 = m_A^2 + M_W^2. \quad (2-20)$$

The tree-level masses of the CP-even Higgs boson particles, h and H , follow as predictions

$$m_{h,H}^2 = \frac{1}{2} \left[m_A^2 + M_{Z^0}^2 \mp \sqrt{(m_A^2 + M_{Z^0}^2)^2 - 4m_A^2 M_{Z^0}^2 \cos^2(2\beta)} \right]. \quad (2-21)$$

From the mass formulas (2-20) and (2-21) the next important inequalities can be derived:

$$m_h \leq M_{Z^0} \quad ; \quad m_A \leq m_H \quad ; \quad M_W \leq m_{\pm}. \quad (2-22)$$

As a consequence, the lightest Higgs boson mass is predicted to be bounded from above by the Z^0 -boson mass, $m_h \leq 91.2$ GeV, modulo radiative corrections. This bound follows from the fact that the quartic coupling of the Higgs boson fields is determined by the size of the EW gauge couplings and therefore m_h is a prediction of the model in the MSSM. The tree-level bound on m_h has already been excluded by the current experimental value of the LHC Higgs boson mass. The other Higgs boson masses grow without boundary when the scale m_A grows.

2.2. Renormalization of the rMSSM Higgs boson masses

Even if the tree-level mass of the light CP-even Higgs boson is excluded by the ATLAS/CMS results, it is very well known that quantum corrections to m_h can shift this tree-level prediction by a substantial amount reaching the experimental value in a large region of the MSSM parameters. There are three different approaches to determine higher order quantum correction to the Higgs boson masses. The first approach is based on a fixed-order calculation, where the quantum corrections contain an explicit diagrammatic calculation of the Higgs self-energy contributions at a given perturbative order. This procedure is invariant under different gauge-fixing elections. The second method uses the 1PI (one-particle-irreducible) Higgs effective potential, which is the classical potential with higher-loop radiative corrections included. The renormalized Higgs boson masses are obtained here through the second derivative of the 1PI effective potential regarding the Higgs fields evaluated at their vacuum expectation values. Due to the potential is expanded around a constant value of the Higgs fields, in this approach the momentum dependence of the Higgs mass corrections cannot be taken into account. The last approach uses the EFT methods to relate the dynamics at high energy scales with a low energy effective model of the MSSM [63]. The techniques of the

RGEs are used here to determine the effective coupling constants where the phenomenology is contained. We have adopted in this work the first method; therefore, we focus in this section on the renormalization of the quantum corrections to the neutral Higgs boson masses computed following a fixed-order Feynman diagrammatic procedure. In this approach, the renormalized CP-even Higgs boson masses are obtained by finding the zero eigenvalues propagator matrix

$$(\Delta_H)^{-1} = -i \begin{pmatrix} p^2 - m_H^2 + \widehat{\Sigma}_{HH} & \widehat{\Sigma}_{hH} \\ \widehat{\Sigma}_{hH} & p^2 - m_h^2 + \widehat{\Sigma}_{hh} \end{pmatrix}, \quad (2-23)$$

which is equivalent to solve the determinantal equation

$$\left[p^2 - m_H^2 + \widehat{\Sigma}_{HH} \right] \left[p^2 - m_h^2 + \widehat{\Sigma}_{hh} \right] - \left[\widehat{\Sigma}_{hH} \right]^2 = 0, \quad (2-24)$$

where m_h and m_H denote the tree-level mass of h and H respectively, p is the external momentum of the self-energies and

$$\widehat{\Sigma}_{\psi_i\psi_j} = \widehat{\Sigma}_{\psi_i\psi_j}^{(1)} + \widehat{\Sigma}_{\psi_i\psi_j}^{(2)} + \cdots + \widehat{\Sigma}_{\psi_i\psi_j}^{(l)} \quad ; \quad \psi_{1,2} = h, H, \quad (2-25)$$

are the corresponding Higgs self-energy corrections evaluated up to l -loop level and renormalized in a specific scheme. These loop corrections contain local UV divergences that have to be removed order by order through appropriated renormalization constants according to

$$\widehat{\Sigma}_{\psi_i\psi_j}^{(l)} = \sum_{\psi_i\psi_j}^{(l)} + \delta^{(l)}\sigma_{\psi_i\psi_j}^2 \quad ; \quad \psi_{1,2} = h, H. \quad (2-26)$$

$\sum_{\psi_i\psi_j}^{(l)}$ represents the l -loop unrenormalized Higgs self-energies while the terms with delta are the counter-terms of the CP-even Higgs boson masses which are responsible for extracting the infinities from the self-energies and producing finite contributions useful to get numerical predictions. Note that the self-energies and counter-terms are in the physical basis; however, their expressions can be derived from the unphysical one ($\phi_1^0 - \phi_2^0$ basis) after diagonalization

$$\sum_{\psi_i\psi_j}^{(l)} + \delta^{(l)}\sigma_{\psi_i\psi_j}^2 = D(\alpha) \left(\sum_{\phi_i^0\phi_j^0}^{(l)} + \delta^{(l)}\sigma_{\phi_i^0\phi_j^0}^2 \right) D(\alpha)^\dagger \quad ; \quad j = 1, 2. \quad (2-27)$$

In the following we specify the necessary conditions to obtain the constants $\delta^{(l)}\sigma_{\phi_i^0\phi_j^0}^2$ in a mixed OS/ \overline{DR} scheme. The abbreviation OS stands for an On-Shell renormalization while \overline{DR} refers to the renormalization by dimensional reduction with minimal subtraction.

The UV divergences contained in the multi-loop radiative corrections are treated through a regularization method. There are different regularization procedures, we briefly described two of them here: the Dimensional Regularization (DREG) [64–66] and the Dimensional Reduction (DRED) [44–47] schemes. The latter is a modification of the DREG procedure.

In order to perform calculations in the SM the method of dimensional regularization is the

preferred option to regularize the Feynman integrals. For this purpose, the four dimensional space-time as well as the gauge fields are analytically continued to a D -dimensional space, where $D = 4 - 2\epsilon$. The divergences are thus expressed in terms of l -order poles of the form $1/\epsilon^l$ in the limit $\epsilon \rightarrow 0$. Additionally, DREG preserves the gauge symmetries, but the chiral symmetry and the supersymmetry are broken in this approach. Since additional degrees of freedom are introduced in the analytic continuation to D dimensions, the number of bosonic no longer coincides with the number of fermionic degrees of freedom and, as a consequence, supersymmetry is broken. In order to avoid this explicit supersymmetry breaking, the method of dimensional reduction has been developed. In contrast to the dimensional regularization, in DRED only the number of space-time dimensions are extended from 4 to D , where D is less than 4, while the number of components of all other tensors, like metric tensors, vector fields and γ matrices, are fixed to four. Fermions, on the other hand, remain as four-component spinors as well. The corresponding Dirac and Lorentz algebra of the different tensor objects in the DREG/DRED schemes will be developed in more detail in Chapter 3 and Appendix A. In the component field language, it is convenient to split the four dimensional vector fields V^μ into a D -dimensional vector V^i plus a $(4 - D)$ -dimensional field V^σ , where $D \leq \sigma \leq 4$. The $(4 - D)$ degrees of freedom transform as scalars under gauge transformations and are known in literature as the ϵ -scalar fields. One can associate a mass m_ϵ to these unphysical ϵ -scalars; however, it is important to ensure that physical observables will be independent of this parameter after renormalization. An important feature of supersymmetric theories is the fact that the renormalized vector and ϵ -scalar coupling constants must be equal, and therefore, their beta functions must be the same. To date, this property has been explicitly proved for the SQCD vertices: $gc\bar{c}$, ggg , $gq\bar{q}$, $\tilde{g}q\bar{q}$, $q\bar{q}\epsilon$, $\tilde{g}\tilde{g}\epsilon$ and $g\epsilon\epsilon$ up to three-loop level [67].

Both regularization procedures DREG and DRED introduce a new non-physical parameter into the theory, the renormalization scale μ_r , which is meant to preserve the mass dimension of the loop integrals and the interaction couplings. A subsequent renormalization procedure is necessary in order to eliminate this dependency on unphysical parameters and establishes a connection between the parameters of the theory and the physical observables, like the particles masses. The result of an exact calculation, in which all orders of perturbation theory are taken into account, is independent of the renormalization scheme. In practice, however, only contributions up to a certain order of the perturbative series can be considered. The dependence on the renormalization scheme of the result of such a calculation reflects the theoretical uncertainty caused mainly by the missing higher order contributions. This work will distinguish between four different renormalization schemes: The \overline{DR} , the \overline{MS} , the \overline{DR}' and the On-Shell scheme.

In the \overline{DR} scheme, loop integrals are regularized with DRED and the renormalization constant belonging to a parameter only absorbs the proportion of the bare parameter which is

proportional to

$$\frac{1}{\bar{\epsilon}} = \frac{2}{\epsilon} - \gamma_E + \ln 4\pi . \quad (2-28)$$

Thus, the bar in \overline{DR} is to underline that an additional factor of $\sqrt{4\pi e^{-\gamma_E}}$ is absorbed into the renormalization scale associated to the loop corrections, where $\gamma_E \approx 0.5772156649$ is the Euler-Mascheroni constant. The \overline{DR} renormalization is of particular interest in SUSY calculations since regularization by dimensional reduction preserves supersymmetry and global gauge invariance up to three-loop level when the EW gaugeless limit is adopted [68]. In contrast, the method of dimensional regularization is used in the \overline{MS} scheme [69–74], usually for calculations in the Standard Model. The \overline{MS} renormalization constants are obtained also from the extraction of the terms proportional to $1/\bar{\epsilon}$. In particular, at the one-loop level, the counterterms in the \overline{DR} scheme do not differ from those in the \overline{MS} scheme. The finite result of a calculation in the \overline{DR} or \overline{MS} scheme is dependent on the renormalization scale which was introduced during regularization. For the complete determination of the renormalization scheme, the specification of μ_r is necessary. Both schemes have the advantage that all UV counter-terms are polynomial in the kinematic invariants, as the external momenta and particle masses.

The \overline{DR}' scheme [46, 75] is a slightly modification of the \overline{DR} procedure where the mass of the ϵ scalars completely decouples from all the anomalous dimensions, beta functions and matching conditions between running parameters and physical observables. In the context of a \overline{DR} renormalization, also the mass m_ϵ is renormalized in the \overline{DR} scheme. In the latter case, the physical observables will depend on the unphysical ϵ -mass and it is important to keep m_ϵ different from zero since the renormalization group equations of the particle masses and m_ϵ are coupled. In order to get rid of this m_ϵ -dependence, one can introduce additional finite shifts in the renormalizations constants associated to the physical parameters. The \overline{DR} renormalization modified to introduce those additional shifts is called the \overline{DR}' scheme.

Finally, in the On-Shell scheme [76, 77] the parameter counterterms absorb finite terms in addition to pole parts in $1/\bar{\epsilon}$. If the mass of a particle is fixed on-shell, then the corresponding mass parameter is given by the real part of the pole of the propagator and can be interpreted as a physical mass. The mass counter-terms then absorb all the corrections to the real part of the propagator's pole. If all quantities are determined on-shell, then the finite result of a calculation no longer depends on the scale μ_r introduced for regularization.

We consider in this section the determination of the Higgs mass counter-terms in the EW gaugeless limit and we derived the counter-term expressions up to three-loop level. The renormalized self-energies are obtained from the unrenormalized Lagrangian \mathcal{L}_{V-H} (eq. 2-2) by replacing the bare parameters and fields with the renormalized ones. Each Higgs scalar doublet of eq. (2-1) gets a multiplicative renormalization

$$H_i \rightarrow H_i \sqrt{Z_i} ; \quad Z_i = 1 + \sum_{l=1}^3 \delta^{(l)} Z_i ; \quad i = 1, 2 . \quad (2-29)$$

The free kinetic part of \mathcal{L}_{V-H} yields the renormalized terms

$$\mathcal{L}_{V-H}^{free} \rightarrow \sum_{j=1}^2 Z_j |\partial_\mu H_j^0|^2 + Z_1 |\partial_\mu H_1^-|^2 + Z_2 |\partial_\mu H_2^+|^2, \quad (2-30)$$

while the mass terms of the classical Higgs potential (eq. 2-12) produce renormalized quantities of the form

$$- \begin{pmatrix} x_1 \sqrt{Z_1} & x_2 \sqrt{Z_2} \end{pmatrix} \left(M^x + \sum_{l=1}^3 \delta^{(l)} M^x \right) \begin{pmatrix} x_1 \sqrt{Z_1} \\ x_2 \sqrt{Z_2} \end{pmatrix} ; \quad x = \phi^0, \chi^0, H^\pm. \quad (2-31)$$

For the off-diagonal terms of the matrix M^x and its counter-terms, $\delta^{(l)} M^x$, the fields x_1 and x_2 are mixed and an expansion of the square root becomes necessary. Keeping terms up to three-loop order one has:

$$\sqrt{Z_1} \sqrt{Z_2} = 1 + \frac{1}{2} \delta^{(1)} Z_{12} + \frac{1}{2} \delta^{(2)} Z_{12} + \frac{1}{2} \delta^{(3)} Z_{12} + \dots, \quad (2-32)$$

where we have used the definitions

$$\begin{aligned} \delta^{(1)} Z_{12} &= \delta^{(1)} Z_1 + \delta^{(1)} Z_2, \\ \delta^{(2)} Z_{12} &= \delta^{(2)} Z_{11} + \delta^{(2)} Z_{22} + \frac{1}{2} \delta^{(1)} Z_1 \delta^{(1)} Z_2, \\ \delta^{(3)} Z_{12} &= \delta^{(3)} Z_{11} + \delta^{(3)} Z_{22} + \frac{1}{2} (\delta^{(1)} Z_1 \delta^{(2)} Z_{22} + \delta^{(1)} Z_2 \delta^{(2)} Z_{11}), \end{aligned} \quad (2-33)$$

with

$$\begin{aligned} \delta^{(1)} Z_{ii} &= \delta^{(1)} Z_i ; \quad i = 1, 2, \\ \delta^{(2)} Z_{ii} &= \delta^{(2)} Z_i - \frac{1}{4} (\delta^{(1)} Z_i)^2 ; \quad i = 1, 2, \\ \delta^{(3)} Z_{ii} &= \delta^{(3)} Z_i - \frac{1}{2} \delta^{(1)} Z_i \delta^{(2)} Z_i + \frac{1}{8} (\delta^{(1)} Z_i)^3 ; \quad i = 1, 2. \end{aligned} \quad (2-34)$$

Solving the matricial product in eq. (2-31) and expanding each resulting term, as well as the Lagrangian terms of eqs. (2-30), up to three-loop level according with the definitions of eqs. (2-32), (2-33) and (2-34), one gets

$$\begin{aligned} \delta^{(l)} \sigma_{\phi_1^0 \phi_2^0}^2 &= -\frac{1}{2} M_{12}^{\phi^0} \delta^{(l)} Z_{12} - \delta^{(l)} M_{12}^{\phi^0} - \frac{1}{2} \boldsymbol{\delta} Z_{12} \boldsymbol{\delta} M_{12}^{\phi^0}, \\ \delta^{(l)} \sigma_{\phi_j^0 \phi_j^0}^2 &= \left(p^2 - M_{jj}^{\phi^0} \right) \delta^{(l)} Z_j - \delta^{(l)} M_{jj}^{\phi^0} - \boldsymbol{\delta} Z_j \boldsymbol{\delta} M_{jj}^{\phi^0} ; \quad j = 1, 2, ; \quad l = 1, 2, 3. \end{aligned} \quad (2-35)$$

The counter-terms with the bolded delta in eq. (2-35) start giving contributions from the two-loop level, these terms contain the sum of all the possible products of the M^x and Z counter-terms at a given l -loop order, that is

$$\boldsymbol{\delta} Z \boldsymbol{\delta} M^x = \sum_{m=1}^{l-1} \sum_{\substack{n=1 \\ m+n=l}}^{l-1} \delta^{(m)} Z \delta^{(n)} M^x ; \quad l = 2, 3, \dots \quad (2-36)$$

In order to derive the explicit expressions of the matrix components $\delta^{(l)} M_{ij}^x$, we require the renormalization of the input parameters contributing to the neutral Higgs boson mass matrices (2-14) and (2-15):

$$M_{Z^0}^2 \rightarrow M_{Z^0}^2 + \sum_{l=1}^3 \delta^{(l)} M_{Z^0}^2, \quad (2-37)$$

$$M_A^2 \rightarrow M_A^2 + \sum_{l=1}^3 \delta^{(l)} M_A^2, \quad (2-38)$$

$$\tan\beta \rightarrow \tan\beta + \sum_{l=1}^3 \delta^{(l)} \tan\beta, \quad (2-39)$$

$$T_i \rightarrow T_i + \sum_{l=1}^3 \delta^{(l)} T_i; \quad i = 1, 2. \quad (2-40)$$

One should also use the Taylor series expansion related to e , M_W and θ_W up to two-loop level as v_1 and v_2 contain parametric dependences on those EW parameters,

$$v_1 = \sqrt{2} \frac{M_W s_{\theta_W}}{e} c_{\beta} \quad ; \quad v_2 = \sqrt{2} \frac{M_W s_{\theta_W}}{e} s_{\beta}. \quad (2-41)$$

However, as we have adopted the gaugeless limit, all the counter-terms associated to the EW gauge particles and their corresponding contributions are discarded. In particular the counter-terms related to $v_{1,2}$ do not make contributions in the limit of vanishing external momentum at order $\alpha_t \alpha_s^2$, as will be discussed in Chapter 3, and therefore the renormalization of the vevs will not be explicitly considered in the following paragraphs of this section. Finally, the renormalization of the remaining terms are performed through the parameter $\tan\beta \equiv t_{\beta}$ according to the eq. (2-39), since the angle β satisfies the conditions

$$\delta^{(l)} s_{\beta} = c_{\beta} (1 - s_{\beta}^2) \delta^{(l)} t_{\beta} \quad ; \quad \delta^{(l)} c_{\beta} = -c_{\beta}^2 s_{\beta} \delta^{(l)} t_{\beta} \quad ; \quad \delta^{(l)} (s_{\beta} c_{\beta}) = c_{\beta}^2 c_{2\beta} \delta^{(l)} t_{\beta}. \quad (2-42)$$

Having in mind the expressions from eq. (2-37) to eq. (2-42) and after a bit of algebra we can derive the following ϕ^0 -mass counter-terms:

$$\begin{aligned} \delta^{(l)} M_{11}^{\phi^0} &= \delta^{(l)} M_A^2 s_{\beta}^2 + 2s_{\beta} c_{\beta}^3 M_A^2 \delta^{(l)} t_{\beta} + 2s_{\beta} c_{\beta}^3 \boldsymbol{\delta} M_A^2 \boldsymbol{\delta} t_{\beta} + \frac{\delta^{(l)} T_1}{\sqrt{2} v_1} + O(\delta^{(l-1)} v_1), \\ \delta^{(l)} M_{22}^{\phi^0} &= \delta^{(l)} M_A^2 c_{\beta}^2 - 2s_{\beta} c_{\beta}^3 M_A^2 \delta^{(l)} t_{\beta} - 2s_{\beta} c_{\beta}^3 \boldsymbol{\delta} M_A^2 \boldsymbol{\delta} t_{\beta} + \frac{\delta^{(l)} T_2}{\sqrt{2} v_2} + O(\delta^{(l-1)} v_2), \\ \delta^{(l)} M_{12}^{\phi^0} &= -\delta^{(l)} M_A^2 s_{\beta} c_{\beta} - c_{\beta}^2 c_{2\beta} M_A^2 \delta^{(l)} t_{\beta} - c_{\beta}^2 c_{2\beta} \boldsymbol{\delta} M_A^2 \boldsymbol{\delta} t_{\beta}. \end{aligned} \quad (2-43)$$

The terms with the bolded delta follow the same definition as in eq. (2-36). Now that we have at hand all the necessary expressions to determine the counter-terms $\delta^{(l)} \sigma_{\phi_i^0 \phi_j^0}^2$ of eq. (2-35) the renormalization constants entering into their definition need to be set. As we mentioned previously, we are going to use a mixed OS/ \overline{DR} renormalization. Specifically, the mass M_A



Figure 2-1.: **Left:** Generic three-loop Higgs tadpole topology with $\phi = \phi_{1,2}^0$, A . There is no momentum dependence. **Right:** Generic three-loop Higgs self-energy diagram where p is the external momentum and $\phi = \phi_{1,2}^0$, A .

and the tadpole parameters $T_{1,2}$ are renormalized using an OS procedure while the Z field contributions and the parameter $\tan\beta$ are renormalized in the \overline{DR} scheme. In particular, the mass counter-terms exhibit a momentum dependence. The tadpoles, $\tan\beta$ and the Higgs field counter-terms are independent of the external momentum p^2 .

Adopting an OS renormalization the tadpole contributions must vanish order by order in the perturbative expansion, yielding the conditions

$$T_{1,2} + \sum_l \left(T_{1,2}^{(l)} + \delta^{(l)} T_{1,2} \right) = 0 \quad \rightarrow \quad \delta^{(l)} T_{1,2} = -T_{1,2}^{(l)}, \quad (2-44)$$

where $T_{1,2}$ are the tree-level tadpoles, which vanish according to eq. (2-8), and $T_{1,2}^{(l)}$ are the sum of all the l -loop Higgs tadpole diagrams (Figure **2-1 Left** shows a schematically representation of a generic three-loop tadpole topology). This is equivalent to impose that the vevs $v_{1,2}$ are the minima of the full effective Higgs potential. Furthermore, the mass parameter M_A is related to the CP-odd Higgs boson mass, m_A , through the eq. (2-20). Therefore, in the EW gaugeless limit the counter-terms of M_A satisfies the condition

$$\delta^{(l)} M_A^2 = \delta^{(l)} m_A^2 - \frac{\delta^{(l)} T_1}{\sqrt{2} v_1} s_\beta^2 - \frac{\delta^{(l)} T_2}{\sqrt{2} v_2} c_\beta^2. \quad (2-45)$$

In the on-shell scheme the renormalization constant of the A -boson mass is determined in terms of the real part of the unrenormalized A -boson self-energy with the external momentum, p , evaluated at the pole mass (see Figure **2-1 Right**),

$$\delta^{(l)} m_A^2 = \text{Re} \left[\sum_{AA}^{(l)} (p^2 = m_A^2) \right]. \quad (2-46)$$

The momentum contribution of $\delta^{(l)} m_A$ is necessary to remove additional divergences coming from the counter-terms involving $\tan\beta$ in eq. (2-43) which contain a dependence on the parameter M_A . Those terms give rise to infinities that cannot be canceled by any of the divergent terms contained in the unrenormalized CP-even Higgs boson self-energies. In the limit of vanishing external momentum one can avoid dealing with these additional divergences.

On the other side, the \overline{DR} renormalization constants of the Higgs fields can be obtained by taking the derivative of the neutral CP-even Higgs self-energies (see Figure **2-1 Right**) with

respect to the external momentum squared,

$$\begin{aligned} \delta^{(l)} Z_j &= \text{Re} \left[\frac{\partial}{\partial p^2} \widehat{\sum}_{\phi_j^0 \phi_j^0}^{(l)}(p^2) - \frac{\partial}{\partial p^2} \sum_{\phi_j^0 \phi_j^0}^{(l)}(p^2) \right]_{p^2=0} \\ &= - \text{Re} \left[\frac{\partial}{\partial p^2} \sum_{\phi_j^0 \phi_j^0}^{(l)}(p^2) \right]_{p^2=0}^{div}. \end{aligned} \quad (2-47)$$

A full \overline{DR} renormalization is convenient because in most of the cases the momentum dependence of the divergent part of the scalar self-energies is known analytically up to three-loop order. In an on-shell scheme it is not possible to take the derivative of the loop integrals regarding p^2 in a fully analytical way since the finite part of some of those integrals at two-loop level and beyond have no closed analytical expressions available until now. There are other alternative choices for the renormalization of the Higgs fields and the parameter $\tan\beta$; however, due to its technical convenience and its process independence the most convenient choice is a \overline{DR} renormalization as was discussed in [78]. The bare parameter $\tan\beta$ can be expressed in terms of the constants $Z_{1,2}$ owing to its definition as the ratio of the vevs $v_{1,2}$ which are renormalized in the same way as the Higgs doublets,

$$v_j \rightarrow \sqrt{Z_j} (v_j + \delta v_j) \approx v_j + \frac{1}{2} \delta^{(1)} Z_{jj} v_j + \frac{1}{2} \delta^{(2)} Z_{jj} v_j + \frac{1}{2} \delta^{(3)} Z_{jj} v_j + \dots ; j = 1, 2, \quad (2-48)$$

where the definitions of eq. (2-34) are required. In eq. (2-48) the dots stand for terms proportional to $\delta^{(l)} v_j$. Having in mind the above equation and the eq. (2-39) we get

$$\delta^{(l)} \tan\beta = \tan\beta \left(\frac{1}{2} (\delta^{(l)} Z_{22} - \delta^{(l)} Z_{11}) + \frac{\delta^{(l)} v_2}{v_2} - \frac{\delta^{(l)} v_1}{v_1} + \frac{\delta Z_{22} \delta v_2}{2v_2} - \frac{\delta Z_{11} \delta v_1}{2v_1} \right). \quad (2-49)$$

If one considers the approximation where the dependence on the external momentum is disregarded ($p^2 \rightarrow 0$) and the limit of vanishing electroweak gauge couplings, then both the Higgs field renormalization constants and the counter-terms of $\tan\beta$ do not make contributions up to three-loop level in the \overline{DR} scheme.

2.3. The SQCD sector of the rMSSM

A particular feature of the rMSSM is the large size of the higher order quantum corrections to masses and couplings. They can lead to a considerably large shift on the value of the Higgs boson masses where the bulk of the corrections comes from the supersymmetric quantum chromodynamics sector of the Lagrangian. The calculation of the SQCD corrections to m_h involves the renormalization of the top quark mass, the gluino mass and the squark mass matrices and mixing angles, when the local divergences coming from a sub-loop diagram have to be removed. An l -loop renormalization of the Higgs boson masses requires the corresponding SQCD counter-terms up to at most $(l - 1)$ -loop order.

2.3.1. The squark masses and mixing angles

At tree-level the squark masses are composed of the soft SUSY breaking terms, the quadratic D-terms and the F-terms coming from the superpotential W after symmetry breaking, where the Higgs bosons acquire vevs. The superpotential is obtained from the Higgs-matter Yukawa and the Higgs self-interaction parts of the rMSSM Lagrangian. It can be written as

$$W = h_u \tilde{u}_R^\dagger \left(\tilde{u}_L H_1^0 - \tilde{d}_L H_2^+ \right) - h_d \tilde{d}_R^\dagger \left(\tilde{u}_L H_2^- - \tilde{d}_L H_2^0 \right) - \mu H_1^0 H_2^0 + \dots, \quad (2-50)$$

where we have made explicit the necessary terms to derive the squark masses. Here $h_{u/d}$ are the up/down Yukawa couplings. For a review of the complete expressions of all the sectors of the rMSSM Lagrangian in terms of mass eigenstates we refer you to the references [24–31]. The mass term of the bare squark Lagrangian is given by

$$\mathcal{L}_{\tilde{m}_f}^{\text{bare}} = -\frac{1}{2} \begin{pmatrix} \tilde{f}_L^\dagger & \tilde{f}_R^\dagger \end{pmatrix} M_{\tilde{f}_{L,R}}^2 \begin{pmatrix} \tilde{f}_L \\ \tilde{f}_R \end{pmatrix}, \quad (2-51)$$

where

$$M_{\tilde{u}_{L,R}}^2 = \begin{pmatrix} m_{\tilde{u}_L}^2 + M_{Z^0}^2 \cos 2\beta (I_3^u - Q_u s_{\theta_W}^2) + M_u^2 & M_u (A_u - \mu \cot \beta) \\ M_u (A_u - \mu \cot \beta) & m_{\tilde{u}_R}^2 + M_{Z^0}^2 \cos 2\beta Q_u s_{\theta_W}^2 + M_u^2 \end{pmatrix} \quad (2-52)$$

for the squarks type up, $f = u$. An analogous expression for the squarks type down ($f = d$) can be obtained just by changing $\cot \beta \rightarrow \tan \beta$. The mass terms, $m_{\tilde{f}_L}$ and $m_{\tilde{f}_R}$, and the trilinear coupling between the squarks and the Higgs bosons, A_f , come from the soft SUSY breaking part of the MSSM Lagrangian. Note that SU(2) invariance requires that $m_{\tilde{u}_L} = m_{\tilde{d}_L}$ for the members of each left-handed sfermion doublet. The off-diagonal terms proportional to $\mu \cot \beta$ come from the F-terms of the form $|\partial W / \partial H_{1,2}^0|^2$ while the diagonal terms M_f^2 , where M_f represents the f -type quark mass, come from $|\partial W / \partial \tilde{f}_R^f|^2$ and $|\partial W / \partial \tilde{f}_L^f|^2$. Additionally Q_f denotes the charge and I_3^f the third isospin component of the f -type squark. The terms proportional to Q_f and I_3^f come respectively from the U(1) and SU(2) contribution to the quadratic term in D .

The u - and d -type squark mass matrices can be rotated into the physical basis, and the physical mass eigenstates \tilde{m}_{f_1} and \tilde{m}_{f_2} can be determined, through the orthogonal transformation

$$\begin{pmatrix} \tilde{f}_1 \\ \tilde{f}_2 \end{pmatrix} = U(\theta_{\tilde{f}}) \begin{pmatrix} \tilde{f}_L \\ \tilde{f}_R \end{pmatrix} \quad ; \quad U(\theta_{\tilde{f}}) = \begin{pmatrix} c_{\theta_{\tilde{f}}} & s_{\theta_{\tilde{f}}} \\ -s_{\theta_{\tilde{f}}} & c_{\theta_{\tilde{f}}} \end{pmatrix}. \quad (2-53)$$

The mixing angle $\theta_{\tilde{f}}$ is given at tree-level and for $\tan \beta > 1$ by

$$s_{\theta_{\tilde{f}}} = \mp \frac{\left(M_{\tilde{f}_{L,R}}^2 \right)_{12}}{\left| \left(M_{\tilde{f}_{L,R}}^2 \right)_{12} \right|} \sqrt{\frac{\left(M_{\tilde{f}_{L,R}}^2 \right)_{12}^2}{\left(M_{\tilde{f}_{L,R}}^2 \right)_{12}^2 + \left(\left(M_{\tilde{f}_{L,R}}^2 \right)_{22} - \tilde{m}_{f_1}^2 \right)^2}}, \quad (2-54)$$

where the negative and positive sign correspond to the u - and d -type squarks respectively. The physical masses of the squarks are given by the eigenvalues:

$$\tilde{m}_{u_j}^2 = \frac{1}{2} [m_{\tilde{u}_L}^2 + m_{\tilde{u}_R}^2] + \frac{1}{2} M_{Z^0}^2 \cos 2\beta I_3^u + M_u^2 + (-1)^{j+1} \frac{\left(M_{\tilde{u}_{L,R}}^2 \right)_{11} - \left(M_{\tilde{u}_{L,R}}^2 \right)_{22}}{\left| \left(M_{\tilde{u}_{L,R}}^2 \right)_{11} - \left(M_{\tilde{u}_{L,R}}^2 \right)_{22} \right|} \times \sqrt{[m_{\tilde{u}_L}^2 - m_{\tilde{u}_R}^2 + M_{Z^0}^2 \cos 2\beta (I_3^u - 2Q_f s_{\theta_W}^2)]^2 + 4M_u^2 (A_u - \mu \cot \beta)^2}; \quad j = 1, 2. \quad (2-55)$$

For squarks type down we have to make the changes $u \rightarrow d$ and $\cot \beta \rightarrow \tan \beta$ in the above equation. Because of the large value of the top quark mass, M_t , mixing effects in the stop sector are expected to be relevant; however, the effects cannot become arbitrarily large to avoid negative values of the physical stop masses. This imposes a bound on the value of the trilinear parameter A_t which cannot be much greater than $m_{\tilde{t}_L}$.

In order to renormalize the squark sector and derive the corresponding counter-term expressions it is convenient to express the squark mass matrix in terms of the physical masses and the squark mixing angle $\theta_{\tilde{f}}$ as follows:

$$M_{\tilde{u}_{L,R}}^2 = \begin{pmatrix} c_{\theta_{\tilde{f}}}^2 \tilde{m}_{f_1}^2 + s_{\theta_{\tilde{f}}}^2 \tilde{m}_{f_2}^2 & s_{\theta_{\tilde{f}}} c_{\theta_{\tilde{f}}} (\tilde{m}_{f_1}^2 - \tilde{m}_{f_2}^2) \\ s_{\theta_{\tilde{f}}} c_{\theta_{\tilde{f}}} (\tilde{m}_{f_1}^2 - \tilde{m}_{f_2}^2) & c_{\theta_{\tilde{f}}}^2 \tilde{m}_{f_2}^2 + s_{\theta_{\tilde{f}}}^2 \tilde{m}_{f_1}^2 \end{pmatrix}. \quad (2-56)$$

Matching the two mass matrices in eq. (2-52) and eq. (2-56) one can derive a tree-level expression for the squark mixing term

$$X_f = A_f - \mu \{ \cot \beta, \tan \beta \} = \frac{\sin \theta_{\tilde{f}} \cos \theta_{\tilde{f}} (\tilde{m}_{f_1}^2 - \tilde{m}_{f_2}^2)}{M_f}. \quad (2-57)$$

The renormalization constants of the masses, the mixing angles and the fields are then defined via the transformations:

$$\tilde{m}_{f_j}^2 \rightarrow \tilde{m}_{f_j}^2 + \delta \tilde{m}_{f_j}^2 \quad ; \quad \delta \tilde{m}_{f_j}^2 = \sum_l \delta^{(l)} \tilde{m}_{f_j}^2, \quad (2-58)$$

$$\theta_{\tilde{f}} \rightarrow \theta_{\tilde{f}} + \delta \theta_{\tilde{f}} \quad ; \quad \delta \theta_{\tilde{f}} = \sum_l \delta^{(l)} \theta_{\tilde{f}}, \quad (2-59)$$

$$\begin{pmatrix} \tilde{f}_1 \\ \tilde{f}_2 \end{pmatrix} \rightarrow Z_{\tilde{f}_{12}} \begin{pmatrix} \tilde{f}_1 \\ \tilde{f}_2 \end{pmatrix} \quad ; \quad Z_{\tilde{f}_{12}} = \begin{pmatrix} 1 + \frac{1}{2} \sum_l \delta^{(l)} Z_{\tilde{f}_{11}} & \frac{1}{2} \sum_l \delta^{(l)} Z_{\tilde{f}_{12}} \\ \frac{1}{2} \sum_l \delta^{(l)} Z_{\tilde{f}_{21}} & 1 + \frac{1}{2} \sum_l \delta^{(l)} Z_{\tilde{f}_{22}} \end{pmatrix}, \quad (2-60)$$

where

$$\delta^{(l)} Z_{\tilde{f}_{12}} = \delta^{(l)} Z_{\tilde{f}_{21}} = \frac{s_{\theta_{\tilde{f}}} c_{\theta_{\tilde{f}}}}{c_{\theta_{\tilde{f}}}^2 - s_{\theta_{\tilde{f}}}^2} (\delta^{(l)} Z_{\tilde{f}_{22}} - \delta^{(l)} Z_{\tilde{f}_{11}}) \quad ; \quad l = 1, 2. \quad (2-61)$$

The bare Lagrangian of eq. (2-51) is therefore transformed to its renormalized version

$$\mathcal{L}_{\tilde{m}_f}^{\text{ren}} = -\frac{1}{2} \begin{pmatrix} \tilde{f}_1^\dagger & \tilde{f}_2^\dagger \end{pmatrix} Z_{\tilde{f}_{12}}^T M_{1,2}^2 Z_{\tilde{f}_{12}} \begin{pmatrix} \tilde{f}_1 \\ \tilde{f}_2 \end{pmatrix} - \frac{1}{2} \begin{pmatrix} \tilde{f}_1^\dagger & \tilde{f}_2^\dagger \end{pmatrix} Z_{\tilde{f}_{12}}^T \Delta M_{1,2}^2 Z_{\tilde{f}_{12}} \begin{pmatrix} \tilde{f}_1 \\ \tilde{f}_2 \end{pmatrix}, \quad (2-62)$$

where $M_{1,2}$ is the squark matrix in the physical basis at tree-level while its related counter-term matrix, $\Delta M_{1,2}^2$, has the expression

$$\begin{pmatrix} \delta\tilde{m}_{f_1}^2 - (\delta\theta_{\tilde{f}})^2 (\tilde{m}_{f_1}^2 - \tilde{m}_{f_2}^2) & (\tilde{m}_{f_1}^2 - \tilde{m}_{f_2}^2) \delta\theta_{\tilde{f}} + \delta\theta_{\tilde{f}} (\delta\tilde{m}_{f_1}^2 - \delta\tilde{m}_{f_2}^2) \\ (\tilde{m}_{f_1}^2 - \tilde{m}_{f_2}^2) \delta\theta_{\tilde{f}} + \delta\theta_{\tilde{f}} (\delta\tilde{m}_{f_1}^2 - \delta\tilde{m}_{f_2}^2) & \delta\tilde{m}_{f_2}^2 + (\delta\theta_{\tilde{f}})^2 (\tilde{m}_{f_1}^2 - \tilde{m}_{f_2}^2) \end{pmatrix}. \quad (2-63)$$

Collecting the counter-terms generated from eq. (2-62) and from the kinetic terms of the squark Lagrangian, we derive the expressions of the renormalized squark self-energies, which are given by

$$\widehat{\Sigma}(p^2) = Z_{\tilde{f}_{12}}^\dagger p^2 Z_{\tilde{f}_{12}} - Z_{\tilde{f}_{12}}^\dagger \left[M_{1,2}^2 + \Delta M_{1,2}^2 - \Sigma(p^2) \right] Z_{\tilde{f}_{12}} - p^2 + M_{1,2}^2. \quad (2-64)$$

Once again we have used the symbol Σ with a hat to represent the renormalized self-energies. Along this work we are going to consider the quantum corrections to the Higgs boson masses up to three-loop level; therefore, the one- and two-loop SQCD counter-terms are required in order to renormalize the non-local divergences coming from a sub-loop diagram. Thus, keeping the terms up to two-loop order in the unrenormalized squark self-energy matrix, we have:

$$\Sigma(p^2) = \begin{pmatrix} \Sigma_{11}^{(1)} + \Sigma_{11}^{(2)} - 2\delta^{(1)}\theta_{\tilde{f}} \Sigma_{12}^{(1)} & \Sigma_{12}^{(1)} + \Sigma_{12}^{(2)} + \delta^{(1)}\theta_{\tilde{f}} (\Sigma_{11}^{(1)} - \Sigma_{22}^{(1)}) \\ \Sigma_{21}^{(1)} + \Sigma_{21}^{(2)} + \delta^{(1)}\theta_{\tilde{f}} (\Sigma_{11}^{(1)} - \Sigma_{22}^{(1)}) & \Sigma_{22}^{(1)} + \Sigma_{22}^{(2)} + 2\delta^{(1)}\theta_{\tilde{f}} \Sigma_{12}^{(1)} \end{pmatrix}. \quad (2-65)$$

Using an analogous expansion over the matrix $\Delta M_{1,2}^2$ (eq. 2-63), one can derive the components of the renormalized squark self-energy matrix of eq. (2-64) at one- and two-loop level, yielding the expressions:

$$\begin{aligned} \widehat{\Sigma}_{ij}^{(1)}(p^2) &= \Sigma_{ij}^{(1)}(p^2) + p^2 \delta^{(1)} Z_{\tilde{f}_{ij}} - \frac{1}{2} (\tilde{m}_{f_i}^2 + \tilde{m}_{f_j}^2) \delta^{(1)} Z_{\tilde{f}_{ij}} \\ &\quad - \delta^{(1)} \tilde{m}_{f_i}^2 \delta_j^i - (-1)^{i+1} (\tilde{m}_{f_i}^2 - \tilde{m}_{f_j}^2) \delta^{(1)} \theta_{\tilde{f}} \quad ; \quad i, j = 1, 2, \end{aligned} \quad (2-66)$$

$$\begin{aligned} \widehat{\Sigma}_{ii}^{(2)}(p^2) &= \Sigma_{ii}^{(2)}(p^2) + \delta^{(1)} Z_{\tilde{f}_{ii}} \Sigma_{ii}^{(1)}(p^2) + p^2 \delta^{(2)} Z_{ii} \\ &\quad - (-1)^{i+1} 2\delta^{(1)}\theta_{\tilde{f}} \Sigma_{12}^{(1)} - \tilde{m}_{f_i}^2 \delta^{(2)} Z_{ii} - \delta^{(2)} \tilde{m}_{f_i}^2 \\ &\quad - \delta^{(1)} \tilde{m}_{f_i}^2 \delta^{(1)} Z_{\tilde{f}_{ii}} - (-1)^i (\delta^{(1)}\theta_{\tilde{f}})^2 (\tilde{m}_{f_1}^2 - \tilde{m}_{f_2}^2) \quad ; \quad i = 1, 2, \end{aligned} \quad (2-67)$$

$$\begin{aligned} \widehat{\Sigma}_{12}^{(2)}(p^2) &= \Sigma_{12}^{(2)}(p^2) + \frac{1}{2} (\delta^{(1)} Z_{\tilde{f}_{11}} + \delta^{(1)} Z_{\tilde{f}_{22}}) \Sigma_{12}^{(1)}(p^2) \\ &\quad + \delta^{(1)}\theta_{\tilde{f}} \left(\Sigma_{11}^{(1)}(p^2) - \Sigma_{22}^{(1)}(p^2) \right) - (\tilde{m}_{f_1}^2 - \tilde{m}_{f_2}^2) \delta^{(2)}\theta_{\tilde{f}} \\ &\quad - (\tilde{m}_{f_1}^2 - \tilde{m}_{f_2}^2) \delta^{(1)} Z_{\tilde{f}_{11}} \delta^{(1)}\theta_{\tilde{f}} - (\delta^{(1)} \tilde{m}_{f_1}^2 - \delta^{(1)} \tilde{m}_{f_2}^2) \delta^{(1)}\theta_{\tilde{f}}. \end{aligned} \quad (2-68)$$

As we are working in the \overline{DR} scheme, the left-handed and right-handed components of the squark fields have the same renormalization constants. Consequently, $\delta^{(l)}Z_{\tilde{f}_{11}} = \delta^{(l)}Z_{\tilde{f}_{22}}$ and therefore we have used $\delta^{(l)}Z_{\tilde{f}_{21}} = 0$ in the derivation of the above two-loop expressions. At one-loop level we have imposed the conditions

$$\text{Dp} \left[\widehat{\sum}_{ii}^{(1)} (\tilde{m}_{f_i}^2) \right] = 0 \quad ; \quad i = 1, 2, \quad (2-69)$$

$$\text{Dp} \left[\widehat{\sum}_{12}^{(1)} (\tilde{m}_{f_2}^2) + \widehat{\sum}_{21}^{(1)} (\tilde{m}_{f_1}^2) \right] = 0, \quad (2-70)$$

$$\text{Dp} \left[\frac{\partial}{\partial p^2} \widehat{\sum}_{ii}^{(1)} (\tilde{m}_{f_i}^2) \right] = 0 \quad ; \quad i = 1, 2. \quad (2-71)$$

The function $\text{Dp}[f]$ takes the pole part (principal part of the Laurent series) of the argument f which is computed in the DRED scheme. Using this prescription we get the one-loop renormalization constants:

$$\delta^{(1)}\tilde{m}_{f_i}^2 = \text{Dp} \left[\widehat{\sum}_{ii}^{(1)} (\tilde{m}_{f_i}^2) \right] \quad ; \quad i = 1, 2, \quad (2-72)$$

$$\delta^{(1)}\theta_{\tilde{f}} = \frac{\text{Dp} \left[\widehat{\sum}_{12}^{(1)} (\tilde{m}_{f_2}^2) + \widehat{\sum}_{21}^{(1)} (\tilde{m}_{f_1}^2) \right]}{2(\tilde{m}_{f_1}^2 - \tilde{m}_{f_2}^2)}, \quad (2-73)$$

$$\delta^{(1)}Z_{\tilde{f}_{ii}} = -\text{Dp} \left[\frac{\partial}{\partial p^2} \widehat{\sum}_{ii}^{(1)} (\tilde{m}_{f_i}^2) \right] \quad ; \quad i = 1, 2. \quad (2-74)$$

At two-loop order the renormalization conditions are derived by imposing

$$\left[p^2 - M_{1,2}^2 - \widehat{\sum}_{1,2} \right]_{fp} = 0, \quad (2-75)$$

that is to say, the finite part of the inverse propagator must be zero since in the \overline{DR} scheme the counterterms have only the pole parts. Explicitly the two-loop conditions are:

$$\left[\widehat{\sum}_{ii}^{(2)} + \delta^{(1)}Z_{\tilde{f}_{ii}} \widehat{\sum}_{ii}^{(1)} + (p^2 - \tilde{m}_{f_i}^2) \delta^{(2)}Z_{ii} - \delta^{(2)}\tilde{m}_{f_i}^2 - \delta^{(1)}\tilde{m}_{f_i}^2 \delta^{(1)}Z_{\tilde{f}_{ii}} \right. \\ \left. - (-1)^{i+1} 2\delta^{(1)}\theta_{\tilde{f}} \widehat{\sum}_{12}^{(1)} + (\delta^{(1)}\theta_{\tilde{f}})^2 (\tilde{m}_{f_1}^2 - \tilde{m}_{f_2}^2) \right]_{fp} = 0 \quad ; \quad i = 1, 2, \quad (2-76)$$

$$\left[\widehat{\sum}_{12}^{(2)} + \delta^{(1)}Z_{\tilde{f}_{11}} \widehat{\sum}_{12}^{(1)} + \delta^{(1)}\theta_{\tilde{f}} \left(\widehat{\sum}_{11}^{(1)} - \widehat{\sum}_{22}^{(1)} \right) - (\tilde{m}_{f_1}^2 - \tilde{m}_{f_2}^2) \delta^{(2)}\theta_{\tilde{f}} \right. \\ \left. - (\delta^{(1)}\tilde{m}_{f_1}^2 - \delta^{(1)}\tilde{m}_{f_2}^2) \delta^{(1)}\theta_{\tilde{f}} - (\tilde{m}_{f_1}^2 - \tilde{m}_{f_2}^2) \delta^{(1)}Z_{\tilde{f}_{11}} \delta^{(1)}\theta_{\tilde{f}} \right]_{fp} = 0. \quad (2-77)$$

Consequently, the corresponding two-loop counter-terms in the \overline{DR} scheme are:

$$\begin{aligned} \delta^{(2)} \tilde{m}_{f_j}^2 = & \text{Dp} \left[\sum_{jj}^{(2)} \left(\tilde{m}_{f_j}^2 \right) \right] - (-1)^{j+1} \frac{\text{Dp} \left[\sum_{21}^{(1)} \left(\tilde{m}_{f_j}^2 \right) \right]^2}{\left(\tilde{m}_{f_1}^2 - \tilde{m}_{f_2}^2 \right)} \\ & + (-1)^{j+1} \frac{\text{Dp} \left[\sum_{12}^{(1)} \left(\tilde{m}_{f_2}^2 \right) - \sum_{21}^{(1)} \left(\tilde{m}_{f_1}^2 \right) \right]^2}{4 \left(\tilde{m}_{f_1}^2 - \tilde{m}_{f_2}^2 \right)} \quad ; \quad j = 1, 2, \end{aligned} \quad (2-78)$$

$$\begin{aligned} 2 \left(\tilde{m}_{f_1}^2 - \tilde{m}_{f_2}^2 \right) \delta^{(2)} \theta_{\bar{f}} = & \text{Dp} \left[\sum_{12}^{(2)} \left(\tilde{m}_{f_1}^2 \right) \right] + \text{Dp} \left[\sum_{12}^{(2)} \left(\tilde{m}_{f_2}^2 \right) \right] \\ & - \text{Dp} \left[\delta^{(1)} \theta_{\bar{f}} \right] \text{Dp} \left[\sum_{11}^{(1)} \left(\tilde{m}_{f_2}^2 \right) - \sum_{11}^{(1)} \left(\tilde{m}_{f_1}^2 \right) \right] \\ & - \text{Dp} \left[\delta^{(1)} \theta_{\bar{f}} \right] \text{Dp} \left[\sum_{22}^{(1)} \left(\tilde{m}_{f_1}^2 \right) - \sum_{22}^{(1)} \left(\tilde{m}_{f_2}^2 \right) \right] \quad , \end{aligned} \quad (2-79)$$

$$\begin{aligned} \delta^{(2)} Z_{ii} = & - \text{Dp} \left[\frac{\partial}{\partial p^2} \sum_{ii}^{(2)} \left(\tilde{m}_{f_i}^2 \right) \right] + \text{Dp} \left[\frac{\partial}{\partial p^2} \sum_{ii}^{(1)} \left(\tilde{m}_{f_i}^2 \right) \right]^2 \\ & + (-1)^{i+1} 2 \text{Dp} \left[\delta^{(1)} \theta_{\bar{f}} \right] \text{Dp} \left[\frac{\partial}{\partial p^2} \sum_{12}^{(1)} \left(\tilde{m}_{f_i}^2 \right) \right] \quad ; \quad i = 1, 2, \end{aligned} \quad (2-80)$$

In the limit where the light fermion masses are neglected (NLF limit) the mixing angles $\theta_{\bar{q}}$ with $q = u, d, b, c, s$ are equal to zero and therefore there are no mixing counter-terms. Thus, the pole equation (2-77) and the counter-term (2-79) do not exist for the q -type squarks. Additionally, the equation (2-76) and the counter-terms (2-78) and (2-80) can be even further reduced just by putting $\delta^{(1)} \theta_{\bar{q}} = 0$.

2.3.2. Renormalization of the fermion masses

In the NLF limit the only fermions that can give a contribution to the Higgs mass corrections is the gluino and the top quark. The gluino mass, $M_{\tilde{g}}$, plays an important role in the determination of the corrections coming from the SQCD sector. A gluino is a Majorana fermion, a spin 1/2-particle whose associated 4-component spinor is even under charge-conjugation, which is the superpartner of the gluon and therefore is a SU(3) color octet fermion that cannot mix with any other MSSM particle. As a consequence, the only contribution to its tree-level mass comes from the soft SUSY breaking term of the Lagrangian,

$$M_{\tilde{g}} = M_3. \quad (2-81)$$

In SUSY-GUTs this mass is related to the U(1) and SU(2) gaugino masses, M_1 and M_2 respectively, through

$$M_3 = \frac{g_s^2}{g^2} M_2 \quad ; \quad M_1 = \frac{5}{3} \frac{s_{\theta_W}^2}{c_{\theta_W}^2} M_2. \quad (2-82)$$

At the perturbative order considered in this work we just need a one-loop renormalization of the gluino mass. On the other hand, we need the renormalization of the top quark mass, M_t , up to two-loop order. We have adopted a quite simple prescription. The fermion self-energies are decomposed into a vector, an axial-vector, a scalar and a pseudo-scalar part as

$$\Sigma_f(p^2) = \not{p}\Sigma_f^V(p^2) + \not{p}\gamma_5\Sigma_f^A(p^2) + M_f\Sigma_f^S(p^2) + M_f\gamma_5\Sigma_f^P(p^2), \quad (2-83)$$

where M_f is the mass of the fermion f , while \not{p} stands for $\gamma_\mu p^\mu$ with γ_μ the Dirac gamma matrices. Each component can be obtained according to

$$\begin{aligned} \Sigma_f^V(p^2) &= \frac{1}{4p^2} \text{Tr} \left(\not{p}\Sigma_f(p^2) \right), & \Sigma_f^A(p^2) &= \frac{1}{4p^2} \text{Tr} \left(\gamma_5\not{p}\Sigma_f(p^2) \right), \\ \Sigma_f^S(p^2) &= \frac{1}{4M_f} \text{Tr} \left(\Sigma_f(p^2) \right), & \Sigma_f^P(p^2) &= \frac{1}{4M_f} \text{Tr} \left(\gamma_5\Sigma_f(p^2) \right). \end{aligned} \quad (2-84)$$

Up to two-loop level the top-quark and the gluino mass counter-terms are derived in the \overline{DR} scheme according with the condition:

$$\frac{\delta M_{\tilde{f}}}{M_{\tilde{f}}} = \text{Dp} \left[\Sigma_{\tilde{f}}^V(M_{\tilde{f}}^2) + \Sigma_{\tilde{f}}^S(M_{\tilde{f}}^2) \right]. \quad (2-85)$$

The one- and two-loop renormalization constants for the top quark and the gluino masses in the \overline{DR} scheme are known for long time [79, 80]. We have put their explicit expression in Appendix B.

2.3.3. Role of the top quark mass

Most of the theoretical predictions of the EW observables, as the Higgs boson mass, as well as the stability analysis of the Higgs potential crucially depends of the specific central values and the uncertainties assigned to M_h and M_t , being M_t the parameter with the higher uncertainty. In general, the vacuum stability analysis in the SM is performed using as renormalized mass for the top quark, the so-called pole mass, in an on-shell renormalization scheme where the pole of the propagator is not a gauge-invariant quantity and is identified with the world average of the Tevatron, CMS and ATLAS measurements, $M_t^{MC} = 173.34 \pm 0.76$ GeV [81]. Since the experimental error on the Higgs mass is already fairly small, the factor that can discriminate between a stable or an unstable potential is the exact value of the top quark mass. This identification is not straightforward, M_t^{MC} cannot be used directly as an input for precise NLO or NNLO theoretical predictions because all measurements included in the world average are calibrated using Monte Carlo (MC) simulations. M_t^{MC} is by definition the MC top quark mass, which are not the renormalized mass appearing in the propagator of an on-shell renormalized theory.

Theoretically, the top quark mass is a renormalized quantity of the QCD Lagrangian. The

renormalized mass is obtained from the top self-energy diagrams, as was discussed in Section 2.3.2. The finite contributions to the self-energies can be absorbed into the renormalized mass and the UV divergences in a suitable counterterm. Different choices for the finite terms define different top mass schemes. In the top quark on-shell scheme all ultraviolet (UV) and finite contributions of the self-energy are absorbed into the mass M_t^{pole} including the dynamics at scales below $\Lambda_{QCD} \sim 1$ GeV (describing the gluon exchange between quarks and gluon radiation) where the perturbation theory breaks down. Consequently, the top quark pole mass is plagued with an intrinsically non-perturbative ambiguity of the order of Λ_{QCD} , the hadronization scale, a problem known in the literature as the infrared (IR) renormalon problem [82]. This ambiguity is a manifestation of the fact that the pole mass for a quark is not well defined as quarks are not free asymptotic states due to the confinement. The Monte Carlo mass M_t^{MC} instead is the mass of the propagator prior to the top quark decay. For scales below 1 GeV the partonic degrees of freedom are not used anymore and a non-perturbative hadronization model is employed. The infrared ambiguity known from perturbative QCD from scales below 1 GeV never arise in this context and there are also no perturbative contributions to the mass parameter coming from this region. This already tells that M_t^{MC} is not identical with the top quark pole mass M_t^{pole} . M_t^{MC} can be interpreted as M_t^{pole} within the intrinsic ambiguity in its definition which is roughly of the order of 1 GeV. In order to reduce the uncertainty introduced by the renormalon ambiguity, a more adequate renormalization scheme must be used. It is well known that short distance masses, such the one defined in the \overline{DR} and \overline{MS} schemes, do not suffer from the IR renormalon problem. In those schemes only pure UV divergences are subtracted [83], as a result, the $\overline{DR}/\overline{MS}$ top mass is renormalization scale dependent. Physically, the scale dependent masses are conceptually and numerically very far away from the notion of a physical particle mass, the difference can amount a size as large as 10 GeV. The scale dependent mass parameter, $m_t(Q)$, should be thought more as a coupling for a heavy quark-antiquark correlation and is therefore a very good scheme for parametrizing the top Yukawa coupling y_t . The mass $m_t(Q)$ can be extracted directly from a measurement of the total top-pair production cross section $\sigma_{\text{exp}}(p\bar{p} \rightarrow t\bar{t} + X)$. Such analysis performed in [84] with NNLO accuracy with inclusion of the full theoretical uncertainties gives rise to the following result

$$m_t(M_t) = 163.3 \pm 2.7 \text{ GeV} , \quad (2-86)$$

a value that translated in terms of pole mass gives

$$M_t^{pole} = 173.3 \pm 2.8 \text{ GeV} . \quad (2-87)$$

The central value is very close to the MC value $M_t^{MC} = 173.34 \pm 0.76$ GeV but the theoretical uncertainty is much larger. To improve the current precision of the top-mass determination one needs to consider, in addition to the QCD NNLO radiative corrections, the EW and the mixed EW \times QCD corrections. In contrast to QCD, where the mass of a quark is the parameter of the Lagrangian, the notion of a running mass in the MSSM, as well as in the

SM, after EW symmetry breaking is not entirely determined by the prescriptions of minimal subtraction. It also depends on the value of the vacuum expectation value (vev) $v(Q)$ chosen as a parameter of the calculations so that the running mass is $m_t(Q) = y_t(Q)v(Q)/\sqrt{2}$. This implies that the definition of a $\overline{DR}/\overline{MS}$ -mass is not unique: it depends upon the definition of the vacuum.

There are two main definitions found in the literature. The first one, called the *tree-level vev*, defines the renormalized vacuum v_{tree} as the minimum of the tree-level Higgs potential. The advantage of a scheme with this vacuum definition is that all the physical observables depending on it are gauge invariant quantities due to the explicit insertion of the tadpoles diagrams. Their insertion is done not only in the diagrams with counterterms but also in the 1PI Feynman diagrams as required to have the gauge independence of renormalized scattering amplitudes according to the gauge Ward identities. However, there is a disadvantage, the inclusion of tadpole diagrams involving the Higgs field, which have to be included in any calculation based on v_{tree} , include negative powers of the Higgs quartic self-coupling leading to a parametrically slower convergence. For instance, in the computation of $m_t(Q)$ in the SM the EW contribution is surprisingly large and has opposite sign relative to the QCD contributions, so that the total correction is small and increases the theoretical error by 0.5 GeV [85].

Using this definition of the vacuum, the relation between the top quark pole mass and the \overline{MS} parameters of the SM have been computed at different perturbative orders. The status of those calculations is the following. The pure QCD contributions, which are dominant, have been computed at one [86], two [87] (confirmed in [88, 89]), three [90], and recently at four-loops order [91]. Besides these pure QCD contributions, the full one-loop contributions to the pole mass have been given in the references [92–94]. The 2-loop mixed $O(\alpha\alpha_s)$ contributions were found in [95]. The full 2-loop contributions have been studied in the EW gaugeless limit approximation in [13]. Most recently, a systematic approach is available to the complete two-loop threshold corrections $O(\alpha^2)$ of all the running parameters of the SM [14,15]. This computation includes the masses of the W , Z^0 , and Higgs bosons and those of the top and bottom quarks as well as the gauge couplings, the Higgs self-coupling, and the top and bottom Yukawa couplings. The full two-loop results was implemented in a C++ library called *mr* (available for download from URL: <http://apik.github.io/mr/>) that allows to calculate the values of the running parameters in the SM at high energy scales [96].

There is an alternative to the above results implemented in the public code SMDR which can be consult in the references [97–99]. In this approach the complex pole mass of the top quark is presented at full two-loop order in the SM, including the known four-loop QCD contributions, in a scheme where the running \overline{MS} squared masses are expressed in terms of the vev v of the Higgs field, where v is defined to be the minimum of the full effective potential calculated in the Landau gauge. By this definition, the sum of all Higgs tadpole graphs, including the tree-level Higgs tadpole, vanishes identically, as is schematically represented in Figure **2-2** for the Higgs self-energy, and therefore negative powers of λ and

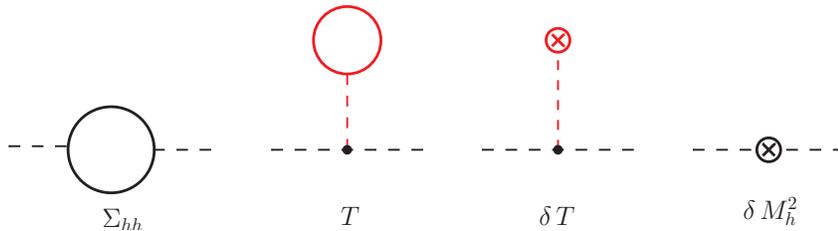


Figure 2-2.: Renormalization of the vev. The sum of the topologies in red color vanishes.

huge EW corrections are absent in the perturbative expansions of the pole masses and their relations with the \overline{MS} parameters. The vev v is in some sense a more faithful description of the true vacuum state. However, there is also a disadvantage. If the scheme is defined in terms of the self-energy diagrams without including the tadpole contribution, it gives rise to radiative corrections that are dependent of the gauge-fixing procedure. As a consequence, in this framework the \overline{MS} masses are gauge-dependent quantities. Nevertheless, a \overline{MS} mass is not a physical quantity nor a Lagrangian parameter and therefore the requirement of gauge-invariance is not mandatory.

By other side, it is worth mentioning that, so far, the precise relationship between the threshold corrections that relate the \overline{MS} masses to the parameters in the pole scheme with the three level vacuum v_{tree} (the computation done by Kniehl et al. in [14]) and the alternative computation done by Martin in [97–99] remains unclear. Recently, it has been argued that would be preferable to avoid the use of the pole mass scheme all-together and directly relate the Monte Carlo mass to a different short distance mass definition, where the top mass could have a numerical value close to the pole mass but without suffering from the renormalon ambiguities. There are several useful definitions of the top-quark mass in these so-called threshold masses schemes that depends on the precise relation to experimental quantities. Those include the potential-subtracted mass [100], the 1S mass [101, 102], and the MSR mass [103].

2.4. State of art of the higher-order corrections to M_h

In most of the relevant phenomenology benchmark scenarios for MSSM Higgs boson searches, the Higgs boson found at LHC corresponds to the lightest CP-even Higgs boson with a mass M_h which is not a free input parameter but it is predicted in the MSSM. The upper bound on its predicted mass at the leading order is given by $M_{Z^0} = 91.2$ GeV, leading to the exclusion of the MSSM at current collider experiments. However, the tree-level prediction of the Higgs boson mass is strongly modified by higher-order quantum corrections making the MSSM compatible with the measured Higgs mass of 125 GeV and consistent with the similarities of the measured Higgs couplings to those in the SM [6].

The state of art of the corrections to the lightest Higgs boson mass in the MSSM is quite

advanced and widely studied. At one-loop level the full quantum corrections can be found in the references [104–107] with real parameters. The dominant contributions come from the top-stop Yukawa corrections at zero external momentum in the EW gaugeless limit, which are proportional to the fourth power of the top mass and to the logarithm of the physical stop masses:

$$\delta_t^{(1)} M_h^2 = \frac{3G_F}{\sqrt{2}\pi^2 s_\beta^2} M_t^4 \ln \left(\frac{\tilde{m}_{t_1} \tilde{m}_{t_2}}{M_t^2} \right), \quad (2-88)$$

where $G_F = 1.16637 \times 10^{-5}$ GeV⁻² is the Fermi constant. The source of this correction is the soft breaking of supersymmetry which produces an incomplete cancellation between virtual top and stop loops. In this approximation the one-loop prediction of the Higgs boson masses can be expressed in the simple compact form:

$$M_h^2 = \frac{1}{2} \left[m_A^2 + \delta_t^{(1)} M_h^2 - \sqrt{\left(m_A^2 + \delta_t^{(1)} M_h^2 \right)^2 - 4m_A^2 s_\beta^2 \delta_t^{(1)} M_h^2} \right],$$

$$M_H^2 = m_A^2 - M_h^2 + \delta_t^{(1)} M_h^2 \quad ; \quad m_\pm^2 = m_A^2 + M_W^2. \quad (2-89)$$

The Higgs mass can be also affected by a potentially large stop mixing X_t (see eq. 2-57) due to the non-leading effects of the one-loop correction:

$$\delta_{X_t}^{(1)} M_h^2 = \frac{3G_F}{2\sqrt{2}\pi^2 s_\beta^2} M_t^4 X_t^2 \left(2f(\tilde{m}_{t_1}^2, \tilde{m}_{t_2}^2) + \frac{2 - (\tilde{m}_{t_1}^2 + \tilde{m}_{t_2}^2) f(\tilde{m}_{t_1}^2, \tilde{m}_{t_2}^2)}{(\tilde{m}_{t_1}^2 - \tilde{m}_{t_2}^2)^2} X_t^2 \right), \quad (2-90)$$

where the function f is defined as:

$$f(x, y) = \frac{1}{x - y} \ln \left(\frac{x}{y} \right). \quad (2-91)$$

We have drawn in Figure **2-3** the dependence of the CP-even and charged Higgs boson masses on the parameter m_A including the dominant one-loop radiative corrections in a scenario where the soft SUSY breaking mass terms of the squarks are put at the same supersymmetric scale, $m_{\tilde{u}_{L,R}} = m_{\tilde{d}_{L,R}} = M_{SUSY}$. Note that for large values of m_A , independently of $\tan\beta$, the masses of the heavy Higgs particles, M_H and m_\pm , grow linearly without boundary and have approximately the same magnitude, $M_H \approx m_\pm$. The lightest Higgs boson mass instead approaches to an asymptotic value, showing a more regular dependence on m_A for large $\tan\beta$, where $M_h \simeq m_A$ for small m_A while $M_h \simeq const$ for large A -mass. The non-leading effects of the stop mixing X_t allow a simple determination of an upper bound on the lightest Higgs boson mass at one-loop level, yielding the expression:

$$M_h^2 \leq M_{Z^0}^2 c_{2\beta}^2 + \delta_t^{(1)} M_h^2 s_\beta^2 + \delta_{X_t}^{(1)} M_h^2 s_\beta^2. \quad (2-92)$$

If one considers large values of the parameter $\tan\beta$ ($\tan\beta \gg 10$) in the scenario of maximal stop mixing, where the value of X_t makes M_h maximal (frequently referred in literature as

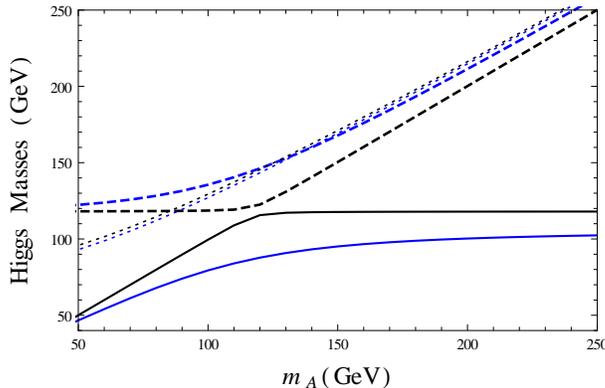


Figure 2-3.: One-loop predictions of the Higgs boson masses M_h (solid), M_H (dashed) and m_{\pm} (dotted) as a function of the CP-odd Higgs boson mass m_A . We have considered $\tan\beta = 3$ (blue) and 30 (black) in a scenario where $M_{SUSY} = 1$ TeV, $\mu = 200$ GeV and the stop mixing parameter X_t vanishes.

the m_h^{max} scenario), a general upper bound given by $M_h \lesssim 140$ GeV is found out. Fortunately for the MSSM, the Higgs boson was discovered at the LHC within this energy region.

The contributions of eqs. (2-88) and (2-90) contain the bulk of the one-loop corrections. The subdominant contributions coming from higher-loop corrections can essentially be reduced to higher-order SQCD effects. The detailed results of a Feynman diagrammatic calculation of the leading two-loop QCD corrections at order $O(\alpha\alpha_s)$ can be found in [108], in particular the $O(\alpha_b\alpha_s)$ [109] and $O(\alpha_t\alpha_s)$ [110] contributions using the FD approach are known in the limit where the external momentum vanishes and in the MSSM version with complex parameters. In this limit there is an alternative procedure to compute the above corrections, the Effective Potential (EP) approach. A comparison of the corresponding two-loop results in the FD and EP approaches at $O(\alpha\alpha_s)$ can be found in [111, 112] and references therein. In contrast to the EP method, the FD approach has the advantage that it can allow for non-vanishing external momentum. An evaluation of the momentum dependence of the two-loop corrections, including all the terms involving the QCD couplings, in the modified dimensional reduction scheme (\overline{DR}) was presented in [113]. The latest status of the momentum-dependent two-loop corrections was discussed recently in [114, 115] using a hybrid on-shell- \overline{DR} scheme and including corrections of $O(p^2\alpha_t\alpha_s)$ for the real version of the MSSM. A complete two-loop QCD contributions to M_h in the MSSM with complex parameters including the full dependence on the external momentum can be found in [116]. The expressions of the leading two-loop quantum corrections to the MSSM Higgs boson mass are quite involved and have a large amount of terms. However, all the above mentioned one- and two-loop M_h -predictions are implemented in the public code FeynHiggs [56] and can be readily used for numerical evaluation purposes. Figure 2-4 Left shows the dependence of the tree-level, full one-loop and leading QCD two-loop M_h -predictions coming from FeynHiggs as a function of the scale m_A in the maximal stop mixing scenario for $\tan\beta = 30$, $M_{SUSY} = 1$ TeV and $\mu = 200$ GeV. In this plot one can clearly see the good behaviour of the perturbative expansion. If one

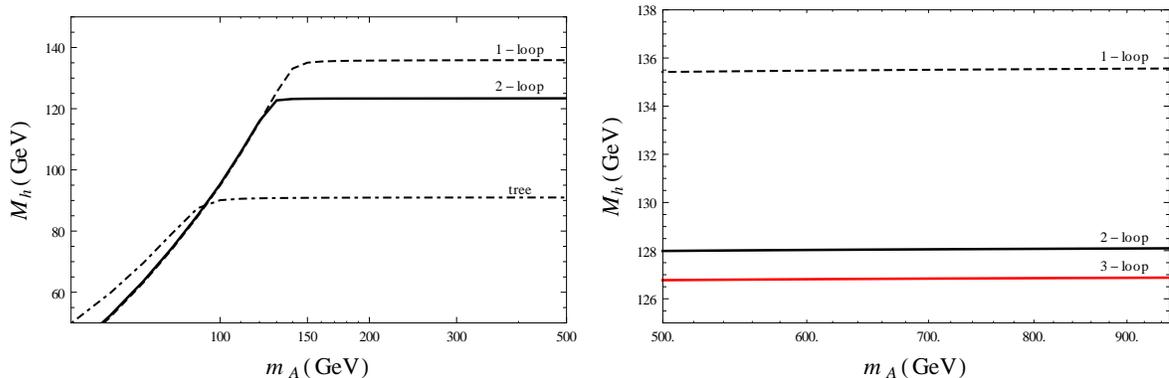


Figure 2-4.: **Left:** Predictions of the lightest Higgs boson mass, M_h , at tree (dot-dashed), one-loop (dashed) and two-loop (black solid) level as a function of the CP-odd Higgs boson mass m_A . We have considered the m_h^{max} scenario ($X_t/M_{SUSY} \approx 2.4$) at the kinematical point $\tan\beta = 30$, $M_{SUSY} = 1$ TeV, $\mu = 200$ GeV and $M_{\tilde{g}} = 1.5$ TeV. **Right:** The three-loop M_h -predictions (red solid line) are included for large m_A in the maximal stop mixing scenario.

looks at the numerical difference between the dashed and the dot-dashed curve as well as the difference between the dashed and the solid line for large m_A , one can easily conclude that the size of the one-loop corrections (estimated to be about 45 GeV) are higher than the size of the two-loop ones (roughly 12 GeV), as expected from a perturbative quantum field theory. Besides, the two-loop corrections give negative contributions in contrast to the one-loop corrections which are positive.

At three-loop level there is a first diagrammatic computation performed by P. Kant and collaborators [117–119], where the radiative corrections to M_h were computed in the SQCD sector including non-logarithmic terms of order $O(M_t^2\alpha_t\alpha_s^2)$. They have exploited the methods of asymptotic expansion in order to provide precise approximations in the relevant mass hierarchies. An alternative computation of the three-loop corrections to M_h at order $\alpha_t\alpha_s^2$, which extends the validity of the leading three-loop predictions to the whole SUSY parameter space of the rMSSM, were recently presented by our group in the reference [2]. The details of our computation are described in the Chapter 3 of this work. In Figure 2-4 **Right** we have depicted the three-loop predictions of M_h as a function of m_A (red solid line) in the m_h^{max} scenario. The complete M_h -prediction is built up as the sum of different contributions. The tree-level value, which accounts for about 60 % of the renormalized mass, the one-loop correction, which represents about 32 % of M_h , the two-loop correction, contributing with about 6 %, and finally the three-loop contribution representing about 1 % of the total mass. The size of the three-loop quantum corrections are of the order of 1 GeV and have an opposite sign regarding the one-loop corrections.

All the fixed-order corrections shown in Figure 2-4 contain logarithmic terms which can spoil their good perturbative behaviour when there is a large numerical difference between

the electroweak scale Λ_{EW} and the supersymmetric scale M_{SUSY} . For this reason, effective field theory (EFT) methods have been considered to resum large-logarithms in case of a large mass hierarchy between Λ_{EW} and M_{SUSY} [120–126]. In particular, for values of M_{SUSY} above a critical point where the fixed-order and EFT combined uncertainties are equal, the EFT computation is more accurate and therefore the usage of the SM [41] or a two-Higgs-doublet-model (THDM) [127–129] as effective theories below the SUSY scale is preferred. In the simplest case where the SM is the low energy EFT, the masses of the SUSY particles are all set to a single scale M_{SUSY} and the physics at this energy is correlated, with the help of the RGEs, to the low scale Λ_{EW} through just one EFT coupling: the effective Higgs self-coupling $\lambda(Q)$. The state of art currently includes full one-loop and complete two-loop matching conditions for λ at the SUSY scale [121, 125, 130], full three-loop RGEs of all the SM parameters [131–136] and full two-loop relations between the running SM parameters and the physical observables including the Higgs boson mass [12, 13, 137]. With the new results presented in [130] a full NNLL resummation of the large logarithmic contributions is now allowed. Finally, a new hybrid computation which includes a partial N³LL resummation and N³LO + N³LL hybrid QCD corrections to the light CP-even Higgs boson mass are also available [138].

Both the fixed-order and the EFT results are implemented in several publicly available codes. For the diagrammatic fixed-order calculations there are the programs SoftSUSY [139], SUSPECT [140], CPsuperH [141] and H3m [55]. The results of H3m are also implemented into the C++ module Himalaya [142, 143] linked to the Mathematica generator FlexibleSUSY [144, 145] in a pure \overline{DR} context. Pure EFT calculations are implemented in SUSYHD [124] and MhEFT [146]. Moreover, different hybrid methods that combine both approaches have been recently developed in order to take profit of the features of each one [147]. FlexibleSUSY [148], based on SARAH [149–152], implements a hybrid method called Flexible-EFT-Higgs [40]. This approach was also included into the program SPHeno [153, 154]. A hybrid method different from the one pursued in Flexible-EFT-Higgs has been implemented in FeynHiggs [155, 156]. There are also in literature detailed numerical comparisons between the different diagrammatic, EFT and hybrid codes. In [40] it is discussed in details how the hybrid method Flexible-EFT-Higgs compares to the other EFT and diagrammatic codes. Finally, several numerical comparisons of the hybrid approach implemented in FeynHiggs to the pure EFT calculations have been studied in [40, 124, 154]. Those papers reported surprising non-negligible numerical differences between FeynHiggs and pure EFT codes for the prediction of M_h at large SUSY scales. The observed differences come mainly from three sources. The scheme conversion of input parameters from OS to \overline{DR} , which can lead to large shifts due to uncontrolled higher-order terms. Unwanted effects from incomplete cancellations with subloop renormalization contributions in the determinations of the Higgs propagator pole and different parametrizations of non-logarithmic terms. After performing the corresponding corrections, FeynHiggs results are in very good agreement with the results of SUSYHD [157].

3. The Lightest MSSM Higgs Boson Mass (M_h) at Three-Loop Accuracy

This chapter is devoted to explain the technical details to the computation of the three-loop corrections to the lightest Higgs boson mass in the rMSSM, starting from the generation of the Feynman diagrams and until the numerical evaluation of the renormalized quantum corrections to M_h . The first part contains the renormalization framework in which the computation was done. The latter includes the explicit expressions of the renormalization conditions for the CP-even Higgs boson mass counter-terms at order $\alpha_t \alpha_s^2$ derived from the relations exposed in Section 2.2. We next describe the technical details related to the generation of the three-loop Higgs self-energy amplitudes and the regularization procedure applied to the resulting Feynman integrals. In particular, we have adopted a DRED regularization scheme in order to preserve supersymmetry at the given perturbative order. The evaluation of the three-loop self-energy integrals obtained after regularization follows a specific treatment. Each of them is reduced to a superposition of a set of irreducible integrals (the so-called master integrals) with the help of the Integration by Parts (IBP) method and the covariant decomposition, which admits either an analytical or a numerical evaluation depending on the number of independent scales involved. When a closed analytical expression of any of the master integrals is missing, we proceed to perform its numerical evaluation through two different numerical techniques: the dispersion method and the method of sector decomposition. Finally, the obtained results will be numerically tested in some phenomenologically relevant benchmark scenarios by the comparison of our three-loop prediction of the lightest Higgs boson mass with the higher-order predictions coming from the public codes FeynHiggs and H3m for the same observable.

3.1. Renormalization of the CP-even Higgs boson masses

In Chapter 2 we have derived the necessary renormalization constants to obtain the renormalized CP-even Higgs boson masses in the EW gaugless limit. However, the numerical dominant contributions to the Higgs self-energy corrections come from the SQCD sector of the rMSSM Lagrangian in two specific limits that can reduce even more the expressions presented in sections 2.2 and 2.3. Those approximations include:

- i) The non-light fermions limit (NLF) where all the fermion masses are put to zero except

the mass of the top quark, M_t . We have computed all the three-loop corrections at the perturbative order $\alpha_t\alpha_s^2$. Consequently, cubic vertices of the Higgs with two light fermions are not considered in this work since the order of the corrections and the NLF limit forbid that kind of vertices.

- ii) The approximation of vanishing external momenta, where the momentum carried by the external lines of the self-energy diagrams is disregarded. Therefore, $p^2 = 0$, where p is the external momentum transferred. This approximation is very well motivated. Up to two-loop level the shift in the mass M_h due to the momentum dependence is below 1 GeV in all scenarios studied, the bulk of the two-loop corrections comes from the effective-potential effects which are of the order of 10 GeV [114]. A well-behaved perturbative expansion will make this dependence even weaker at three-loop level.

In our computation we have followed the above observations to get the dominant contributions at three-loop order and therefore we have adopted the approximation of zero external momentum and the NLF limit. Further reductions in the Higgs mass counter-terms are obtained because of the tree-level relation

$$\alpha = \beta - \pi/2 \quad \text{for} \quad m_A^2 \gg M_{Z^0}^2, \quad (3-1)$$

which is satisfied in the gaugeless limit, and also due to the definition of the the vevs of the Higgs fields ($v_{1,2}$) as the minima of the full effective potential, see eq. (2-44). The latter implies that the condition $\langle \Omega | H_{1,2}^0 | \Omega \rangle = 0$ must be satisfied order by order in the perturbative expansion of the one-point Green function and brings as an effect that just 1PI self-energy diagrams have to be evaluated, self-energies with tadpole insertions do not make contributions.

Taking in consideration the above restrictions the expressions in eq. (2-26) and eq. (2-27) for the renormalized three-loop corrections to the neutral CP-even Higgs bosons are reduced to

$$\widehat{\sum}_{\psi_i\psi_j}^{(3)} = \sum_{\psi_i\psi_j}^{(3)} - \delta^{(3)} M_{\psi_i\psi_j}^2 \quad ; \quad \psi_{1,2} = h, H. \quad (3-2)$$

The terms with delta, $\delta^{(3)} M_{\psi_i\psi_j}^2$, are the counter-terms of the physical CP-even Higgs boson masses whose expressions are obtained from the rotation of the mass counter-terms in the unphysical basis (see eq. 2-43) according to

$$\begin{aligned} \delta^{(3)} M_{hh}^2 &= \delta^{(3)} M_{11}^{\phi^0} s_\alpha^2 + \delta^{(3)} M_{22}^{\phi^0} c_\alpha^2 - 2\delta^{(3)} M_{12}^{\phi^0} s_\alpha c_\alpha, \\ \delta^{(3)} M_{HH}^2 &= \delta^{(3)} M_{11}^{\phi^0} c_\alpha^2 + \delta^{(3)} M_{22}^{\phi^0} s_\alpha^2 + 2\delta^{(3)} M_{12}^{\phi^0} s_\alpha c_\alpha, \\ \delta^{(3)} M_{hH}^2 &= \delta^{(3)} M_{12}^{\phi^0} (c_\alpha^2 - s_\alpha^2) - \left(\delta^{(3)} M_{11}^{\phi^0} - \delta^{(3)} M_{22}^{\phi^0} \right) c_\alpha s_\alpha. \end{aligned} \quad (3-3)$$

Some clarifications need to be done regarding the renormalization constants of the Higgs fields and the parameter $\tan\beta$ which are included in eq. (2-27) and eq. (2-35) but are not anymore considered in the eqs. (3-2) and (3-3).

The Higgs field renormalization constants represented with the Z_j factors are obtained from the terms proportional to p^2 in the divergent part of the CP-even Higgs boson self-energies according with the eq. (2-47). The perturbative order of the Z_j counter-terms is the same as the Higgs self-energies. Therefore, all the terms which are products of one and two-loop counter-terms, as the products of $\delta^{(1,2)}Z_j$ counter-terms in eq. (2-34) or the bolded delta terms in eq. (2-35), cannot match the order $\alpha_t\alpha_s^2$ since there is no cubic or quartic vertex with a Higgs external line that is proportional to the strong coupling g_s in the rMSSM. Besides, the three-loop constants $\delta^{(3)}Z_j$ do not make contributions provided that the divergent part of the three-loop Higgs self-energies do not contain an external momentum dependence at the considered order $\alpha_t\alpha_s^2$. Having that in mind, we have put

$$\delta^{(l)}Z_{1,2} = 0 \quad \text{for } l = 1, 2, 3, \quad (3-4)$$

in the renormalization of the CP-even Higgs self-energies. As a result of eq. (3-4) the \overline{DR} renormalization of the parameter $\tan\beta$ (see eq. 2-49) is determined only by the counter-terms $\delta^{(l)}v_1/v_1$ and $\delta^{(l)}v_2/v_2$. However, as the difference $\delta^{(3)}v_1/v_1 - \delta^{(3)}v_2/v_2$ is UV-finite at the order $\alpha_t\alpha_s^2$, we lastly get

$$\delta^{(3)}\tan\beta = 0, \quad (3-5)$$

and therefore all the terms of eq. (2-43) with a dependence on the $\tan\beta$ -counterterm and also the $O(\delta^{(l-1)}v_j)$ terms are disregarded. Considering all the above approximations the mass counter-terms of eq. (2-43) are reduced to

$$\begin{aligned} \delta^{(3)}M_{11}^{\phi^0} &= s_\beta^2\delta^{(3)}m_A^2 - \frac{T_1^{(3)}}{\sqrt{2}v_1}(1 - s_\beta^4) + s_\beta^2c_\beta^2\frac{T_2^{(3)}}{\sqrt{2}v_2}, \\ \delta^{(3)}M_{22}^{\phi^0} &= c_\beta^2\delta^{(3)}m_A^2 - \frac{T_2^{(3)}}{\sqrt{2}v_2}(1 - c_\beta^4) + s_\beta^2c_\beta^2\frac{T_1^{(3)}}{\sqrt{2}v_1}, \\ \delta^{(3)}M_{12}^{\phi^0} &= -\delta^{(3)}m_A^2s_\beta c_\beta - s_\beta^3c_\beta\frac{T_1^{(3)}}{\sqrt{2}v_1} - c_\beta^3s_\beta\frac{T_2^{(3)}}{\sqrt{2}v_2}, \end{aligned} \quad (3-6)$$

leading to the following counter-terms in the physical basis:

$$\delta^{(3)}M_{\psi_i\psi_j}^2 = \delta^{(3)}m_A^2c_{\psi_i\psi_j}^A + \left(\frac{h_t}{2M_t}s_\beta\right)\left(\frac{T_h^{(3)}}{\sqrt{2}}c_{\psi_i\psi_j}^h + \frac{T_H^{(3)}}{\sqrt{2}}c_{\psi_i\psi_j}^H\right); \quad \psi_{1,2} = h, H. \quad (3-7)$$

The coefficients $c_{\psi_i\psi_j}^{A,h,H}$ are functions of the angles α and β and are given by the expressions

$$\begin{aligned} c_{hh}^A &= c_{\alpha-\beta}^2; & c_{hh}^h &= \frac{1}{4}(5s_{\alpha-\beta} + s_{3(\alpha-\beta)}); & c_{hh}^H &= c_{\alpha-\beta}s_{\alpha-\beta}^2, \\ c_{HH}^A &= s_{\alpha-\beta}^2; & c_{HH}^h &= -c_{\alpha-\beta}^2s_{\alpha-\beta}; & c_{HH}^H &= \frac{1}{4}(c_{3(\alpha-\beta)} - 5c_{\alpha-\beta}), \\ c_{hH}^A &= \frac{1}{2}s_{2(\alpha-\beta)}; & c_{hH}^h &= -c_{\alpha-\beta}^3; & c_{hH}^H &= s_{\alpha-\beta}^3, \end{aligned} \quad (3-8)$$

h_t is the top Yukawa coupling,

$$\begin{pmatrix} T_H \\ T_h \end{pmatrix} = D(\alpha) \begin{pmatrix} T_1 \\ T_2 \end{pmatrix} \quad \text{and} \quad \delta^{(3)} m_A^2 = \text{Re} \left[\sum_{AA}^{(3)} (p^2 = 0) \right]. \quad (3-9)$$

Due to the relation (3-1), the expressions of $c_{\psi_i \psi_j}^{A,h,H}$ can be further reduced. Therefore, in the gaugeless limit but also in the decoupling limit, $m_A \gg M_{Z^0}$, only the coefficients $c_{hh}^h = -1$, $c_{HH}^A = 1$ and $c_{hH}^H = -1$ give a contribution.

The three-loop counter-terms described in the above expressions are useful to cancel local UV divergences. However, the unrenormalized topologies, consisting of self-energies as well as tadpoles of the neutral CP-even and CP-odd Higgs boson fields, can contain also non-local divergences coming from a sub-loop in the three-loop diagrams. It is therefore necessary an additional sub-renormalization procedure to remove these infinities. The procedure consists in the inclusion of additional three-loop diagrams which are built from either one-loop topologies with a two-loop or two one-loop counter-term insertions or two-loop topologies with a one-loop counter-term inserted. Each of those three-loop counter-term diagrams is meant to cancel the non-local divergences arising in a sub-loop of a given three-loop topology. At order $O(\alpha_t \alpha_s^2)$ the counter-terms comes from the SQCD sector of the rMSSM Lagrangian. Specifically, we need the $O(\alpha_s)$ -contribution of the one-loop counter-terms coming from the renormalization of the gluino mass, the top quark mass, the squark masses and the stop mixing angles. In addition, we need the two-loop renormalization of the top mass, the stop masses and stop mixing angles at order $O(\alpha_s^2)$. We have got all the one and two-loop counter-terms in the \overline{DR} scheme, where the UV divergences are minimally subtracted. In order to preserve supersymmetry to all perturbative orders we have used the regularization procedure DRED [44–47]. The main renormalization conditions to derive the necessary one- and two-loop SQCD counter-terms are described in Section 2.3 and their explicit expressions in terms of fundamental functions are consigned in Appendix B.

3.2. Three-loop fixed-order calculation of M_h

In this section we are going to discuss the technical details of our three-loop diagrammatic computation. Considering that we are interested in terms of order $\alpha_t \alpha_s^2$ from the perturbative expansion of the Higgs mass, we have restricted the calculations to the SQCD sector where the Higgs couples just to the top quark or its super-partner. The three-loop radiative correction to M_h is obtained by evaluating the neutral Higgs boson self-energies (Σ) and the tadpoles (T) for the fields h , H and A according with the equations (3-2) and (3-7). All the Feynman diagrams and their corresponding amplitudes are generated with the Mathematica package FeynArts [158]. In FeynArts one can specify the number of external lines and the number of loops in order to create a set of topologies obtained from connecting incoming and outgoing lines of tree-level vertices in all distinct ways. For the purposes of FeynArts,

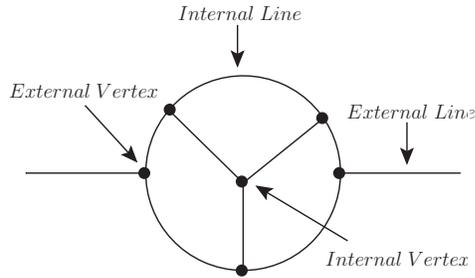


Figure 3-1.: Generic three-loop topology. An external vertex is a vertex joined to an external line. An internal vertex is a vertex joined only to internal lines (propagators).

a topology is a connected diagram without the insertion of quantum fields on any of their lines. We are interested in three-loop topologies with one (tadpoles) and two (self-energies) external lines which are 1PI. Note that besides pure three-loop topologies, there are also contained one-loop diagrams with first- and second-order counter-term insertions, two-loop diagrams with first-order counter-terms and tree diagrams with third-order counter-terms, which will be involve in the renormalization of local and non-local divergences. In Appendix D we show a simple Mathematica routine that generates and draws all the three-loop topologies needed in our calculation. The output of this code shows that there are 80 pure three-loop self-energies, 63 self-energies with counter-term insertions, 15 pure three-loop tadpoles and 16 tadpoles with counter-term insertions.

The next step consists in the introduction of the quantum fields on the lines of each topology according with the interaction vertices of the rMSSM. We have used a modification of the model `MSSMCT.mod` of FeynArts where all the MSSM vertices are contained. The modifications include the addition of the counter-term vertices of Appendix B as well as tree-level vertices with ϵ -scalars into the model. The latter requires also a modification of the generic model file `Lorentz.gen` where the analytical propagators and couplings are defined. In the external lines the only fields to take into consideration are the neutral Higgs fields: h , H and A . The internal lines (propagators) would contain the SQCD fields (heavy quarks, squarks, gluon, gluino and ϵ -scalar) whose vertices lead to the generation of the amplitudes with the required perturbative order. The needed vertices can be consulted in Appendix C. In the language of FeynArts, the insertion of the fields can be done with the function `InsertFields` and it is possible to exclude the unnecessary insertions with the help of the functions `DiagramSelect`, `ExcludeParticles` and `LastSelections`. `DiagramSelect` is the most efficient function to pick a selected set of diagrams because it applies a test function to every diagram, and returns only those for which the result of the test is `True`. We have written a routine in Mathematica, which can be consulted in Appendix E, where the test functions impose selection rules over each topology in order to extract the desired Feynman diagrams. The selection rules were designed according with the definitions in Figure 3-1 and the following simple statements:

- In a renormalized QFT in four dimensions, only cubic and quartic vertices can be considered.
- There is no quartic vertex which is linear in g_s or h_t .
- There is no vertex with a neutral Higgs field on any of their lines which is proportional to the strong coupling constant g_s .
- For self-energy diagrams with two external vertices, each external vertex must be a cubic vertex of the order of h_t . In self-energies with one external vertex, the vertex must be a quartic vertex proportional to h_t^2 .
- Tadpole diagrams must be of the order of $h_t g_s^4$; therefore, its external vertex must be a cubic vertex proportional to the first power of h_t .
- Internal vertices must be only SQCD vertices of the order of g_s^n with $1 \leq n \leq 2$.
- As we are assuming the limit of vanishing external momentum, only mass counter-terms of the order of g_s^2 (first-order) or g_s^4 (second-order) inserted into the propagators are considered. Diagrams with counter-terms insertions on the vertices are disregarded.

As a result, the 32 self-energy topologies with two quartic external vertices and the four tadpole topologies with a quartic external vertex, drawn by the code in Appendix D, are excluded. At order $\alpha_t \alpha_s^2$, after the insertion of the fields and the application of the selection rules, we obtain a total set of 3869×4 Feynman diagrams for the pure three-loop neutral Higgs self-energies case and 3590×2 three-loop neutral Higgs tadpoles. The counter-term diagrams include 523×2 tadpoles and 3491×4 self-energies. A total of 37666 diagrams have been created. The routine in Appendix E also generates the amplitudes of the resulting diagrams with the help of the FeynArts function `CreateFeynAmp`. The generated FeynArts amplitudes have a quite involved structure, we have to deal with three-loop four-dimensional integrals of the form

$$\mathcal{A}_{v_1 v_2 v_3 v_4 v_5 v_6}^{(4)} = \frac{1}{\pi^{12}} \iiint \frac{d^4 q_1 d^4 q_2 d^4 q_3}{P_1^{v_1} P_2^{v_2} P_3^{v_3} P_4^{v_4} P_5^{v_5} P_6^{v_6}} N(q_j^\mu, p^\nu, \gamma^\mu, \gamma^5, g^{\mu\nu}, T_{kl}^a, f^{abc}), \quad (3-10)$$

where the denominator contains the Feynman propagators

$$P_j = \left(\sum_{n=1}^3 x_j^n q_n + y_j p \right)^2 - m_j^2 \quad ; \quad x_j, y_j = 1, 0, -1, \quad (3-11)$$

raised to the powers v_j , which can be zero or a positive integer number. The numerator, in turn, is a complicated combination of the tensor structures included into the parenthesis of the function N , that is to say, the loop-momenta q_j^μ , the external momentum p^ν , the Dirac gamma matrix γ^μ , the chiral gamma matrix γ^5 , the metric tensor $g^{\mu\nu}$ and the $SU(3)$

generators in the real (T_{kl}^a) and the adjoint (f^{abc}) representation. The resulting FeynArts amplitudes are not regularized. The loop/external momenta, the metric tensor and the gamma matrices are in four dimensions. Besides the tensor structures in the numerators are written without taking the contractions of the Lorentz, Dirac and Color indices. With the help of the Mathematica package FeynCalc [159] we have written a routine that implements the regularization of the Feynman integrals by dimensional reduction. We have used the version 9.0.1 of FeynCalc where DRED is not implemented; however, some of the FeynCalc functions can be used in order to get the DRED regularized amplitudes. Also, the language of FeynCalc is more convenient for calculational purposes and can be easily imported from FeynArts through the function `FCFAConvert`. There are three different but equivalent ways to implement DRED, which differ basically in how the algebra of the Dirac matrices on the numerators is solved. In this regularization scheme all gamma matrices coming from a vertex with a vector field and the metric tensor in a vector propagator belong to the quasi-four-dimensional space ($Q4S$) [68, 160, 161] while loop/external momenta coming from a fermion propagator, and any metric tensor or gamma matrix contracted to them, remain in the quasi- D -dimensional space (QDS). Such spaces were first postulated in [162, 163] and guarantees that all calculational rules are consistent and that all practical calculations lead to unambiguous and well-defined results. The details of the algebra in the quasi-four, $-D$ and $-\epsilon$ -dimensional spaces can be found in Appendix A. One can regularize a loop-integral by

- i) splitting each $Q4S$ matrix in the numerator into a sum of $QDS \oplus Q\epsilon S$ matrices and therefore, for our purposes, splitting the four-dimensional gamma and metric tensor matrices according with:

$$\gamma_\mu = \gamma_{\hat{\mu}} + \gamma_{\tilde{\mu}} \quad ; \quad g_{\mu\nu} = g_{\hat{\mu}\hat{\nu}} + g_{\tilde{\mu}\tilde{\nu}} \quad , \quad (3-12)$$

where the indices with a hat and a tilde run the QDS and $Q\epsilon S$ spaces, respectively. Then, one has to perform the corresponding algebra of the tensors involved, products of gamma matrices and Dirac traces, according with the rules of each QDS and $Q\epsilon S$ spaces and solve the resulting integrals using the usual techniques of the dimensional regularization. Note that this procedure do not require the inclusion of additional vertices in the MSSM model file of FeynArts, just the identification and splitting of the $Q4S$ matrices in the amplitudes.

- ii) In the second procedure, diagrams generated with the original MSSM vertices are regularized in the usual DREG; however, in order to preserve supersymmetry, the diagrams with the inclusion of the vertices involving ϵ -scalars (see Appendix C) coming from the split of the vector fields ($V^\mu = V^{\hat{\mu}} + V^{\tilde{\mu}}$) must be added. The amplitudes of the diagrams with ϵ -scalars have the same expressions as the integrals with $Q\epsilon S$ objects obtained after the splitting of the $Q4S$ matrices in the first approach. In this procedure the cubic and quartic vertices involving ϵ -scalars must be added to the model file `MSSMCT.mod` of FeynArts.

- iii) Finally, one can perform the regularization of the Feynman integrals directly in the $Q4S$ space following their calculational rules and without the introduction of additional ϵ -scalar vertices. In particular, due to all traces of γ matrices can be reduced to $\text{Tr}1 = 4$ times metric

tensors by applying the anticommutation relations, results of traces are formally the same in the actual four-dimensional space and in $Q4S$ as long as no γ^5 is present; therefore, in this approach FeynCalc functions as `DiracTrace` or `Tr` can be used to sort out traces of gamma matrices. It is worth to mention that the $Q4S$ algebra for diagrams which contain the cubic vertex quark-squark-gluino requires a special treatment. This vertex introduces the γ_5 matrix in the Dirac traces. We can deal γ_5 as an anti-commuting object provided that traces with an odd number of γ_5 contain less than four gamma matrices [164]. This γ^5 -regularization is allowed in our computation of the three-loop Higgs self-energies because after expanding the numerator of each three-loop integral (which contain products of Higgs/SQCD vertices and the numerator of vector/fermion propagators) with the help of the FeynCalc functions `DiracOrder` and `DiracSimplify`, we only find traces of a single γ_5 and at most three gamma-matrices besides of traces with just γ^μ products. We point out, however, that this treatment of γ^5 is not valid in general. For instance, three-point three-loop Green functions could contain non-vanishing traces with a single γ^5 , as is shown in [67].

Even though the three procedures are completely equivalent, in practice the third one is the easiest to implement since we avoid the introduction of the diagrams involving ϵ -scalars and the algebra in the $Q\epsilon S$. Nevertheless, for the pure three-loop amplitudes we have implemented the second and the third procedure in a Mathematica routine to cross-check the results and for the diagrams with counter-term insertions we have used directly the second method provided that the anomalous dimensions of the squarks contain an ϵ -mass dependence starting from the two-loop level, as you can see in eq. (B-12). An example routine of the regularization of three-loop self-energy integrals using the third approach is shown in Appendix F. The code in Appendix F also applies the approximation of vanishing external momentum and performs the sum over the Color indices of the $SU(3)$ generators, with the help of the package `SUNSimplify` of FeynCalc. In this way, after performing the Dirac and the Color algebra, the numerator of each three-loop amplitude is expressed in terms of the Casimir operator eigenvalues, the scalar products of loop momenta and the kinematic invariants, besides of the coupling constants and the other rMSSM involved parameters.

The scalar products of loop-momenta over the numerators can be expressed in terms of scalar propagators according to:

$$\begin{aligned} q_j^2 &\rightarrow (q_j^2 - m_j^2) + m_j^2, \\ q_i \cdot q_j &\rightarrow \frac{1}{2} [(q_i + q_j)^2 - m_{i+j+1}^2 - (q_i^2 - m_i^2) - (q_j^2 - m_j^2) + f(m_i, m_j, m_{i+j+1})], \end{aligned} \quad (3-13)$$

where

$$f(m_i, m_j, m_{i+j+1}) = m_{i+j+1}^2 - m_i^2 - m_j^2. \quad (3-14)$$

Applying the changes defined in eqs. (3-13) and (3-14) and a further partial fractioning over propagators with equal loop momenta but different masses,

$$\left(\frac{1}{k_i^2 - m_i^2} \right) \left(\frac{1}{k_i^2 - m_j^2} \right) \rightarrow \frac{1}{m_i^2 - m_j^2} \left(\frac{1}{k_i^2 - m_i^2} - \frac{1}{k_i^2 - m_j^2} \right), \quad (3-15)$$

each three-loop amplitude can be expressed as a superposition of a set of *scalar integrals* of the form

$$\sum_j c_j \text{INT} [\{v_{j_1}, m_{j_1}\}, \{v_{j_2}, m_{j_2}\}, \{v_{j_3}, m_{j_3}\}, \{v_{j_4}, m_{j_4}\}, \{v_{j_5}, m_{j_5}\}, \{v_{j_6}, m_{j_6}\}], \quad (3-16)$$

where the coefficients c_j are functions of the Casimir operator's eigenvalues of the non Abelian color algebra, the coupling constants and the squared masses, while

$$\begin{aligned} \text{INT} [\{a, m_1\}, \{b, m_2\}, \{c, m_3\}, \{d, m_4\}, \{e, m_5\}, \{f, m_6\}] = \\ \left\langle \frac{1}{(k_1^2 - m_1^2)^a} \frac{1}{(k_2^2 - m_2^2)^b} \frac{1}{(k_3^2 - m_3^2)^c} \frac{1}{(k_4^2 - m_4^2)^d} \frac{1}{(k_5^2 - m_5^2)^e} \frac{1}{(k_6^2 - m_6^2)^f} \right\rangle_{3l}, \\ \langle (\dots) \rangle_{3l} = \prod_{j=1}^3 \int d^D q_j, \end{aligned} \quad (3-17)$$

with $k_1^2 = q_1^2$, $k_2^2 = q_2^2$, $k_3^2 = q_3^2$, $k_4^2 = (q_1 + q_2)^2$, $k_5^2 = (q_1 + q_3)^2$ and $k_6^2 = (q_2 + q_3)^2$. The powers a, b, c, \dots can be zero, negative or positive integer numbers. Thus, the scalar integrals can contain propagators with negative powers and therefore irreducible numerators. The total set of pure three-loop Higgs self-energies and tadpoles can be expressed as a linear combination of 3525 different scalar integrals (with different configuration of powers and masses).

So as to evaluate each scalar integral in terms of a general expression valid for any election of the input masses, we have avoided the use of asymptotic expansions at the integral level. Instead, we have exploited the fact that this set of integrals are not independent of each other but related by the integration by parts (IBP) relations, which are obtained after working out the differentiation in

$$\int d^D q_j \frac{\partial}{\partial q_j^\nu} [k^\mu \text{I}(p_1, \dots, p_e, q_1, \dots, q_l)] = 0. \quad (3-18)$$

The momentum k^μ represents an arbitrary loop/external momentum. The index μ is summed over but the index j is not. If there are l loop momenta and e independent external momenta one can therefore build $l(l + e)$ equations from one seed integral. Additional relations can be obtained from the Lorentz invariance (LI) identities,

$$\sum_{n=1}^e \left(p_n^\nu \frac{\partial}{\partial p_{n\mu}} - p_n^\mu \frac{\partial}{\partial p_{n\nu}} \right) \text{I}(p_1, \dots, p_e) = 0. \quad (3-19)$$

The eq. (3-19) leads to $e(e - 1)/2$ identities, where e denotes the number of independent external momenta. We have used the IBPs to generate a homogeneous system of linear equations where the scalar integrals are the unknowns. The system can be reduced to a small set of irreducible integrals, the so called Master Integrals. This is something that cannot be done by hand because there are thousand of equations. Thus, we have used the program Reduze [165], an implementation of the Laporta algorithm, in order to carry out

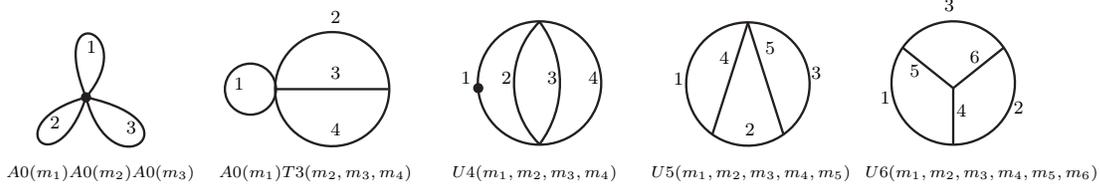


Figure 3-2.: Basis of three-loop vacuum integrals obtained from the IBP reduction with Reduze.

this reduction. Reduze requires the definition of a set of integral families, which is a minimal ordinary set of propagators P_1, \dots, P_n with the specification of their permutation symmetries, where any scalar product of a loop-momentum with a loop/external momentum can be uniquely expressed as a linear combination of inverse propagators and kinematic invariants. A selection of t propagators P_{j_1}, \dots, P_{j_t} , where $\{j_1, \dots, j_t\} \subset \{1, \dots, n\}$, defines a sector of a family. Each sector have an identification number defined as

$$ID = \sum_{k=1}^t 2^{j_k-1}. \quad (3-20)$$

In the Reduze notation an arbitrary scalar integral belongs to a sector and is expressed as:

$$\text{INT} [F, t, ID, r, s, \{v_1, \dots, v_n\}], \quad (3-21)$$

where F denotes the integral family, t is the number of propagators, v_i is the exponent of the propagator P_i , r is the sum of the propagator exponents which are positive, $r = \sum_{i=1}^t r_i$ with $\{r_i \in v_i \mid v_i > 0\}$, s is the sum of the propagator powers which are negative, $s = \sum_{i=1}^{n-t} s_i$ with $\{s_i \in v_i \mid v_i < 0\}$. A code devoted to change the notation of the scalar integrals from (3-17) to (3-21) and to identify the corresponding integral families at which the scalar integrals belong is shown in Appendix G.

We have found a basis of 32 master integrals, which correspond to different mass configurations for the five vacuum diagrams depicted in Figure 3-2, where each topology can contain at most four independent mass scales. Those integrals are independent of each other, in the sense that they cannot be related by permutation symmetries of the propagators. Specifically, the basis includes the integrals depicted in Figure 3-3. The divergent and the finite part as well as the evanescent terms, which are the terms of order ϵ^n with $n > 0$, of the Laurent expansion of the one-loop function

$$A0(m) = \frac{e^{\gamma_E \epsilon}}{i\pi^{D/2}} \int d^D q \frac{1}{q^2 - m^2}, \quad (3-22)$$

and the two-loop function

$$T3(m_1, m_2, m_3) = i \frac{e^{2\gamma_E \epsilon}}{\pi^D} \int \prod_{j=1}^3 d^D q_j \frac{1}{[q_1^2 - m_1^2]^1 [q_2^2 - m_2^2]^1 [(q_1 - q_2)^2 - m_3^2]^1}, \quad (3-23)$$

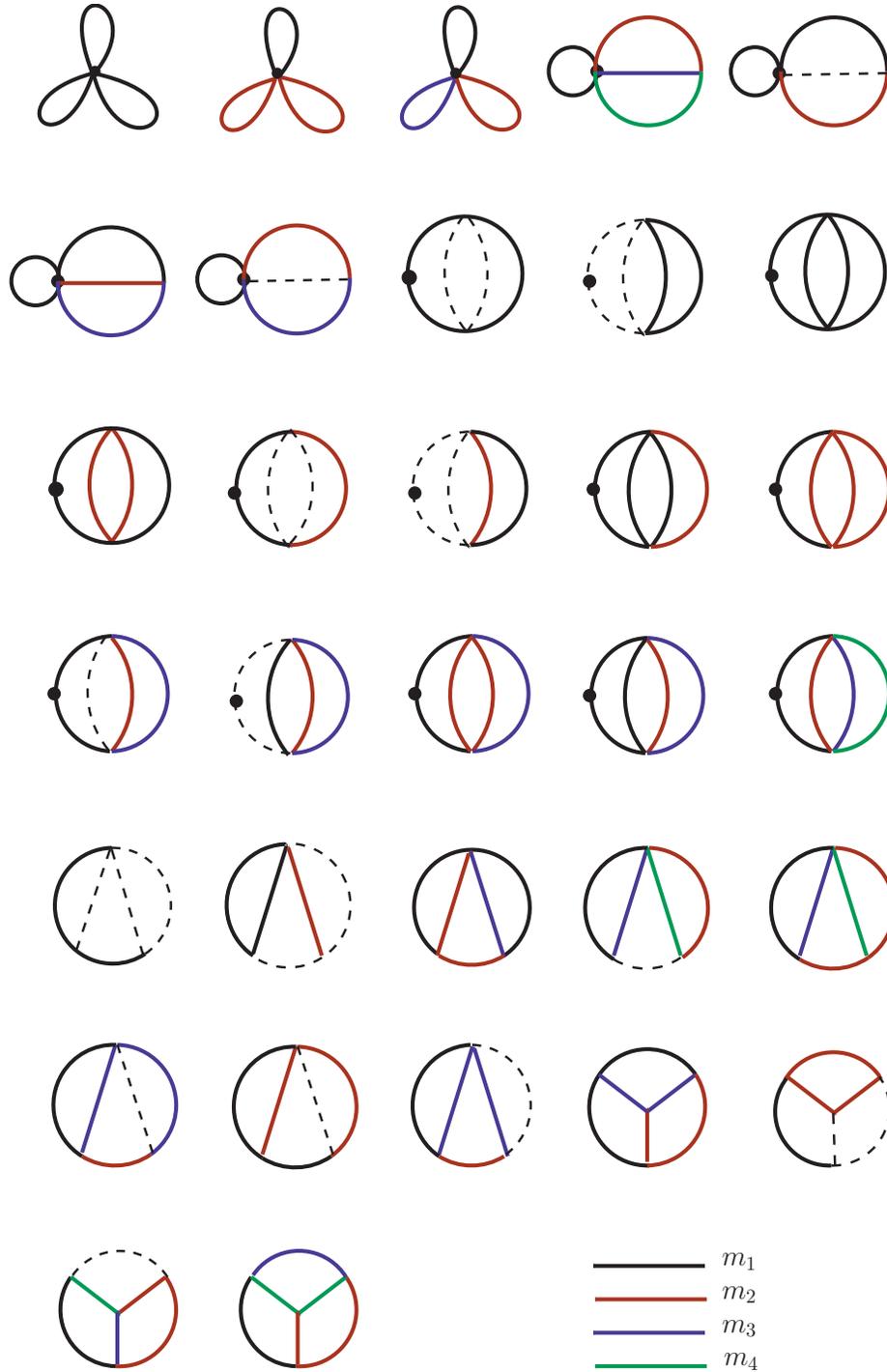


Figure 3-3.: Basis of three-loop Master Integrals. The dashed line represents a massless propagator. The solid lines are massive propagators, each color represent an independent mass scale.

have very well known analytical expressions for any configuration of masses. Furthermore, the three-loop vacuum integrals $U4$, $U5$ and $U6$, are defined as:

$$U4(m_1, m_2, m_3, m_4) \equiv \text{INT}[2, 1, 1, 1, 0, 0], \quad (3-24)$$

$$U5(m_1, m_2, m_3, m_4, m_5) \equiv \text{INT}[1, 1, 1, 1, 1, 0], \quad (3-25)$$

$$U6(m_1, m_2, m_3, m_4, m_5, m_6) \equiv \text{INT}[1, 1, 1, 1, 1, 1], \quad (3-26)$$

with

$$\text{INT}[\nu_1, \nu_2, \nu_3, \nu_4, \nu_5, \nu_6] = i \frac{e^{3\gamma_E \epsilon}}{\pi^{3D/2}} \int \prod_{j=1}^3 d^D q_j \frac{1}{[q_1^2 - m_1^2]^{\nu_1} [(q_1 - q_2)^2 - m_2^2]^{\nu_2}} \times \frac{1}{[(q_2 - q_3)^2 - m_3^2]^{\nu_3} [q_3^2 - m_4^2]^{\nu_4} [q_2^2 - m_5^2]^{\nu_5} [(q_1 - q_3)^2 - m_6^2]^{\nu_6}}, \quad (3-27)$$

where the indices ν_j are integers numbers, $\epsilon = (4 - D)/2$ and D is the number of the space-time dimensions. For each of those three-loop functions it is possible to find an analytical expression of the divergent part, which can be consulted in Appendix I, independent of the mass configuration in the propagators. An analytical solution to all orders in ϵ can be obtained just for the cases where there are one or two massive propagators, the main expressions can be consulted in Appendix J. However, when there are three or four independent mass scales a numerical evaluation of the finite part and the evanescent terms of the three-loop master integrals is required. In this work we have used a method based on dispersion relations, implemented in the public code TVID developed by A. Freitas [166–168], in order to make the analysis of the convergence and get a numerical integration of the master integrals which are unknown analytically. TVID uses the discontinuities coming from the one-loop self-energy

$$B0(p^2, m_1, m_2) = \frac{e^{\gamma_E \epsilon}}{i\pi^{D/2}} \int d^D q \frac{1}{[q^2 - m_1^2] [(q+p)^2 - m_2^2]}, \quad (3-28)$$

and the one-loop vertex

$$C0(p_1^2, p_2^2, m_1, m_2, m_3) = \frac{e^{\gamma_E \epsilon}}{i\pi^{D/2}} \int d^D q \frac{1}{[q^2 - m_1^2] [(q+p_1)^2 - m_2^2] [(q+p_1+p_2)^2 - m_3^2]}, \quad (3-29)$$

to produce dispersion relations that are useful in the evaluation of the U -functions in terms of one- and two-dimensional integral representations. The four-propagator function $U4$ and the five-propagator function $U5$ can be represented in terms of one-dimensional integrals. In analogous way the six-propagator function $U6$ can be represented by a two-dimensional numerical integral. For the case of the $U4$ function the representation is

$$\begin{aligned} U4(m_1, m_2, m_3, m_4) &= -\frac{e^{\gamma_E \epsilon}}{i\pi^{D/2}} \int d^D q_3 \int_0^\infty ds \frac{\Delta I_{db}(s)}{q_3^2 - s + i\epsilon} \\ &= U4_{div} - \int_0^\infty ds A0_{fin}(s) \Delta I_{db,fin}(s), \end{aligned} \quad (3-30)$$

where $U4_{div}$ contains the UV divergences of $U4$, $A0_{fin}$ is the finite part of the one-loop function $A0$, while

$$\begin{aligned} \Delta I_{db,fin}(s, m_1^2, m_2^2, m_3^2, m_4^2) &= \Delta B_{0,m_1}(s, m_1^2, m_2^2) \operatorname{Re} [B0(s, m_3^2, m_4^2) - B0(s, 0, 0)] \\ &\quad - \Delta B_{0,m_1}(s, m_1^2, 0) \operatorname{Re} [B0(s, m_3^2, 0) + B0(s, m_4^2, 0) - 2B0(s, 0, 0)] \\ &\quad + \operatorname{Re} [B_{0,m_1}(s, m_1^2, m_2^2)] (\Delta B0(s, m_3^2, m_4^2) - \Delta B0(s, 0, 0)) \\ &\quad - \operatorname{Re} [B_{0,m_1}(s, m_1^2, 0)] (\Delta B0(s, m_3^2, 0) + \Delta B0(s, m_4^2, 0) - 2\Delta B0(s, 0, 0)). \end{aligned} \quad (3-31)$$

$\Delta B0$ and $\Delta B_{0,m_j}$ are the discontinuities of the scalar one-loop self-energy function, $B0$, and its mass derivative, $B_{0,m_j} = \frac{\partial}{\partial m_j^2} B0$, given by

$$\Delta B0(s, m_a^2, m_b^2) = \frac{1}{s} \lambda(s, m_a^2, m_b^2) \Theta(s - (m_a + m_b)^2), \quad (3-32)$$

$$\Delta B_{0,m_1}(s, m_a^2, m_b^2) = \frac{m_a^2 - m_b^2 - s}{s \lambda(s, m_a^2, m_b^2)} \Theta(s - (m_a + m_b)^2). \quad (3-33)$$

Here $\lambda(x, y, z)$ is the Källén function defined as

$$\lambda(x, y, z) = \sqrt{x^2 + y^2 + z^2 - 2(xy + yz + zx)} \quad (3-34)$$

and Θ is the Heaviside step function. The finite part of the vacuum integral $U4$ is therefore expressed as a numerical integral of a combination of elementary functions, such as logarithms and square roots, which can be efficiently evaluated with numerical methods for general mass patterns without making any assumptions about the mass hierarchy of the SUSY particles.

Analogous but more complicated dispersion relations in terms of fundamental functions, whose explicit form is too lengthy to be included here, were already obtained for the finite part of the three-loop integrals $U5$ and $U6$ and can be consulted in [166] and the ancillary files included in the program TVID [167, 168]. In any case the dispersion relation techniques lead to one- and two-dimensional integrals of the form

$$\int_{s_0}^{\infty} ds \frac{f(s)}{s - s' \pm i\varepsilon}, \quad (3-35)$$

which can be efficiently evaluated for any mass hierarchy with numerical methods. This is an important feature that is worth pointing out. The three-loop corrections to M_h are expressed in terms of a basis of master integrals which can be numerically evaluated for an arbitrary hierarchy of the mass scales. For $s' > s_0$, those integrals can be split into a residue contribution and a principal value integral, yielding

$$\int_{s_0}^{\infty} ds \frac{f(s)}{s - s' \pm i\varepsilon} = \mp i\pi f(s') + \int_{s_0}^{s'} ds \frac{f(s) - f(2s' - s)}{s - s'} + \int_{2s' - s_0}^{\infty} ds \frac{f(s)}{s - s'}. \quad (3-36)$$

In the eq. (3-36), the integrand of the first remaining integral is regular at the point $s = s'$. If $f(s)$ is real, the residue contribution can be dropped provided that only the real part

is needed in the evaluation of the three-loop vacuum functions. With the dispersion method implemented in TVID the finite part of the three-loop U -integrals can be numerically evaluated with up to 10 digits of accuracy. Internally the program uses the Gauss-Kronrod routine QAG from the Quadpack library [169] to evaluate the dispersion integrals. This routine has been amended to facilitate 30 digit floating point arithmetic from the package doubledouble [170] allowing results with at least ten digits of precision for the $U4$ and $U5$ integrals and a precision of eight digits for the $U6$ vacuum integral. It is possible to reach this precision because the numerical integrations are at most 2-dimensional and therefore there is a controlled treatment of any singularities.

The code devoted to express each three-loop amplitude as a linear combination of the integrals drawn in Figure 3-2, with coefficients that are ratios of polynomials in the masses and the space-time dimension, is shown in Appendix H. These coefficients can contain poles of first and second order and therefore the renormalized correction to M_h requires also the evaluation of the evanescent terms of the master integrals up to second order, that is to say, the terms at order $O(\epsilon)$ and $O(\epsilon^2)$ in the Laurent expansion. It is not possible to evaluate these contributions with TVID because the higher- ϵ terms of the real and imaginary parts of $B0$ and $C0$ and therefore of $U4$, $U5$ and $U6$ are not included in the program. For this reason we have used the code SecDec [171] which admit a numerical evaluation of the evanescent terms.

3.2.1. Three-loop counter-term diagrams

On the other hand, we also need to generate the amplitudes for the diagrams which are responsible for removing the non-local sub-divergences. This includes the generation and insertion of the needed SQCD mass counter-terms. We have written a routine in Mathematica that generates all the expressions for the counter-terms listed in Appendix B. The generation of the involved regularized amplitudes was done with the help of the FeynArts and FeynCalc functions. In contrast to the three-loop diagrams, the one and two-loop counter-terms are determined from the evaluation of fermionic and scalar self-energies with the external momentum transferred different from zero, $p^2 \neq 0$. The resulting self-energies can be further reduced using the Tarasov method [172], that is implemented in the code TARCER [173], to the basis of one and two-loop master integrals represented by the diagrams of Figure 3-4. The one-loop counter-terms of the top quark mass, the gluino mass, the sfermion masses and the stop mixing angles can be determined in terms of the Passarino-Veltman functions $A0$ and $B0$. The two-loop counter-terms of the stop masses and mixing angles can be expressed as a superposition of the eleven master integrals depicted in Figure 3-4.

In the \overline{DR} scheme we just need the divergent parts of the integrals. The one-loop functions $A0$ and $B0$ have the analytical expressions found in Appendix J. The functions Dm_1m_2J , $Dm_1m_2m_3J$ and $D2m_1m_2J$ are finite. $D2m_1J$ has only a $1/\epsilon$ divergence with coefficient $-1/2m_1^2$, independent of the values of m_2 and m_3 . Dm_1J has poles of one and second order,

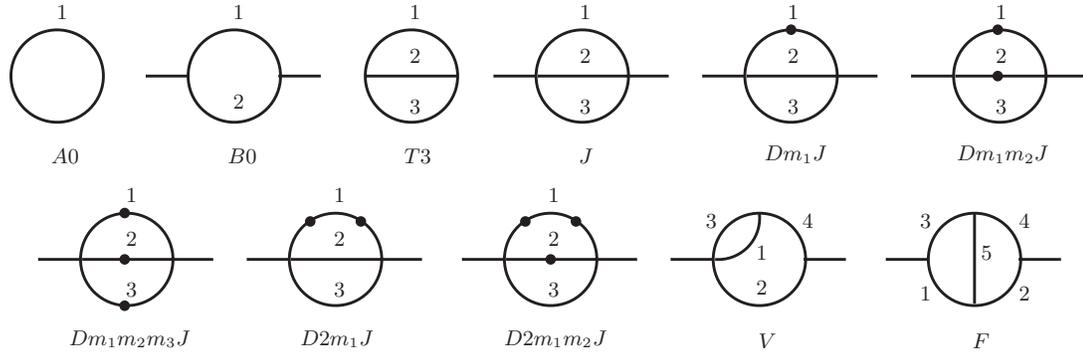


Figure 3-4.: Basis of one and two-loop master integrals obtained from the Tarasov method. The dot over the internal line j represents a partial derivative of the propagator regarding the squared mass m_j^2 .

its $1/\epsilon^2$ divergence is $1/2$, mass independent while its $1/\epsilon$ divergence is $1/2 - \ln(m_1^2/\mu_r^2)$. The $1/\epsilon^2$ divergence coefficient of J is $1/2(m_1^2 + m_2^2 + m_3^2)$ while the $1/\epsilon$ divergence coefficient is

$$\frac{3}{2} (m_1^2 + m_2^2 + m_3^2) - \frac{p^2}{4} - \sum_{j=1}^3 m_j^2 \ln(m_j^2/\mu_r^2). \quad (3-37)$$

For the cases where one or more masses m_j^2 vanish in the expression (3-37) one should take the zero order term of the Taylor expansion around $m_j^2 = 0$ to get the right expression. The same apply for $T3$ but choosing the external momentum p^2 equal to zero. Finally, we need the functions F and V with at most three independent mass scales. The function F is finite, while $V[p^2, m_1^2, m_2^2, m_3^2, m_4^2]$ have a divergence $1/\epsilon^2$ with coefficient $1/2$ and a $1/\epsilon$ divergence equal to $B0_{fin}[p^2, m_2^2, m_4^2] + 1/2$, where $B0_{fin}$ refers to the finite part of the function $B0$. All these analytical expressions were numerically checked with the code SecDec, where the prefactor $Exp[-2\gamma_E\epsilon]$ must be specified in order to get the correct result. In Appendix B the counter-term expressions involved in the renormalization of the non-local ultraviolet divergences are listed. These results can be checked with those of the review [174] and references therein.

Once the needed mass counter-terms are generated, we need to insert their expressions into the counter-terms diagrams, which are Higgs self-energies and tadpoles at one- and two-loop level with counter-term insertions. The code devoted to this aim is shown in Appendix K. A further expansion in ϵ is performed over the amplitudes. The coefficients of the poles are saved by the program in a list and used to remove the sub-divergences appearing in the pure three-loop diagrams. Besides the $O(\epsilon^0)$ term of each counter-term diagram is also generated and added to the finite contributions coming from the pure three-loop Higgs tadpoles and self-energies. These cancellations and additions are performed in an automatized way with the help of a Mathematica routine.

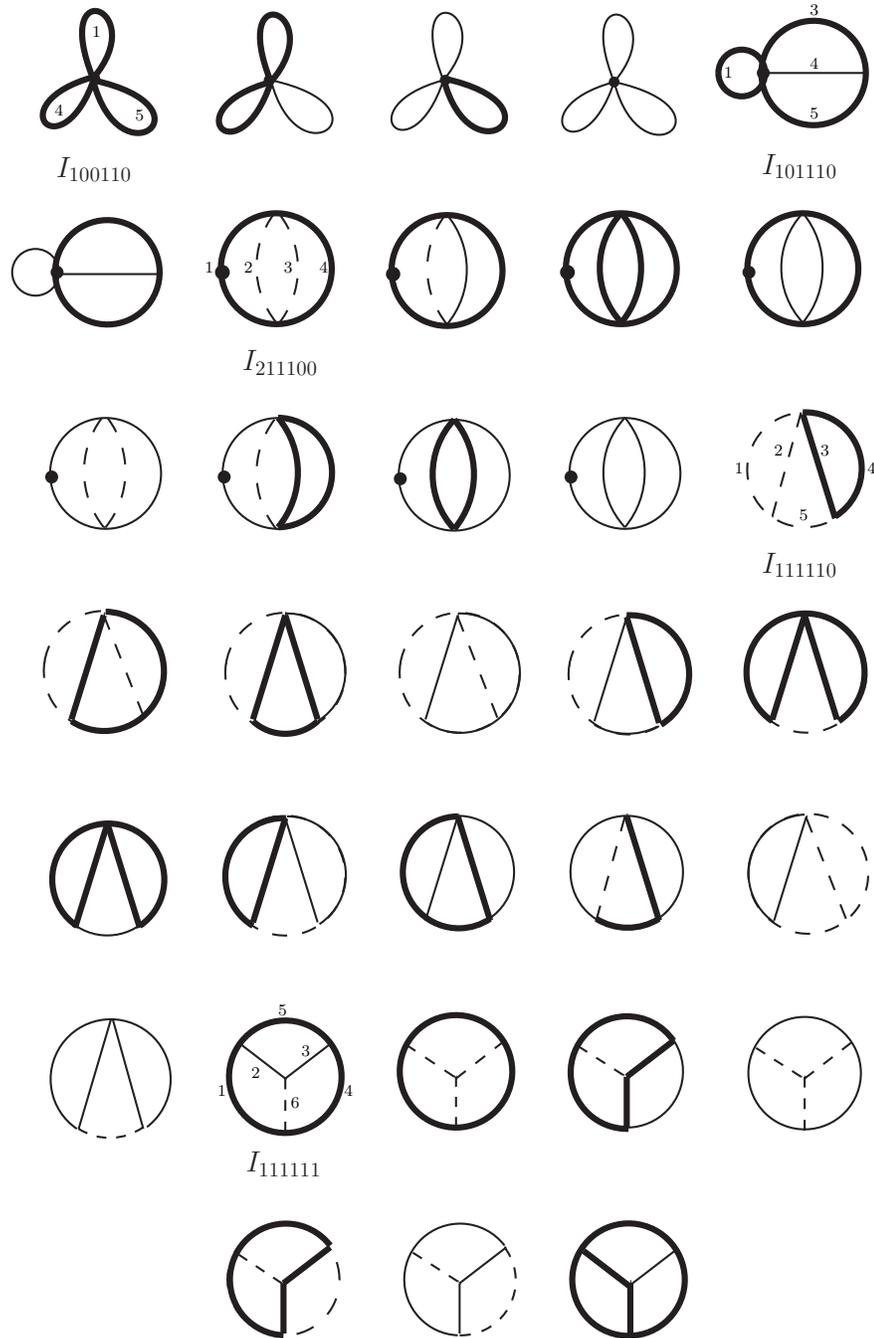


Figure 3-5.: Basis of three-loop Master Integrals in the heavy SUSY limit. The dashed line represents a massless propagator. The thin solid line is the propagator with a mass at the electroweak scale M_t and the thick solid line depicts the propagator involving the SUSY scale M_{SUSY} .

3.2.2. Three-loop M_h -corrections in the heavy SUSY limit

We have also considered a degenerate single-scale scenario where all the super-symmetric masses are set equal to an effective scale M_{SUSY} ,

$$M_{L,R} = M_{\tilde{g}} = M_A = \mu = M_{SUSY}. \quad (3-38)$$

Here μ is the Higgsino mass and $M_{L,R}$ are the soft SUSY-breaking masses. We have identified the lightest Higgs boson h as the SM-like Higgs boson and therefore we have assumed the decoupling limit, $M_A = M_{SUSY} \gg M_t$. This degenerate scenario in the decoupling limit is known as the ‘‘heavy SUSY’’ limit. As a consequence, the three-loop self-energy corrections to $m_{h,H}^2$ can approximately be obtained as a superposition of the 33 vacuum integrals depicted in Figure 3-5 with coefficients that are functions of the kinematic invariants and the space-time dimension, D . In some particular cases the coefficients can contain poles; that is to say, terms of the form $(D - 4)^{-1}$. Thus, the basis integrals could also require a numerical evaluation of their evanescent terms. Besides, the mixed $h - H$ self-energy contributions vanish and therefore the propagator equation (2-24) reduces to

$$p^2 - m_h^2 + \widehat{\Sigma}_{hh} = 0, \quad (3-39)$$

where

$$\widehat{\Sigma}_{hh} = \Sigma_{hh} + \frac{h_t}{2M_t} s_\beta \frac{T_h}{\sqrt{2}}. \quad (3-40)$$

Each diagram of the basis in Figure 3-5 represents a three-loop Master Integral of the form

$$I_{v_1 \dots v_6} = i \frac{e^{3\gamma_E \epsilon}}{\pi^{3D/2}} \int \prod_{l=1}^3 d^D q_l \left[\prod_{j=1}^6 \frac{1}{P_j^{n_j}} \right], \quad (3-41)$$

with

$$\begin{aligned} P_1 &= q_1^2 - m_1^2, & P_2 &= (q_1 - q_2)^2 - m_2^2, & P_3 &= (q_2 - q_3)^2 - m_3^2, \\ P_4 &= q_3^2 - m_4^2, & P_5 &= q_2^2 - m_5^2, & P_6 &= (q_1 - q_3)^2 - m_6^2. \end{aligned}$$

There are two scales involved, the electroweak scale M_t , whose associated propagator is represented with a thin solid line and the super-symmetric scale M_{SUSY} represented with a thick solid line. Massless propagators are represented with a dashed line. This basis was obtained using the integration by parts (IBP) method implemented in the code Reduze. Main part of the diagrams shown on Figure 3-5 have been analytically evaluated in [175–182]. The numerical evaluation of this basis was done also with TVID and SecDec. In particular, the integral I_{211100} requires a Laurent expansion up to first order in ϵ . The evanescent terms of $\mathcal{O}(\epsilon^1)$ was numerically evaluated with the help of SecDec.

3.3. Numerical M_h -predictions in the diagrammatic approach

Once the local and non-local UV divergences have been subtracted from the Higgs self-energies, we get finite three-loop corrections to the CP-even and CP-odd Higgs boson masses that are useful in the derivation of the renormalized value of M_h which is obtained as a solution of the pole equation (2-24). Our corrections depend upon 26 parameters: the renormalization scale μ_r , the SM \overline{DR} parameters h_t , M_t , α_s and the MSSM parameters μ , $\tan\beta$, M_A , $M_{\tilde{g}}$, θ_t , $\tilde{m}_{f_{1,2}}$ and A_f , with $f = u, d, t, b, c, s$. Their values as well as the renormalization group evolution of the SM parameters are determined with the help of the spectrum generator SoftSUSY [139]. We use the package SLAM [183] (Supersymmetry Les Houches Accord with Mathematica) in order to export to Mathematica any needed parameter generated with SoftSUSY. In the \overline{DR} scheme the two-loop anomalous dimension of the stop mass contain a non-physical dependence on the ϵ -scalar mass, m_ϵ . At order $\alpha_t\alpha_s^2$ a one-loop renormalization of m_ϵ is required. In order to decouple the ϵ -scalar mass from the physical observables we have renormalized m_ϵ in the on-shell scheme [91, 184] and we have imposed $m_\epsilon^{OS} \rightarrow 0$ at the given perturbative order. Strictly speaking, this procedure does not coincide with a \overline{DR} renormalization due to m_ϵ is not renormalized minimally. However, as all the other parameters entering the two-loop counter-term of the stop mass are \overline{DR} parameters and the $O(\alpha_t\alpha_s^2)$ correction to M_h is independent from m_ϵ , we maintain the nomenclature " \overline{DR} scheme".

We have performed a numerical comparison between our three-loop predictions and the other fixed-order corrections currently included in FeynHiggs [56, 155, 156] and the three-loop results implemented in H3m [55, 117, 118] combined with the lower-order results of FeynHiggs. We discuss our results in three different limits: i) the m_h^{free} scenario, where μ_r , $\tan\beta$, M_A and A_t are left as free input parameters. ii) The m_h^{max} and m_h^{mod+} scenarios analyzed in [37]. In these three different scenarios we do not make any specific assumptions about the soft SUSY-breaking mechanism and we interpret the LHC signal at 125 GeV as the lightest CP-even Higgs boson. We consider values of the SUSY scale in the region $M_{SUSY} < 1.2$ TeV, where the combined theoretical uncertainty of the fixed-order calculation is lesser than the combined uncertainty of the effective field theory (EFT) calculation [41]. At the critical point $M_{SUSY} = 1.2$ TeV, the fixed-order and EFT combined uncertainties are equal and a hybrid calculation should be used [128, 147, 157]. Above the critical point the EFT computation is more accurate and therefore an EFT approach, where an effective SM is used below a super-symmetric scale [122–125], should be preferred.

Throughout this section, we will discuss our numerical results in scenarios where a fixed-order calculation is recommended. A numerical analysis considering large SUSY scales of the order of $M_{SUSY} \gg 1.2$ TeV will be the subject of the Chapter 4. In the m_h^{free} scenario we fix the parameters

$$M_{\tilde{t}_L} = M_{\tilde{t}_R} = \tilde{m}_{q_{1,2}} = M_{SUSY} = 1 \text{ TeV}, \quad (3-42)$$

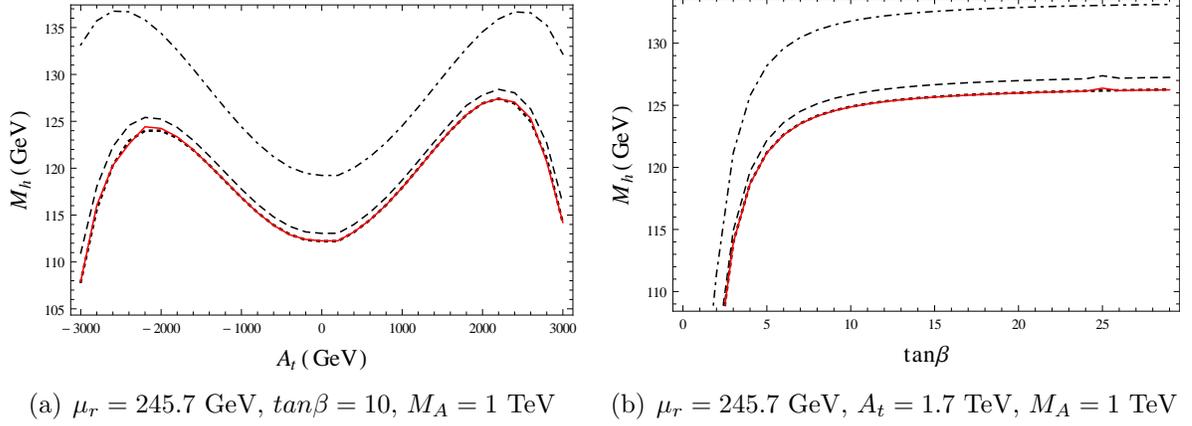


Figure 3-6.: Dependence of M_h on (a) A_t and (b) $\tan\beta$. The dot-dashed and dashed lines are the one and two-loop predictions of FeynHiggs. The dotted line is the three-loop prediction of H3m and the red solid line depicts our three-loop predictions.

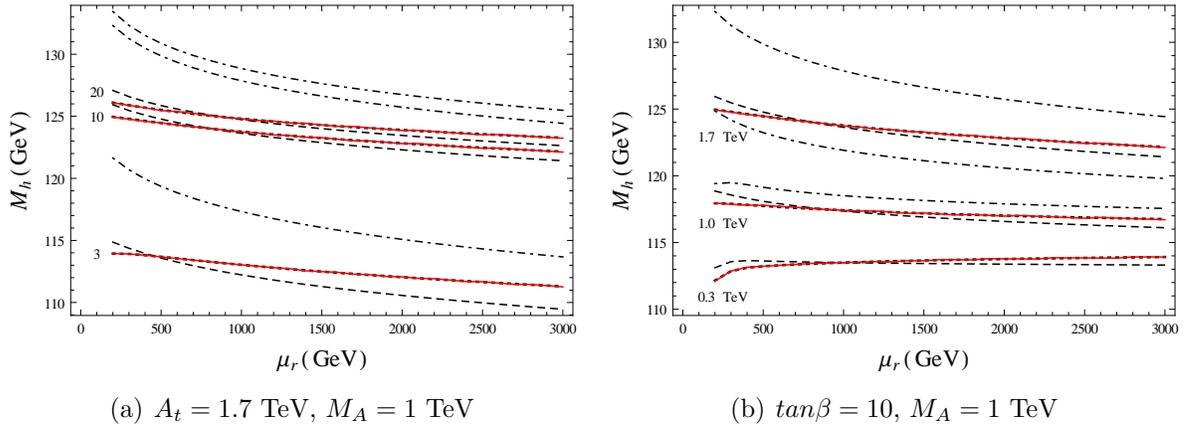


Figure 3-7.: Dependence of M_h on μ_r . (a) The evolution for three different values of $\tan\beta$ is studied. We consider $\tan\beta = 3, 10$ and 20 . (b) M_h is plotted for the scenarios with $A_t = 0.3$ TeV, 1 TeV and 1.7 TeV. The inclusion of three-loop corrections reduces the scale dependence by a factor between $1.5 - 2.0$. The scale dependence is improved when we consider lower values of $\tan\beta$ and A_t . To draw these plots we have used the same conventions as in the Figure **3-6**.

| | M_t | M_{SUSY} | X_t | $M_{\tilde{g}}$ | μ |
|--------------|-----------|------------|----------------|-----------------|---------|
| m_h^{max} | 173.2 GeV | 1000 GeV | $2M_{SUSY}$ | 1500 GeV | 200 GeV |
| m_h^{mod+} | 173.2 GeV | 1000 GeV | $+1.5M_{SUSY}$ | 1500 GeV | 200 GeV |

Table 3-1.: Input parameters for the m_h^{max} and m_h^{mod+} scenarios.

where q denotes any quark different than the top quark. We also set $M_{\tilde{g}} = 1500$ GeV, $\mu = 200$ GeV and $M_A = 1000$ GeV. Using this limit, we have studied the dependence of the Higgs boson mass M_h on the soft-breaking parameter A_t (Fig-3.6(a)) on the input parameter $\tan\beta$ (Fig-3.6(b)) and on the renormalization scale μ_r (Fig-3.7(a) and Fig-3.7(b)).

At one- and two-loop level we have generated the Higgs mass predictions with the help of the code FeynHiggs. These contributions are represented in the plots with the dot-dashed and dashed curves respectively. This convention has been used in all panels. We have included the full one and two-loop corrections ($\alpha_s\alpha_t$, $\alpha_s\alpha_b$, α_t^2 , $\alpha_t\alpha_b$, α_b^2) in the rMSSM. The one-loop field-renormalization constants and the one-loop $\tan\beta$ counter-term are set in the \overline{DR} scheme. We do not assume any approximation for the external momentum value for the one and two-loop corrections, i.e. we set in FeynHiggs a full determination of the propagator matrix poles (2-23). Besides, the dotted curve represents the three-loop predictions at order $O(M_t^2\alpha_t\alpha_s^2)$ coming from the program H3m while the red solid line represents our three-loop prediction evaluated at the same order. Our three-loop results shown in Figure 3-6 are quite sizeable, amounting a size between 0.8 to 3.1 GeV compared to the two-loop corrections and -0.373 to 0.418 GeV regarding the three-loop prediction of H3m. The relative size and sign of the corrections depend on our election of the renormalization scheme.

Figure 3.6(b) shows a strong dependence on $\tan\beta$ for small values close to $\tan\beta = 3$, while for large values above $\tan\beta = 10$ the variation of M_h is marginal and closer to the LHC Higgs mass value. Figure 3-7 depicts the dependence of M_h on the renormalization scale μ_r . In Fig-3.7(a) the dependence is studied for three different values of $\tan\beta$, namely $\tan\beta = 3, 10$ and 20 . The three-loop corrections lead to a more stable dependence of M_h with the renormalization scale μ_r than the one and two-loop predictions, reducing the scale dependence by a factor between 1.5 and 2.0. This stability increases for lower values of $\tan\beta$ in the m_h^{free} scenario. Fig-3.7(b) shows the RG evolution for three values of the soft breaking parameter, $A_t = 0.3$ TeV, 1 TeV and 1.7 TeV. The evolution is more stable when the three-loop corrections are added and when the value of A_t decreases, reducing the scale dependence by a factor of about 1.6 compared to the two-loop predictions. In the m_h^{max} and m_h^{mod+} scenarios the renormalization scale is set to $\mu_r = m_t = 173.2$ GeV, where m_t represents the combined Tevatron and LHC experimental value of the top quark mass [81]. Besides one has to fix $M_{\tilde{t}_L} = M_{\tilde{t}_R} = M_{SUSY}$, $A_q = 0$ and $\tilde{m}_{q_{1,2}} = 1500$ GeV. The parameter A_t is fixed through the mixing term in the squark sector, $X_t = A_t - \mu\cot\beta$, while M_A and $\tan\beta$ are left as free parameters. Within the m_h^{max} scenario X_t is chosen in order to maximize the value of M_h for a given election of μ and $\tan\beta$. This occurs when $|X_t/M_{SUSY}| \approx 2$, where the

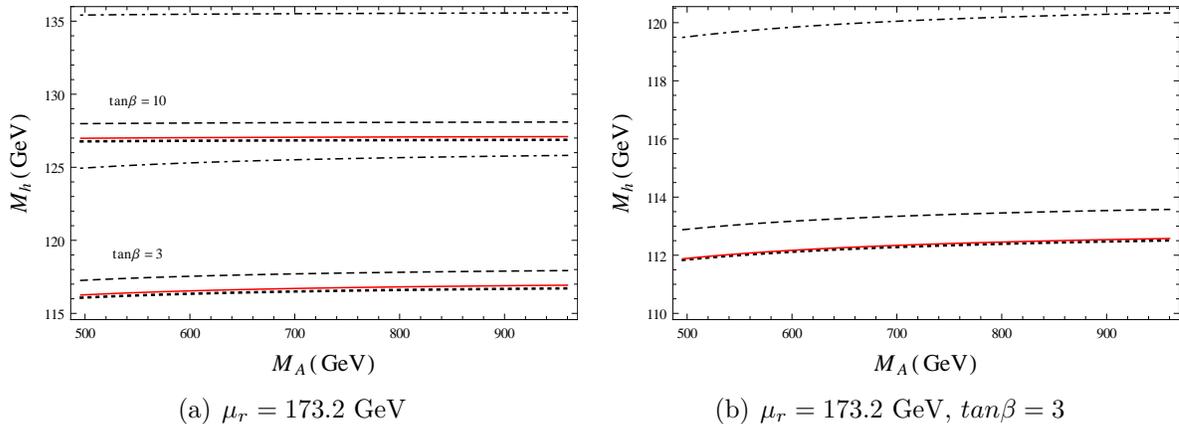


Figure 3-8.: The lightest Higgs boson mass M_h as a function of M_A in (a) the m_h^{max} limit for $\tan\beta = 3, 10$ and (b) in the m_h^{mod+} scenario. Our three-loop corrections are, within theoretical uncertainties, in agreement with the predictions of H3m. The difference can amount a size of about 0.2 GeV in m_h^{max} and 0.05 GeV in m_h^{mod+} . These plots follow the same conventions as in the Figure 3-6.

radiative corrections in the FD calculation reach to the largest positive contribution. With this election of parameters the mass of the lightest CP-even Higgs boson is in agreement with the LHC Higgs boson signal just in a relatively small strip in the M_A - $\tan\beta$ plane. A convenient way to enlarge the region of validity is to decrease the amount of mixing in the stop sector. The m_h^{mod+} scenario is a modification of m_h^{max} where this mixing represented by $|X_t/M_{SUSY}|$ is reduced. In detail we consider the input parameters shown in Table 3-1 for each scenario. The stop mixing angle θ_t and the stop masses \tilde{m}_{t_1} , \tilde{m}_{t_2} are functions of the parameters specified in Table 3-1.

To draw the plots in Figure 3-8 the CP-odd Higgs boson mass M_A is varied in the interval: $500 \text{ GeV} \leq M_A \leq 1 \text{ TeV}$ and we consider the values of $\tan\beta = 3$ and $\tan\beta = 10$. The numerical values of our three loop corrections to M_h are reduced compared with the two-loop predictions showing a good behaviour of the perturbative expansion. In both scenarios the three-loop corrections give rise to a significant reduction of about 1 GeV to the two-loop value of the Higgs boson mass. In addition the values of the corrections are consistent with the results obtained with H3m. The difference can amount a size of about 0.2 GeV in the m_h^{max} limit and 0.05 GeV in m_h^{mod+} . The detailed analysis of the individual sources of uncertainty of the three-loop fixed order \overline{DR}' Higgs boson mass prediction of SoftSUSY, developed recently in [41], shows a combined uncertainty for a maximal stop mixing scenario who varies between 1-4 GeV depending on the SUSY scale. Our results have then very similar numerical values to the ones obtained with H3m with differences which are within the combined theoretical uncertainty.

4. M_{SUSY} Constraints and Vacuum Stability Analysis in the SM

The numerical analysis presented in the last section of Chapter 3 was done for a scenario where the squark masses are of the order of 1 TeV; however, due to the lack of experimental evidence of supersymmetric particles at this energy, we have to consider much larger values for these masses. In this chapter, we are going to study the Higgs mass predictions, coming from our three-loop fixed-order computation and the EFT hybrid calculation included in the public code FeynHiggs, evaluated at the decoupling limit introduced in Section 3.3. Therefore, we consider the limit where all the soft SUSY-breaking masses as well as the CP-odd Higgs mass (m_A) lie around a characteristic scale, M_{SUSY} , and we focus on the dependence of the M_h -predictions on this scale. The effect of the large logarithms occurring in the fixed-order contributions, when supersymmetry is broken at some energy scale greater than the electroweak symmetry breaking scale ($M_{SUSY} \gg M_t$) will be also discussed. A further phenomenological analysis, where we look for constraints on the M_{SUSY} value coming from the LHC measurements for the Higgs boson mass and the vacuum stability analysis in the SM, is developed.

4.1. EFT and hybrid calculation of M_h

When there is a large mass hierarchy between the electroweak scale and the scale of the SUSY particles, the fixed-order computations of the Higgs self-energy corrections contain large logarithms that can spoil the convergence of the perturbative expansion and yield unreliable predictions of the Higgs boson masses. A fixed-order computation is thus recommended for low values of M_{SUSY} not separated too much from M_t . There is an alternative approach to calculate M_h which yield accurate results for high SUSY scales. This approach is based on the EFT techniques [124, 185] and allows the resummation of the large logarithmic terms and the incorporation of higher-order contributions beyond the order of the fixed-order diagrammatic calculations. In the heavy SUSY limit discussed in Section 3.3 the low-scale EFT below M_{SUSY} is the SM. In this approximation, the lightest CP-even Higgs is uniquely identified as the combination of the original neutral Higgs fields

$$h = \frac{v_1 H_1^0 + v_2 H_2^0}{\sqrt{v_1^2 + v_2^2}}, \quad (4-1)$$

which yields a non-vanishing vacuum expectation value $\langle h \rangle = v = \sqrt{v_1^2 + v_2^2} \simeq 174$ GeV. In terms of the light Higgs field h , the rMSSM Higgs potential (eq. 2-6) becomes

$$V(h) = \frac{1}{2}\lambda|\Phi|^4 - \frac{1}{2}m^2|\Phi|^2 \quad ; \quad \Phi = \begin{pmatrix} 0 \\ h/\sqrt{2} + v \end{pmatrix}. \quad (4-2)$$

The parameter m^2 is a function of m_{H_1} , m_{H_2} , μ , b and $v_{1,2}$ which satisfies the minimization condition $\partial V/\partial h = 0$ at $h = v$, while λ is the SM Higgs quartic coupling given at leading order by

$$\lambda = \frac{1}{4}(g^2 + g'^2)c_{2\beta}^2. \quad (4-3)$$

Here g and g' are the running electroweak gauge couplings evaluated at M_{SUSY} , which at tree-level are the same in both theories: the SM and the rMSSM. The SM coupling of the light Higgs to the top quark and the strong coupling constant at tree-level are:

$$y_t = h_t s_\beta, \quad g_s = g_s. \quad (4-4)$$

Note that g_s is the same in the two theories, while h_t is the running top Yukawa coupling at M_{SUSY} in the rMSSM, which differs from the SM top Yukawa coupling y_t by the factor s_β . Solving the n -loop renormalization group equations (RGEs) for the SM couplings,

$$\frac{dg_k}{dt} = \beta_{g_k}, \quad t \equiv \log(Q), \quad \beta_{g_k} = \frac{1}{16\pi^2}\beta_{g_k}^{(1)} + \dots + \frac{1}{(16\pi^2)^n}\beta_{g_k}^{(n)}, \quad g_k = \lambda, y_t, g_s, \dots, \quad (4-5)$$

the effective Higgs self coupling λ can correlate the high scale M_{SUSY} with the next threshold, the low scale M_t , and capture radiative corrections of the form

$$\alpha_j^{m+n-1} \log^m(M_{SUSY}/M_t) \quad ; \quad j = \lambda, y_t, g_s, \dots, \quad (4-6)$$

into the coupling $\lambda(Q)$ for $m \geq 1$, where Q represents the renormalization scale. Thus, with 1, 2, \dots , n -loop RGEs a perturbative solution of $\lambda(M_t)$ can extract the leading (L), next to leading (NL), \dots , $N^{n-1}L$ -logarithmic terms of a fixed-order calculation, respectively. For a complicated set of SM beta functions, an analytical solution of $\lambda(M_t)$ is typically not possible; however, a numerical solution of the system (4-5) allows a very precise evaluation in the EFT approach. On the other hand, in order to numerically solve the system of RGEs it is necessary to impose boundary conditions to obtain the couplings $g_k(t)$ as a function of $g_k(\tilde{t})$ at the scale $\tilde{t} = \log(M_{SUSY})$. The matching conditions in eqs. (4-3) and (4-4) are the boundaries at leading order for the dominant SM couplings. However, this matching procedure is subject to higher-order threshold corrections from loops involving heavy fields. In general, an n -loop RGE requires the specification of boundary conditions with $(n-1)$ -loop threshold corrections. For the Higgs quartic coupling λ at the SUSY scale, the state of art now includes two-loop matching conditions which combined with the three-loop SM RGEs

allows a full NNLL resummation of the large logarithmic corrections. The matching takes the form

$$\lambda(Q) = \frac{1}{4} [g^2(Q) + g'^2(Q)] c_{2\beta}^2 + \Delta^{(1)}\lambda + \Delta^{(2)}\lambda^{\text{gaugeless}} + \Delta^{(2)}\lambda^{\text{EW-QCD}}. \quad (4-7)$$

The complete result for the one-loop correction $\Delta^{(1)}\lambda$ and a complete determination of the two-loop correction $\Delta^{(2)}\lambda^{\text{gaugeless}}$ in the limit of vanishing EW gauge couplings at order $y_{t,b,\tau}^4 g_s^2$ can be found in refs. [121, 125]. The dominant contributions comes from the terms proportional to the fourth power of a third-family Yukawa coupling, which have the form:

$$\Delta\lambda^{y_f^4} = \sum_{f=t,b,\tau} \frac{3y_f^4}{(4\pi)^2} \left(\ln \frac{\tilde{m}_{fL}^2 \tilde{m}_{fR}^2}{Q^4} + 2 \frac{X_f^2}{\tilde{m}_{fL} \tilde{m}_{fR}} \left[F_1(x_f) - \frac{1}{12} \frac{X_f^2}{\tilde{m}_{fL} \tilde{m}_{fR}} F_2(x_f) \right] \right), \quad (4-8)$$

where

$$F_1(x) = \frac{x \ln x^2}{x^2 - 1}, \quad F_2(x) = \frac{6x^2(2 - 2x^2 + (1 + x^2)\ln x^2)}{(x^2 - 1)^3} \quad (4-9)$$

and $x_f = \tilde{m}_{fL}/\tilde{m}_{fR}$. The remaining two-loop corrections, $\Delta^{(2)}\lambda^{\text{EW-QCD}}$, that involves terms with a mixture between the EW and the strong gauge couplings at $O(y_{t,b}^2 g^2 g_s^2)$, $O(y_{t,b}^2 g'^2 g_s^2)$, $O(g^4 g_s^2)$ and $O(g'^4 g_s^2)$, have been recently computed in [130]. The SM parameters in the threshold corrections of eq. (4-7) are \overline{MS} -renormalized quantities. The matching conditions for the dominant SM parameters, y_t and g_s , can also be found in [121, 125].

In order to get a three-loop running Higgs boson mass in the \overline{MS} scheme at the scale M_t , one has to multiply $\lambda(M_t)$, which comes from the solution of the three-loop SM RGEs with the boundary condition in eq. (4-7) evaluated at $Q = M_{SUSY}$, by $2v^2(M_t)$, where $v(M_t)$ is the \overline{MS} vev evaluated at M_t . In turn, the physical Higgs mass requires to solve the pole equation

$$p^2 - 2\lambda(M_t)v^2(M_t) + \widetilde{\prod}_{hh}^{SM}(p^2) = 0, \quad (4-10)$$

with the SM Higgs boson self-energy,

$$\widetilde{\prod}_{hh}^{SM}(p^2) = \left[\prod_{hh}^{SM}(p^2) - \frac{1}{\sqrt{2}v} T_h^{SM} \right]_{fin}, \quad (4-11)$$

renormalized in the \overline{MS} scheme but with the Higgs tadpoles renormalized to zero, i.e. $\delta T_h^{SM} = -T_h^{SM}$. Thus, self-energy diagrams with tadpole insertions are not considered and the vev corresponds to the minimum of the Higgs effective potential.

The procedure of matching the MSSM to a renormalizable EFT in the unbroken phase of the EW symmetry amounts to neglecting corrections suppressed by powers of v^2/M_{SUSY}^2 . Those corrections can in fact be mapped to the effect of non-renormalizable, higher-dimensional operators in the EFT Lagrangian. If the higher dimensional operators are not included, such as the pure SM as EFT, the contributions suppressed by the heavy scale M_{SUSY} are not

considered. Consequently, the EFT calculation is less accurate than the fixed-order one for low SUSY scales of the order of $M_{SUSY} \lesssim 1$ TeV. Due to the presence of the large logarithms, the fixed-order calculation loses accuracy for M_{SUSY} above a critical SUSY mass scale, estimated to be about $M_{SUSY}^C \approx 1.2$ TeV in [41], whereas above that scale the EFT calculation is more accurate.

In the version 2.14 of FeynHiggs [56] both approaches, the fixed-order and the EFT approach, are combined in order to supplement the full one-loop, leading and sub-leading two-loop diagrammatic results with a resummation of the leading + next to leading (LL+NLL) [120] and next to next to leading (NNLL) [147] logarithmic contributions coming from the top/stop sector. For the resummation of large logarithms up to NLL two-loop RGEs and one-loop matching conditions are needed, accordingly, the resummation up to NNLL requires three-loop RGEs and two-loop matching conditions. The hybrid results obtained from the combination of the two approaches are added into the pole equation of the full MSSM

$$p^2 - m_h^2 + \widetilde{\prod}_{hh} (p^2) + \Delta_{hh}^{log} = 0, \quad (4-12)$$

through the shift Δ_{hh}^{log} which contains the resummed large logarithms from the EFT as well as the logarithmic terms already present in the fixed-order Higgs self-energies,

$$\Delta_{hh}^{log} = - [2\lambda(M_t)v^2(M_t)]_{log} - \left[\widetilde{\prod}_{hh} (m_h^2) \right]_{log}. \quad (4-13)$$

The subscript "log" means that only logarithmic terms are considered. The logarithms in the Higgs self-energy appear explicitly only after expanding in v/M_{SUSY} . This subtraction term ensures that the one- and two-loop logarithms, already contained in the fixed-order FD computation, are not counted twice. In general the higher-order logarithms obtained from the EFT and the hybrid approaches are not the same because the determination of the poles of the propagators (eq. 4-10 and eq. 4-12) are performed in different models. However, this difference, which comes from the momentum dependence of the two-loop order non-SM contributions to the Higgs self-energy, cancels out with contributions coming from the subloop renormalization in the heavy SUSY limit, as was explicitly shown in [157]. Besides the unwanted effects from incomplete cancellations in the determination of the Higgs propagator pole, the effects due to non-logarithmic terms and its parametrization as well as the higher-order terms coming from the scheme conversion between OS and \overline{DR} parameters are all included into FeynHiggs 2.14 [56].

4.2. Comparison of the EFT hybrid and three-loop fixed-order calculations of M_h

In this section we present a numerical comparison of our three-loop fixed-order predictions of M_h to the numerical predictions coming from FeynHiggs 2.14. We have chosen a \overline{DR}

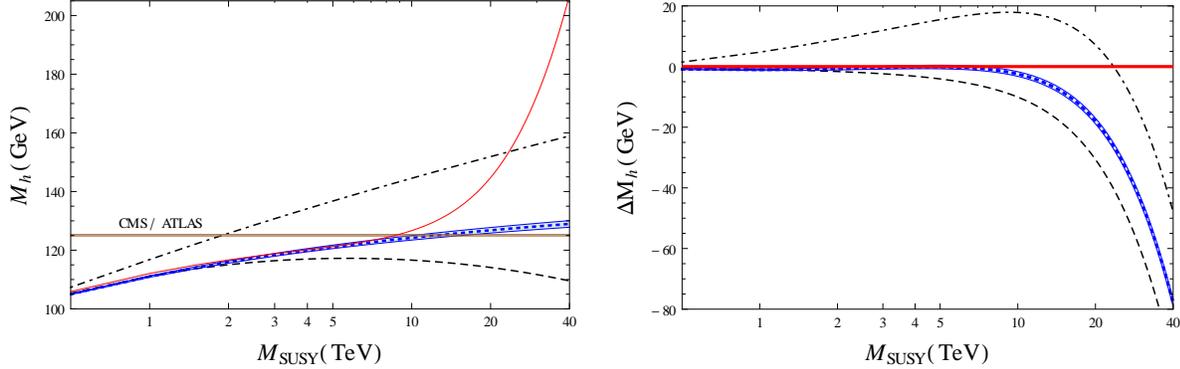


Figure 4-1.: Comparison of the M_h predictions of FeynHiggs with the three-loop fixed-order computation of M_h at $O(\alpha_t\alpha_s^2)$ in the heavy SUSY limit. The dot-dashed and the dashed lines are the fixed-order results of FeynHiggs at one and two -loop level respectively. The blue dotted line contains the NNLL resummation of the large logarithms in FeynHiggs. The blue band corresponds to the uncertainty in the NNLL prediction taken from FeynHiggs. The brown band is the CMS/ATLAS Higgs boson mass, $M_h^{exp} = 125.09 \pm 0.24$ GeV. The red solid line represents our three-loop fixed-order predictions. **Left:** Dependence of M_h on the super-symmetric scale M_{SUSY} for a vanishing stop mixing, $X_t/M_{SUSY} = 0$. **Right:** Numerical differences between the FeynHiggs predictions and the three-loop fixed-order predictions of M_h .

renormalization of the stop sector with the renormalization scale set to M_{SUSY} , which is equivalent to set $Q_t = -1$ in FeynHiggs. The one-/two-loop fixed-order and the EFT-hybrid FeynHiggs predictions are fixed such that the full MSSM is considered (`mssmpart=4`) in its real version (`higgsmix=2`, `tlCplxApprox=0`), no approximation is taken for the one-loop result (`p2approx=4`) and the $O(\tan^n\beta)$ corrections are resummed (`botResum=1`). In particular, when the resummation of the large logarithms is included, we use the full LL, NLL and NNLL resummation (`looplevel=2`, `loglevel=3`). The top quark mass is renormalized in the SM \overline{MS} scheme at NNLO (`runningMT=1`) since for loglevel different from zero a \overline{DR} renormalization is not allowed. The input flags of FeynHiggs 2.14.3 are explicitly indicated, for more details the online manual of the code can be consulted at [186]. To obtain the pole mass M_h at three-loop level in the fixed-order approach, we have introduced the $O(\alpha_t\alpha_s^2)$ corrections as constant shifts in the FeynHiggs 1-loop + 2-loop Higgs renormalized self-energies (`looplevel=2` and `loglevel=0`) with the help of the function `FHAddSelf` but in this case we have used a \overline{DR} renormalization of the top quark mass. In order to assure a correct evaluation of the parameters α_s and M_t in the \overline{DR} scheme at the desired perturbative order, we have used the program RunDec [187–189] and its supersymmetric extension, decSUSY. We start by considering the FeynHiggs fixed-order, FeynHiggs NNLL hybrid and three-loop $O(\alpha_t\alpha_s^2)$ predictions. The left plot of Figure 4-1 shows the dependence of M_h on M_{SUSY} for a vanishing stop mixing, $X_t/M_{SUSY} = 0$, at the kinematic point $A_{e,\mu,\tau,u,d,c,s,b} = 0$ and

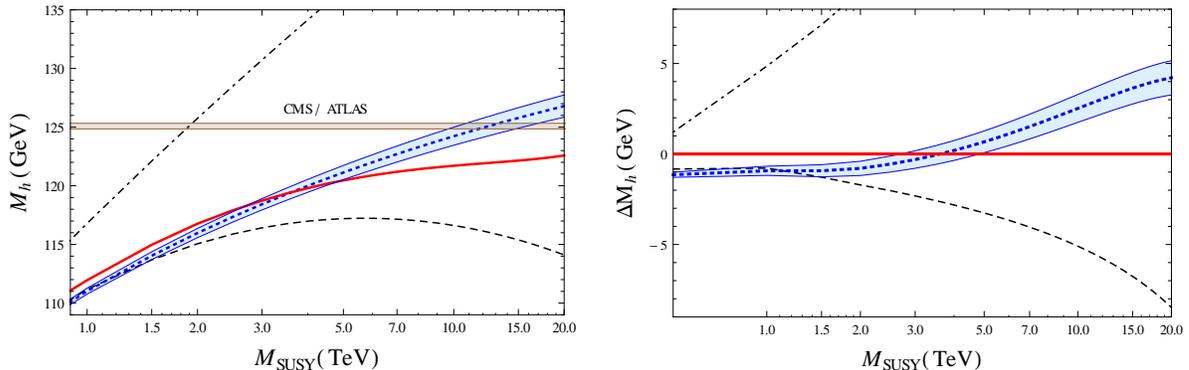


Figure 4-2.: Numerical comparison of the M_h predictions in a scenario where $M_{\tilde{g}} = 1.5$ TeV and $X_t/M_{SUSY} = 0$. These plots follow the same conventions as in the Figure 4-1. **Left:** Evolution of M_h as a function of M_{SUSY} . **Right:** Differences between the three-loop fixed-order and the FeynHiggs predictions.

$\tan\beta = 10$, whereas the right plot shows the numerical differences between all the considered FeynHiggs results and the $O(\alpha_t\alpha_s^2)$ prediction of M_h . In order to draw these plots we have adopted the heavy SUSY limit (eq. 3-38) and we have followed the next conventions. The one and two-loop fixed-order results of FeynHiggs are represented with the dot-dashed and the dashed lines respectively. The blue dotted line contains, in addition, the resummation of the large logarithms up to NNLL order. The blue band corresponds to the uncertainty in the NNLL prediction computed with the help of the FeynHiggs function `FHUncertainties` for the flag choice: `mssmpart = 4, looplevel = 2, loglevel = 3, runningMT = 1`. In principle three effects are taken into account: i) the variation of the renormalization scale from $M_t/2$ to $2M_t$, ii) the use of M_t^{pole} instead of M_t^{run} in the two-loop corrections and iii) the exclusion of higher order resummation effects in M_b . The brown band is the experimental Higgs boson mass and its corresponding uncertainty, we have adopted the combined CMS/ATLAS result of the RUN 1 at the LHC, $M_h^{exp} = 125.09 \pm 0.24$ GeV [6], since there is not yet an official combined result for RUN 2 [7,8] observations. Finally, the red solid line contains our three-loop fixed-order corrections.

The first thing to note here (and also in Figure 4-2) is that the higher-order large logarithms coming from the EFT hybrid approach at NNLL level produce a growing positive shift on the two-loop predictions reaching a size of about 20 GeV for $M_{SUSY} = 40$ TeV. Additionally, the NNLL predictions are in a very good agreement with the three-loop $O(\alpha_t\alpha_s^2)$ results for M_{SUSY} less than the value $M_{SUSY} \lesssim 10$ TeV. On the right graph of Figure 4-1 one can see that in the region 2.2 TeV $\lesssim M_{SUSY} \lesssim 7.4$ TeV there is an approximately constant difference of about 0.2 GeV between the red solid and the blue dotted line which is within the theoretical uncertainty (blue band) estimated to be about 0.6 GeV. Below this region the agreement is still good with a numerical difference of at most 1 GeV. However, for scales above 10 TeV the effects of the large logarithms in the red curve start to be relevant, the

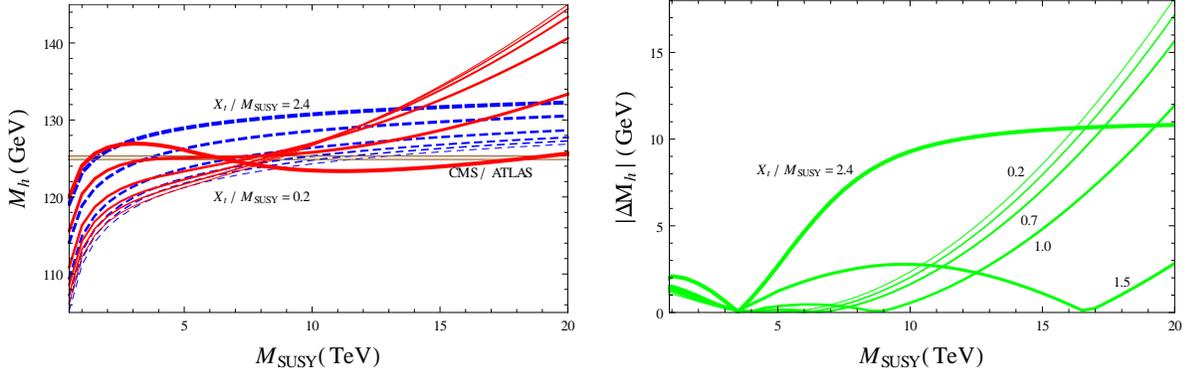


Figure 4-3.: Numerical comparison of the M_h predictions for a non-vanishing stop mixing in the heavy SUSY limit. The blue dashed lines are the NNLL predictions of FeynHiggs and the red solid lines represent our three-loop fixed-order predictions. The brown band is the CMS/ATLAS Higgs boson mass, $M_h^{exp} = 125.09 \pm 0.24$ GeV. **Left:** M_h as a function of M_{SUSY} for different stop mixing values, $X_t/M_{SUSY} = 0.2, 0.5, 0.7, 1.0, 1.5$ and 2.4 . **Right:** Absolute numerical differences between the three-loop fixed-order predictions and the NNLO results of FeynHiggs plotted in the left figure.

difference between the two results rapidly increases up to ~ 21 GeV when M_{SUSY} grows to up to 20 TeV and grows monotonically reaching 78 GeV at $M_{SUSY} = 40$ TeV. This pronounced behaviour depends crucially on our election of the input parameters $M_{\tilde{g}}$ and X_t . Note that according with the discussion of Section 3.3, the presence of n -loop logarithms of the form $\log^n(M_{SUSY}/M_t)$ in the master integrals of Figure 3-5, which are the basis for the three-loop fixed-order Higgs self-energy corrections in the heavy SUSY limit, are the source of these additional large contributions in the three-loop predictions of M_h .

In Figure 4-2 we show the numerical comparison between two results. i) Our three-loop $O(\alpha_t\alpha_s^2)$ predictions of M_h (red curve), where the heavy SUSY limit has been smoothed to include an additional SUSY scale, the gluino mass $M_{\tilde{g}}$. ii) The FeynHiggs prediction of M_h including the resummation of the large logarithms up to NNLL order (blue dashed curve). The effects of a gluino threshold are not included in the NNLL resummation procedure since three-loop RGEs for an appropriate extension of the Standard Model with the gluino as additional fermion, for instance as a singlet of the gauge group, are not included in FeynHiggs. The NNLL resummation is thus restricted to the case $M_{\tilde{g}} = M_{SUSY}$. However, the numerical effects due to a gluino threshold in the EFT computation of M_h is numerically small, about 0.2 GeV [147], and therefore can be safely neglected. The fixed-order corrections instead, capture almost the entire effect of varying $M_{\tilde{g}}$. In [147] was shown that the diagrammatic two-loop correction to M_h gives a sizable contribution of up to ~ 2 GeV for the case of maximal stop mixing. The three-loop fixed-order corrections with the added gluino can also be sizeable, specially for large SUSY scales. We have considered a gluino mass of $M_{\tilde{g}} = 1.5$ TeV. The inclusion of this additional scale produces significant differences between the $O(\alpha_t\alpha_s^2)$ and the NNLL results. Note that the red curve includes not only the gluino effects

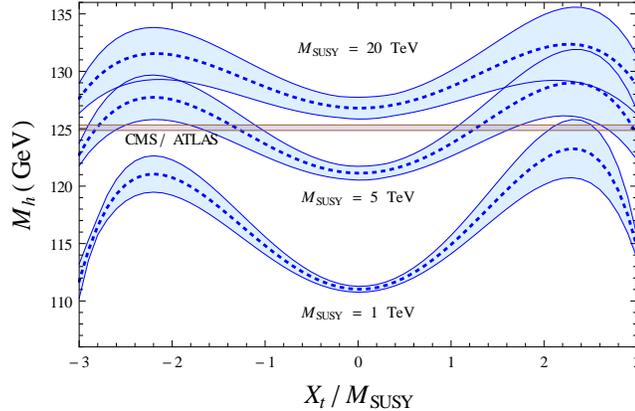


Figure 4-4.: Dependence of M_h on X_t/M_{SUSY} in the heavy SUSY limit evaluated at the same kinematic point considered in Figure 4-3 with $\tan\beta = 10$ and $M_{SUSY} = 1$ TeV, 5 TeV and 20 TeV. The blue lines represent the NNLL predictions coming from FeynHiggs and the blue bands are their corresponding theoretical uncertainties.

but the complete dynamics, that is to say, the large logarithms of the form $\ln(M_{SUSY}/M_t)$ and $\ln(M_{SUSY}/M_{\tilde{g}})$ are included. For small SUSY scales below ~ 3.5 TeV the difference is always less than 1.3 GeV. For large SUSY scales ($M_{SUSY} > 3.5$ TeV) this difference grows to a maximum value of 4 GeV when $M_{SUSY} = 20$ TeV. Nevertheless, the numerical effect of the large logarithms in the red curve is reduced by a factor of around 5 regarding the results shown in Figure 4-1. Lastly, we have studied the dependence of the NNLL and three-loop M_h predictions on the stop mixing parameter X_t in the heavy SUSY limit.

In Figure 4-3 we have increased the value of X_t/M_{SUSY} from 0.2 (thin curves) to 2.4 (thick curves). We observe a good agreement between the two predictions for small SUSY scales up to $M_{SUSY} = 10$ TeV, which is in accordance with previous comparisons of fixed-order and EFT calculations [138, 143]. However, for high energy scales above $M_{SUSY} \gtrsim 10$ TeV there is a large variation of the three-loop fixed-order curves which is observed neither in the NNLL FeynHiggs curves nor in the three-loop EFT and hybrid results presented in [55, 138, 143] where the resummation of the large logarithmic contributions is included. In particular, when X_t/M_{SUSY} is equal to 1.5, which is an inflexion point where the curvature of $M_h(X_t)$ changes its sign as you can visualize with the help of the Figure 4-4, the numerical differences between the red and the blue curve remain lesser than 3 GeV up to $M_{SUSY} = 20$ TeV. In the case of maximal stop mixing, $X_t/M_{SUSY} = 2.4$, where the prediction of M_h takes its higher value (see thickest lines in Figure 4-3 and also Figure 4-4), the difference between the two results is almost constant for large SUSY scales amounting a size of about 10 GeV. The other considered X_t values show a numerical difference that grows without boundary as a function of M_{SUSY} . Due to the large variation observed in the red and green curves, it is not possible to derive a systematic improvement of the effect of the large logarithms in the three-loop fixed-order curves when X_t is changed.

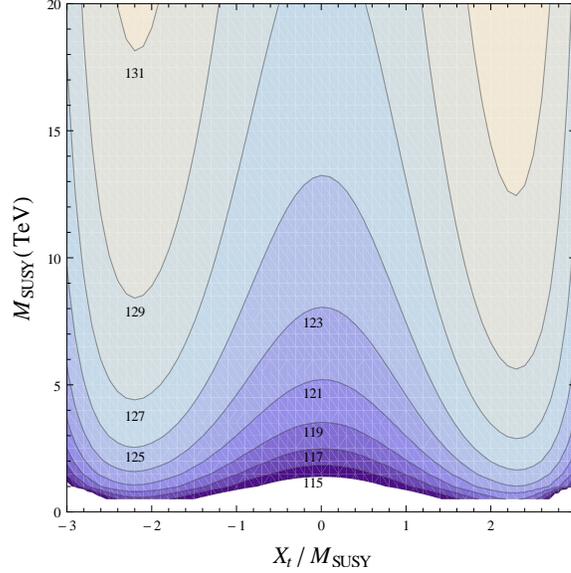


Figure 4-5.: Dependence of M_h on M_{SUSY} and X_t in the heavy SUSY limit. We have used $\tan\beta = 10$. The gray lines represent the values of M_{SUSY} and X_t which produce the same Higgs boson mass. The predicted value of M_h increases monotonically with M_{SUSY} .

4.3. Phenomenological bounds on the SUSY scale

We further explore the dependence of the Higgs boson mass on the SUSY input parameters M_{SUSY} , X_t and $\tan\beta$ in the heavy SUSY limit. The figures 4-1 to 4-4 show that the predicted value of M_h grows when M_{SUSY} increases and reach a maximum value at the critical point $X_t/M_{SUSY} = 2.4$, whose location is independent of M_{SUSY} . It suggests that one can find boundaries for the region of rMSSM parameters which put further constraints on M_h . Figure 4-5 shows the numerical values of X_t/M_{SUSY} and M_{SUSY} which produce the same Higgs mass prediction (gray curves). We have considered values of M_h from 115 GeV to 131 GeV and set $\tan\beta = 10$. We observed here that there is a minimum value of M_{SUSY} , located at the maximal point $X_t/M_{SUSY} = 2.4$, which is compatible with some election of the Higgs boson mass. Moreover, in the case of non stop mixing ($X_t = 0$) one can find the higher value of M_{SUSY} compatible with a given M_h . These extrema values grow when we consider higher values of M_h . This behaviour can also be seen at the intersection of the brown band with the blue dashed lines in Figure 4-3 for a 125 GeV Higgs mass.

If we use the combined CMS/ATLAS measured Higgs boson mass within the actual combined uncertainties, $M_h^{exp} = 125.09 \pm 0.24$ GeV, we will be able to fix upper and lower bounds on the SUSY scale M_{SUSY} in the benchmark scenario considered in this work. Figure 4-6 shows the 125.09 GeV contours (gray lines) as a function of M_{SUSY} , $\tan\beta$ (**Left:** for values of X_t/M_{SUSY} from 0 to 2.4) and X_t/M_{SUSY} (**Right:** for values of $\tan\beta$ from 4 to 30). The blue and the brown regions refer to the SUSY parameters compatible with M_h^{exp} . The purple lines

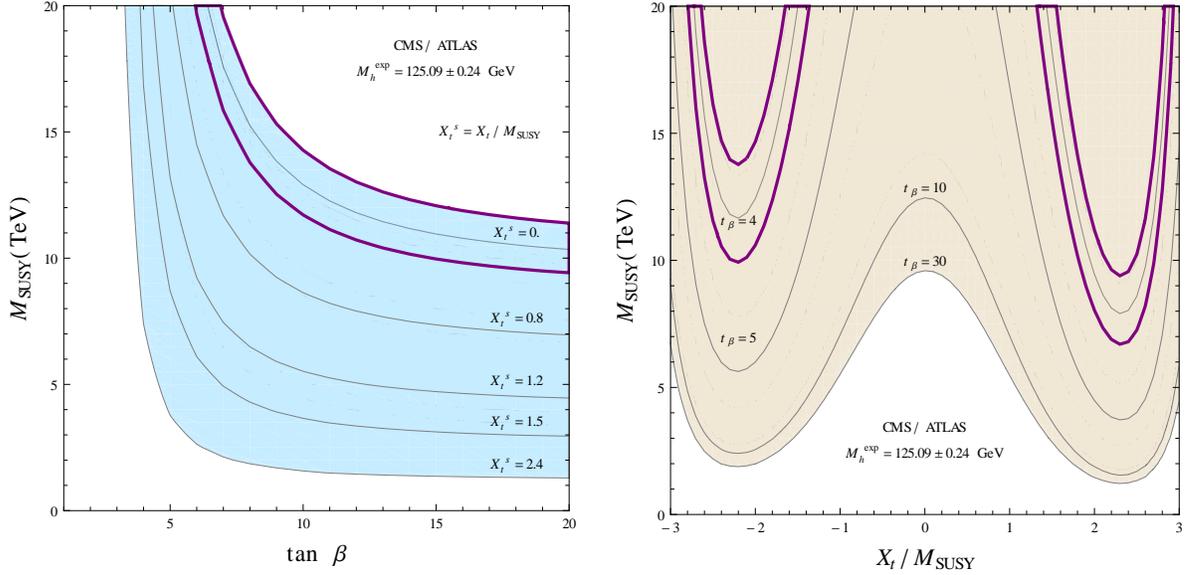


Figure 4-6.: Region of rMSSM parameters in the heavy SUSY limit which is compatible with the central value and the combined uncertainty of the CMS/ATLAS Higgs boson mass, $M_h^{exp} = 125.09 \pm 0.24$ GeV. **Left:** Gray lines represent the points $(M_{SUSY}, \tan \beta)$ compatible with a 125.09 GeV Higgs mass for different values of the stop mixing parameter, $X_t/M_{SUSY} = 0, 0.8, 1.2, 1.5, 2.4$. The purple line represents the combined uncertainty for the case of zero stop mixing. **Right:** Gray lines are the 125.09 GeV contours as a function of M_{SUSY} and X_t/M_{SUSY} for different values of the parameter $\tan \beta$, $\tan \beta = 4, 5, 10, 30$. The purple lines are the points compatible with the combined uncertainty for the lowest value of $\tan \beta$ considered.

represent the combined uncertainty for the cases enclosed inside. Notice that if $\tan \beta \leq 10$ then M_{SUSY} strongly depends on $\tan \beta$, moreover the parameter region of $\tan \beta \lesssim 3$ is incompatible with the LHC observations of the Higgs boson mass if one considers SUSY scales below 20 TeV. For values above 10, the dependence is marginal and the curves flatten. As a consequence, at low $\tan \beta$ values, independent of the election of X_t , it is not possible to find upper bounds on the required SUSY scale from the CMS/ATLAS Higgs mass value. However, for higher values ($\tan \beta \gtrsim 10$), due to the curves are almost constant, one can identify a lower bound for $X_t/M_{SUSY} = 2.4$ and an upper bound for a vanishing stop mixing parameter ($X_t = 0$). When $\tan \beta = 10$, which is the point considered in all the above plots of this section, we find that M_{SUSY} must be at most 12.5 ± 1.2 TeV (see purple line in left plot) in order to be in agreement with the CMS/ATLAS Higgs mass value. Besides, the upper bound on M_{SUSY} can be reduced up to 9.6 TeV for $\tan \beta = 30$ and $X_t = 0$. One can significantly lower the required value of M_{SUSY} to 1.2 TeV when $|X_t/M_{SUSY}|$ increases up to 2.4 and for $\tan \beta = 30$.

The region $M_{SUSY} > 12.5 \pm 1.2$ TeV, where the three-loop fixed-order results blow up, is excluded by the combined CMS/ATLAS Higgs mass value in the simple scenario consider

here where $\tan\beta$ takes large values. The coming combined result for RUN 2 by ATLAS and CMS will reduce the current uncertainty and therefore the upper bound on the SUSY scale could be reduced even more.

4.4. Vacuum stability problem

In the previous section we have been able to find an upper bound on the SUSY scale in a scenario where $\tan\beta$ is large; however, for small $\tan\beta$ values such an upper bound is missing. There is still the possibility to use the vacuum stability of the Higgs potential to find a global upper bound on M_{SUSY} including the region $\tan\beta < 10$, as was discussed in [41]. The estimated bound obtained in this work is of the order of 10^{11} GeV; nevertheless, this result is not conclusive because it was derived without including the full MSSM Higgs potential and is valid in the \overline{DR}' scheme, where m_ϵ is minimally renormalized and its dependence is decoupled from the observables through appropriated shifts of the physical parameters [46, 75]. A phenomenological analysis in the \overline{DR} scheme including small $\tan\beta$ values and the SM-like Higgs effective potential in the heavy SUSY limit will be the subject of discussion in this section. We start by describing the vacuum stability problem in the SM and then we use this analysis to derive the required M_{SUSY} upper bounds.

The stability of the SM vacuum is determined from the 1PI Higgs effective potential. This potential contains all the SM dynamics and allows obtaining the vacuum expectation value from the electroweak phase transition. Although the effective potential is gauge and scheme dependent, its value at any stationary point is gauge and scheme invariant, as can be seen from the Nielsen identity [190]. Correspondingly, the vev of the Higgs field can be calculated at any particular gauge. The Higgs effective potential in the SM is completely known up to two-loop order [191] while at three [192] and four [193] -loop level it is known in the approximation where the strong and top-Yukawa coupling are large compared to all the other SM parameters. The analysis of the stability must be obtained from a renormalization group improved (RGI) version of the effective potential and requires the study of the renormalization group equations of all the SM couplings ($g_k = \lambda, y_t, g, g', g_s$, etc) that includes the determination of the matching relations between the running coupling constants and the values of the SM observables [194], a sort of boundary conditions for those RGEs which can include the effects of a heavy SUSY threshold according to eq. (4-7) when the SM is considered as a low-energy EFT of the rMSSM. For large values of the Higgs classical field, $h_c \gg v$ where v is the EW minimum, the effective potential of eq. (4-2) improved by the RGEs approximates to

$$V(h_c)^{RGI} \approx \frac{\lambda(Q)}{4} h_c^4(Q). \quad (4-14)$$

The stability of the potential translates to the study of the evolution of the Higgs self-coupling $\lambda(Q)$ as a function of the scale Q , more precisely to its positivity at large scales.

As was discussed in Section 4.1, the running of $\lambda(Q)$ is obtained by numerically solving the system of non-linear ordinary differential equations defined by the beta functions of the SM couplings (see eq. 4-5) while the boundary conditions are determined from the relations between the parameters in the \overline{MS} scheme and the physical masses of the particles (M_k) according to

$$g_k(Q) = c_i \frac{G_F}{\sqrt{2}} M_k^2 + \Delta g_i(Q), \quad (4-15)$$

where G_F is the Fermi coupling constant which is related to the Higgs vev as $v = \frac{2^{-1/4}}{G_F^{1/2}}$, c_i are normalization constants and $\Delta g_i(Q)$ are the threshold corrections to the matching conditions. Currently, the vacuum stability analysis is done at next to next to leading order (NNLO) involving the state-of-the-art computations for the running couplings, i.e. three-loop beta functions and two-loop matching conditions. The three-loop beta functions have been completely computed. For the EW gauge couplings g , g' and the strong gauge coupling g_s the beta functions can be found in [131, 132]. The beta function of the top Yukawa coupling was fully computed in [133] and finally the RGEs of the quartic coupling λ and the quadratic parameter m^2 up to three-loop level was obtained in [134, 135]. In the context of the pure SM, that is without including the SUSY effects, the two-loop threshold corrections of all the relevant SM couplings are found in [10], where the NNLO corrections of $\lambda(Q)$ was computed in the EW gaugeless limit. The full NNLO computation for λ , m^2 and y_t is found in [12]. An implementation of the three-loop SM beta functions and anomalous dimensions as well as the corresponding two-loop matching conditions can be found in the public codes `mr` [96] and `SMDR` [97–99]. The main references containing the threshold corrections in the heavy SUSY limit of the rMSSM were given in Section 4.1. It is worth mentioning that the three-loop threshold corrections are not relevant in the NNLO stability analysis as was proved in [195, 196]. The L-loop effective potential improved by (L+1)-loop RGEs resums all the Lth-to-leading logarithm contributions. Therefore, for the L-loop vacuum stability analysis, the L-loop threshold corrections to the matching conditions are sufficient.

If one makes the bold assumption that there is no new physics up to very high energies, the parameter $\lambda(Q)$ remains weak from the EW scale until the Planck scale and runs negative at an intermediate scale of the order of $\Lambda_I = 10^{10}$ GeV for the central values of the top mass ($M_t \approx 173.3$ GeV) and the Higgs mass ($M_h \approx 125.09$ GeV) as is shown in Figure 4-7 Left. The trouble with λ becoming negative at a scale lower than Λ_P is that it will cause an instability in the Higgs effective potential at the scale Λ_I . The instability occurs due to the effects of the top quark corrections. For instance in the one-loop RGI potential and therefore in $\lambda(Q)$ they contribute as $-\frac{3y_t^4}{16\pi^2} 2\Gamma$, being Γ the integral of the Higgs anomalous dimension. For small values of λ this is the term dominating the evolution and λ is going to evolve towards smaller values eventually crossing zero. Consequently, at high energy scales the RGI potential is either not bounded from below or it develops a second minimum that can be deeper than the EW one. In both cases the idea that the SM can be considered as a valid

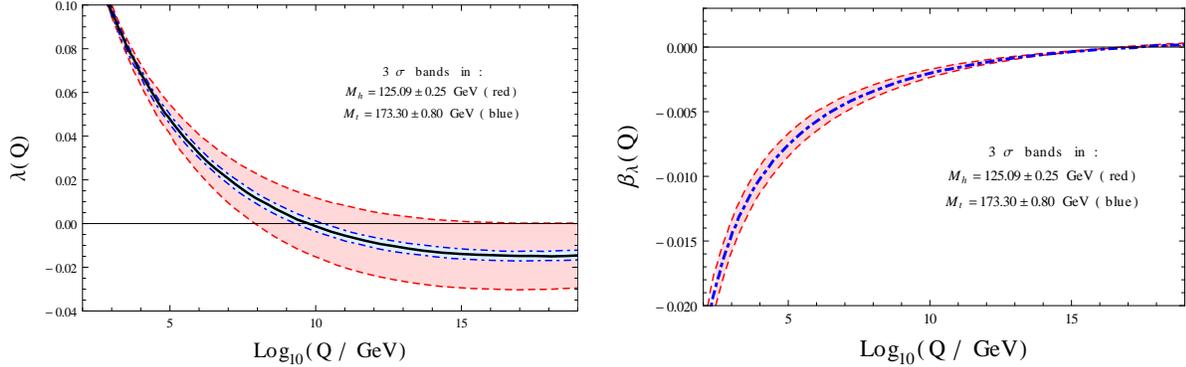


Figure 4-7.: **Left:** Evolution of the Higgs quartic self-coupling λ as a function of the renormalization scale Q . **Right:** Beta function of the Higgs self-coupling. We have included the uncertainties in M_t and M_h as is indicated. The plots were drawn with the help of the program SMDR.

theory up to Λ_P is in trouble because v is no longer the true minimum of the potential and there is a tunnelling probability between the false vacuum v and the true vacuum at high field values.

The requirement of new physics appearing below the instability scale to cure the instability of the SM potential is mandatory if the lifetime of EW vacuum is shorter than the life of the universe. In other case, we can accept a metastable SM vacuum. In fact, the Figure 4-7 Left shows that λ does become negative but never too negative, it is bounded from below with a bound higher than $\lambda_0 = -0.025$, its evolution is slowing down and is bounded at high energy because its beta function at high energy becomes very small, vanishing close to Λ_P as can be seen in Figure 4-7 Right. This implies a total probability for vacuum decay,

$$\wp \sim \tau_U^4 \Lambda_B^4 e^{-S(\Lambda_B)} \quad ; \quad S(\Lambda_B) = \frac{8\pi^2}{3|\lambda(\Lambda_B)|}, \quad (4-16)$$

extremely small, less than 10^{-100} , or a lifetime of the EW vacuum much larger than the age of the universe $\tau_U \approx 14 \times 10^9$ years, stating that our vacuum is metastable. In Eq. (4-16) Λ_B is determined as the scale at which \wp is maximized [197].

The metastability condition is generally presented with the help of a phase diagram in the $M_h - M_t$ plane. Neglecting the presence of new interactions up to Λ_P , the zero-temperature meta-stability analysis provides the graph given by Figure 4-8. This phase diagram is divided into three different sectors. An absolute stability region where the effective potential evaluated in the EW minimum v is lower than the effective potential evaluated at the new minimum v' , $V_{RGI}(v) < V_{RGI}(v')$. A meta-stability region where the effective potential at the new minimum is lower than the effective potential at the electroweak minimum, $V_{RGI}(v') < V_{RGI}(v)$, but with the life-time of the EW vacuum larger than the age of the universe, $\tau > \tau_U$. An instability region where $V_{RGI}(v') < V_{RGI}(v)$ but the life-time of the EW vacuum is lower than the age of the universe, $\tau < \tau_U$. The phase diagram also has two division lines. The

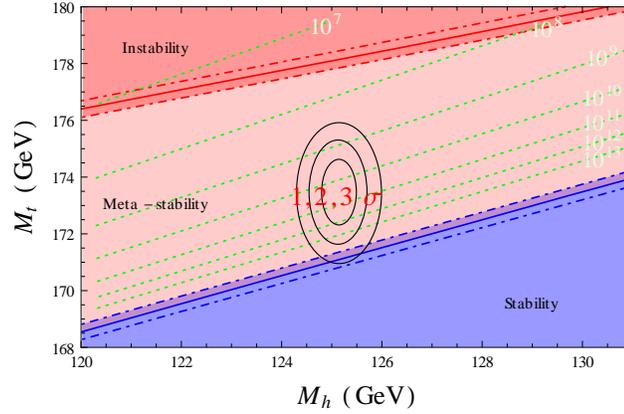


Figure 4-8.: SM vacuum stability phase diagram in terms of the Higgs and top quark masses. The region plotted shows the dominant experimental range of M_h and M_t .

stability line separates the stability and the meta-stability regions, this line is obtained when $V_{RGI}(v) = V_{RGI}(v')$. Whereas, the instability line separates the metastability and the instability regions, this line is obtained when the life-time of the electroweak vacuum is equal to the age of the universe, $\tau = \tau_U$. Finally, the red dot-dashed lines along the borders indicate the uncertainty from $\alpha_s = 0.1184 \pm 0.0007$ GeV and from theoretical errors. The measured values of M_h and M_t appear to be rather special, the SM vacuum is at the border between stability and metastability regions. When its experimental and perturbative errors are taken into account, represented with the 1σ , 2σ and 3σ ellipses in Figure 4-8, the SM could be sitting on the stability region, i.e. it could reach and even cross the stability line, this scenario is known as the *near-criticality*. Including the two-loop threshold corrections of all SM parameters, the estimated overall theory error on $M_h \pm 1.0$ GeV combined with the experimental errors on M_t and α_s gives as result that vacuum stability of the SM up to the Planck scale is excluded at 2.5σ (99.3% C.L. one sided) [10]. There is no conclusive result about the state of the SM vacuum, however the metastability is the preferred option with 99.3% of probability. As a consequence, owing to an intriguing conspiracy of the SM particles masses, it is likely that the higgs potential develops a second minimum as deep as the one corresponding to the electroweak vev.

4.4.1. Vacuum stability constraints on the SUSY scale

In this section we are going to see that it is possible to derive upper bounds over M_{SUSY} for small $\tan\beta$ values if we impose the positivity of the running Higgs self-coupling $\lambda(Q)$ from the EW scale until the next threshold, $Q = M_{SUSY}$, which is equivalent to impose the stability of the SM renormalization group improved Higgs effective potential (see eq. 4-14) up to the scale where supersymmetry is supposed to appear. The SM is considered here as a low-energy EFT of the rMSSM valid in the heavy SUSY limit, where we integrate out all

SQCD particles at the scale M_{SUSY} , and therefore the RGEs correspond to the three-loop SM beta functions while the threshold corrections to the boundary condition for the Higgs quartic coupling (see eq. 4-7) takes the form:

$$\Delta^{(1)}\lambda = \Delta^{(1)}\lambda^{reg} + \Delta^{(1)}\lambda^\phi + \Delta^{(1)}\lambda^{x^1} + \Delta^{(1)}\lambda^{x^2}. \quad (4-17)$$

Note that the effects of the SUSY parameters affects only the boundary conditions. Those parameters are renormalized in the \overline{MS} scheme, for this reason it is necessary to include the term $\Delta^{(1)}\lambda^{reg}$ which accounts for the conversion from the \overline{DR} , where the SUSY parameters are defined, to the \overline{MS} scheme, usually used in the SM:

$$(4\pi)^2\Delta^{(1)}\lambda^{reg} = -\frac{1}{4}g'^4 - \frac{1}{2}g^2g'^2 - \left(\frac{3}{4} - \frac{c_{2\beta}^2}{6}\right)g^4. \quad (4-18)$$

On the other hand, the term $\Delta^{(1)}\lambda^\phi$ in eq. (4-17) represents the one-loop threshold corrections coming from the heavy scalars contributions. Considering only the terms involving the top Yukawa coupling, the correction $\Delta^{(1)}\lambda^\phi$ is reduced to the form:

$$\begin{aligned} (4\pi)^2\Delta^{(1)}\lambda^\phi = & 3y_t^2 \left[y_t^2 + \frac{1}{2} \left(g^2 - \frac{g'^2}{3} \right) c_{2\beta} \right] \ln \left(\frac{m_{\tilde{t}_L}^2}{M_{SUSY}^2} \right) + 3y_t^2 \left[y_t^2 + \frac{2}{3} g'^2 c_{2\beta} \right] \ln \left(\frac{m_{\tilde{t}_R}^2}{M_{SUSY}^2} \right) \\ & + \frac{c_{2\beta}^2}{300} \sum_{i=1}^3 \left[3 \left(\frac{25}{9} g'^4 + 25g^4 \right) \ln \left(\frac{m_{\tilde{u}_{iL}}^2}{M_{SUSY}^2} \right) + \frac{200}{3} g'^4 \ln \left(\frac{m_{\tilde{u}_{iR}}^2}{M_{SUSY}^2} \right) \right. \\ & + \left. \frac{50}{3} g'^4 \ln \left(\frac{m_{\tilde{d}_{iR}}^2}{M_{SUSY}^2} \right) + (25g'^4 + 25g^4) \ln \left(\frac{m_{\tilde{l}_i}^2}{M_{SUSY}^2} \right) + 50g'^4 \ln \left(\frac{m_{\tilde{e}_i}^2}{M_{SUSY}^2} \right) \right] \\ & + \frac{1}{4800} \left[725g'^4 + 1050g'^2g^2 + 1325g^4 - 4c_{4\beta} (25g'^4 + 150g'^2g^2 + 175g^4) \right. \\ & - \left. 9c_{8\beta} (5g'^2 + 5g^2)^2 \right] \ln \left(\frac{m_A^2}{M_{SUSY}^2} \right) - \frac{3}{16} (g'^2 + g^2)^2 s_{4\beta}^2 \\ & + 6y_t^4 \tilde{X}_t \left[F_1(x_t) - \frac{\tilde{X}_t}{12} F_2(x_t) \right] + \frac{3}{4} y_t^2 \tilde{X}_t c_{2\beta} [g'^2 F_3(x_t) + g^2 F_4(x_t)] \\ & - \frac{1}{4} y_t^2 \tilde{X}_t c_{2\beta}^2 (g'^2 + g^2) F_5(x_t). \end{aligned} \quad (4-19)$$

Here $\tilde{X}_t = X_t^2/(m_{\tilde{t}_L} m_{\tilde{t}_R})$ and $x_t = m_{\tilde{t}_L}/m_{\tilde{t}_R}$. In the heavy SUSY limit, where all of the soft breaking masses have a common value M_{SUSY} , the first, second and third lines of eq. (4-19) vanish, leaving only the contribution of the heavy Higgs doublet and the corrections controlled by X_t . Besides the functions F_j with $j = 1, \dots, 5$ become equal to one. The definition of the functions F_j can be consulted in Appendix L. Finally, the terms $\Delta^{(1)}\lambda^{x^1}$ and $\Delta^{(1)}\lambda^{x^2}$ come from the higgsino-gaugino contributions. The first one contains the proper

threshold corrections to the Higgs quartic coupling:

$$\begin{aligned}
(4\pi)^2 \Delta^{(1)} \lambda^{\chi^4} = & \frac{1}{2} \tilde{\beta}_\lambda \ln \left(\frac{\mu^2}{M_{SUSY}^2} \right) + \left[-\frac{7}{12} f_1(r_1) (g'^4 c_\beta^4 + g^4 s_\beta^4) - \frac{9}{4} f_2(r_2) (g^4 c_\beta^4 + g^4 s_\beta^4) \right. \\
& - \frac{3}{2} f_3(r_1) g'^4 s_\beta^2 c_\beta^2 - \frac{7}{2} f_4(r_2) g^4 s_\beta^2 c_\beta^2 - \frac{8}{3} f_5(r_1, r_2) g^2 g'^2 s_\beta^2 c_\beta^2 \\
& - \frac{7}{6} f_6(r_1, r_2) g^2 g'^2 (c_\beta^4 + s_\beta^4) - \frac{1}{3} f_7(r_1, r_2) g^2 g'^2 c_\beta^2 s_\beta^2 - \frac{8}{3} f_8(r_1, r_2) g^2 g'^2 s_\beta c_\beta \\
& + \frac{2}{3} f(r_1) g'^2 s_\beta c_\beta [\lambda - 2g'^2] + 2f(r_2) g^2 s_\beta c_\beta [\lambda - 2g^2] \\
& \left. + \frac{1}{3} G(r_1) \lambda g'^2 + G(r_2) \lambda g^2 \right], \tag{4-20}
\end{aligned}$$

where $r_j = M_j/\mu$, with M_j the masses of the gauginos, and

$$\begin{aligned}
\tilde{\beta}_\lambda = & 2\lambda (g'^2 + 3g^2) - g'^4 (c_\beta^4 + s_\beta^4) - 5g^4 (c_\beta^4 + s_\beta^4) \\
& - 4g^2 g'^2 s_\beta^2 c_\beta^2 - 2 (g'^2 c_\beta^2 + g^2 s_\beta^2) (g'^2 s_\beta^2 + g^2 c_\beta^2). \tag{4-21}
\end{aligned}$$

Here λ must be expressed in terms of β and the EW gauge couplings according with the eq. (4-3). The definition of the functions f_j , f and G are written in Appendix L. The second higgsino-gaugino contribution emerges in the heavy SUSY limit from the fact that the tree-level part of the matching condition for λ is a function of the EW gauge couplings. The expression is quite simple:

$$(4\pi)^2 \Delta^{(1)} \lambda^{\chi^2} = -\frac{1}{6} c_{2\beta}^2 \left[2g^2 \ln \left(\frac{M_2^2}{M_{SUSY}^2} \right) + (g^2 + g'^2) \ln \left(\frac{\mu^2}{M_{SUSY}^2} \right) \right]. \tag{4-22}$$

For the two-loop threshold corrections, on the other hand, the formula of $\Delta^{(2)} \lambda^{\text{gaugeless}}$ with the full dependence on the SQCD masses is too lengthy to be included here. The derivation of the terms including all contributions controlled by the strong gauge coupling and by the third-family Yukawa couplings can be consulted in [121, 125]. However, in the decoupling limit discussed in this section, the dominant threshold correction at order $g_s^2 y_t^4$ can be recovered directly from the $O(g_s^2 y_t^4 M_t^2)$ correction to the lightest MSSM Higgs boson mass. In particular, it is sufficient to subtract the top-quark contribution from the full MSSM correction, as the given in eq. (21) of [198]. The derived expression is the following:

$$\Delta^{(2)} \lambda^{\text{gaugeless}} \approx \frac{g_s^2 y_t^4}{96\pi^4} \left[-12 \frac{X_t}{M_{SUSY}} - 6 \frac{X_t^2}{M_{SUSY}^2} + 14 \frac{X_t^3}{M_{SUSY}^3} + \frac{1}{2} \frac{X_t^4}{M_{SUSY}^4} - \frac{X_t^5}{M_{SUSY}^5} \right]. \tag{4-23}$$

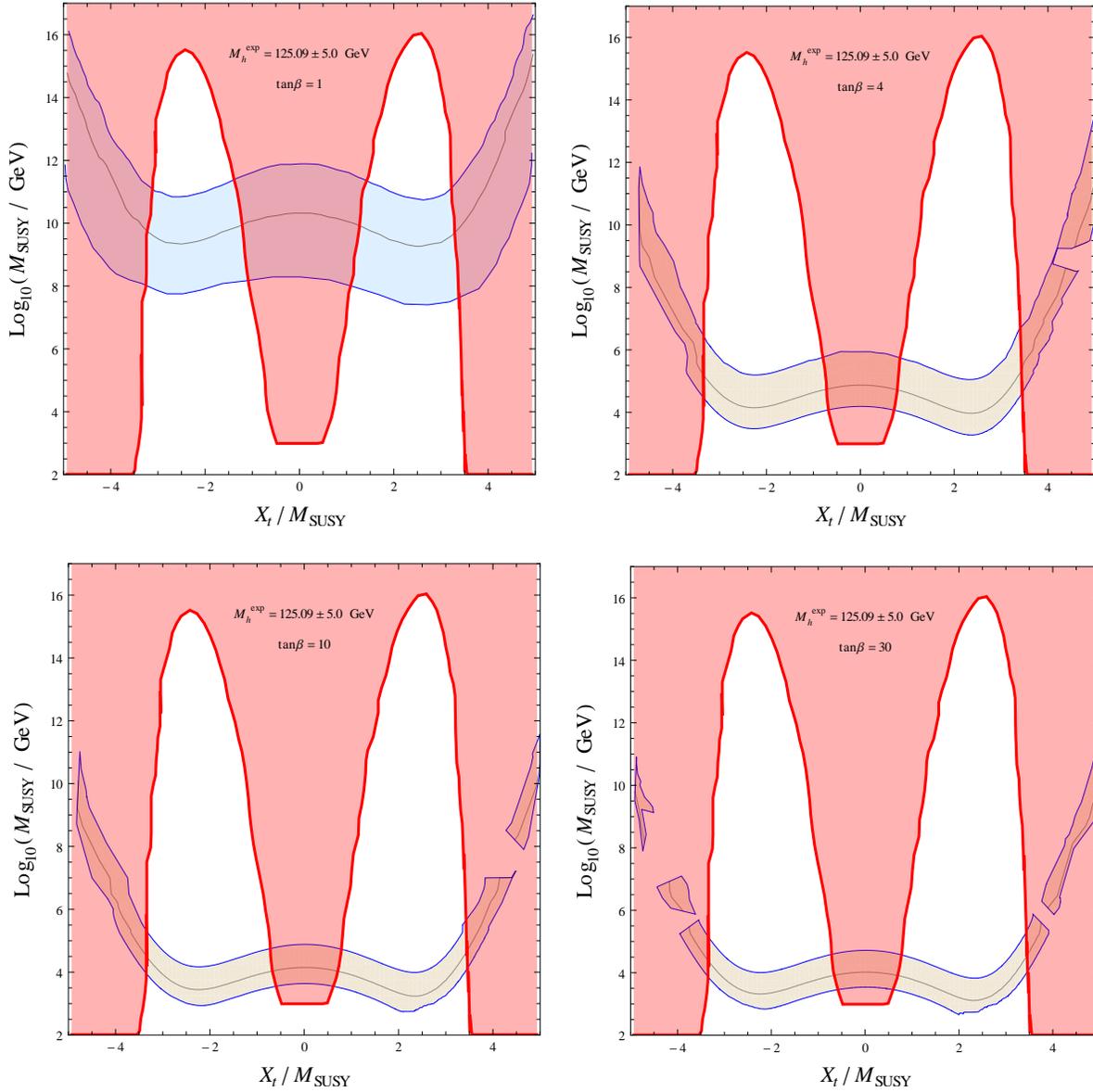


Figure 4-9.: Higgs boson mass predictions as a function of the SUSY scale and the stop mixing parameter in the \overline{DR} scheme. The light blue regions correspond to the points compatible with $M_h^{\text{exp}} = 125.09 \pm 5.0$ GeV for $\tan\beta = 1, 4, 10$ and 30 . The gray lines are the contours for the central value of the CMS/ATLAS Higgs mass. The red regions represent the values of X_t and M_{SUSY} where $\lambda(M_{SUSY})$ becomes negative while the red lines display the parameter space which have $\lambda(M_{SUSY}) = 0$.

Finally, the full expression for the sub-dominant contribution of $\Delta^{(2)}\lambda^{\text{EW}\times\text{QCD}}$ can be consulted in [130], we put here only the terms proportional to the top Yukawa coupling:

$$\begin{aligned}
(16\pi^2)^2\Delta^{(2)}\lambda^{\text{EW}\times\text{QCD}} = & \\
& 4g_s^2y_t^2 \left\{ c_{2\beta}^2(g^2 + g'^2) \left[-\frac{11}{8} - \frac{3}{2}\ln\left(\frac{M_{SUSY}^2}{Q^2}\right) - \frac{1}{2}\ln^2\left(\frac{M_{SUSY}^2}{Q^2}\right) + \right. \right. \\
& \left. \frac{X_t}{3M_{SUSY}} \left(4 + \ln\left(\frac{M_{SUSY}^2}{Q^2}\right) \right) - \frac{X_t^2}{12M_{SUSY}^2} \left(5 - 2\ln\left(\frac{M_{SUSY}^2}{Q^2}\right) \right) - \frac{X_t^3}{6M_{SUSY}^3} \right] \\
& + c_{2\beta}(g^2 + g'^2) \left[-1 - \ln\left(\frac{M_{SUSY}^2}{Q^2}\right) - 2\ln^2\left(\frac{M_{SUSY}^2}{Q^2}\right) + \right. \\
& \left. \left. 3\frac{X_t}{M_{SUSY}}\ln\left(\frac{M_{SUSY}^2}{Q^2}\right) + \frac{X_t^2}{2M_{SUSY}^2} \left(1 - \ln\left(\frac{M_{SUSY}^2}{Q^2}\right) \right) + \frac{X_t^3}{2M_{SUSY}^3} \right] \right\}. \quad (4-24)
\end{aligned}$$

Considering the threshold corrections in eqs. (4-18) - (4-24), the requirement of the positivity of the running Higgs quartic coupling λ can allow an estimation of additional upper bounds for the SUSY scale in a given kinematical point of the supersymmetric parameter space. With this objective, we have studied the dependence of the Higgs boson mass on the SUSY scale, M_{SUSY} , and the stop mixing parameter, X_t , for a given $\tan\beta$ between 1 and 30. The Higgs mass is extracted from the hybrid approach of FeynHiggs 2.14 with the large logarithms resummed at NNLL in the \overline{MS} scheme. We have used the same benchmark scenario considered in sections 4.2 and 4.3 to be consistent with the results of Figure 4-6, but this time we let M_{SUSY} evolve up to 10^{17} GeV and we span values of X_t/M_{SUSY} from -5 to 5 . We have also identified, in a phase diagram X_t vs M_{SUSY} , the values for which λ gets negative.

In Figure 4-9 we show the region of SUSY parameters which are compatible with a Higgs boson mass of $M_h^{exp} = 125.09 \pm 5.0$ GeV (light blue regions) for different values of $\tan\beta$: $\tan\beta = 1, 4, 10$ and 30 . The gray lines correspond to the 125.09 GeV contours. We have pictured the region where the quartic Higgs self-coupling is negative at the SUSY scale, $\lambda(M_{SUSY}) < 0$, leading to an unstable electroweak vacuum (see the red regions). If one demands the stability of the EW vacuum, then the parameter space in the red region are excluded and the intersection of the red border line with the blue region could give us constrains on the M_{SUSY} value as a function of M_h . Note that the region of exclusion occurs in general around $|X_t/M_{SUSY}| \approx 0$ and for large values of X_t , $|X_t/M_{SUSY}| \gtrsim 3$. When X_t is close to zero, the dominant contributions to $\lambda(M_{SUSY})$ come from the Higgsinos and EW gauginos terms of eqs. (4-20) and (4-22) which are negative; however, for slightly large values, $|X_t| \gtrsim 0.5M_{SUSY}$, the positive stop contribution in eq. (4-19) becomes dominant. In particular, for large stop mixing, the stop contribution gets negative, due to the negative terms in eqs. (4-19) and (4-23) are dominant, leading $\lambda(M_{SUSY})$ to negative values as well. On the other hand, we can see that for smaller values of $\tan\beta$ the required M_{SUSY} compatible with M_h^{exp} increases. Thus, the left-top plot of Figure 4-9, with $\tan\beta = 1$, contains the highest upper bound of the SUSY scale derived from the vacuum instability region. Specifically, for

a 125.09 GeV Higgs boson mass and a stop mixing of $|X_t/M_{SUSY}| = 1.2$, the intersection of the gray curve with the blue line provides the bound $M_{SUSY} < 8.34 \times 10^9$ GeV. Assuming an uncertainty of ± 5 GeV on the Higgs boson mass, this bound can reach a maximum value of $M_{SUSY} < 2.39 \times 10^{11}$ GeV for $|X_t/M_{SUSY}| = 1.4$. This result is not very encouraging, the bounds obtained from the positivity of λ for small $\tan\beta$ values are very far away from the M_{SUSY} bounds derived in Section 4.3, where $\tan\beta$ was taken to be large.

5. Conclusions and Perspectives

The main contribution of this thesis is the determination of UV finite expressions for the renormalized three-loop corrections to the neutral CP-even and CP-odd Higgs boson masses of the rMSSM following the Feynman diagrammatic approach at the fixed-order $O(\alpha_t \alpha_s^2)$. We have computed only the dominant contributions coming from the EW gaugeless and the non-light-fermions limits and the approximation of vanishing external momentum transferred in the calculation of the involved self-energy functions. The DRED procedure was adopted to regularize the Feynman amplitudes associated to the Higgs self-energies. Besides, a precise prescription of a mixed \overline{DR}/OS scheme was developed in order to renormalize the local and non-local UV divergences from the three-loop corrections. In particular, the non-local infinities contained in sub-loop diagrams require an additional treatment which includes the evaluation of two-loop SQCD counter-term insertions computed in the \overline{DR} scheme. After regularization, we have reduced the three-loop corrections, using the integration-by-parts recurrence relations, to a small set of master integrals which are different realizations of five three-loop vacuum topologies with at most four independent mass scales. Their numerical evaluation is possible thanks to the dispersion relation techniques. The three-loop vacuum topologies are expressed in terms of one and two-dimensional numerical integrals of elementary functions which can be efficiently evaluated for a general mass pattern. In this way we avoided the asymptotic expansions on the amplitudes at the integral level in the realistic mass hierarchies proposed in [118]. Thus, our work represents an independent check of the results implemented in H3m but also provides a numerical evaluation of the three-loop corrections in the whole supersymmetric parameter space without any assumption about the mass hierarchy.

We have studied the numerical impact of our three-loop corrections in the value of the pole mass M_h for three different benchmark limits: the m_h^{free} , m_h^{max} and m_h^{mod+} scenarios. We have considered scenarios with the SUSY scale M_{SUSY} lower than 1.2 TeV, where a fixed-order calculation have a combined theoretical uncertainty better than the estimated uncertainty from an EFT calculation [41] since the effects of the large logarithmic terms are not relevant when the sparticle masses have values close to M_t . We have investigated the dependence of M_h on the ratio between the vacuum expectation values of the two CP-even Higgs bosons, $\tan\beta$, the soft-breaking trilinear parameter A_t , the renormalization scale μ_r and the CP-odd Higgs boson mass m_A . The three-loop corrections show a good perturbative behaviour, their numerical size is about ten times lesser than the two-loop predictions and the dependence on the renormalization scale is reduced by around a factor two. The contributions yield a

shift in the value of the lightest Higgs boson mass of the order of 1 GeV compared with the two-loop results of FeynHiggs and a shift between -0.4 and 0.4 GeV compared with the three-loop predictions of H3m combined with the lower-order contributions of FeynHiggs. Our results are in agreement within the theoretical composited uncertainty with the predictions of M_h obtained from H3m if the same kinematical limits of the SQCD mass spectrum are employed.

The three-loop fixed-order computation of the lightest rMSSM Higgs boson mass [2] is in a very good agreement with the results of H3m [55] for low SUSY scales ($M_{SUSY} \lesssim 1.2$ TeV). However, for large M_{SUSY} values significant differences are expected and therefore a numerical comparison with the available codes for large SUSY scales was included in this work. We have decided to check our computation of M_h with the three-loop results coming from the EFT hybrid approach implemented in FeynHiggs 2.14 [56] for the same observable. FeynHiggs includes a hybrid procedure which uses an EFT in order to perform a resummation of the large logarithms at high SUSY scales. Their numerical predictions are in a very good agreement with the other fixed-order and EFT codes found in literature. This allowed us to compare our results with a reliable three-loop M_h -prediction for M_{SUSY} up to scales of the order of 40 TeV. We focused on a single SUSY scale scenario in the decoupling limit (heavy SUSY limit) where the heavy particles are integrated out at the scale M_{SUSY} which can take values considerably larger than the EW scale. This limit is considered in order to compare our three-loop results with the hybrid corrections included in FeynHiggs where the SM is the low-energy EFT. Moreover, the region of free SUSY parameters is significantly reduced to just three: $\tan\beta$, X_t and M_{SUSY} , which is convenient from the phenomenological point of view. We specifically contrasted our $O(\alpha_t\alpha_s^2)$ and the FeynHiggs NNLL predictions of M_h at the kinematical point $A_{e,\mu,\tau,u,d,c,s,b} = 0$ and $\tan\beta = 10$. The stop sector was renormalized in the \overline{DR} scheme with the renormalization scale set to $= M_{SUSY}$. We find a very good agreement between the two results for SUSY scales below 10 TeV in the case of vanishing stop mixing ($X_t = 0$). The difference is estimated to be in the range $0.2 \text{ GeV} \lesssim \Delta M_h \lesssim 1 \text{ GeV}$ for the region $M_{SUSY} \lesssim 10$ TeV. Above $M_{SUSY} = 10$ TeV we have observed meaningful differences that increase monotonically with M_{SUSY} . Such a behaviour is expected for high SUSY scales since the $O(\alpha_t\alpha_s^2)$ computation contains now the effects of the large logarithmic contributions. The numerical differences can be reduced through the introduction of an additional SUSY scale, the gluino mass $M_{\tilde{g}}$. The variation of the stop mixing parameter X_t instead does not produce a systematic improvement of the large logarithm effects in the three-loop fixed-order corrections.

A phenomenological analysis where the LHC results are used to study the compatibility of the SUSY parameters space with the combined CMS/ATLAS Higgs boson mass, $M_h^{exp} = 125.09 \pm 0.24$ GeV, shows that the region where the contributions of the large logarithms blow up, is actually excluded. However, this exclusion is valid just for large $\tan\beta$ values, $\tan\beta \gtrsim 10$, where we have derived an upper bound on the needed SUSY scale. For values above $\tan\beta = 10$ the region $M_{SUSY} > 12.5 \pm 1.2$ TeV is ruled out, independent of the

election of the stop mixing value. A global upper bound valid also for any value of $\tan\beta$ cannot be derived from the experimental Higgs mass value. Nevertheless, there is the possibility to use the stability of the SM Higgs effective potential, which translates to the positivity of the running Higgs self-coupling $\lambda(Q)$, to derive upper bounds for the required SUSY scale as a function of M_h for small $\tan\beta$ values. In this case the SM is considered as a low-energy EFT of the rMSSM in the heavy SUSY limit. Thus, $\lambda(Q)$ is numerically obtained from the solution of the system of RGEs of the SM parameters at three-loop order, where the boundary conditions are matching relations that relates the running couplings to the physical observables with two-loop threshold corrections which includes the effects of the rMSSM particles. The bound obtained was far less restrictive. Imposing the stability of the EW vacuum, the instability region $\lambda(M_{SUSY}) < 0$ excludes values above $M_{SUSY} = 8.34 \times 10^9$ GeV for $M_h = 125.09$ GeV. Accepting an uncertainty of ± 5 GeV on the Higgs boson mass, the upper bound can reach a maximum value of $M_{SUSY} < 2.39 \times 10^{11}$ GeV.

As a result of this thesis new perspectives for future research projects are opened. The corrections presented along this work were computed without taking any assumption about the soft SUSY-breaking mechanism so that a direct comparison with the H3m results in the MSUGRA scenarios requires a reparametrization of our expressions and therefore is beyond the scope of this work. Moreover, there is still missing an estimation of the theoretical uncertainties in the fixed-order determination of M_h at three-loop level and the corresponding numerical comparison, including these uncertainties, with the other three-loop contributions currently found in literature, namely the pure \overline{DR} three-loop results recently presented in [142] and implemented in FlexibleSUSY+Himalaya, the EFT calculations implemented in HSSUSY [40], the hybrid implementations in FlexibleSUSY [148], SPheno [153, 154], etc. In this work we have studied the effects of the large logarithmic terms; however, an analysis of the effects of the non-logarithmic terms is still missing. There is a complication to separate these contributions. All the three-loop corrections were computed in terms of the finite part of three-loop vacuum integrals which are expressed in terms of one- and two-dimensional integral representations. For master integrals where there are three or four independent mass scales, an analytical expression of the finite parts in terms of special functions, as the polylogarithms, are usually not possible. Yet, it is possible to find a more adequate basis to isolate the non-logarithmic terms and measure their numerical effects.

A more technical issue related with the basis of master integrals are also left open. In this work we have used SecDec in order to evaluate the evanescent terms of the three-loop vacuum integrals. However, the evaluation could be done in a more efficiently way with the dispersion method if one finds integral representations for those contributions in terms of fundamental functions. Examples of three-loop vacuum integrals which have never been published are: $U5(m_1, m_2, m_1, m_2, m_3)$, $U5(m_1, 0, m_2, m_3, m_4)$ or $U5(m_1, m_2, m_2, m_3, m_4)$. Recently, a version 2.0 of the program TVID was released [168]. This could allow a better election of the basis of master integrals, but also can be used to estimate the size of the momentum dependence contribution to the fixed-order three-loop M_h -corrections.

A. DRED: Notation and Technical Setup

In this appendix we show the needed gamma algebra and tensor relations for a practical calculation regularized in the dimensional reduction scheme, where momenta are continued from 4 to D dimensions, while gauge fields and γ -matrices remain as four-dimensional objects. We have implemented DRED by introducing the quasi-four, $-D$ and $-\epsilon$ dimensional spaces: $Q4S$, QDS and $Q\epsilon S$, where $D = 4 - 2\epsilon$,

$$Q4S = QDS \cup Q\epsilon S \quad \text{and} \quad QDS \cap Q\epsilon S = 0. \quad (\text{A-1})$$

The space $Q4$ retains the essential 4-dimensional properties but is in fact an infinite-dimensional space which contain the QDS . The complement of the D -dimensional space is a $(4 - D)$ -dimensional space, $Q\epsilon S$. The four-dimensional quantities live in $Q4S$ with metric tensor $g^{\mu\nu}$ while the D -dimensional and ϵ -dimensional objects live in QDS and $Q\epsilon S$ with metric tensors $g^{\hat{\mu}\hat{\nu}}$ and $g^{\tilde{\mu}\tilde{\nu}}$, respectively. Those metric tensors satisfy

$$g^{\mu\nu} = g^{\hat{\mu}\hat{\nu}} + g^{\tilde{\mu}\tilde{\nu}}, \quad g^{\hat{\mu}\hat{\sigma}} g_{\hat{\sigma}\tilde{\nu}} = g^{\hat{\mu}\tilde{\nu}} = 0, \quad g_{\mu}^{\mu} = 4, \quad g_{\hat{\mu}}^{\hat{\mu}} = D, \quad g_{\tilde{\mu}}^{\tilde{\mu}} = 2\epsilon. \quad (\text{A-2})$$

In $Q4S$, QDS and $Q\epsilon S$, gamma-matrices satisfy the usual Dirac algebra:

$$\{\gamma^{\mu}, \gamma^{\nu}\} = 2g^{\mu\nu}, \quad \{\gamma^{\hat{\mu}}, \gamma^{\hat{\nu}}\} = 2g^{\hat{\mu}\hat{\nu}}, \quad \{\gamma^{\tilde{\mu}}, \gamma^{\tilde{\nu}}\} = 2g^{\tilde{\mu}\tilde{\nu}}, \quad \{\gamma^{\hat{\mu}}, \gamma^{\tilde{\nu}}\} = 0. \quad (\text{A-3})$$

For any vector $v \in Q4S$ the following relation is satisfied:

$$v^{\mu} = v^{\hat{\mu}} + v^{\tilde{\mu}} \quad (\text{A-4})$$

$v^{\hat{\mu}}$ and $v^{\tilde{\mu}}$ denote the projection of v^{μ} to the subspaces QDS and $Q\epsilon S$ according to

$$v^{\hat{\mu}} = g^{\hat{\mu}\hat{\nu}} v_{\nu} \quad ; \quad v^{\tilde{\mu}} = g^{\tilde{\mu}\tilde{\nu}} v_{\nu}. \quad (\text{A-5})$$

Provided that QDS is a subspace of $Q4S$ the next identities are satisfied:

$$p^{\hat{\mu}} \gamma_{\hat{\mu}} = \begin{pmatrix} p^{\hat{\mu}} & 0 \end{pmatrix} \begin{pmatrix} \gamma_{\hat{\mu}} \\ 0 \end{pmatrix} = \begin{pmatrix} p^{\hat{\mu}} & 0 \end{pmatrix} \begin{pmatrix} \gamma_{\hat{\mu}} \\ \gamma_{\tilde{\mu}} \end{pmatrix} = p^{\hat{\mu}} \gamma_{\mu} = p_{\nu} \gamma^{\hat{\nu}}. \quad (\text{A-6})$$

In particular, the relation

$$\not{p}\not{p} = \frac{1}{2} p^{\hat{\mu}} p^{\hat{\nu}} \{\gamma_{\mu}, \gamma_{\nu}\} = p^{\hat{\mu}} p^{\hat{\nu}} g_{\mu\nu} = \hat{p}^2, \quad (\text{A-7})$$

appearing in the fermion propagators, holds for a D -dimensional momenta \hat{p} . Concerning the chiral matrix γ_5 , we have used the usual definition in DRED, that is, we have defined γ_5 as an object that anticommutes with all infinitely many γ^μ ,

$$\{\gamma_5, \gamma^\mu\} = 0 \quad \rightarrow \quad \{\gamma_5, \gamma^{\hat{\mu}}\} = \{\gamma_5, \gamma^{\tilde{\mu}}\} = 0, \quad (\text{A-8})$$

and holds the properties

$$(\gamma_5)^2 = 1, \quad \gamma_5^\dagger = \gamma_5. \quad (\text{A-9})$$

The relations (A-2) to (A-9) together with the constraint $\text{Tr}1 = 4$ in $Q4S$ allow the evaluation of fermion traces in the following way:

$$\begin{aligned} \text{Tr}\gamma_\mu &= \text{Tr}\gamma_{\hat{\mu}} = \text{Tr}\gamma_{\tilde{\mu}} = 0, \\ \text{Tr}(\gamma_\mu\gamma_\nu) &= 4g_{\mu\nu}, \quad \text{Tr}(\gamma_{\hat{\mu}}\gamma_{\hat{\nu}}) = 4g_{\hat{\mu}\hat{\nu}}, \quad \text{Tr}(\gamma_{\tilde{\mu}}\gamma_{\tilde{\nu}}) = 4g_{\tilde{\mu}\tilde{\nu}}, \\ \text{Tr}(\gamma_\mu\gamma_\nu\gamma_\rho\gamma_\sigma) &= 4(g_{\mu\nu}g_{\rho\sigma} - g_{\mu\rho}g_{\nu\sigma} + g_{\mu\sigma}g_{\nu\rho}), \\ \text{Tr}(\gamma_{\hat{\mu}}\gamma_{\hat{\nu}}\gamma_{\hat{\rho}}\gamma_{\hat{\sigma}}) &= 4(g_{\hat{\mu}\hat{\nu}}g_{\hat{\rho}\hat{\sigma}} - g_{\hat{\mu}\hat{\rho}}g_{\hat{\nu}\hat{\sigma}} + g_{\hat{\mu}\hat{\sigma}}g_{\hat{\nu}\hat{\rho}}), \\ \text{Tr}(\gamma_{\tilde{\mu}}\gamma_{\tilde{\nu}}\gamma_{\tilde{\rho}}\gamma_{\tilde{\sigma}}) &= 4(g_{\tilde{\mu}\tilde{\nu}}g_{\tilde{\rho}\tilde{\sigma}} - g_{\tilde{\mu}\tilde{\rho}}g_{\tilde{\nu}\tilde{\sigma}} + g_{\tilde{\mu}\tilde{\sigma}}g_{\tilde{\nu}\tilde{\rho}}), \\ \text{Tr}(\gamma_{\hat{\mu}}\dots\gamma_{\hat{\sigma}}\gamma_{\tilde{\mu}}\dots\gamma_{\tilde{\sigma}}) &= \frac{1}{4}\text{Tr}(\gamma_{\hat{\mu}}\dots\gamma_{\hat{\sigma}})\text{Tr}(\gamma_{\tilde{\mu}}\dots\gamma_{\tilde{\sigma}}), \\ \text{Tr}(\gamma_5(\text{arbitrary number of } \gamma_{\mu_j})) &= 0. \end{aligned} \quad (\text{A-10})$$

Further relations of the gamma-matrices can also be obtained:

$$\begin{aligned} \gamma_\mu\gamma^\mu &= 4, \quad \gamma_{\hat{\mu}}\gamma^{\hat{\mu}} = D, \quad \gamma_{\tilde{\mu}}\gamma^{\tilde{\mu}} = 2\epsilon, \\ \gamma_\mu\gamma^\nu\gamma^\mu &= -2\gamma^\nu, \quad \gamma_{\hat{\mu}}\gamma^{\hat{\nu}}\gamma^{\hat{\mu}} = -(D-2)\gamma^{\hat{\nu}}, \quad \gamma_{\tilde{\mu}}\gamma^{\tilde{\nu}}\gamma^{\tilde{\mu}} = -2\epsilon\gamma^{\tilde{\nu}}. \end{aligned} \quad (\text{A-11})$$

B. DRED Renormalization Constants

In this appendix we are going to list the relevant counter-terms involved in the three-loop calculation of the Lightest CP-even Higgs boson mass at order $\alpha_t\alpha_s^2$. The next listed counter-terms were computed using the renormalization scheme DRED with minimal subtraction. Their explicit expressions are required in the analysis presented in Chapters 3 and 4.

The one-loop counter-term of the top quark mass in the \overline{DR} scheme is:

$$\begin{aligned} M_t\delta^{(1)}M_t &= \frac{\alpha_s}{6\pi}\text{Dp} \left[A0(\tilde{m}_{t_1}) + A0(\tilde{m}_{t_2}) - 2A0(M_{\tilde{g}}) - 2A0(M_t) - 4M_t^2 B0(M_t^2, M_t, 0) \right. \\ &+ (M_{\tilde{g}}^2 + M_t^2 - \tilde{m}_{t_1}^2) B0(M_t^2, \tilde{m}_{t_1}, M_{\tilde{g}}) + (M_{\tilde{g}}^2 + M_t^2 - \tilde{m}_{t_2}^2) B0(M_t^2, \tilde{m}_{t_2}, M_{\tilde{g}}) \\ &\left. + 2M_{\tilde{g}}M_t s_{2\theta_{\tilde{t}}} (B0(M_t^2, \tilde{m}_{t_2}, M_{\tilde{g}}) - B0(M_t^2, \tilde{m}_{t_1}, M_{\tilde{g}})) \right] . \end{aligned} \quad (\text{B-1})$$

Using the analytical expression of the one-loop functions $A0$ and $B0$, which can be consulted in Appendix J, and the definitions of the $SU(3)$ group invariants:

$$\begin{aligned} b &= 1, \quad N = 3, \quad C_A = bN = 3, \quad C_R = b\frac{N^2 - 1}{2N} = \frac{4}{3}, \quad I_2(R) = \frac{b}{2} = \frac{1}{2}, \\ n_q &= 5, \quad n_t = 1, \quad n_f = n_q + n_t = 6, \quad T_f = n_f I_2(R) = 3, \end{aligned} \quad (\text{B-2})$$

we have

$$\delta^{(1)}M_t = -\frac{\alpha_s}{2\pi}M_t C_R \frac{1}{\epsilon}. \quad (\text{B-3})$$

The gluino mass counter-term at one-loop order is:

$$\begin{aligned} M_{\tilde{g}}\delta^{(1)}M_{\tilde{g}} &= \frac{\alpha_s}{8\pi}\text{Dp} \left[\sum_f \sum_{j=1}^2 A0(\tilde{m}_{f_j}) - 6A0(M_{\tilde{g}}) - 2A0(M_t) - 12M_{\tilde{g}}^2 B0(M_{\tilde{g}}^2, M_{\tilde{g}}, 0) + \right. \\ &\left. \sum_f \sum_{j=1}^2 \left(M_{\tilde{g}}^2 + M_f^2 - \tilde{m}_{f_j}^2 - 2M_{\tilde{g}}M_f s_{2\theta_{f_j}} \right) B0(M_{\tilde{g}}^2, \tilde{m}_{f_j}, M_f) \right] ; f = u, d, t, b, c, s. \end{aligned} \quad (\text{B-4})$$

Explicitly we have:

$$\delta^{(1)}M_{\tilde{g}} = \frac{\alpha_s}{4\pi}M_{\tilde{g}} (-3C_A + 2T_f) \frac{1}{\epsilon}. \quad (\text{B-5})$$

In the NLF limit $M_q = 0$ where $q = u, d, b, c, s$. From now on we are going to preserve the definitions of the indices f and q . The one-loop counter-terms of the squark sector are:

$$\begin{aligned} \delta^{(1)}\tilde{m}_{f_1}^2 &= \frac{\alpha_s}{3\pi} \text{Dp} \left[A0(\tilde{m}_{f_1}) c_{2\theta_{\bar{f}}}^2 + A0(\tilde{m}_{f_2}) s_{2\theta_{\bar{f}}}^2 + A0(\tilde{m}_{f_1}) - 4\tilde{m}_{f_1}^2 B0(\tilde{m}_{f_1}^2, \tilde{m}_{f_1}, 0) \right] \\ &\quad - 2\frac{\alpha_s}{3\pi} \text{Dp} \left[\left(M_{\bar{g}}^2 + M_f^2 - \tilde{m}_{f_1}^2 + (-1)^1 2M_{\bar{g}}M_f s_{2\theta_{\bar{f}}} \right) B0(\tilde{m}_{f_1}^2, M_f, M_{\bar{g}}) \right] \\ &\quad - 2\frac{\alpha_s}{3\pi} \text{Dp} [A0(M_{\bar{g}}) + A0(M_f)], \end{aligned} \quad (\text{B-6})$$

which leads to

$$\delta^{(1)}\tilde{m}_{f_1}^2 = \frac{\alpha_s}{\pi} C_R \left(-M_{\bar{g}}^2 - M_f^2 + M_{\bar{g}}M_f s_{2\theta_{\bar{f}}} + \frac{\tilde{m}_{f_1}^2 - \tilde{m}_{f_1}^2}{4} s_{\theta_{\bar{f}}}^2 \right) \frac{1}{\epsilon}. \quad (\text{B-7})$$

The expression for $\delta^{(1)}\tilde{m}_{f_2}^2$ is obtained by interchanging $1 \leftrightarrow 2$ in the above equation. Besides

$$\begin{aligned} \delta^{(1)}\theta_{\bar{t}} &= \left\{ 4\frac{\alpha_s}{3\pi} M_{\bar{g}}M_t \left(c_{2\theta_{\bar{t}}}^2 - s_{2\theta_{\bar{t}}}^2 \right) \text{Dp} [B0(\tilde{m}_{t_1}^2, M_t, M_{\bar{g}}) + B0(\tilde{m}_{t_2}^2, M_t, M_{\bar{g}})] \right. \\ &\quad \left. - \frac{\alpha_s}{3\pi} \text{Dp} [A0(\tilde{m}_{t_1}) - A0(\tilde{m}_{t_2})] s_{4\theta_{\bar{t}}} \right\} / 2 (\tilde{m}_{t_1}^2 - \tilde{m}_{t_2}^2), \end{aligned} \quad (\text{B-8})$$

that yields

$$(\tilde{m}_{t_1}^2 - \tilde{m}_{t_2}^2) \delta^{(1)}\theta_{\bar{t}} = C_R c_{2\theta_{\bar{t}}} \left(M_{\bar{g}}M_t - \frac{\tilde{m}_{t_1}^2 - \tilde{m}_{t_2}^2}{4} s_{2\theta_{\bar{t}}} \right) \frac{1}{\epsilon}, \quad (\text{B-9})$$

and

$$\begin{aligned} \delta^{(1)}Z_{\bar{f}jj} &= \frac{\alpha_s}{3\pi} \text{Dp} \left[2 \left(M_{\bar{g}}^2 + M_f^2 - \tilde{m}_{f_j}^2 + (-1)^j 2M_{\bar{g}}M_f s_{2\theta_{\bar{f}}} \right) \frac{\partial}{\partial p^2} B0(p^2, M_f, M_{\bar{g}}) \right. \\ &\quad \left. - 2B0(\tilde{m}_{f_j}^2, M_f, M_{\bar{g}}) + 4\tilde{m}_{f_j}^2 \frac{\partial}{\partial p^2} B0(p^2, \tilde{m}_{f_j}, 0) + 2B0(\tilde{m}_{f_j}^2, \tilde{m}_{f_j}, 0) \right] \Big|_{p^2=\tilde{m}_{f_j}^2}; \quad j = 1, 2. \end{aligned} \quad (\text{B-10})$$

At two-loop level we need the \overline{DR} counter-terms:

$$\delta^{(2)}M_t^2 = \left(\frac{\alpha_s}{4\pi} \right)^2 M_t^2 \left[\frac{68}{9} \frac{1}{\epsilon^2} - \frac{41}{9} \frac{1}{\epsilon} \right], \quad (\text{B-11})$$

$$\begin{aligned} \delta^{(2)}\tilde{m}_{t_1}^2 &= \left(\frac{\alpha_s}{\pi} \right)^2 \left\{ \frac{16}{9} c_{2\theta_{\bar{t}}}^2 \frac{M_{\bar{g}}^2 M_t^2}{(\tilde{m}_{t_1}^2 - \tilde{m}_{t_2}^2)} + \left(\frac{1}{9} (1 + c_{2\theta_{\bar{t}}}^2) + \frac{1}{8} \right) s_{2\theta_{\bar{t}}}^2 (\tilde{m}_{t_1}^2 - \tilde{m}_{t_2}^2) \right. \\ &\quad \left. + \frac{25}{18} M_t^2 + \frac{3}{2} M_{\bar{g}}^2 - \left(\frac{8}{9} (1 + c_{2\theta_{\bar{t}}}^2) + 1 \right) s_{2\theta_{\bar{t}}} M_{\bar{g}} M_t \right\} \frac{1}{\epsilon^2} \\ &\quad + \left(\frac{\alpha_s}{\pi} \right)^2 \left\{ \frac{1}{6} (\tilde{m}_{t_1}^2 + \tilde{m}_{t_2}^2) - \frac{1}{72} s_{2\theta_{\bar{t}}}^2 (\tilde{m}_{t_1}^2 - \tilde{m}_{t_2}^2) - \frac{7}{18} M_t^2 \right. \\ &\quad \left. - \frac{7}{6} M_{\bar{g}}^2 + \frac{1}{9} s_{2\theta_{\bar{t}}} M_{\bar{g}} M_t + \frac{1}{6} \sum_q \sum_{j=1}^2 \tilde{m}_{q_j}^2 - \frac{1}{2} m_\epsilon^2 \right\} \frac{1}{\epsilon}. \end{aligned} \quad (\text{B-12})$$

The expression for $\delta^{(2)}\tilde{m}_{t_2}$ can be derived from (B-12) by interchanging the indices $1 \leftrightarrow 2$ and changing the sign of $\theta_{\bar{t}}$. Furthermore, in the \overline{DR} scheme the two-loop counter-terms of the stop masses have a dependence on the ϵ -scalar mass m_ϵ . This dependence must cancel in the final result of the three-loop correction to M_h . At the perturbative order considered in this work, just a one-loop renormalization of m_ϵ is required. Three different approaches with equivalent results can be used. i) If one renormalizes the ϵ -scalar mass in the \overline{DR} scheme, it is enough to consider the simple \overline{DR} counter-term

$$\delta^{(1)}m_\epsilon^2 = \frac{\alpha_s}{\pi}m_\epsilon^2 \left\{ -\frac{3}{4} + \left[-\frac{3}{2}M_g^2 + \frac{1}{2} \sum_f \sum_{j=1}^2 \tilde{m}_{f_j}^2 - M_t^2 \right] \frac{1}{2m_\epsilon^2} \right\} \frac{1}{\epsilon}. \quad (\text{B-13})$$

and appropriated shifts over the stop quark masses. ii) Instead, if one considers an on-shell renormalization and chooses $m_\epsilon \neq 0$, one has to consider the one-loop counter-term

$$\begin{aligned} -\frac{\pi}{\alpha_s}\delta^{(1)}m_\epsilon^2 &= \left[\frac{C_A}{4} (3m_\epsilon^2 + 2M_g^2) - \frac{n_q}{4} (m_\epsilon^2 + 2\tilde{m}_q^2) - \frac{n_t}{2} (m_\epsilon^2 + \tilde{m}_{t_1}^2 + \tilde{m}_{t_2}^2 - 2M_t^2) \right] \frac{1}{\epsilon} \\ &+ \frac{C_A}{4} \left[\left(6 + 4\ln\left(\frac{\mu^2}{m_\epsilon^2}\right) - \ln\left(\frac{\mu^2}{M_g^2}\right) \right) m_\epsilon^2 + 2 \left(1 + \ln\left(\frac{\mu^2}{M_g^2}\right) \right) M_g^2 \right] \\ &- \frac{n_q}{4} \left[\left(2 + \ln\left(\frac{\mu^2}{m_\epsilon^2}\right) \right) m_\epsilon^2 + 2 \left(1 + \ln\left(\frac{\mu^2}{\tilde{m}_q^2}\right) \right) \tilde{m}_q^2 \right] \\ &- \frac{n_t}{4} \left[\ln\left(\frac{\mu^2}{M_t^2}\right) m_\epsilon^2 + \sum_{j=1}^2 \left(1 + \ln\left(\frac{\mu^2}{\tilde{m}_{t_j}^2}\right) \right) \tilde{m}_{t_j}^2 - 2 \left(1 + \ln\left(\frac{\mu^2}{M_t^2}\right) \right) M_t^2 \right]. \end{aligned} \quad (\text{B-14})$$

accompanied by the corresponding shifts over the stop masses. iii) If we assume $m_\epsilon \neq 0$ in the on-shell scheme, no finite counter-term is needed at all. This is the best choice for practical calculations. Finally, we need the two-loop counter-term of the stop mixing angle:

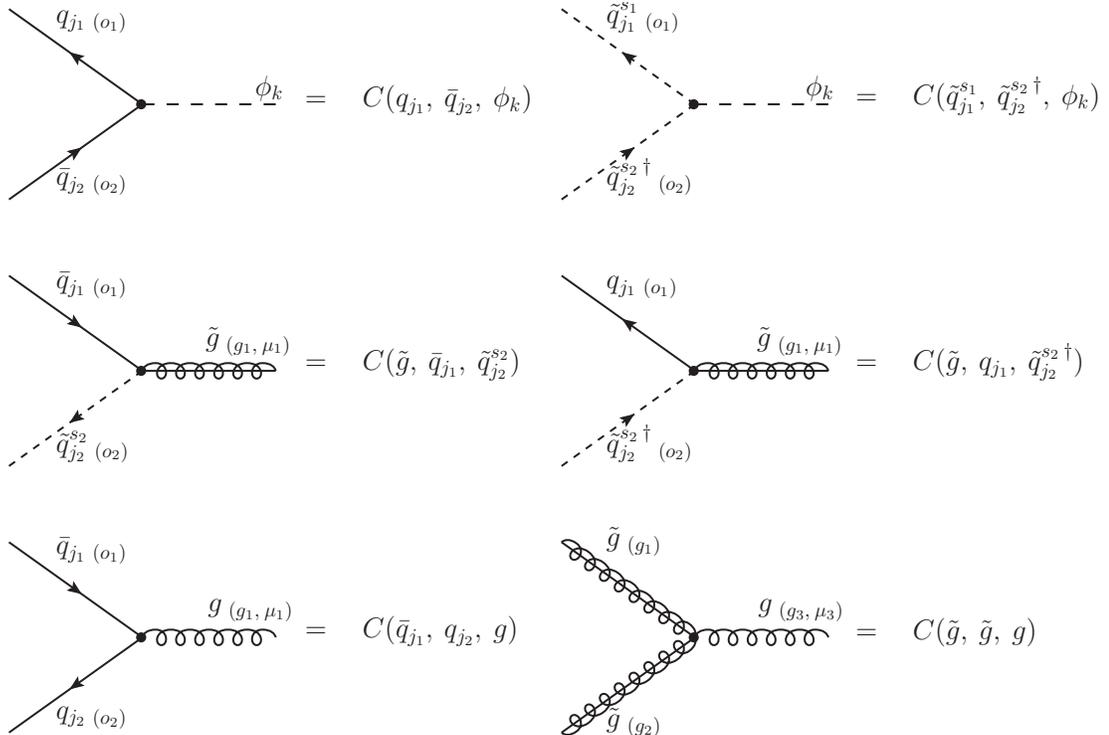
$$\begin{aligned} (\tilde{m}_{t_1}^2 - \tilde{m}_{t_2}^2) \delta^{(2)}\theta_{\bar{t}} &= \left(\frac{\alpha_s}{\pi} \right)^2 \left\{ \left(\frac{1}{8}s_{2\theta_{\bar{t}}}c_{2\theta_{\bar{t}}} - \frac{1}{9}(s_{2\theta_{\bar{t}}}^2 - c_{2\theta_{\bar{t}}}^2) \right) s_{2\theta_{\bar{t}}} (\tilde{m}_{t_1}^2 - \tilde{m}_{t_2}^2) + \right. \\ &\left. \left(\frac{8}{9}c_{2\theta_{\bar{t}}}(s_{2\theta_{\bar{t}}}^2 - c_{2\theta_{\bar{t}}}^2) - c_{2\theta_{\bar{t}}} \right) M_{\bar{g}}M_t - \frac{32}{9}s_{2\theta_{\bar{t}}}c_{2\theta_{\bar{t}}}\frac{M_{\bar{g}}^2M_t^2}{(\tilde{m}_{t_1}^2 - \tilde{m}_{t_2}^2)} \right\} \frac{1}{\epsilon^2} \\ &+ \left(\frac{\alpha_s}{\pi} \right)^2 \left\{ \frac{1}{9}c_{2\theta_{\bar{t}}}M_{\bar{g}}M_t - \frac{1}{72}s_{2\theta_{\bar{t}}}c_{2\theta_{\bar{t}}}(\tilde{m}_{t_1}^2 - \tilde{m}_{t_2}^2) \right\} \frac{1}{\epsilon}. \end{aligned} \quad (\text{B-15})$$

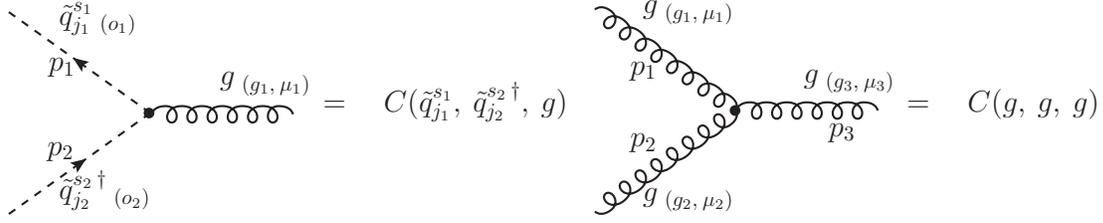
C. Feynman Rules in the SQCD Sector

| Index | Type | Range | Particles |
|---------------------------------------|------------|-----------------|--|
| j_i | Generation | $1 \dots 3$ | $\phi_k = h, H, A$ $q = u, d$ $\tilde{q} = \tilde{u}, \tilde{d}$ |
| s_i | Sfermion | $1 \dots 2$ | |
| o_i | Colour | $1 \dots 3$ | |
| g_i | Gluon | $1 \dots 8$ | |
| $(\mu_i, \hat{\mu}_i, \tilde{\mu}_i)$ | Lorentz | $(4, D, 4 - D)$ | |

Table C-1.: Index labels and ranges included in the Feynman rules of the vertex diagrams.

This appendix contains the needed rMSSM vertices for the computation of the Higgs mass M_h at order $\alpha_t \alpha_s^2$. The notation of Table C-1 for the index labels and ranges are used to draw the vertex diagrams and derive their corresponding Feynman rules. For cubic vertices we have the rules:





where

$$C(u_{j_1}, \bar{u}_{j_2}, h) = -i \frac{ec_\alpha}{2s_\beta M_W s_{\theta_W}} m_{u_{j_1}} \delta_{j_1 j_2} \delta_{o_1 o_2}$$

$$C(d_{j_1}, \bar{d}_{j_2}, h) = i \frac{es_\alpha}{2c_\beta M_W s_{\theta_W}} m_{d_{j_1}} \delta_{j_1 j_2} \delta_{o_1 o_2}$$

$$C(u_{j_1}, \bar{u}_{j_2}, H) = -i \frac{es_\alpha}{2s_\beta M_W s_{\theta_W}} m_{u_{j_1}} \delta_{j_1 j_2} \delta_{o_1 o_2}$$

$$C(d_{j_1}, \bar{d}_{j_2}, H) = -i \frac{ec_\alpha}{2c_\beta M_W s_{\theta_W}} m_{d_{j_1}} \delta_{j_1 j_2} \delta_{o_1 o_2}$$

$$C(u_{j_1}, \bar{u}_{j_2}, A) = -\frac{e\gamma^5}{2t_\beta M_W s_{\theta_W}} m_{u_{j_1}} \delta_{j_1 j_2} \delta_{o_1 o_2}$$

$$C(d_{j_1}, \bar{d}_{j_2}, A) = -\frac{et_\beta \gamma^5}{2M_W s_{\theta_W}} m_{d_{j_1}} \delta_{j_1 j_2} \delta_{o_1 o_2}$$

$$C(\tilde{u}_{j_1}^{s_1}, \tilde{u}_{j_2}^{s_2 \dagger}, h) = -i \frac{e}{6s_{\theta_W} c_{\theta_W} M_W s_\beta} \delta_{j_1 j_2} \left\{ \begin{array}{l} U_{s_1,1}^{\tilde{u},j_1} U_{s_2,2}^{\tilde{u},j_1} 3c_{\theta_W} m_{u_{j_1}} (A_{j_1 j_1}^u c_\alpha + \mu s_\alpha) + \\ U_{s_1,1}^{\tilde{u},j_1} U_{s_2,1}^{\tilde{u},j_1} \left(6c_{\theta_W} c_\alpha m_{u_{j_1}}^2 - M_W M_Z s_{\alpha+\beta} s_\beta (3 - 4s_{\theta_W}^2) \right) + \\ U_{s_1,2}^{\tilde{u},j_1} U_{s_2,2}^{\tilde{u},j_1} \left(6c_{\theta_W} c_\alpha m_{u_{j_1}}^2 - 4M_W M_Z s_{\alpha+\beta} s_\beta s_{\theta_W}^2 \right) + \\ U_{s_1,2}^{\tilde{u},j_1} U_{s_2,1}^{\tilde{u},j_1} 3c_{\theta_W} m_{u_{j_1}} (A_{j_1 j_1}^u c_\alpha + \mu s_\alpha) \end{array} \right\}$$

$$C(\tilde{d}_{j_1}^{s_1}, \tilde{d}_{j_2}^{s_2 \dagger}, h) = i \frac{e}{6s_{\theta_W} c_{\theta_W} M_W c_\beta} \delta_{j_1 j_2} \left\{ \begin{array}{l} U_{s_1,1}^{\tilde{d},j_1} U_{s_2,2}^{\tilde{d},j_1} 3c_{\theta_W} m_{d_{j_1}} (A_{j_1 j_1}^d s_\alpha + \mu c_\alpha) + \\ U_{s_1,1}^{\tilde{d},j_1} U_{s_2,1}^{\tilde{d},j_1} \left(6c_{\theta_W} s_\alpha m_{d_{j_1}}^2 - M_W M_Z s_{\alpha+\beta} c_\beta (3 - 2s_{\theta_W}^2) \right) + \\ U_{s_1,2}^{\tilde{d},j_1} U_{s_2,2}^{\tilde{d},j_1} \left(6c_{\theta_W} s_\alpha m_{d_{j_1}}^2 - 2M_W M_Z s_{\alpha+\beta} c_\beta s_{\theta_W}^2 \right) + \\ U_{s_1,2}^{\tilde{d},j_1} U_{s_2,1}^{\tilde{d},j_1} 3c_{\theta_W} m_{d_{j_1}} (A_{j_1 j_1}^d s_\alpha + \mu c_\alpha) \end{array} \right\}$$

$$C(\tilde{u}_{j_1}^{s_1}, \tilde{u}_{j_2}^{s_2 \dagger}, H) = i \frac{e}{6s_{\theta_W} c_{\theta_W} M_W s_\beta} \delta_{j_1 j_2} \left\{ \begin{array}{l} U_{s_1,1}^{\tilde{u},j_1} U_{s_2,2}^{\tilde{u},j_1} 3c_{\theta_W} m_{u_{j_1}} (\mu c_\alpha - A_{j_1 j_1}^u s_\alpha) - \\ U_{s_1,1}^{\tilde{u},j_1} U_{s_2,1}^{\tilde{u},j_1} \left(6c_{\theta_W} s_\alpha m_{u_{j_1}}^2 + M_W M_Z c_{\alpha+\beta} s_\beta (3 - 4s_{\theta_W}^2) \right) - \\ U_{s_1,2}^{\tilde{u},j_1} U_{s_2,2}^{\tilde{u},j_1} \left(6c_{\theta_W} s_\alpha m_{u_{j_1}}^2 + 4M_W M_Z c_{\alpha+\beta} s_\beta s_{\theta_W}^2 \right) - \\ U_{s_1,2}^{\tilde{u},j_1} U_{s_2,1}^{\tilde{u},j_1} 3c_{\theta_W} m_{u_{j_1}} (\mu c_\alpha - A_{j_1 j_1}^u s_\alpha) \end{array} \right\}$$

$$C(\tilde{d}_{j_1}^{s_1}, \tilde{d}_{j_2}^{s_2 \dagger}, H) = -i \frac{e}{6s_{\theta_W} c_{\theta_W} M_W c_\beta} \delta_{j_1 j_2} \left\{ \begin{array}{l} U_{s_1,1}^{\tilde{d},j_1} U_{s_2,2}^{\tilde{d},j_1} 3c_{\theta_W} m_{d_{j_1}} (A_{j_1 j_1}^d c_\alpha - \mu s_\alpha) + \\ U_{s_1,1}^{\tilde{d},j_1} U_{s_2,1}^{\tilde{d},j_1} \left(6c_{\theta_W} c_\alpha m_{d_{j_1}}^2 - M_W M_Z c_{\alpha+\beta} c_\beta (3 - 2s_{\theta_W}^2) \right) + \\ U_{s_1,2}^{\tilde{d},j_1} U_{s_2,2}^{\tilde{d},j_1} \left(6c_{\theta_W} c_\alpha m_{d_{j_1}}^2 - 2M_W M_Z c_{\alpha+\beta} c_\beta s_{\theta_W}^2 \right) + \\ U_{s_1,2}^{\tilde{d},j_1} U_{s_2,1}^{\tilde{d},j_1} 3c_{\theta_W} m_{d_{j_1}} (A_{j_1 j_1}^d c_\alpha - \mu s_\alpha) \end{array} \right\}$$

$$\begin{aligned}
C(\tilde{u}_{j_1}^{s_1}, \tilde{u}_{j_2}^{s_2 \dagger}, A) &= \frac{e}{2s_{\theta_W} M_W t_\beta} \delta_{j_1 j_2} \left\{ \begin{array}{l} U_{s_1,1}^{\tilde{u},j_1} U_{s_2,2}^{\tilde{u},j_1} m_{u_{j_1}} (A_{j_1 j_1}^u + \mu t_\beta) - \\ U_{s_1,2}^{\tilde{u},j_1} U_{s_2,1}^{\tilde{u},j_1} m_{u_{j_1}} (A_{j_1 j_1}^u + \mu t_\beta) \end{array} \right\} \\
C(\tilde{d}_{j_1}^{s_1}, \tilde{d}_{j_2}^{s_2 \dagger}, A) &= \frac{e}{2s_{\theta_W} M_W} \delta_{j_1 j_2} \left\{ \begin{array}{l} U_{s_1,1}^{\tilde{d},j_1} U_{s_2,2}^{\tilde{d},j_1} m_{d_{j_1}} (A_{j_1 j_1}^d t_\beta + \mu) - \\ U_{s_1,2}^{\tilde{d},j_1} U_{s_2,1}^{\tilde{d},j_1} m_{d_{j_1}} (A_{j_1 j_1}^d t_\beta + \mu) \end{array} \right\} \\
C(\tilde{g}, \tilde{u}_{j_1}, \tilde{u}_{j_2}^{s_2}) &= i\sqrt{2} g_s \delta_{j_1 j_2} T_{o_1 o_2}^{g_1} (U_{s_2,2}^{\tilde{u},j_1} \gamma^6 - U_{s_2,1}^{\tilde{u},j_1} \gamma^7) \\
C(\tilde{g}, \tilde{d}_{j_1}, \tilde{d}_{j_2}^{s_2}) &= i\sqrt{2} g_s \delta_{j_1 j_2} T_{o_1 o_2}^{g_1} (U_{s_2,2}^{\tilde{d},j_1} \gamma^6 - U_{s_2,1}^{\tilde{d},j_1} \gamma^7) \\
C(\tilde{g}, u_{j_1}, \tilde{u}_{j_2}^{s_2 \dagger}) &= -i\sqrt{2} g_s \delta_{j_1 j_2} T_{o_2 o_1}^{g_1} (U_{s_2,1}^{\tilde{u},j_1} \gamma^6 - U_{s_2,2}^{\tilde{u},j_1} \gamma^7) \\
C(\tilde{g}, d_{j_1}, \tilde{d}_{j_2}^{s_2 \dagger}) &= -i\sqrt{2} g_s \delta_{j_1 j_2} T_{o_2 o_1}^{g_1} (U_{s_2,1}^{\tilde{d},j_1} \gamma^6 - U_{s_2,2}^{\tilde{d},j_1} \gamma^7) \\
C(\tilde{q}_{j_1}, q_{j_2}, g) &= -i g_s \delta_{j_1 j_2} T_{o_1 o_2}^{g_1} \gamma^{\mu_1} \\
C(\tilde{g}, \tilde{g}, g) &= -g_s f^{g_1 g_2 g_3} \gamma^{\mu_3} \\
C(\tilde{q}_{j_1}^{s_1}, \tilde{q}_{j_2}^{s_2 \dagger}, g) &= -i g_s \delta_{j_1 j_2} \delta_{o_1 o_2} T_{o_1 o_2}^{g_1} (p_2 - p_1)^{\mu_1} \\
C(g, g, g) &= -g_s f^{g_1 g_2 g_3} (g^{\mu_1 \mu_3} (p_1 + p_3)^{\mu_2} + g^{\mu_2 \mu_3} (p_2 - p_3)^{\mu_1} - g^{\mu_1 \mu_2} (p_1 + p_2)^{\mu_3}).
\end{aligned}$$

In the above expressions we have used the definitions $\gamma^6 = (1 + \gamma^5)/2$ and $\gamma^7 = (1 - \gamma^5)/2$. Besides, p_i represents the momentum carried by the line i , while $U_{s_1, s_2}^{\tilde{q}, j_i}$ is the $s_1 s_2$ -component of the squark mixing matrix (see eq. 2-53) associated to the squark type \tilde{q}_{j_i} .

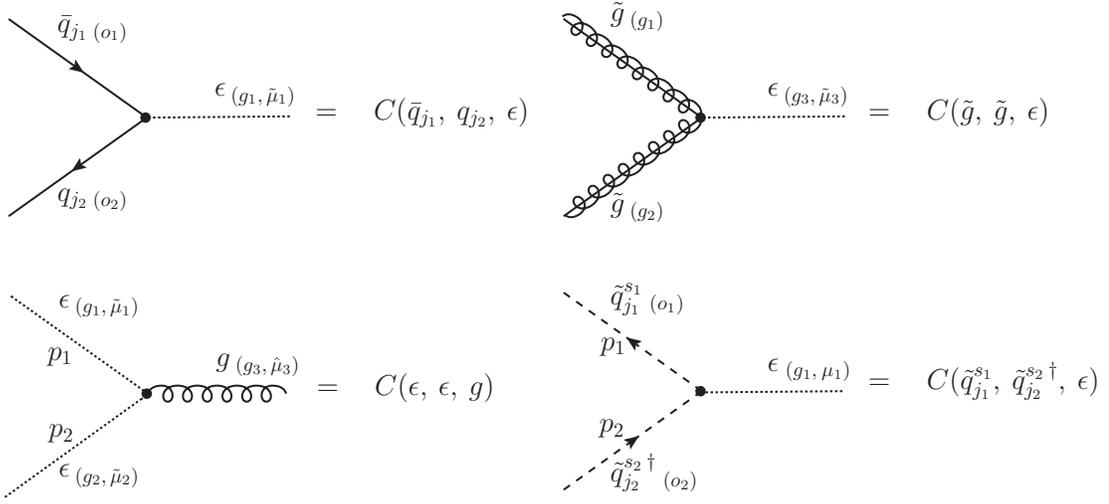
For the quartic vertices the Feynman rules are:

$$\begin{aligned}
& \begin{array}{c} \tilde{q}_{j_2}^{s_2 \dagger} (o_2) \quad \phi_{k_2} \\ \diagdown \quad \diagup \\ \tilde{q}_{j_1}^{s_1 \dagger} (o_1) \quad \phi_{k_1} \end{array} = C(\tilde{q}_{j_1}^{s_1 \dagger}, \tilde{q}_{j_2}^{s_2 \dagger}, \phi_{k_1}, \phi_{k_2}) \\
& \begin{array}{c} \tilde{q}_{j_2}^{s_2 \dagger} (o_2) \quad \tilde{q}_{j_4}^{s_4 \dagger} (o_4) \\ \diagdown \quad \diagup \\ \tilde{q}_{j_1}^{s_1} (o_1) \quad \tilde{q}_{j_3}^{s_3} (o_3) \end{array} = C(\tilde{q}_{j_1}^{s_1}, \tilde{q}_{j_2}^{s_2 \dagger}, \tilde{q}_{j_3}^{s_3}, \tilde{q}_{j_4}^{s_4 \dagger}) \\
& \begin{array}{c} \tilde{q}_{j_2}^{s_2 \dagger} (o_2) \quad g(g_1, \mu_1) \\ \diagdown \quad \diagup \\ \tilde{q}_{j_1}^{s_1} (o_1) \quad g(g_2, \mu_2) \end{array} = C(\tilde{q}_{j_1}^{s_1}, \tilde{q}_{j_2}^{s_2 \dagger}, g, g) \\
& \begin{array}{c} g(g_1, \mu_1) \quad g(g_4, \mu_4) \\ \diagdown \quad \diagup \\ g(g_2, \mu_2) \quad g(g_3, \mu_3) \end{array} = C(g, g, g, g)
\end{aligned}$$

where

$$\begin{aligned}
C(\tilde{u}_{j_1}^{s_1 \dagger}, \tilde{u}_{j_2}^{s_2}, h, h) &= -i \frac{e^2}{12s_{\theta_W}^2 c_{\theta_W}^2 M_W^2 s_\beta^2} \delta_{j_1 j_2} \left\{ \begin{aligned} &2U_{s_1, 2}^{\tilde{u}, j_1} U_{s_2, 2}^{\tilde{u}, j_1} \left(3c_{\theta_W}^2 c_\alpha^2 m_{u_{j_1}}^2 - 2M_W^2 c_{2\alpha} s_\beta^2 s_{\theta_W}^2 \right) + \\ &U_{s_1, 1}^{\tilde{u}, j_1} U_{s_2, 1}^{\tilde{u}, j_1} \left(6c_{\theta_W}^2 c_\alpha^2 m_{u_{j_1}}^2 - M_W^2 c_{2\alpha} s_\beta^2 (3 - 4s_{\theta_W}^2) \right) \end{aligned} \right\} \\
C(\tilde{d}_{j_1}^{s_1 \dagger}, \tilde{d}_{j_2}^{s_2}, h, h) &= -i \frac{e^2}{12s_{\theta_W}^2 c_{\theta_W}^2 M_W^2 c_\beta^2} \delta_{j_1 j_2} \left\{ \begin{aligned} &2U_{s_1, 2}^{\tilde{d}, j_1} U_{s_2, 2}^{\tilde{d}, j_1} \left(3c_{\theta_W}^2 s_\alpha^2 m_{d_{j_1}}^2 + M_W^2 c_{2\alpha} c_\beta^2 s_{\theta_W}^2 \right) + \\ &U_{s_1, 1}^{\tilde{d}, j_1} U_{s_2, 1}^{\tilde{d}, j_1} \left(6c_{\theta_W}^2 s_\alpha^2 m_{d_{j_1}}^2 + M_W^2 c_{2\alpha} c_\beta^2 (3 - 2s_{\theta_W}^2) \right) \end{aligned} \right\} \\
C(\tilde{u}_{j_1}^{s_1 \dagger}, \tilde{u}_{j_2}^{s_2}, H, H) &= -i \frac{e^2}{12s_{\theta_W}^2 c_{\theta_W}^2 M_W^2 s_\beta^2} \delta_{j_1 j_2} \left\{ \begin{aligned} &2U_{s_1, 2}^{\tilde{u}, j_1} U_{s_2, 2}^{\tilde{u}, j_1} \left(3c_{\theta_W}^2 s_\alpha^2 m_{u_{j_1}}^2 + 2M_W^2 c_{2\alpha} s_\beta^2 s_{\theta_W}^2 \right) + \\ &U_{s_1, 1}^{\tilde{u}, j_1} U_{s_2, 1}^{\tilde{u}, j_1} \left(6c_{\theta_W}^2 s_\alpha^2 m_{u_{j_1}}^2 + M_W^2 c_{2\alpha} s_\beta^2 (3 - 4s_{\theta_W}^2) \right) \end{aligned} \right\} \\
C(\tilde{d}_{j_1}^{s_1 \dagger}, \tilde{d}_{j_2}^{s_2}, H, H) &= -i \frac{e^2}{12s_{\theta_W}^2 c_{\theta_W}^2 M_W^2 c_\beta^2} \delta_{j_1 j_2} \left\{ \begin{aligned} &2U_{s_1, 2}^{\tilde{d}, j_1} U_{s_2, 2}^{\tilde{d}, j_1} \left(3c_{\theta_W}^2 c_\alpha^2 m_{d_{j_1}}^2 - M_W^2 c_{2\alpha} c_\beta^2 s_{\theta_W}^2 \right) + \\ &U_{s_1, 1}^{\tilde{d}, j_1} U_{s_2, 1}^{\tilde{d}, j_1} \left(6c_{\theta_W}^2 c_\alpha^2 m_{d_{j_1}}^2 - M_W^2 c_{2\alpha} c_\beta^2 (3 - 2s_{\theta_W}^2) \right) \end{aligned} \right\} \\
C(\tilde{u}_{j_1}^{s_1 \dagger}, \tilde{u}_{j_2}^{s_2}, A, A) &= -i \frac{e^2}{12s_{\theta_W}^2 c_{\theta_W}^2 M_W^2 t_\beta^2} \delta_{j_1 j_2} \left\{ \begin{aligned} &2U_{s_1, 2}^{\tilde{u}, j_1} U_{s_2, 2}^{\tilde{u}, j_1} \left(3c_{\theta_W}^2 m_{u_{j_1}}^2 - 2M_W^2 c_{2\beta} t_\beta^2 s_{\theta_W}^2 \right) + \\ &U_{s_1, 1}^{\tilde{u}, j_1} U_{s_2, 1}^{\tilde{u}, j_1} \left(6c_{\theta_W}^2 m_{u_{j_1}}^2 - M_W^2 c_{2\beta} t_\beta^2 (3 - 4s_{\theta_W}^2) \right) \end{aligned} \right\} \\
C(\tilde{d}_{j_1}^{s_1 \dagger}, \tilde{d}_{j_2}^{s_2}, A, A) &= -i \frac{e^2}{12s_{\theta_W}^2 c_{\theta_W}^2 M_W^2} \delta_{j_1 j_2} \left\{ \begin{aligned} &2U_{s_1, 2}^{\tilde{d}, j_1} U_{s_2, 2}^{\tilde{d}, j_1} \left(3c_{\theta_W}^2 t_\beta^2 m_{d_{j_1}}^2 + M_W^2 c_{2\beta} s_{\theta_W}^2 \right) + \\ &U_{s_1, 1}^{\tilde{d}, j_1} U_{s_2, 1}^{\tilde{d}, j_1} \left(6c_{\theta_W}^2 t_\beta^2 m_{d_{j_1}}^2 + M_W^2 c_{2\beta} (3 - 2s_{\theta_W}^2) \right) \end{aligned} \right\} \\
C(\tilde{u}_{j_1}^{s_1 \dagger}, \tilde{u}_{j_2}^{s_2}, H, h) &= -i \frac{e^2 s_{2\alpha}}{12s_{\theta_W}^2 c_{\theta_W}^2 M_W^2 s_\beta^2} \delta_{j_1 j_2} \left\{ \begin{aligned} &U_{s_1, 2}^{\tilde{u}, j_1} U_{s_2, 2}^{\tilde{u}, j_1} \left(3c_{\theta_W}^2 m_{u_{j_1}}^2 - 4M_W^2 s_\beta^2 s_{\theta_W}^2 \right) + \\ &U_{s_1, 1}^{\tilde{u}, j_1} U_{s_2, 1}^{\tilde{u}, j_1} \left(3c_{\theta_W}^2 m_{u_{j_1}}^2 - M_W^2 s_\beta^2 (3 - 4s_{\theta_W}^2) \right) \end{aligned} \right\} \\
C(\tilde{d}_{j_1}^{s_1 \dagger}, \tilde{d}_{j_2}^{s_2}, H, h) &= i \frac{e^2 s_{2\alpha}}{12s_{\theta_W}^2 c_{\theta_W}^2 M_W^2 c_\beta^2} \delta_{j_1 j_2} \left\{ \begin{aligned} &U_{s_1, 2}^{\tilde{d}, j_1} U_{s_2, 2}^{\tilde{d}, j_1} \left(3c_{\theta_W}^2 m_{d_{j_1}}^2 - 2M_W^2 c_\beta^2 s_{\theta_W}^2 \right) + \\ &U_{s_1, 1}^{\tilde{d}, j_1} U_{s_2, 1}^{\tilde{d}, j_1} \left(3c_{\theta_W}^2 m_{d_{j_1}}^2 - M_W^2 c_\beta^2 (3 - 2s_{\theta_W}^2) \right) \end{aligned} \right\} \\
C(\tilde{u}_{j_1}^{s_1}, \tilde{u}_{j_2}^{s_2 \dagger}, \tilde{u}_{j_3}^{s_3}, \tilde{u}_{j_4}^{s_4 \dagger}) &= \frac{ig_s^2 T_{o_2 o_3}^x T_{o_1 o_4}^x}{ig_s^2 T_{o_1 o_2}^x T_{o_4 o_3}^x} \left(U_{s_2, 1}^{\tilde{u}, j_2} U_{s_3, 1}^{\tilde{u}, j_2} - U_{s_2, 2}^{\tilde{u}, j_2} U_{s_3, 2}^{\tilde{u}, j_2} \right) \left(U_{s_1, 1}^{\tilde{u}, j_1} U_{s_4, 1}^{\tilde{u}, j_1} - U_{s_1, 2}^{\tilde{u}, j_1} U_{s_4, 2}^{\tilde{u}, j_1} \right) \delta_{j_1 j_4} \delta_{j_2 j_3} + \\ &\frac{ig_s^2 T_{o_1 o_2}^x T_{o_4 o_3}^x}{ig_s^2 T_{o_1 o_2}^x T_{o_4 o_3}^x} \left(U_{s_1, 1}^{\tilde{u}, j_1} U_{s_2, 1}^{\tilde{u}, j_1} - U_{s_1, 2}^{\tilde{u}, j_1} U_{s_2, 2}^{\tilde{u}, j_1} \right) \left(U_{s_3, 1}^{\tilde{u}, j_3} U_{s_4, 1}^{\tilde{u}, j_3} - U_{s_3, 2}^{\tilde{u}, j_3} U_{s_4, 2}^{\tilde{u}, j_3} \right) \delta_{j_1 j_2} \delta_{j_3 j_4} \\
C(\tilde{d}_{j_1}^{s_1}, \tilde{d}_{j_2}^{s_2 \dagger}, \tilde{d}_{j_3}^{s_3}, \tilde{d}_{j_4}^{s_4 \dagger}) &= \frac{ig_s^2 T_{o_2 o_3}^x T_{o_1 o_4}^x}{ig_s^2 T_{o_1 o_2}^x T_{o_4 o_3}^x} \left(U_{s_2, 1}^{\tilde{d}, j_2} U_{s_3, 1}^{\tilde{d}, j_2} - U_{s_2, 2}^{\tilde{d}, j_2} U_{s_3, 2}^{\tilde{d}, j_2} \right) \left(U_{s_1, 1}^{\tilde{d}, j_1} U_{s_4, 1}^{\tilde{d}, j_1} - U_{s_1, 2}^{\tilde{d}, j_1} U_{s_4, 2}^{\tilde{d}, j_1} \right) \delta_{j_1 j_4} \delta_{j_2 j_3} + \\ &\frac{ig_s^2 T_{o_1 o_2}^x T_{o_4 o_3}^x}{ig_s^2 T_{o_1 o_2}^x T_{o_4 o_3}^x} \left(U_{s_1, 1}^{\tilde{d}, j_1} U_{s_2, 1}^{\tilde{d}, j_1} - U_{s_1, 2}^{\tilde{d}, j_1} U_{s_2, 2}^{\tilde{d}, j_1} \right) \left(U_{s_3, 1}^{\tilde{d}, j_3} U_{s_4, 1}^{\tilde{d}, j_3} - U_{s_3, 2}^{\tilde{d}, j_3} U_{s_4, 2}^{\tilde{d}, j_3} \right) \delta_{j_1 j_2} \delta_{j_3 j_4} \\
C(\tilde{d}_{j_1}^{s_1}, \tilde{d}_{j_2}^{s_2 \dagger}, \tilde{u}_{j_3}^{s_3}, \tilde{u}_{j_4}^{s_4 \dagger}) &= ig_s^2 T_{o_2 o_1}^x T_{o_4 o_3}^x \left(U_{s_1, 1}^{\tilde{d}, j_1} U_{s_2, 1}^{\tilde{d}, j_1} - U_{s_1, 2}^{\tilde{d}, j_1} U_{s_2, 2}^{\tilde{d}, j_1} \right) \left(U_{s_3, 1}^{\tilde{u}, j_3} U_{s_4, 1}^{\tilde{u}, j_3} - U_{s_3, 2}^{\tilde{u}, j_3} U_{s_4, 2}^{\tilde{u}, j_3} \right) \delta_{j_1 j_2} \delta_{j_3 j_4} \\
C(\tilde{q}_{j_1}^{s_1}, \tilde{q}_{j_2}^{s_2 \dagger}, g, g) &= -ig_s^2 \delta_{j_1 j_2} \delta_{s_1 s_2} \left((T^{g_1} T^{g_2})_{o_1 o_2} + (T^{g_2} T^{g_1})_{o_1 o_2} \right) g^{\mu_1 \mu_2} \\
C(g, g, g, g) &= -ig_s^2 \left\{ \begin{aligned} &g^{\mu_1 \mu_4} g^{\mu_2 \mu_3} (f_{g_1 g_2 x} f_{x g_3 g_4} + f_{g_1 g_3 x} f_{x g_2 g_4}) - \\ &g^{\mu_1 \mu_2} g^{\mu_3 \mu_4} (f_{g_1 g_3 x} f_{x g_2 g_4} + f_{g_1 g_4 x} f_{x g_2 g_3}) - \\ &g^{\mu_1 \mu_3} g^{\mu_2 \mu_4} (f_{g_1 g_2 x} f_{x g_3 g_4} - f_{g_1 g_4 x} f_{x g_2 g_3}) \end{aligned} \right\}.
\end{aligned}$$

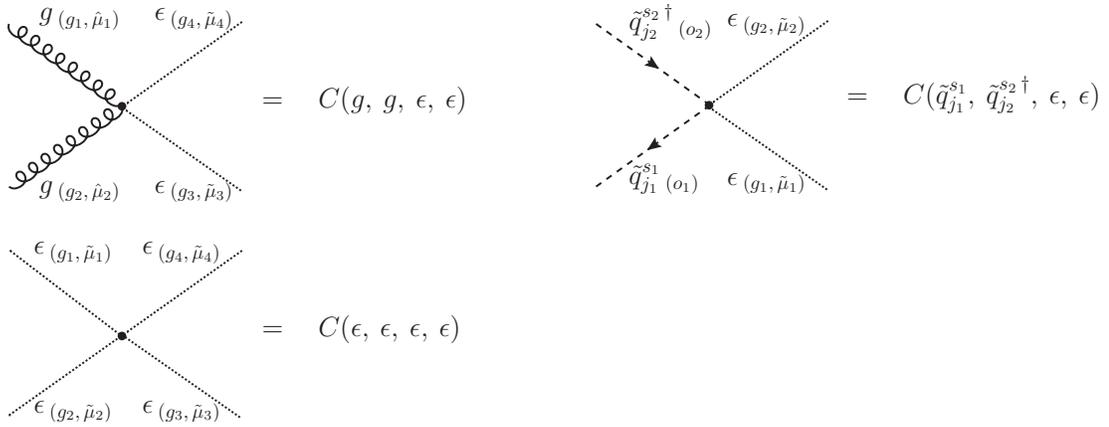
The Lorentz indices of all the above diagrams are supposed to be in $Q4S$; however, when ϵ -scalars are included in the regularization of Feynman amplitudes, those Lorentz indices have to be changed from $Q4S$ to QDS , according to $\mu \rightarrow \hat{\mu}$, and the following additional cubic and quartic vertices involving ϵ -scalars have to be considered:



with

$$\begin{aligned}
 C(\bar{q}_{j_1}, q_{j_2}, \epsilon) &= -ig_s \delta_{j_1 j_2} T_{o_1 o_2}^{g_1} \gamma^{\tilde{\mu}_1} \\
 C(\tilde{g}, \tilde{g}, \epsilon) &= -g_s f^{g_1 g_2 g_3} \gamma^{\tilde{\mu}_3} \\
 C(g, \epsilon, \epsilon) &= g_s f^{g_1 g_2 g_3} g^{\tilde{\mu}_1 \tilde{\mu}_2} (p_1 + p_2)^{\tilde{\mu}_3} \\
 C(\tilde{q}_{j_1}^{s_1}, \tilde{q}_{j_2}^{s_2 \dagger}, \epsilon) &= -ig_s \delta_{j_1 j_2} \delta_{o_1 o_2} T_{o_1 o_2}^{g_1} (p_2 - p_1)^{\tilde{\mu}_1}
 \end{aligned}$$

and



where

$$\begin{aligned}
 C(g, g, \epsilon, \epsilon) &= ig_s^2 g^{\tilde{\mu}_1 \tilde{\mu}_2} g^{\tilde{\mu}_3 \tilde{\mu}_4} (f^{g_1 g_3 x} f^{x g_2 g_4} + f^{g_1 g_4 x} f^{x g_2 g_3}) \\
 C(\tilde{q}_{j_1}^{s_1}, \tilde{q}_{j_2}^{s_2 \dagger}, \epsilon, \epsilon) &= -ig_s^2 \delta_{j_1 j_2} \delta_{s_1 s_2} ((T^{g_1} T^{g_2})_{o_1 o_2} + (T^{g_2} T^{g_1})_{o_1 o_2}) g^{\tilde{\mu}_1 \tilde{\mu}_2} \\
 C(\epsilon, \epsilon, \epsilon, \epsilon) &= -ig_s^2 \left\{ \begin{array}{l} g^{\tilde{\mu}_1 \tilde{\mu}_4} g^{\tilde{\mu}_2 \tilde{\mu}_3} (f^{g_1 g_2 x} f^{x g_3 g_4} + f^{g_1 g_3 x} f^{x g_2 g_4}) - \\ g^{\tilde{\mu}_1 \tilde{\mu}_2} g^{\tilde{\mu}_3 \tilde{\mu}_4} (f^{g_1 g_3 x} f^{x g_2 g_4} + f^{g_1 g_4 x} f^{x g_2 g_3}) - \\ g^{\tilde{\mu}_1 \tilde{\mu}_3} g^{\tilde{\mu}_2 \tilde{\mu}_4} (f^{g_1 g_2 x} f^{x g_3 g_4} - f^{g_1 g_4 x} f^{x g_2 g_3}) \end{array} \right\}.
 \end{aligned}$$

D. Three-loop 1PI Topologies

This appendix contains a Mathematica package for the generation of the three-loop 1PI Topologies with FeynArts. The code and their outputs are shown below.

```
PrependTo[$Path, ToFileName[{"Directory","to","FeynCalc901","FeynCalc"}]];
$LoadFeynArts = True;
Get["FeynCalc.m"];
Off[Paint::nolevel]

SETP=CreateTopologies[3, 1 -> 1, ExcludeTopologies -> Internal];
CTSE=CreateCTTopologies[3, 1 -> 1, ExcludeTopologies -> Internal];
TPTP=CreateTopologies[3, 1 -> 0, ExcludeTopologies -> Internal];
CTTP=CreateCTTopologies[3, 1 -> 0, ExcludeTopologies -> Internal];

(*****
**** Drawing the Three-loop Topologies and Exporting to *.ps ****
*****)

TempDirName=ToFileName[{"Directory","to","save","files"}];

If[!DirectoryQ[ToFileName[{TempDirName,ToString[TOP]}]],
  CreateDirectory[ToFileName[{TempDirName,ToString[TOP]}]]];

Paint[SETP,FieldNumbers->True,ColumnsXRows->{5,5},
Numbering-> Simple, SheetHeader-> "Topologies for the Self-energies",
DisplayFunction->(Export[ToFileName[{TempDirName,"TOP"},"HiggsSETop"<>".ps"],#]&));

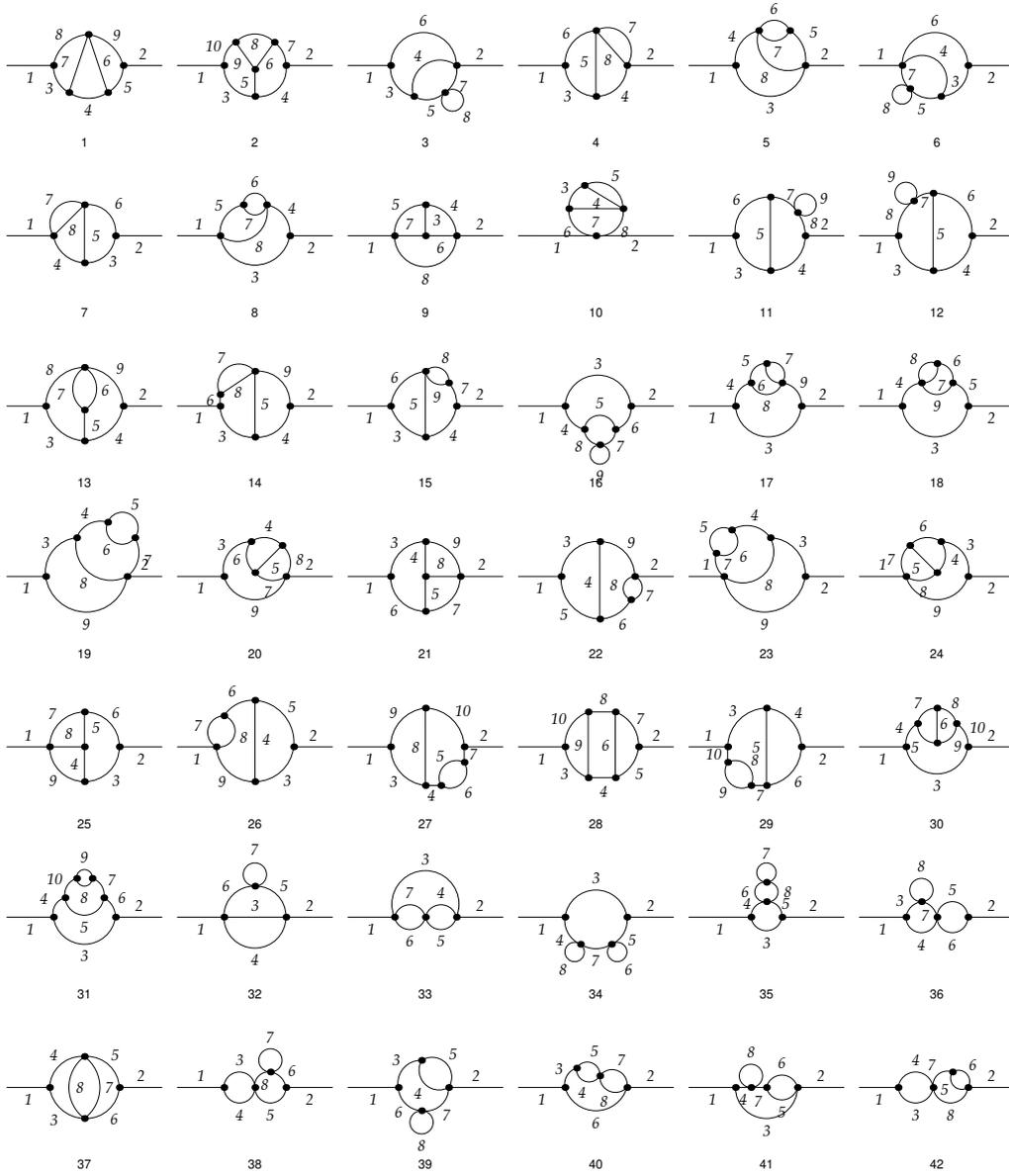
Paint[CTSE,FieldNumbers->True,ColumnsXRows->{8,8}, Numbering-> Simple,
SheetHeader-> "Topologies for the Renormalization of Subdivergences of Self-Energies",
DisplayFunction->(Export[ToFileName[{TempDirName,"TOP"},"HiggsCTSETop"<>".ps"],#]&));

Paint[TPTP,FieldNumbers->True,ColumnsXRows->{3,5},
Numbering-> Simple, SheetHeader-> "Topologies for the Tadpoles",
DisplayFunction->(Export[ToFileName[{TempDirName,"TOP"},"HiggsTPTop"<>".ps"],#]&));

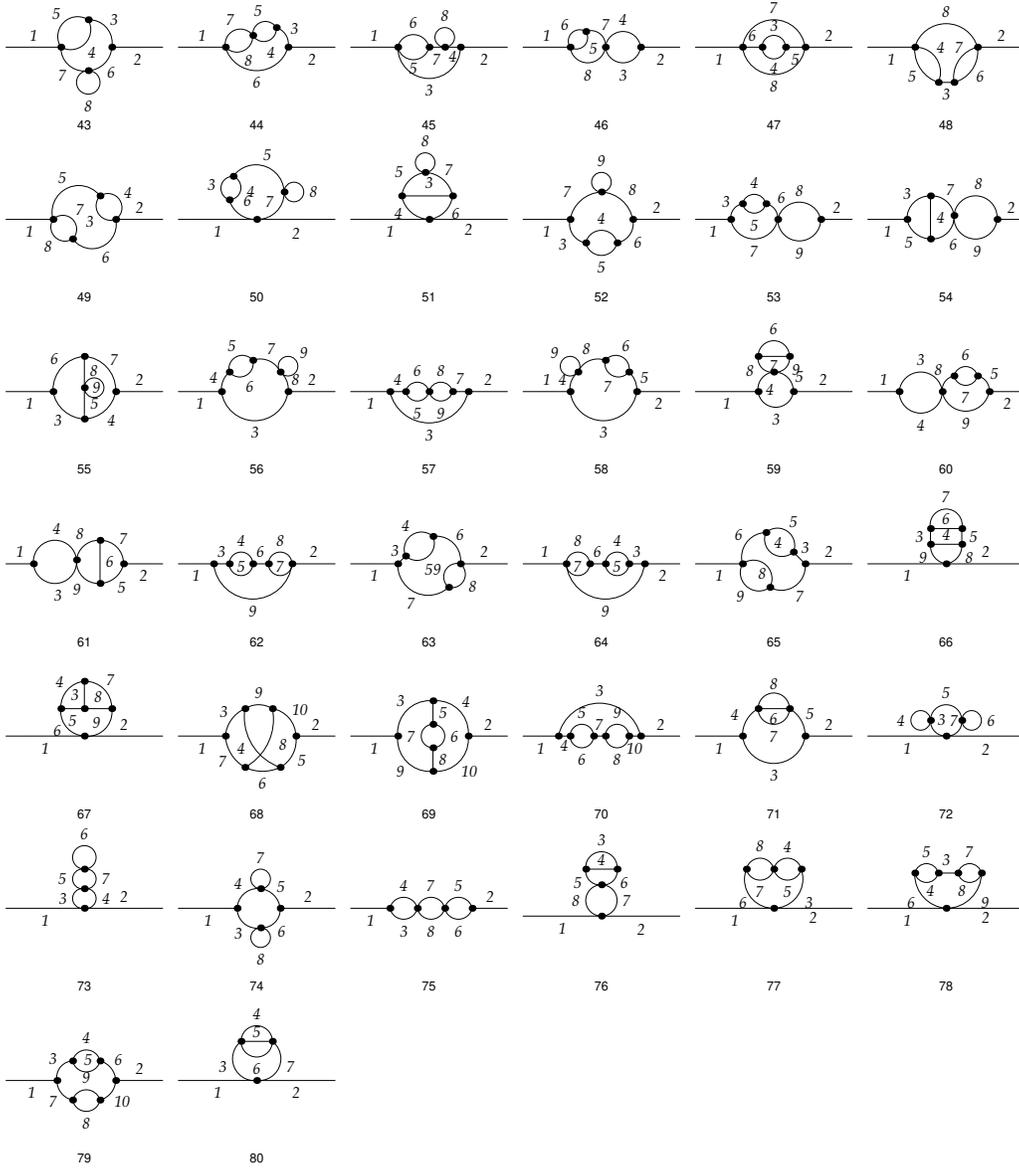
Paint[CTTP,FieldNumbers->True,ColumnsXRows->{4,4}, Numbering-> Simple,
SheetHeader-> "Topologies for the Renormalization of Subdivergences of Tadpoles",
DisplayFunction->(Export[ToFileName[{TempDirName,"TOP"},"HiggsCTTPTop"<>".ps"],#]&));

Quit[];
```

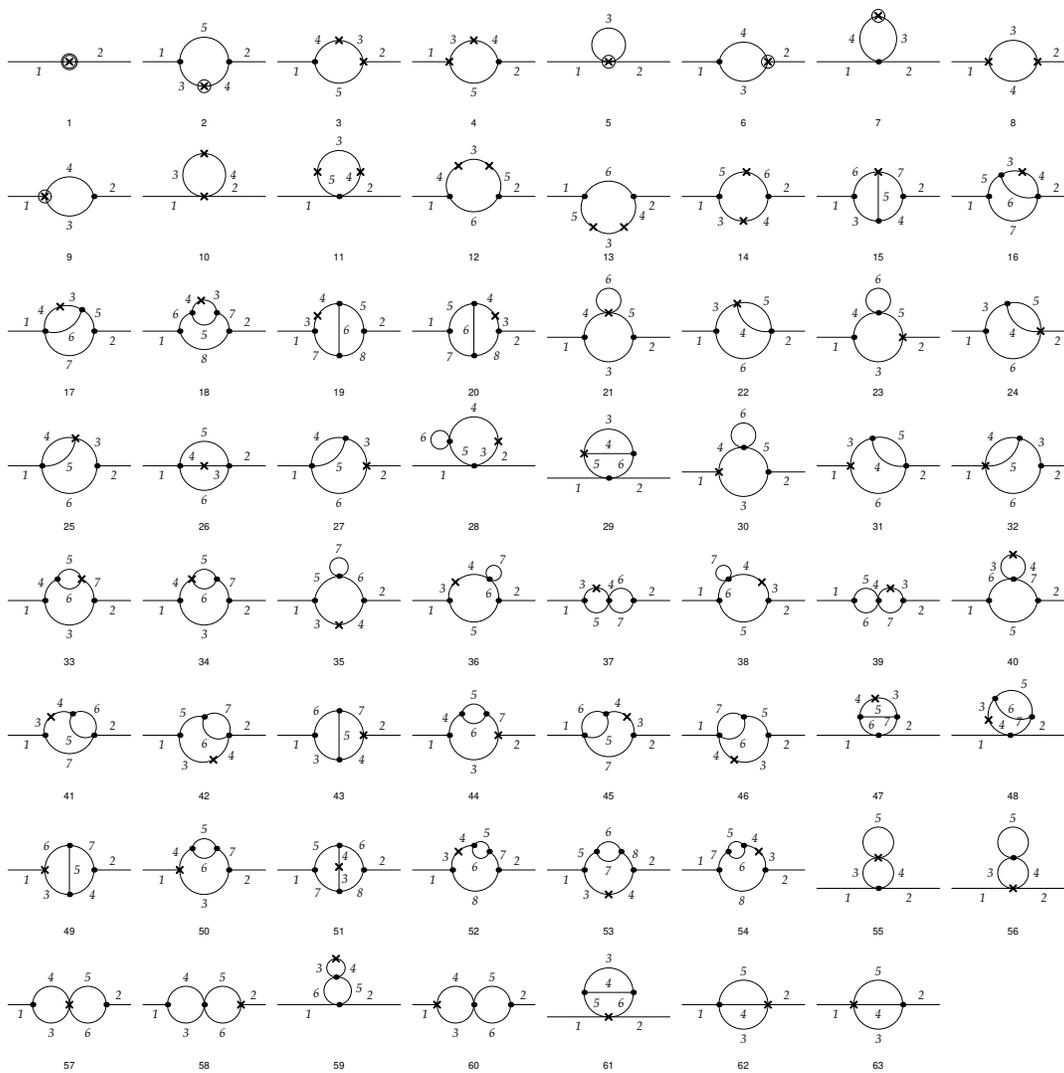
Topologies for the Self-energies



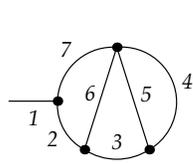
Topologies for the Self-energies



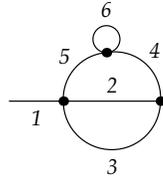
Topologies for the Renormalization of Subdivergences of Self-Energies



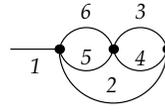
Topologies for the Tadpoles



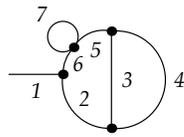
1



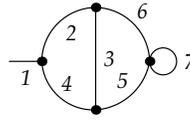
2



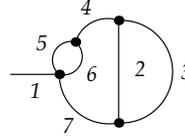
3



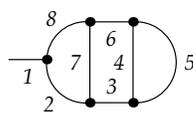
4



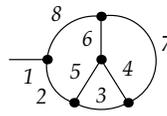
5



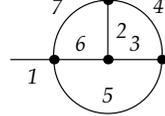
6



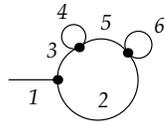
7



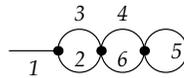
8



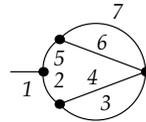
9



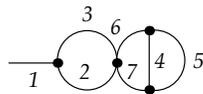
10



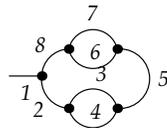
11



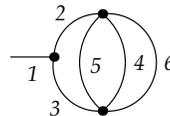
12



13

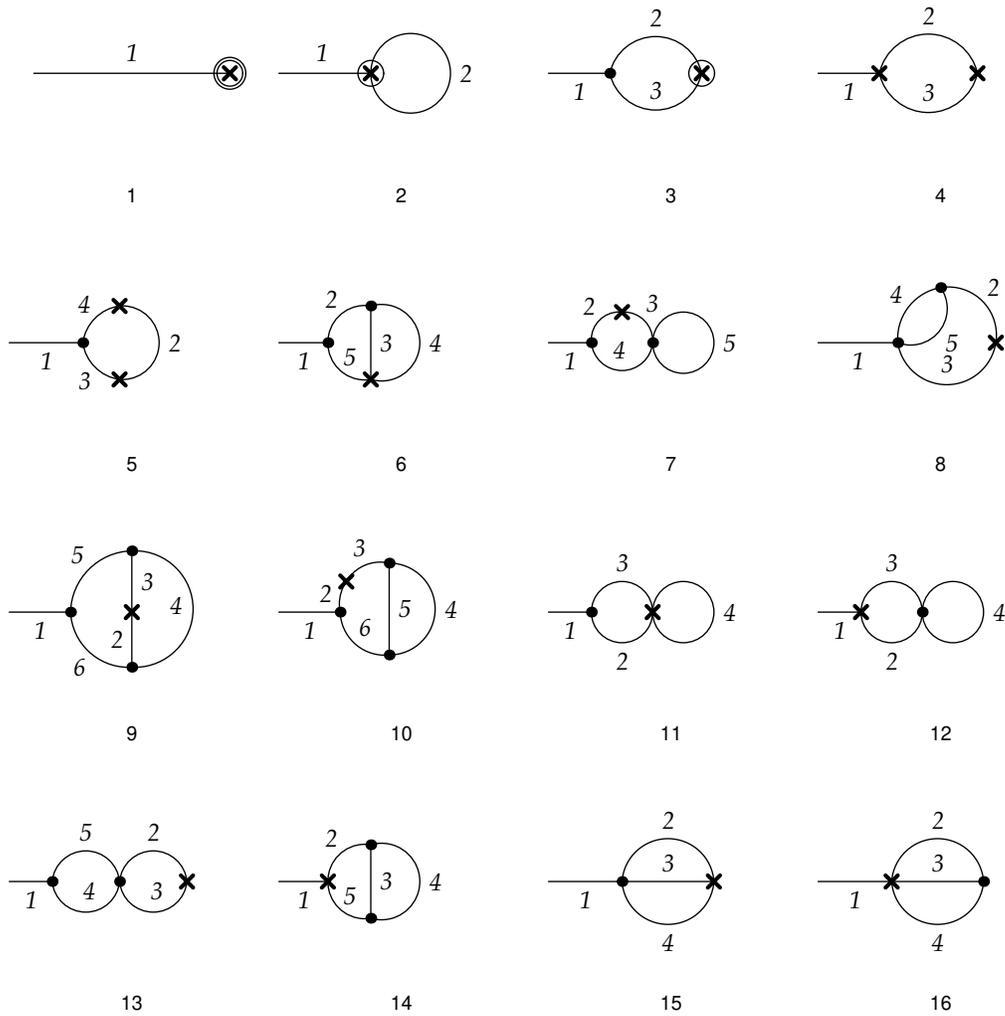


14



15

Topologies for the Renormalization of Subdivergences of Tadpoles



E. Generation of Amplitudes at $O(\alpha_t \alpha_s^2)$

In this appendix we show an example routine to generate the amplitudes of the three-loop neutral Higgs self-energies at order $\alpha_t \alpha_s^2$ in the MSSM. The routine includes a set of test functions to select only the needed diagrams at the given order. We include also the selection rules for the tadpole topologies and the diagrams with counter-term insertions.

E.1. Three-loop Higgs self-energies at $O(\alpha_t \alpha_s^2)$

```
PrependTo[$Path, ToFileName[{"Directory", "to", "FeynCalc901", "FeynCalc"}]];
$LoadFeynArts = True;
Get["FeynCalc.m"];
Off[Paint::nolevel]

LaunchKernels[ ]; Print["Number of Kernels: ", Length[ Kernels[] ] ]

ParallelEvaluate[
PrependTo[$Path, ToFileName[{"Directory", "to", "FeynCalc901", "FeynCalc"}]];
$LoadFeynArts = True;
Get["FeynCalc.m"]
Off[Paint::nolevel]
];

(*****
(** Generation of diagrams: creation of topologies, **)
(** definition and insertion of fields. **)
(*****)

TP=CreateTopologies[3, 1 -> 1, ExcludeTopologies -> Internal];
Print["Number of Topologies = ", Length[TP]]

CPHiggsF={S[1], S[2], S[3]};
$short1=Length[CPHiggsF];

InsFTP[topol_, field1_, field2_, selfields_, excludefields_] := InsertFields[topol,
field1->field2, Model->"MSSMCT", InsertionLevel->Particles,
ExcludeParticles -> excludefields, LastSelections -> selfields];

DistributeDefinitions[InsFTP]
```

```

selfields={};
exclufields={F[1, _], F[2, _], F[11, _], F[12, _], S[1], S[2], S[3], S[4], S[5],
S[6], S[11, _], S[12, _], V[1], V[2], V[3], V[6], U[1 | 2 | 3 | 4]};

(*****)
(** Patterns definitions **)
(*****)

upatt = F[3, {1, _}] | -F[3, {1, _}];
supatt = S[13, {_, 1, _}] | -S[13, {_, 1, _}];
dpatt = F[4, {1, _}] | -F[4, {1, _}];
sdpatt = S[14, {_, 1, _}] | -S[14, {_, 1, _}];
cpatt = F[3, {2, _}] | -F[3, {2, _}];
scpatt = S[13, {_, 2, _}] | -S[13, {_, 2, _}];
spatt = F[4, {2, _}] | -F[4, {2, _}];
sspatt = S[14, {_, 2, _}] | -S[14, {_, 2, _}];
tpatt = F[3, {3, _}] | -F[3, {3, _}];
stpatt = S[13, {_, 3, _}] | -S[13, {_, 3, _}];
bpatt = F[4, {3, _}] | -F[4, {3, _}];
sbpatt = S[14, {_, 3, _}] | -S[14, {_, 3, _}];
gpatt = V[5, {_}] | F[15, {_}] | V[6, {_}];
ghpatt = U[15, {_}];
tstpatt= Flatten[stpatt | tpatt];
sfgpatt = Flatten[supatt | sdpatt | scpatt | sspatt | spatt | sbpatt | gpatt];

(*****)
(* Selection rules for 3L Higgs Self-Energy diagrams at order \alpha_s^2\alpha_t, *)
(* There is a selection rule for each self-energy topology, e.g. there are 80 rules. *)
(*****)

SESelRules = {
(*1*) (MemberQ[#, Field[8] -> stpatt] && MemberQ[#, Field[9] -> stpatt] &&
      MemberQ[#, Field[4] -> Flatten[tpatt | stpatt | gpatt]])&,
(*2*) (MemberQ[#, Field[3] -> tstpatt] && MemberQ[#, Field[4] -> tstpatt])&,
(*3*) (MemberQ[#, Field[6] -> tpatt] && MemberQ[#, Field[4|7] -> gpatt])&,
(*4*) (MemberQ[#, Field[6] -> tpatt] && MemberQ[#, Field[4|8|7] -> tpatt])&,
(*5*) (MemberQ[#, Field[4] -> tpatt] && MemberQ[#, Field[3|5|8] -> tpatt])&,
(*6*) (MemberQ[#, Field[6] -> tpatt] && MemberQ[#, Field[4|7] -> gpatt])&,
(*7*) (MemberQ[#, Field[6] -> tpatt] && MemberQ[#, Field[4|8|7] -> tpatt])&,
(*8*) (MemberQ[#, Field[4] -> tpatt] && MemberQ[#, Field[3|5|8] -> tpatt])&,
(*9*) (MemberQ[#, Field[8] -> tpatt] && MemberQ[#, Field[6|7] -> tpatt])&,
(*10*) (MemberQ[#, Field[6|8] -> stpatt] && MemberQ[#, Field[3|7] ->
      Flatten[tpatt | stpatt | gpatt]])&,
(*11*) (MemberQ[#, Field[3] -> tstpatt] && MemberQ[#, Field[4] -> stpatt] &&
      MemberQ[#, Field[9] -> stpatt])&,
(*12*) (MemberQ[#, Field[4] -> tstpatt] && MemberQ[#, Field[3] -> stpatt] &&
      MemberQ[#, Field[9] -> stpatt])&,
(*13*) (MemberQ[#, Field[8] -> stpatt] && MemberQ[#, Field[9] -> stpatt] &&

```

```

MemberQ[#, Field[5] -> gpatt])&,
(*14*)(MemberQ[#, Field[6] -> stpatt] && MemberQ[#, Field[4] -> stpatt] &&
MemberQ[#, Field[5|8] -> gpatt])&,
(*15*)(MemberQ[#, Field[3] -> stpatt] && MemberQ[#, Field[7] -> stpatt] &&
MemberQ[#, Field[5|9] -> gpatt])&,
(*16*)(MemberQ[#, Field[3] -> tstpatt] && MemberQ[#, Field[5] ->
Flatten[tpatt | stpatt | gpatt]] && MemberQ[#, Field[9] -> stpatt])&,
(*17*)(MemberQ[#, Field[3] -> stpatt] && MemberQ[#, Field[5] ->
Flatten[tpatt | stpatt | gpatt]])&,
(*18*)(MemberQ[#, Field[3] -> stpatt] && MemberQ[#, Field[6] ->
Flatten[tpatt | stpatt | gpatt]])&,
(*19*)(MemberQ[#, Field[9] -> tpatt] && MemberQ[#, Field[7|8] -> gpatt])&,
(*20*)(MemberQ[#, Field[9] -> tpatt] && MemberQ[#, Field[7|8] -> gpatt])&,
(*21*)(MemberQ[#, Field[7] -> tpatt] && MemberQ[#, Field[8|9] -> gpatt])&,
(*22*)(MemberQ[#, Field[9] -> tpatt] && MemberQ[#, Field[7|8] -> gpatt])&,
(*23*)(MemberQ[#, Field[9] -> tpatt] && MemberQ[#, Field[7|8] -> gpatt])&,
(*24*)(MemberQ[#, Field[9] -> tpatt] && MemberQ[#, Field[7|8] -> gpatt])&,
(*25*)(MemberQ[#, Field[9] -> tpatt] && MemberQ[#, Field[7|8] -> gpatt])&,
(*26*)(MemberQ[#, Field[9] -> tpatt] && MemberQ[#, Field[7|8] -> gpatt])&,
(*27*)(MemberQ[#, Field[7] -> tstpatt] && MemberQ[#, Field[9] -> tstpatt] &&
MemberQ[#, Field[8] -> gpatt])&,
(*28*)(MemberQ[#, Field[3] -> tstpatt] && MemberQ[#, Field[5] -> tstpatt] &&
MemberQ[#, Field[4|9] -> Flatten[tpatt | stpatt | gpatt]])&,
(*29*)(MemberQ[#, Field[10] -> tstpatt] && MemberQ[#, Field[4] -> tstpatt] &&
MemberQ[#, Field[5] -> gpatt])&,
(*30*)(MemberQ[#, Field[4] -> tstpatt] && MemberQ[#, Field[10] -> tstpatt])&,
(*31*)(MemberQ[#, Field[3] -> tstpatt] && MemberQ[#, Field[5] ->
Flatten[tpatt | stpatt | gpatt]])&,
(*32*)(MemberQ[#, Field[5] -> tpatt] && MemberQ[#, Field[6] -> tpatt])&,
(*33*)(MemberQ[#, Field[6] -> tpatt] && MemberQ[#, Field[7] -> tpatt])&,
(*34*)(MemberQ[#, Field[3] -> stpatt] && MemberQ[#, Field[7] -> stpatt] &&
MemberQ[#, Field[6] -> stpatt] && MemberQ[#, Field[8] -> stpatt])&,
(*35*)(MemberQ[#, Field[3] -> stpatt] && MemberQ[#, Field[7] -> stpatt] &&
MemberQ[#, Field[6|8] -> sfgpatt])&,
(*36*)(MemberQ[#, Field[3] -> stpatt] && MemberQ[#, Field[5] -> stpatt] &&
MemberQ[#, Field[8] -> stpatt])&,
(*37*)(MemberQ[#, Field[3] -> stpatt] && MemberQ[#, Field[5] -> stpatt])&,
(*38*)(MemberQ[#, Field[6] -> stpatt] && MemberQ[#, Field[3] -> stpatt] &&
MemberQ[#, Field[7] -> stpatt])&,
(*39*)(MemberQ[#, Field[4] -> tpatt] && MemberQ[#, Field[5|7] -> gpatt])&,
(*40*)(MemberQ[#, Field[6] -> tpatt] && MemberQ[#, Field[7|8] -> gpatt])&,
(*41*)(MemberQ[#, Field[3|5|6] -> tpatt])&,
(*42*)(MemberQ[#, Field[8|5|6] -> tpatt])&,
(*43*)(MemberQ[#, Field[4|5|7] -> tpatt])&,
(*44*)(MemberQ[#, Field[6|7|8] -> tpatt])&,
(*45*)(MemberQ[#, Field[3|5|6] -> tpatt])&,
(*46*)(MemberQ[#, Field[8|5|6] -> tpatt])&,
(*47*)(MemberQ[#, Field[8|5|7] -> tpatt])&,

```

```

(*48*)(MemberQ[#, Field[4|5|8] -> tpatt])&,
(*49*)(MemberQ[#, Field[5|7|8] -> tpatt])&,
(*50*)(MemberQ[#, Field[5] -> stpatt] && MemberQ[#, Field[6] -> stpatt] &&
MemberQ[#, Field[8] -> stpatt] && MemberQ[#, Field[3|4] ->
Flatten[tpatt | stpatt | gpatt]])&,
(*51*)(MemberQ[#, Field[4] -> stpatt] && MemberQ[#, Field[8] -> stpatt] &&
MemberQ[#, Field[3|5|7] -> Flatten[tpatt | stpatt | gpatt]])&,
(*52*)(MemberQ[#, Field[3] -> stpatt] && MemberQ[#, Field[6] -> stpatt] &&
MemberQ[#, Field[9] -> stpatt] && MemberQ[#, Field[4|5] ->
Flatten[tpatt | stpatt | gpatt]])&,
(*53*)(MemberQ[#, Field[3] -> stpatt] && MemberQ[#, Field[9] -> stpatt] &&
MemberQ[#, Field[4|5] -> Flatten[tpatt | stpatt | gpatt]])&,
(*54*)(MemberQ[#, Field[3] -> tstpatt] && MemberQ[#, Field[7] -> stpatt] &&
MemberQ[#, Field[8] -> stpatt])&,
(*55*)(MemberQ[#, Field[6] -> tstpatt] && MemberQ[#, Field[7] -> tstpatt] &&
MemberQ[#, Field[9] -> stpatt] && MemberQ[#, Field[5] -> gpatt] &&
MemberQ[#, Field[8]->gpatt])&,
(*56*)(MemberQ[#, Field[3] -> stpatt] && MemberQ[#, Field[9] -> stpatt] &&
MemberQ[#, Field[5|6] -> Flatten[tpatt | stpatt | gpatt]])&,
(*57*)(MemberQ[#, Field[3] -> stpatt] && MemberQ[#, Field[5|6] -> gpatt] &&
MemberQ[#, Field[8|9] -> gpatt])&,
(*58*)(MemberQ[#, Field[3] -> stpatt] && MemberQ[#, Field[9] -> stpatt] &&
MemberQ[#, Field[6|7] -> Flatten[tpatt | stpatt | gpatt]])&,
(*59*)(MemberQ[#, Field[3] -> stpatt] && MemberQ[#, Field[8|9] -> sfgpatt])&,
(*60*)(MemberQ[#, Field[5] -> stpatt] && MemberQ[#, Field[4] -> stpatt] &&
MemberQ[#, Field[6|7] -> Flatten[tpatt | stpatt | gpatt]])&,
(*61*)(MemberQ[#, Field[7] -> tstpatt] && MemberQ[#, Field[3] -> stpatt] &&
MemberQ[#, Field[6] -> Flatten[tpatt | stpatt | gpatt]])&,
(*62*)(MemberQ[#, Field[7|8|9] -> tpatt])&,
(*63*)(MemberQ[#, Field[6|8|9] -> tpatt])&,
(*64*)(MemberQ[#, Field[7|8|9] -> tpatt])&,
(*65*)(MemberQ[#, Field[6|8|9] -> tpatt])&,
(*66*)(MemberQ[#, Field[8|9] -> stpatt] && MemberQ[#, Field[3|4|5] ->
Flatten[tpatt | stpatt | gpatt]])&,
(*67*)(MemberQ[#, Field[6|9] -> stpatt] && MemberQ[#, Field[4|7] ->
Flatten[tpatt | stpatt | gpatt]])&,
(*68*)(MemberQ[#, Field[7] -> tstpatt] && MemberQ[#, Field[5] -> tstpatt] &&
MemberQ[#, Field[4|8] -> Flatten[tpatt | stpatt | gpatt]])&,
(*69*)(MemberQ[#, Field[3] -> tstpatt] && MemberQ[#, Field[4] -> tstpatt] &&
MemberQ[#, Field[5] -> gpatt] && MemberQ[#, Field[8] -> gpatt])&,
(*70*)(MemberQ[#, Field[3] -> tstpatt] && MemberQ[#, Field[7] -> tstpatt] &&
MemberQ[#, Field[5|6] -> Flatten[tpatt | stpatt | gpatt]] &&
MemberQ[#, Field[8|9]->Flatten[tpatt | stpatt | gpatt]])&,
(*71*)(MemberQ[#, Field[3] -> stpatt] && MemberQ[#, Field[6|7|8] -> sfgpatt])&,
(*72*)(MemberQ[#, Field[3] -> stpatt] && MemberQ[#, Field[5] -> stpatt] &&
MemberQ[#, Field[4] -> stpatt] && MemberQ[#, Field[6] -> stpatt])&,
(*73*)(MemberQ[#, Field[3] -> stpatt] && MemberQ[#, Field[6] -> stpatt] &&
MemberQ[#, Field[5|7] -> sfgpatt])&,

```

```

(*74*)(MemberQ[# , Field[3] -> stpatt] && MemberQ[# , Field[5] -> stpatt] &&
  MemberQ[# , Field[7] -> stpatt] && MemberQ[# , Field[8] -> stpatt])&,
(*75*)(MemberQ[# , Field[3] -> stpatt] && MemberQ[# , Field[6] -> stpatt] &&
  MemberQ[# , Field[7|8] -> sfgpatt])&,
(*76*)(MemberQ[# , Field[7] -> stpatt] && MemberQ[# , Field[5|6] -> sfgpatt])&,
(*77*)(MemberQ[# , Field[3] -> stpatt] && MemberQ[# , Field[4|5] ->
  Flatten[tpatt | stpatt | gpatt]] &&
  MemberQ[# , Field[7|8] -> Flatten[tpatt | stpatt | gpatt]])&,
(*78*)(MemberQ[# , Field[6] -> stpatt] && MemberQ[# , Field[3] -> stpatt] &&
  MemberQ[# , Field[4|5] -> Flatten[tpatt | stpatt | gpatt]] &&
  MemberQ[# , Field[7|8] -> Flatten[tpatt | stpatt | gpatt]])&,
(*79*)(MemberQ[# , Field[3] -> tstpatt] && MemberQ[# , Field[6] -> tstpatt] &&
  MemberQ[# , Field[4|5] -> Flatten[tpatt | stpatt | gpatt]] &&
  MemberQ[# , Field[8|9] -> Flatten[tpatt | stpatt | gpatt]])&,
(*80*)(MemberQ[# , Field[3] -> stpatt] && MemberQ[# , Field[4|5|6] -> sfgpatt])&;

(*****
(* Choosing the diagrams for which the function InsFTP[_] with the given criteria *)
(* in "SESelRules" yields True. *)
(*****

DiagSelHiggsSE[i_] := Parallelize[ MapThread[ DiagramSelect[
  InsFTP[Take[TP,{#1}],CPHiggsF[[i]],CPHiggsF[[i]],selfields, excludefields],#2]&,
{Range[Length[TP]],SESelRules}]];

HiggsSE = Array[ DiagSelHiggsSE, $short1];
Print["Number of Higgs SE = ", Length[HiggsSE[[1]]]]
DistributeDefinitions[HiggsSE]

(*****
(** Drawing the self-energy diagrams and exporting to *.ps **)
(*****

TempDirName=ToFileName[{"Directory","to","save","files"}];

Table[ If[!DirectoryQ[ ToFileName[{ TempDirName,
  ToString[CPHiggsF[[j]]]<>ToString[CPHiggsF[[j]]],
  StringJoin[ToString[Top],ToString[1]]}],
CreateDirectory[ ToFileName[{ TempDirName,
  ToString[CPHiggsF[[j]]]<>ToString[CPHiggsF[[j]]],
  StringJoin[ToString[Top],ToString[1]]}],
{j,3,3}, {1,1,Length[SESelRules]}];

PaintHiggsSE[dir1_,dir2_,dir3_,name_,top_,level_, tittle_] := Paint[ top,
PaintLevel -> level, FieldNumbers -> True, ColumnsXRows -> {10,10},
Numbering -> Simple, SheetHeader -> tittle,
DisplayFunction -> (Export[ToFileName[{dir1,dir2,dir3},StringJoin[dir2,name]],#]&);

```

```

DistributeDefinitions[PaintHiggsSE];

Table[ Parallelize[ MapThread[ PaintHiggsSE[ TempDirName,
ToString[CPHiggsF[[j]]]<>ToString[CPHiggsF[[j]]],
StringJoin[ToString[Top],ToString[#1]],"HiggsSE"<>ToString[#1]<>".ps",#2,Particles,
"Selfenergy Diagrams at 0(\[Alpha]_t(\[Alpha]_s)^2)"]&,
{Range[Length[SESelRules]], HiggsSE[[j]] }]],{j,3,3}];

(*****
(** Generation of the Amplitudes. The amplitudes are saved in txt files **)
(** with the name S[?]S[?]Amps. **)
(*****)

TxtFile[dir1_,dir2_, dir3_, Amp_, name_] := Put[ Amp,
ToFileName[{dir1,dir2,dir3},StringJoin[dir2,name]]];
DistributeDefinitions[TxtFile];

Table[ Parallelize[ MapThread[
TxtFile[ TempDirName, ToString[CPHiggsF[[j]]]<>ToString[CPHiggsF[[j]]],
StringJoin[ToString[Top],ToString[#1] ],
CreateFeynAmp[#2, AmplitudeLevel -> {Particles}],ToString[Amps]<>ToString[#1]]&,
{Range[Length[SESelRules]],HiggsSE[[j]]} ] ], {j,3,3}];

CloseKernels[];

Quit[];

```

E.2. Selection rules for Higgs tadpole topologies

```

(*****
(** Patterns defined here correspond to the diagrams at order  $O(h_t g_s^4)$  **)
(*****)

t[n_] := MemberQ[#, Field[n] -> tpatt]&;
st[n_] := MemberQ[#, Field[n] -> stpatt]&;
g[n_] := MemberQ[#, Field[n] -> gpatt]&;
stg[n_] := MemberQ[#, Field[n] -> Flatten[tpatt | stpatt | gpatt]]&;
tst[n_] := MemberQ[#, Field[n] -> tstpatt]&;
sfg[n_] := MemberQ[#, Field[n] -> sfgpatt]&;
Nog[n_] := FreeQ[#, Field[n]-> gpatt]&;

(*****
(** Selection rules for 3L Higgs tadpole diagrams at  $O(h_t g_s^4)$  **)
(*****)

```



```
(*****)

TPSelRules={
(*1*) tst[2],
(*2*) t[2],
(*3*) t[2],
(*4*) (MemberQ[#, Field[2] -> stpatt] && FreeQ[#, Field[7] -> gpatt])&,
(*5*) (MemberQ[#, Field[2] -> tstpatt] && FreeQ[#, Field[7] -> gpatt])&,
(*6*) t[7],
(*7*) tst[2],
(*8*) tst[2],
(*9*) t[5],
(*10*)(MemberQ[#, Field[2] -> tstpatt] && FreeQ[#, Field[6] -> gpatt] &&
      FreeQ[#, Field[4]-> gpatt])&,
(*11*)(MemberQ[#, Field[2] -> stpatt] && FreeQ[#, Field[5] -> gpatt])&,
(*12*)tst[2],
(*13*)st[2],
(*14*)tst[2],
(*15*)st[2]};
```

E.3. Selection rules for counter-term diagrams

```
(*****)
(** Patterns defined here correspond to the CT at order  $O(\alpha_s^2 \alpha_t)$  **)
(*****)

t[n_] := MemberQ[#, Field[n] -> tpatt]&;
st[n_] := MemberQ[#, Field[n] -> stpatt]&;
g[n_] := MemberQ[#, Field[n] -> gpatt]&;
stg[n_] := MemberQ[#, Field[n] -> Flatten[tpatt | stpatt | gpatt]]&;
tst[n_] := MemberQ[#, Field[n] -> tstpatt]&;
sfg[n_] := MemberQ[#, Field[n] -> sfgpatt]&;
Aux[n_] := FreeQ[#, Field[n]-> tpatt]&;

(* Selection rules for self-energy counter-terms to renormalize the subdivergences *)
(*****)

CTSelRules={
Aux[1], tst[5], tst[5], tst[5], st[3], tst[3], st[3],
(MemberQ[#, Field[3] -> tstpatt]&&MemberQ[#, Field[4] -> tstpatt])&,
tst[3], st[3], st[4],
(MemberQ[#, Field[3] -> tstpatt]&&MemberQ[#, Field[6] -> tstpatt])&,
(MemberQ[#, Field[3] -> tstpatt]&&MemberQ[#, Field[6] -> tstpatt])&,
(MemberQ[#, Field[5] -> tstpatt]&&MemberQ[#, Field[6] -> tstpatt])&,
```

```

(MemberQ[#, Field[3] -> tstpatt]&&MemberQ[#, Field[5] -> gpatt])&,
t[7], t[7], tst[8],
(MemberQ[#, Field[7] -> tstpatt]&&MemberQ[#, Field[6] -> gpatt])&,
(MemberQ[#, Field[7] -> tstpatt]&&MemberQ[#, Field[6] -> gpatt])&,
(FreeQ[#, Field[6]->gpatt]&&MemberQ[#, Field[3]->tstpatt])&,
t[6], (FreeQ[#, Field[6]->gpatt]&&MemberQ[#,Field[3]->tstpatt])&,
t[6], t[6], t[6], t[6],
(FreeQ[#, Field[6]->gpatt]&&MemberQ[#,Field[5]->stpatt])&,
st[5], (FreeQ[#, Field[6]->gpatt]&&MemberQ[#,Field[3]->stpatt])&,
t[6], t[6], tst[3], tst[3],
(FreeQ[#, Field[7]->gpatt]&&MemberQ[#,Field[3]->tstpatt])&,
(FreeQ[#, Field[7]->gpatt]&&MemberQ[#,Field[5]->tstpatt])&,
(MemberQ[#, Field[5] -> stpatt]&&MemberQ[#, Field[7] -> stpatt])&,
(FreeQ[#, Field[7]->gpatt]&&MemberQ[#,Field[3]->tstpatt])&,
(MemberQ[#, Field[6] -> stpatt]&&MemberQ[#,Field[7] -> stpatt])&,
tst[5], t[7], t[4],
(MemberQ[#, Field[3] -> tstpatt]&&MemberQ[#, Field[5] -> gpatt])&,
tst[3], t[7], t[4], tst[7], tst[7],
(MemberQ[#, Field[4] -> tstpatt]&&MemberQ[#, Field[5] -> gpatt])&,
tst[3], tst[8], tst[8], tst[5], tst[8],
(FreeQ[#, Field[5]->gpatt] && MemberQ[#, Field[3] -> stpatt] &&
MemberQ[#, Field[4] -> stpatt])&,
(FreeQ[#, Field[5]->gpatt] && MemberQ[#, Field[3] -> stpatt] &&
MemberQ[#, Field[4] -> stpatt])&,
(MemberQ[#, Field[3] -> stpatt]&&MemberQ[#, Field[6] -> stpatt])&,
(MemberQ[#, Field[3] -> stpatt]&&MemberQ[#, Field[6] -> stpatt])&,
(MemberQ[#, Field[5] -> stpatt]&&MemberQ[#, Field[6] -> stpatt])&,
(MemberQ[#, Field[3] -> stpatt]&&MemberQ[#, Field[6] -> stpatt])&,
(MemberQ[#, Field[3] -> stpatt]&&MemberQ[#, Field[6] -> stpatt])&,
(MemberQ[#, Field[5] -> stpatt]&&MemberQ[#, Field[6] -> stpatt])&,
t[4], t[4]};

```

```

(*****
(* Selection rules for tadpole counter-terms to renormalize the subdivergences *)
*****

```

```

CTTPSelRules={
Aux[1], tst[2], tst[2],
(MemberQ[#, Field[2] -> tstpatt]&&MemberQ[#, Field[3] -> tstpatt])&,
(MemberQ[#, Field[3] -> tstpatt]&&MemberQ[#, Field[2] -> tstpatt])&,
(MemberQ[#, Field[2] -> tstpatt])&,
(MemberQ[#, Field[2] -> stpatt] && MemberQ[#, Field[3] -> stpatt] &&
FreeQ[#, Field[5]->gpatt])&,
t[4], (MemberQ[#, Field[5] -> tstpatt])&,
(MemberQ[#, Field[6] -> tstpatt]&&MemberQ[#, Field[3] -> tstpatt])&,
(MemberQ[#, Field[3]->stpatt]&&FreeQ[#, Field[4]->gpatt])&,
(MemberQ[#, Field[3] -> stpatt] && MemberQ[#, Field[2] -> stpatt] &&
FreeQ[#, Field[4]->gpatt])&,
st[5], (MemberQ[#, Field[2] -> tstpatt])&, t[3], t[3]};

```

F. Regularization of Three-Loop Integrals in DRED

This appendix contain a simple routine where the three-loop self-energy amplitudes generated with FeynArts (see Appendix E) are regularized using DRED. Besides, the sum over the color indices and, in general, the color algebra of the SU(3) generators are performed.

```
#!/path/to/MathematicaScript -script

$LoadFeynArts = True;
Get["/path/to/FeynCalc901/FeynCalc/FeynCalc.m"];

PrependTo[$Path, ToFileName[{"Directory", "of", "external", "routines"}]];

Off[DeleteFile::nffil];
Off[ParallelCombine::nopar1];
Off[Simplify::time];

(*****
(** We have used the package "SimplificationDefinitions" to Simplify      **)
(** algebraic expressions. This package can be found into the installation **)
(** folders of FeynHiggs: ~/FeynHiggs/gen/tlsp/packages/                    **)
(*****

<< SimplificationDefinitions';

LaunchKernels[20];

ParallelEvaluate[

$LoadFeynArts = True;
Get["/path/to/FeynCalc901/FeynCalc/FeynCalc.m"];
PrependTo[$Path, ToFileName[{"Directory", "of", "external", "routines"}]];

Off[DeleteFile::nffil];
Off[ParallelCombine::nopar1];
Off[Simplify::time];

<< SimplificationDefinitions';

];
```

```

CPEHiggsF={S[1], S[2], S[3]};

$short1=Length[CPEHiggsF];

TempDirName=ToFileName[{"Directory","where","FeynArts","amplitudes","were","saved"}];

(*****
(** Calling the FeynArts amplitudes **)
(*****)

Amp[n_, m_, l_] := Get[ToString[
    CPEHiggsF[[n]]<>ToString[CPEHiggsF[[m]]<>"Amps"<>ToString[l],
    Path -> { ToFileName[{ TempDirName,
    ToString[CPEHiggsF[[n]]<>ToString[CPEHiggsF[[m]]],
    ToString[Top]<>ToString[l]}]}];

(*****
(** We have used FeynCalc patched with FeynArts in order to perform the Dirac **)
(** and the Color algebra with the FeynCalc tools. For this reason we have **)
(** made the next changes over the amplitudes. CA -> ca means that cos(alpha) **)
(** is changed to avoid the conflict of notation with the FC casimir CA. **)
(*****)

changesFAFC = { CA -> ca, SumOver[___]-> 1,
FASUNT[Index[Gluon,g1_],Index[Gluon,g2_],Index[Colour,o2_],Index[Colour, o1_]]
:> FASUNT[Index[Gluon,g1], Index[Colour,o2], c].FASUNT[ Index[Gluon,g2], c,
    Index[Colour,o1]],
FASUNTSum[Index[Colour,o2_],Index[Colour,o1_],Index[Colour,o4_],Index[Colour,o3_]]
:> FASUNT[ x, Index[Colour,o2], Index[Colour,o1]].FASUNT[ x, Index[Colour,o4],
    Index[Colour,o3]] };

(* Assuming NLF limit *)
changesNLF = {MB -> 0, MC -> 0, MD -> 0, MS -> 0, MU -> 0, MZ -> MW/CW}

(*****
(** Changes also include the substitutions to compute the amplitudes in **)
(** the real MSSM. **)
(*****)

changesreal = { SqrtEG1 -> 1, USf[a_][b_] :> USf[b, a],
Conjugate[USf[a_][b_]] :> USf[b, a], Conjugate[UChC[a_]] :> UChC[a],
Conjugate[VChC[a_]]:>VChC[a], Conjugate[Af[a_]]:>Af[a], Conjugate[MUE]->MUE};

(*****
(** The function FCFAConvert transforms the amplitude from FeynArts notation **)
(** to FeynCalc notation. We identified the external momentum with the letter **)
(*****)

```

```

(** "p" and then we have assumed the limit of vanishing external momentum **)
(*****)

SetOptions[FCFAConvert,UndoChiralSplittings-> True];
SetOptions[DiracSimplify,DiracSubstitute67-> True,Expanding-> True,Factoring-> True];

ParallelEvaluate[
SetOptions[FCFAConvert,UndoChiralSplittings-> True];
SetOptions[DiracSimplify,DiracSubstitute67-> True,Expanding-> True,Factoring-> True];
];

SEFC[n_, m_, l_] := FCFAConvert[Amp[n,m,l] //. changesFAFC //. changesNLF //. changesreal,
IncomingMomenta -> {p}, OutgoingMomenta -> {p},
LoopMomenta-> {q1,q2,q3} /. {p -> 0} ;

(*****)
(** The next functions performs the DRED regularization of the three-loop **)
(** amplitudes using the Q4S algebra. **)
(*****)

Regul[n_,m_,l_] := ParallelMap[ DiracSimplify[
DiracSimplify[SEFC[n,m,l][[#]]] /. {DiracGamma[5]->0}&,
Range[Length[SEFC[n,m,l]]] ];

TxtFile[dir1_,dir2_, dir3_, Amp_, name_] := Put[Amp,
ToFileName[{dir1,dir2,dir3},StringJoin[dir2,name]]];

Table[ Map[ TxtFile[ TempDirName,
ToString[CPEHiggsF[[i]]]<>ToString[CPEHiggsF[[j]]],StringJoin[ToString[Top],ToString[#]],
Regul[i,j,#],ToString[RampsFC]<>ToString[#]]&, Range[1,48] ], {i,1,1}, {j,1,1} ];

SetOptions[DiracTrace,DiracTraceEvaluate-> True];
SetOptions[SUNSSimplify,SUNTrace-> True];
Off[DotSimplify::argrx]

ParallelEvaluate[

SetOptions[DiracTrace,DiracTraceEvaluate-> True];
SetOptions[SUNSSimplify,SUNTrace-> True];
Off[DotSimplify::argrx]

];

RegAmp[n_, m_, j_] := Get[
ToString[CPEHiggsF[[n]]]<>ToString[CPEHiggsF[[m]]]<>"RampsFC"<>ToString[j],
Path -> { ToFileName[TempDirName,
ToString[CPEHiggsF[[n]]]<>ToString[CPEHiggsF[[m]]],

```

```

ToString[Top]<>ToString[j]]} ]];

(*****)
(** The next functions performs the Color algebra on the SU(3) generators      **)
(** in the numerators of the amplitudes.                                     **)
(*****)

SUNSAmp[a_,b_,c_] := ParallelMap[ MagicSimplify[ Calc[ SUNSimplify[
Expand[ Contract[ RegAmp[a,b,c][[#]] ]]] /. False -> True ],
Feedback->False ]&, Range[Length[RegAmp[a,b,c]] ]];

Map[ Table[
  TxtFile[ TempDirName, ToString[CPEHiggsF[[i]]]<>ToString[CPEHiggsF[[j]]],
  StringJoin[ToString[Top],ToString[#]], SUNSAmp[i,j,#],
  ToString[AlgebraAmps]<>ToString[#],
  {i, 1, 1}, {j, 1, 1}]&, Range[1, 48] ]];

Print["The End!"]

CloseKernels[];

Quit[];

```

We next show the outputs of the functions defined in the above routine for the amplitude of the diagram pictured in Fig. **F-1**.

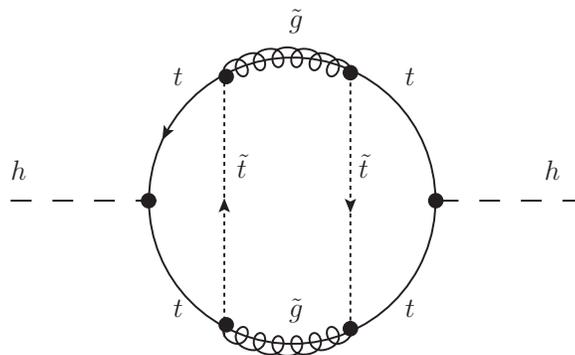


Figure F-1.: Generic three-loop Higgs self-energy diagram. The field h stands for the lightest Higgs boson, t is the top quark field, \tilde{t} is the stop and \tilde{g} represents the gluino field.

The amplitude $\text{Amp}[1,1,13][[5]]$ of the diagram in Fig. F-1 is one of the amplitudes that have the most complicated numerator structure. The vertex expressions were simplified taking into account the unitarity of the sfermion mixing matrix and disregarding the electroweak gauge couplings.

Amp[1, 1, 13][[5]]

$$\begin{aligned}
& \text{FAFeynAmp} \left(\text{GraphID} \text{ Topology} = 1, \text{Generic} = 2, \text{Classes} = 2, \text{Particles} = 1, \text{Number} = 5 \right), \\
& \text{Integral}[q1, q2, q3], \frac{1}{4096 \pi^{12}} \\
& i \text{FAFeynAmpDenominator} \left(\frac{1}{(q1)^2 - MT^2}, \frac{1}{(q2)^2 - MG^2}, \frac{1}{(q2 - q1)^2 - MSf(1, 3, 3)^2}, \frac{1}{(q3)^2 - MT^2}, \right. \\
& \left. \frac{1}{(q2 + q3)^2 - MSf(1, 3, 3)^2}, \frac{1}{(q3 - k1)^2 - MT^2}, \frac{1}{(k1 + q1)^2 - MT^2}, \frac{1}{(k1 + q2)^2 - MG^2} \right) \\
& \text{tr} \left(\bar{\gamma} \cdot (-\bar{k}1 - \bar{q}2) + MG1, -i \sqrt{2} \text{FAGS}(\bar{\gamma}^6 \text{USf}(1, 1, 3, 3) - \bar{\gamma}^7 \text{USf}(1, 2, 3, 3)) \right. \\
& \left. \text{FASUNT}(\text{Glu}4, \text{Col}4, \text{Col}5), \bar{\gamma} \cdot (\bar{q}3 - \bar{k}1) + MT, -\frac{i \text{caht}(\bar{\gamma}^6 + \bar{\gamma}^7)}{\sqrt{2}}, \bar{\gamma} \cdot \bar{q}3 + MT, \right. \\
& \left. -i \sqrt{2} \text{FAGS}(\bar{\gamma}^7 \text{USf}(1, 1, 3, 3) - \bar{\gamma}^6 \text{USf}(1, 2, 3, 3)) \text{FASUNT}(\text{Glu}3, \text{Col}5, \text{Col}4), \right. \\
& \left. MG1 - \bar{\gamma} \cdot \bar{q}2, -i \sqrt{2} \text{FAGS}(\bar{\gamma}^7 \text{USf}(1, 1, 3, 3) - \bar{\gamma}^6 \text{USf}(1, 2, 3, 3)) \right. \\
& \left. \text{FASUNT}(\text{Glu}3, \text{Col}6, \text{Col}3), MT - \bar{\gamma} \cdot \bar{q}1, -\frac{i \text{caht}(\bar{\gamma}^6 + \bar{\gamma}^7)}{\sqrt{2}}, \bar{\gamma} \cdot (-\bar{k}1 - \bar{q}1) + MT, \right. \\
& \left. -i \sqrt{2} \text{FAGS}(\bar{\gamma}^6 \text{USf}(1, 1, 3, 3) - \bar{\gamma}^7 \text{USf}(1, 2, 3, 3)) \text{FASUNT}(\text{Glu}4, \text{Col}3, \text{Col}6) \right) \Big)
\end{aligned}$$

Note that the gammas and the loop momenta in the numerators are defined in four dimensions (the quantities with a bar) whereas the momenta in the denominators are defined in D dimensions. There are two reasons to define the numerators in four dimensions: i) Even if we know that in DRED all the momenta are in the QDS, they appear in the numerators contracted with the gammas, which by definition are in the Q4S. We are assuming a subtlety of DRED, the scalar product of a QDS momentum with a Q4S gamma is equivalent to the product of a Q4S momentum (where the epsilon-components remain to be zero) and a Q4S gamma. Besides, this product is equivalent to the product of a QDS momentum and a QDS gamma too. The gamma matrices coming from the fermion propagators (together with the momentum) or the gammas in the kinetic term of the Lagrangian (together with the spacial derivative) are in D-dim. But, due to the above identities in DRED, all gammas on the numerator are put in Q4S. ii) In FeynCalc DRED is not implemented, so that products of a gamma with a momentum of different dimensions cannot be solved; however, the Dirac algebra in the Q4S is the same algebra of the actual four-dimensional space (except for the cases involving $\backslash\gamma_{-5}$). The definition of a Q4S momentum does not affect the final result because they are expressed as a superposition of scalar products of the loop momenta. If the epsilon-components are zero, we will recover the original D-dimensional momenta.

Using the function `FCFAConvert`, the amplitude transforms to:

SEFC [1, 1, 13][[5]]

$$\begin{aligned}
& \left(i \operatorname{tr} \left((\operatorname{MGl} - \bar{\gamma} \cdot \bar{q}2) \cdot \left(-i \sqrt{2} g_s (\bar{\gamma}^6 \operatorname{USf}(1, 1, 3, 3) - \bar{\gamma}^7 \operatorname{USf}(1, 2, 3, 3)) T_{\operatorname{Col}4 \operatorname{Col}5}^{\operatorname{Glu}4} \right) \right. \right. \\
& \quad \left. \left. (\bar{\gamma} \cdot \bar{q}3 + \operatorname{MT}) \cdot \left(-\frac{i \operatorname{ca} \operatorname{ht}(\bar{\gamma}^6 + \bar{\gamma}^7)}{\sqrt{2}} \right) \cdot (\bar{\gamma} \cdot \bar{q}3 + \operatorname{MT}) \right. \right. \\
& \quad \left. \left. \left(-i \sqrt{2} g_s (\bar{\gamma}^7 \operatorname{USf}(1, 1, 3, 3) - \bar{\gamma}^6 \operatorname{USf}(1, 2, 3, 3)) T_{\operatorname{Col}5 \operatorname{Col}4}^{\operatorname{Glu}3} \right) \right. \right. \\
& \quad \left. \left. (\operatorname{MGl} - \bar{\gamma} \cdot \bar{q}2) \cdot \left(-i \sqrt{2} g_s (\bar{\gamma}^7 \operatorname{USf}(1, 1, 3, 3) - \bar{\gamma}^6 \operatorname{USf}(1, 2, 3, 3)) T_{\operatorname{Col}6 \operatorname{Col}3}^{\operatorname{Glu}3} \right) \right. \right. \\
& \quad \left. \left. (\operatorname{MT} - \bar{\gamma} \cdot \bar{q}1) \cdot \left(-\frac{i \operatorname{ca} \operatorname{ht}(\bar{\gamma}^6 + \bar{\gamma}^7)}{\sqrt{2}} \right) \cdot (\operatorname{MT} - \bar{\gamma} \cdot \bar{q}1) \right. \right. \\
& \quad \left. \left. \left(-i \sqrt{2} g_s (\bar{\gamma}^6 \operatorname{USf}(1, 1, 3, 3) - \bar{\gamma}^7 \operatorname{USf}(1, 2, 3, 3)) T_{\operatorname{Col}3 \operatorname{Col}6}^{\operatorname{Glu}4} \right) \right) \right) / \\
& \quad (4096 \pi^{12} (q1^2 - \operatorname{MT}^2) \cdot (q2^2 - \operatorname{MGf}^2) \cdot ((q2 - q1)^2 - \operatorname{MSf}(1, 3, 3)^2) \cdot (q3^2 - \operatorname{MT}^2) \cdot \\
& \quad ((q2 + q3)^2 - \operatorname{MSf}(1, 3, 3)^2) \cdot (q3^2 - \operatorname{MT}^2) \cdot (q1^2 - \operatorname{MT}^2) \cdot (q2^2 - \operatorname{MGf}^2))
\end{aligned}$$

Now we expand the product of terms inside the Dirac trace in such a way that terms with the product of a $\backslash\gamma_5$ and any number of $\backslash\gamma_{\mu}$ appear explicitly:

```

SetOptions [ DiracSimplify , DiracSubstitute67 -> True , Expanding -> True , Factoring -> True ]
{ DiracCanonical-> False , DiracSigmaExplicit-> True , DiracSimpCombine-> False , DiracSubstitute67-> True ,
  Expanding-> True , Factoring-> True , SirlinRelations-> True , FeynCalcInternal-> False , InsideDiracTrace-> False }

```

DiracSimplify [SEFC [1, 1, 13][[5]]]

$$\begin{aligned}
& \left(i \operatorname{tr} \left(2 \operatorname{ca}^2 g_s^4 \operatorname{ht}^2 T_{\operatorname{Col}5 \operatorname{Col}4}^{\operatorname{Glu}3} T_{\operatorname{Col}6 \operatorname{Col}3}^{\operatorname{Glu}3} T_{\operatorname{Col}3 \operatorname{Col}6}^{\operatorname{Glu}4} T_{\operatorname{Col}4 \operatorname{Col}5}^{\operatorname{Glu}4} \right. \right. \\
& \quad \left. \left(-\operatorname{MGl} \bar{\gamma} \cdot \bar{q}2 \operatorname{USf}(1, 1, 3, 3) \operatorname{USf}(1, 2, 3, 3)^3 \operatorname{MT}^4 + \operatorname{MGl} (\bar{\gamma} \cdot \bar{q}2) \cdot \bar{\gamma}^5 \operatorname{USf}(1, 1, 3, 3) \right. \right. \\
& \quad \left. \left. \operatorname{USf}(1, 2, 3, 3)^3 \operatorname{MT}^4 - \operatorname{MGf}^2 \operatorname{USf}(1, 1, 3, 3)^2 \operatorname{USf}(1, 2, 3, 3)^2 \operatorname{MT}^4 - \right. \right. \\
& \quad \left. \left. \bar{q}2^2 \operatorname{USf}(1, 1, 3, 3)^2 \operatorname{USf}(1, 2, 3, 3)^2 \operatorname{MT}^4 - \operatorname{MGl} \bar{\gamma} \cdot \bar{q}2 \operatorname{USf}(1, 1, 3, 3)^3 \right. \right. \\
& \quad \left. \left. \operatorname{USf}(1, 2, 3, 3) \operatorname{MT}^4 - \operatorname{MGl} (\bar{\gamma} \cdot \bar{q}2) \cdot \bar{\gamma}^5 \operatorname{USf}(1, 1, 3, 3)^3 \operatorname{USf}(1, 2, 3, 3) \operatorname{MT}^4 + \right. \right. \\
& \quad \left. \left. \operatorname{MGf}^2 \bar{\gamma} \cdot \bar{q}1 \operatorname{USf}(1, 1, 3, 3)^4 \operatorname{MT}^3 + \operatorname{MGf}^2 (\bar{\gamma} \cdot \bar{q}1) \cdot \bar{\gamma}^5 \operatorname{USf}(1, 1, 3, 3)^4 \operatorname{MT}^3 + \right. \right. \\
& \quad \left. \left. \operatorname{MGf}^2 \bar{\gamma} \cdot \bar{q}1 \operatorname{USf}(1, 2, 3, 3)^4 \operatorname{MT}^3 - \operatorname{MGf}^2 (\bar{\gamma} \cdot \bar{q}1) \cdot \bar{\gamma}^5 \operatorname{USf}(1, 2, 3, 3)^4 \operatorname{MT}^3 + \right. \right. \\
& \quad \left. \left. \operatorname{MGl} (\bar{\gamma} \cdot \bar{q}1) \cdot (\bar{\gamma} \cdot \bar{q}2) \operatorname{USf}(1, 1, 3, 3) \operatorname{USf}(1, 2, 3, 3)^3 \operatorname{MT}^3 + \right. \right. \\
& \quad \left. \left. \operatorname{MGl} (\bar{\gamma} \cdot \bar{q}2) \cdot (\bar{\gamma} \cdot \bar{q}1) \operatorname{USf}(1, 1, 3, 3) \operatorname{USf}(1, 2, 3, 3)^3 \operatorname{MT}^3 - \right. \right. \\
& \quad \left. \left. \operatorname{MGl} (\bar{\gamma} \cdot \bar{q}2) \cdot (\bar{\gamma} \cdot \bar{q}3) \operatorname{USf}(1, 1, 3, 3) \operatorname{USf}(1, 2, 3, 3)^3 \operatorname{MT}^3 - \right. \right. \\
& \quad \left. \left. \operatorname{MGl} (\bar{\gamma} \cdot \bar{q}3) \cdot (\bar{\gamma} \cdot \bar{q}2) \operatorname{USf}(1, 1, 3, 3) \operatorname{USf}(1, 2, 3, 3)^3 \operatorname{MT}^3 + \right. \right. \\
& \quad \left. \left. \operatorname{MGl} (\bar{\gamma} \cdot \bar{q}1) \cdot (\bar{\gamma} \cdot \bar{q}2) \cdot \bar{\gamma}^5 \operatorname{USf}(1, 1, 3, 3) \operatorname{USf}(1, 2, 3, 3)^3 \operatorname{MT}^3 - \right. \right. \\
& \quad \left. \left. \operatorname{MGl} (\bar{\gamma} \cdot \bar{q}2) \cdot (\bar{\gamma} \cdot \bar{q}1) \cdot \bar{\gamma}^5 \operatorname{USf}(1, 1, 3, 3) \operatorname{USf}(1, 2, 3, 3)^3 \operatorname{MT}^3 - \right. \right. \\
& \quad \left. \left. \operatorname{MGl} (\bar{\gamma} \cdot \bar{q}2) \cdot (\bar{\gamma} \cdot \bar{q}3) \cdot \bar{\gamma}^5 \operatorname{USf}(1, 1, 3, 3) \operatorname{USf}(1, 2, 3, 3)^3 \operatorname{MT}^3 + \right. \right. \\
& \quad \left. \left. \operatorname{MGl} (\bar{\gamma} \cdot \bar{q}3) \cdot (\bar{\gamma} \cdot \bar{q}2) \cdot \bar{\gamma}^5 \operatorname{USf}(1, 1, 3, 3) \operatorname{USf}(1, 2, 3, 3)^3 \operatorname{MT}^3 - \right. \right. \\
& \quad \left. \left. 2 \operatorname{MGf}^2 \bar{\gamma} \cdot \bar{q}3 \operatorname{USf}(1, 1, 3, 3)^2 \operatorname{USf}(1, 2, 3, 3)^2 \operatorname{MT}^3 + \right. \right. \\
& \quad \left. \left. 4 \bar{\gamma} \cdot \bar{q}2 (\bar{q}1 \cdot \bar{q}2) \operatorname{USf}(1, 1, 3, 3)^2 \operatorname{USf}(1, 2, 3, 3)^2 \operatorname{MT}^3 - \right. \right.
\end{aligned}$$

$$\begin{aligned}
& 2 \text{MGI } \bar{\gamma} \cdot \bar{q}_3 \bar{q}_1^2 (\bar{q}_2 \cdot \bar{q}_3) \text{USf}(1, 1, 3, 3) \text{USf}(1, 2, 3, 3)^3 - \\
& 2 \text{MGI}(\bar{\gamma} \cdot \bar{q}_3) \cdot \bar{\gamma}^5 \bar{q}_1^2 (\bar{q}_2 \cdot \bar{q}_3) \text{USf}(1, 1, 3, 3) \text{USf}(1, 2, 3, 3)^3 + \\
& \text{MGI } \bar{\gamma} \cdot \bar{q}_2 \bar{q}_1^2 \bar{q}_3^2 \text{USf}(1, 1, 3, 3) \text{USf}(1, 2, 3, 3)^3 + \\
& \text{MGI}(\bar{\gamma} \cdot \bar{q}_2) \cdot \bar{\gamma}^5 \bar{q}_1^2 \bar{q}_3^2 \text{USf}(1, 1, 3, 3) \text{USf}(1, 2, 3, 3)^3 - \\
& \text{MGF}^2 \bar{q}_1^2 \bar{q}_3^2 \text{USf}(1, 1, 3, 3)^2 \text{USf}(1, 2, 3, 3)^2 - \bar{q}_1^2 \bar{q}_2^2 \bar{q}_3^2 \text{USf}(1, 1, 3, 3)^2 \\
& \quad \text{USf}(1, 2, 3, 3)^2 - 2 \text{MGI } \bar{\gamma} \cdot \bar{q}_3 \bar{q}_1^2 (\bar{q}_2 \cdot \bar{q}_3) \text{USf}(1, 1, 3, 3)^3 \text{USf}(1, 2, 3, 3) + \\
& 2 \text{MGI}(\bar{\gamma} \cdot \bar{q}_3) \cdot \bar{\gamma}^5 \bar{q}_1^2 (\bar{q}_2 \cdot \bar{q}_3) \text{USf}(1, 1, 3, 3)^3 \text{USf}(1, 2, 3, 3) + \\
& \text{MGI } \bar{\gamma} \cdot \bar{q}_2 \bar{q}_1^2 \bar{q}_3^2 \text{USf}(1, 1, 3, 3)^3 \text{USf}(1, 2, 3, 3) - \\
& \text{MGI}(\bar{\gamma} \cdot \bar{q}_2) \cdot \bar{\gamma}^5 \bar{q}_1^2 \bar{q}_3^2 \text{USf}(1, 1, 3, 3)^3 \text{USf}(1, 2, 3, 3) \Big) \Big) / \\
& (4096 \pi^{12} (q_1^2 - \text{MT}^2) \cdot (q_2^2 - \text{MGF}^2) \cdot ((q_2 - q_1)^2 - \text{MSf}(1, 3, 3)^2) \cdot \\
& (q_3^2 - \text{MT}^2) \cdot \\
& ((q_2 + q_3)^2 - \text{MSf}(1, 3, 3)^2) \cdot \\
& (q_3^2 - \text{MT}^2) \cdot \\
& (q_1^2 - \text{MT}^2) \cdot \\
& (q_2^2 - \text{MGF}^2))
\end{aligned}$$

Regul[1, 1, 13][[5]] = DiracSimplify [DiracSimplify [SEFC[1, 1, 13][[5]]] /. {DiracGamma [5] → 0}]

$$\begin{aligned}
& \left(i \text{tr} \left(2 \text{ca}^2 \text{ht}^2 g_s^4 T_{\text{Col6 Col3}}^{\text{Glu3}} T_{\text{Col3 Col6}}^{\text{Glu4}} T_{\text{Col5 Col4}}^{\text{Glu3}} T_{\text{Col4 Col5}}^{\text{Glu4}} \right. \right. \\
& \quad \left(2 \text{MGF}^2 \text{MT}^2 \text{USf}(1, 1, 3, 3)^4 (\bar{q}_1 \cdot \bar{q}_3) + 2 \text{MGF}^2 \text{MT}^2 \text{USf}(1, 2, 3, 3)^4 (\bar{q}_1 \cdot \bar{q}_3) - \right. \\
& \quad \text{MGF}^2 \text{MT}^2 \bar{q}_1^2 \text{USf}(1, 1, 3, 3)^2 \text{USf}(1, 2, 3, 3)^2 - \text{MGF}^2 \text{MT}^2 \bar{q}_3^2 \text{USf}(1, 1, 3, 3)^2 \\
& \quad \text{USf}(1, 2, 3, 3)^2 - \text{MGF}^2 \bar{q}_1^2 \bar{q}_3^2 \text{USf}(1, 1, 3, 3)^2 \text{USf}(1, 2, 3, 3)^2 + \\
& \quad 2 \text{MGI} \text{MT}^3 \text{USf}(1, 1, 3, 3) \text{USf}(1, 2, 3, 3)^3 (\bar{q}_1 \cdot \bar{q}_2) + 2 \text{MGI} \text{MT}^3 \text{USf}(1, 1, 3, 3)^3 \\
& \quad \text{USf}(1, 2, 3, 3) (\bar{q}_1 \cdot \bar{q}_2) - 2 \text{MGI} \text{MT}^3 \text{USf}(1, 1, 3, 3) \text{USf}(1, 2, 3, 3)^3 (\bar{q}_2 \cdot \bar{q}_3) - \\
& \quad 2 \text{MGI} \text{MT}^3 \text{USf}(1, 1, 3, 3)^3 \text{USf}(1, 2, 3, 3) (\bar{q}_2 \cdot \bar{q}_3) - 2 \text{MGI} \text{MT} \bar{q}_1^2 \text{USf}(1, 1, 3, 3) \\
& \quad \text{USf}(1, 2, 3, 3)^3 (\bar{q}_2 \cdot \bar{q}_3) + 2 \text{MGI} \text{MT} \bar{q}_3^2 \text{USf}(1, 1, 3, 3) \text{USf}(1, 2, 3, 3)^3 (\bar{q}_1 \cdot \bar{q}_2) - \\
& \quad 2 \text{MGI} \text{MT} \bar{q}_1^2 \text{USf}(1, 1, 3, 3)^3 \text{USf}(1, 2, 3, 3) (\bar{q}_2 \cdot \bar{q}_3) + \\
& \quad 2 \text{MGI} \text{MT} \bar{q}_3^2 \text{USf}(1, 1, 3, 3)^3 \text{USf}(1, 2, 3, 3) (\bar{q}_1 \cdot \bar{q}_2) - \text{MT}^4 \bar{q}_2^2 \text{USf}(1, 1, 3, 3)^2 \\
& \quad \text{USf}(1, 2, 3, 3)^2 - 4 \text{MT}^2 \bar{q}_2^2 \text{USf}(1, 1, 3, 3)^2 \text{USf}(1, 2, 3, 3)^2 (\bar{q}_1 \cdot \bar{q}_3) + \\
& \quad 8 \text{MT}^2 \text{USf}(1, 1, 3, 3)^2 \text{USf}(1, 2, 3, 3)^2 (\bar{q}_1 \cdot \bar{q}_2) (\bar{q}_2 \cdot \bar{q}_3) - \\
& \quad \text{MT}^2 \bar{q}_1^2 \bar{q}_2^2 \text{USf}(1, 1, 3, 3)^2 \text{USf}(1, 2, 3, 3)^2 - \\
& \quad \left. \left. \text{MT}^2 \bar{q}_2^2 \bar{q}_3^2 \text{USf}(1, 1, 3, 3)^2 \text{USf}(1, 2, 3, 3)^2 - \bar{q}_1^2 \bar{q}_2^2 \bar{q}_3^2 \text{USf}(1, 1, 3, 3)^2 \right. \right. \\
& \quad \left. \left. \text{USf}(1, 2, 3, 3)^2 - \text{MGF}^2 \text{MT}^4 \text{USf}(1, 1, 3, 3)^2 \text{USf}(1, 2, 3, 3)^2 \right) \right) \Big) / \\
& (4096 \pi^{12} (q_1^2 - \text{MT}^2) \cdot (q_2^2 - \text{MGF}^2) \cdot ((q_2 - q_1)^2 - \text{MSf}(1, 3, 3)^2) \cdot \\
& (q_3^2 - \text{MT}^2) \cdot \\
& ((q_2 + q_3)^2 - \text{MSf}(1, 3, 3)^2) \cdot \\
& (q_3^2 - \text{MT}^2) \cdot (q_1^2 - \text{MT}^2) \cdot \\
& (q_2^2 - \text{MGF}^2))
\end{aligned}$$

According with DRED, if we define γ_5 as a totally anticommuting object, the trace of a single γ_5 and an arbitrary number of gamma matrices vanishes in contrast to the four-dimensional case

where for four gamma matrices and a single γ_5 the trace is different from zero. However, as we mentioned above, DRED is not implemented in FeynCalc, FeynCalc performs this kind of traces only in 4-dim, so we must not take the traces with FeynCalc, instead we should disregard the terms with a single γ_5 :

Once the γ_5 terms are disregarded one can proceed to perform the Dirac trace with FeynCalc, here the Q4S algebra is the same as the actual 4-dimensional algebra.

```

SetOptions [ DiracTrace , DiracTraceEvaluate → True ]

{EpsContract→ False, Factoring→ Automatic, FeynCalcExternal→ False,
 Mandelstam→ {}, PairCollect→ True, DiracTraceEvaluate→ True, Schouten→ 0,
 LeviCivitaSign→ $LeviCivitaSign TraceOfOne→ 4, FCVerbose→ False}

Simplify [ Tr [ Regul [1, 1, 13][[13]]]]

- ( i ca^2 ht^2 g_s^4 T_Col6^Glu3 Col3 T_Col3^Glu4 Col6 T_Col5^Glu3 Col4 T_Col4^Glu4 Col5
  ( USf(1, 1, 3, 3) USf(1, 2, 3, 3) ( (q1^2 + MT^2) ( USf(1, 1, 3, 3) USf(1, 2, 3, 3) (q2^2 + MGf^2)
    (q3^2 + MT^2) + 2 MGf MT ( USf(1, 1, 3, 3)^2 + USf(1, 2, 3, 3)^2) (q2 · q3) ) -
    2 MT (q1 · q2) ( MT ( 4 USf(1, 1, 3, 3) USf(1, 2, 3, 3) (q2 · q3) + MGf
      MT ( USf(1, 1, 3, 3)^2 + USf(1, 2, 3, 3)^2) ) +
      MGf q3^2 ( USf(1, 1, 3, 3)^2 + USf(1, 2, 3, 3)^2) ) ) -
    2 MT^2 (q1 · q3) ( MGf^2 ( USf(1, 1, 3, 3)^4 + USf(1, 2, 3, 3)^4) -
      2 q2^2 USf(1, 1, 3, 3)^2 USf(1, 2, 3, 3)^2 ) ) ) /
  ( 512 pi^12 (q1^2 - MT^2) · (q2^2 - MGf^2) · ((q2 - q1)^2 - MSf(1, 3, 3)^2) ·
    (q3^2 - MT^2) ·
    ((q2 + q3)^2 - MSf(1, 3, 3)^2) ·
    (q3^2 - MT^2) ·
    (q1^2 - MT^2) · (q2^2 - MGf^2) )

```

We now perform the Colour algebra:

```

SetOptions [ SUNSimplify , SUNTrace → True ]

{Expanding→ False, Explicit→ False, Factoring→ False,
 SUNIndexRename→ True, SUNFJacobi→ False, SUNNToCACF→ True, SUNTrace→ True}

SUNSAmp [1, 1, 13][[5]]

```

$$\begin{aligned}
& -\left(i \, c a^2 \, h t^2 \, C_A \, C_F \, g_s^4 \right. \\
& \quad \left(\text{USf}(1, 1, 3, 3) \, \text{USf}(1, 2, 3, 3) \left((\overline{q1}^2 + \text{MT}^2) \left(\text{USf}(1, 1, 3, 3) \, \text{USf}(1, 2, 3, 3) \left(\overline{q2}^2 + \text{MGf}^2 \right) \right. \right. \right. \\
& \quad \left. \left. \left(\overline{q3}^2 + \text{MT}^2 \right) + 2 \, \text{MGl} \, \text{MT} \left(\text{USf}(1, 1, 3, 3)^2 + \text{USf}(1, 2, 3, 3)^2 \right) \left(\overline{q2} \cdot \overline{q3} \right) \right) - \right. \\
& \quad \left. 2 \, \text{MT} \left(\overline{q1} \cdot \overline{q2} \right) \left(\text{MT} \left(4 \, \text{USf}(1, 1, 3, 3) \, \text{USf}(1, 2, 3, 3) \left(\overline{q2} \cdot \overline{q3} \right) + \text{MGl} \right. \right. \right. \\
& \quad \left. \left. \left. \text{MT} \left(\text{USf}(1, 1, 3, 3)^2 + \text{USf}(1, 2, 3, 3)^2 \right) \right) + \right. \right. \\
& \quad \left. \left. \text{MGl} \, \overline{q3}^2 \left(\text{USf}(1, 1, 3, 3)^2 + \text{USf}(1, 2, 3, 3)^2 \right) \right) \right) - \\
& \quad \left. 2 \, \text{MT}^2 \left(\overline{q1} \cdot \overline{q3} \right) \left(\text{MGf}^2 \left(\text{USf}(1, 1, 3, 3)^4 + \text{USf}(1, 2, 3, 3)^4 \right) - \right. \right. \\
& \quad \left. \left. 2 \, \overline{q2}^2 \, \text{USf}(1, 1, 3, 3)^2 \, \text{USf}(1, 2, 3, 3)^2 \right) \right) \Big/ \\
& \quad \left(1024 \, \pi^{12} \left(q1^2 - \text{MT}^2 \right) \cdot \left(q2^2 - \text{MGf}^2 \right) \cdot \left((q2 - q1)^2 - \text{MSf}(1, 3, 3)^2 \right) \cdot \right. \\
& \quad \left(q3^2 - \text{MT}^2 \right) \cdot \\
& \quad \left((q2 + q3)^2 - \text{MSf}(1, 3, 3)^2 \right) \cdot \\
& \quad \left(q3^2 - \text{MT}^2 \right) \cdot \\
& \quad \left. \left(q1^2 - \text{MT}^2 \right) \cdot \left(q2^2 - \text{MGf}^2 \right) \right)
\end{aligned}$$

Nota that the numerator of the resulting amplitude is a superposition of scalar products of the loop-momenta, which in this case are in the Q4S, but according with the above statements the epsilon-components are zero so actually they are in the QDS. The next step consists in express these scalar products in terms of the propagators and rewrite all the expression in the Reduze notation to perform the IBP reduction.


```

Position[{i, j, k, l, m, n}, MSf[1, 4, 2]][[All, 1]],
Position[{i, j, k, l, m, n}, MSf[1, 4, 3]][[All, 1]],
Position[{i, j, k, l, m, n}, MSf[2, 4, 1]][[All, 1]],
Position[{i, j, k, l, m, n}, MSf[2, 4, 2]][[All, 1]],
Position[{i, j, k, l, m, n}, MSf[2, 4, 3]][[All, 1]]}], {1,10}];

```

```

INToReduce = {
  INT[{a_, i_}, {b_, j_}, {c_, k_}, {d_, l_}, {e_, m_}, {f_, n_}] :>
  MRULES @@ PadRight[ DeleteDuplicates[ Flatten[
    Table[Pick[{i, j, k, l, m, n}, {1, 2, 3, 4, 5, 6},
              Flatten[FamDiff[i, j, k, l, m, n]][[h]] ],
    {h, 1, Length[Flatten[FamDiff[i, j, k, l, m, n]]]}], 4]*(INT @@ {
    FamDiff[i, j, k, l, m, n] /. NameChanges,
    Length[Cases[{a, b, c, d, e, f}, p_ /; Positive[p], Infinity]],
    Sum[Power[2, Flatten[Position[Sign[{a, b, c, d, e, f}], 1]][[q]] - 1],
    {q, 1, Length[Position[Sign[{a, b, c, d, e, f}], 1]}],
    Sum[Cases[{a, b, c, d, e, f}, p_ /; Positive[p], Infinity]][[q]],
    {q, 1, Length[Cases[{a, b, c, d, e, f}, p_ /; Positive[p], Infinity]}],
    Abs[ Sum[Cases[{a, b, c, d, e, f}, p_ /; Negative[p], Infinity]][[q]],
    {q, 1, Length[Cases[{a, b, c, d, e, f}, p_ /; Negative[p], Infinity]}],
    {a, b, c, d, e, f, 0, 0, 0}]]];

```

The output for an arbitrary three-loop scalar integral would be of the form:

```
In[1]:= INT[{0, 0}, {1, MT}, {1, MT}, {1, 0}, {1, 0}, {1, 0}] /. INToReduce
```

```
Out[1]:= INT["INT-m1_23", 5, 62, 5, 0, {0, 1, 1, 1, 1, 1, 0, 0, 0}]*MRULES[MT, 0, 0, 0]
```

H. Amplitudes of the Three-Loop Diagrams

This chapter contains a Mathematica code that performs the evaluation of the three-loop amplitudes in terms of the set of the master integrals depicted in Figure 3-3. Besides, the divergent and the finite contributions are extracted from the amplitudes.

```
#!/path/to/MathematicaScript -script

nofk = ToExpression[$ScriptCommandLine[[2]]];

(*****)
(** In order to read this package it is necessary to run the codes: **)
(** i) SimplificationDefinitions **)
(** ii) TVID **)
(*****)

PrependTo[$Path, ToFileName[{"path", "to", "SimplificationDefinitions", "code"}]];
<< SimplificationDefinitions';

PrependTo[$Path, ToFileName[{"path", "to", "tvid"}]]; (* A. Freitas program*)
Get["i3.m"];
$Directory = ToFileName[{"path", "to", "tvid"}];

LaunchKernels[nofk];

ParallelEvaluate[

PrependTo[$Path, ToFileName[{"path", "to", "SimplificationDefinitions", "code"}]];
<< SimplificationDefinitions';

PrependTo[$Path, ToFileName[{"path", "to", "tvid"}]]; (* A. Freitas program*)
Get["i3.m"];
$Directory = ToFileName[{"path", "to", "tvid"}];

];

TempDirName = ToFileName[{"directory", "where", "outputs", "are", "saved"}];
```



```
(* Load a regularized three-loop amplitude *)

AmpShifts = Get["ReduceAmp", Path -> {ToFileName[{TempDirName}]}];
$Lamp = Length[AmpShifts];
Put[$Lamp, ToFileName[{TempDirName}, "Lamp" ]];

(*****
(** A list of rules, where each scalar integral is changed by its IBP      **)
(** reduction in terms of a set of MI is contained in the file "preferreduc". **)
(** The list contain 3525 rules of the form:                               **)
(**                                                                           **)
(**     INT["INT-m1_12", 4, 51, 6, 0, {3, 1, 0, 0, 1, 1, 0, 0, 0}] ->     **)
(**     -((-8 + 3*d)*(-40 + 22*d - 3*d^2)*INT["INT-m1_12", 4, 51, 4, 0,   **)
(**     {1, 1, 0, 0, 1, 1, 0, 0, 0}])/(16*(-7 + 2*d)*m1^2),                **)
(**                                                                           **)
(** obtained with the program Reduce, and is so large that cannot be included **)
(** in this work (the file have about 200000 lines).                       **)
(*****)

preferreduc = Get["preferreduc"];
DistributeDefinitions[preferreduc];

(*****
(** The list "basispref" changes the notation of the master integrals from  **)
(** Reduce to TVID notation. For instance:                                **)
(**                                                                           **)
(**     INT["INT-m1_1-m2_2", 5, 59, 5, 0, {1, 1, 0, 1, 1, 1, 0, 0, 0}] -> **)
(**     U5[m1,m2,0,0,0],                                                  **)
(**                                                                           **)
(** and so on for the other master integrals.                            **)
(*****)

basispref = Get["basispref"];
DistributeDefinitions[basispref];

(*****
(** Applying the changes in "preferreduc" and "basispref" to each amplitude. **)
(*****)

ParallelMap[
If[!FileExistsQ[FileNameJoin[{TempDirName, "AmpsTVID"<>ToString[#]}]]] ,
Put[ Expand[ Part[AmpShifts, #] ] /. preferreduc /. basispref,
  ToFileName[{TempDirName}, "AmpsTVID"<>ToString[#]}] ]& , Range[$Lamp]];

```

```

ClearAll[AmpShifts,preferredred, basispref];
ParallelEvaluate[
ClearAll[AmpShifts,preferredred, basispref];
];

AmpsTVID[l_] := Get["AmpsTVID"<>ToString[l], Path -> {ToFileName[{TempDirName}]}]

$factor = (-I)*(Pi^(6)); (* changing Reduze notation to Ayres Freytas notation *)

rules[amp_] := Union@Cases[amp,
    MRULES[a_, b_, c_, d_] :> Level[MRULES[a, b, c, d], 1], Infinity]

ampstest[amp_] := Coefficient[amp, Union@Cases[amp, MRULES[_], Infinity]];

replacements3[amp_] := Plus @@ MapThread[
    $factor*(#1 /. {m1 -> Part[#2, 1]^2, m2 -> Part[#2, 2]^2,
        m3 -> Part[#2, 3]^2, m4 -> Part[#2, 4]^2})&,
    {ampstest[amp], rules[amp]} ]

DistributeDefinitions[$factor, rules, ampstest, replacements3];

ParallelMap[
    Put[replacements3[AmpsTVID[#]],
    ToFileName[{TempDirName}, "AmpsTVIDMOD"<>ToString[#]]&,
    Range[$Lamp] ];

Print["Preferred basis applied and backup saved"];

(*****
(** 1) Reduction of the function M[m1,m2,m3,m4] in terms of U4.      **)
(** 2) Rules for some reductions taking into account the unitarity  **)
(**   of the sfermion matrices                                     **)
(*****

Mredu = { M[m1_,m2_,m3_,m4_] :> (2/(3*d - 8))*(
    m1*U4[m1,m2,m3,m4]
    + m2*U4[m2,m3,m4,m1] + m3*U4[m3,m4,m1,m2]
    + m4*U4[m4,m1,m2,m3] ) };

AmpShifts[m_] := AmpShifts[m] = Get["AmpsTVIDMOD" <> ToString[m],
    Path->{ToFileName[{TempDirName}]}];

Amplitude[m_] := Normal@Series[
    AmpShifts[m] /. Mredu /. {d -> 4-2*$eps}, {$eps, 0, 3}]

```

```

stopmixing = {
  USf[i_, 1, 3, 3]^2 + USf[i_, 2, 3, 3]^2 -> 1,
  USf[1, i_, 3, 3]^2 + USf[2, i_, 3, 3]^2 -> 1,
  USf[1, 1, 3, 3]*USf[1, 2, 3, 3] + USf[2, 1, 3, 3]*USf[2, 2, 3, 3] -> 0,
  USf[1, 1, 3, 3]*USf[2, 1, 3, 3] + USf[1, 2, 3, 3]*USf[2, 2, 3, 3] -> 0,
  USf[1, 1, 3, 3]*USf[2, 2, 3, 3] - USf[1, 2, 3, 3]*USf[2, 1, 3, 3] -> 1 };

USFchanges = {
  USf[1, 1, 3, 3]->Cos[tht], USf[1, 2, 3, 3]->Sin[tht], USf[2, 1, 3, 3]->-Sin[tht],
  USf[2, 2, 3, 3]->Cos[tht], USf[1, 1, 3, 1]->1, USf[1, 2, 3, 1]->0,
  USf[2, 1, 3, 1]->0, USf[2, 2, 3, 1]->1, USf[1, 1, 3, 2]->1, USf[1, 2, 3, 2]->0,
  USf[2, 1, 3, 2]->0, USf[2, 2, 3, 2]->1, USf[1, 1, 4, 1]->1, USf[1, 2, 4, 1]->0,
  USf[2, 1, 4, 1]->0, USf[2, 2, 4, 1]->1, USf[1, 1, 4, 2]->1, USf[1, 2, 4, 2]->0,
  USf[2, 1, 4, 2]->0, USf[2, 2, 4, 2]->1, USf[1, 1, 4, 3]->1, USf[1, 2, 4, 3]->0,
  USf[2, 1, 4, 3]->0, USf[2, 2, 4, 3]->1 };

stopmixingB = {
UCSf[i_, j_, 3, 3] := Cos[tht]^2*KroneckerDelta[i, j]
  + Sin[tht]^2*(KroneckerDelta[i+1, j]
  + KroneckerDelta[i-1, j]) /; !(i===3)&&!(j===3),
UCSf[a_, b_, 3, 1] := KroneckerDelta[a, b] /; !(a===3)&&!(b===3),
UCSf[a_, b_, 3, 2] := KroneckerDelta[a, b] /; !(a===3)&&!(b===3),
UCSf[a_, b_, 4, c_] := KroneckerDelta[a, b] /; !(a===3)&&!(b===3),
UCSf[a_, 3, 3, 3] := Sin[tht]*Cos[tht]*KroneckerDelta[a, 1]
  - Sin[tht]*Cos[tht]*KroneckerDelta[a, 2] /; !(a===3),
UCSf[a_, 3, 3, c_] := 0 /; !(a===3)&&!(c===3), UCSf[a_, 3, 4, c_] := 0 /; !(a===3),
UCSf[3, a_, 3, 3] := Sin[tht]*Cos[tht]*KroneckerDelta[a, 2]
  - Sin[tht]*Cos[tht]*KroneckerDelta[a, 1] /; !(a===3)&&!(a===4),
UCSf[3, a_, 3, c_] := 0 /; !(a===3)&&!(a===4)&&!(c===3),
UCSf[3, a_, 4, c_] := 0 /; !(a===3)&&!(a===4),
UCSf[3, 3, 3, a_] := 1 /; !(a===3), UCSf[3, 4, 3, a_] := 0 /; !(a===3),
UCSf[3, 3, 3, 3] -> Cos[tht]^2, UCSf[3, 4, 3, 3] -> -Sin[tht]^2,
UCSf[3, 3, 4, a_] -> 1, UCSf[3, 4, 4, a_] -> 0, Cos[tht]^2 + Sin[tht]^2 -> 1,
Cos[tht]*Sin[tht] -> Sin[2*tht]/2, Cos[tht]^2 - Sin[tht]^2 -> Cos[2*tht],
Sin[tht]^2 - Cos[tht]^2 -> -Cos[2*tht] };

DistributeDefinitions[stopmixing, USFchanges, stopmixingB];

Print[" Amps Loaded and Replacement of M[] Done! "];

(*****
(** The following functions extract the coefficient of each master integral      **)
(** contained in a three-loop amplitude.                                          **)
(*****

```

```

ListA0[num_] := Union@Cases[Amplitude[num], A0[___], Infinity]
ListT3[num_] := Union@Cases[Amplitude[num], T3[___], Infinity]
ListU4[num_] := Union@Cases[Amplitude[num], U4[___], Infinity]
ListU5[num_] := Union@Cases[Amplitude[num], U5[___], Infinity]
ListU6[num_] := Union@Cases[Amplitude[num], U6[___], Infinity]
ListAOT3[num_] := Union@Map[(Times @@ #)&, Tuples[{ListA0[num], ListT3[num]}]]
ListA0A0A0[num_] := Union@Map[(Times @@ #)&,
                               Tuples[{ListA0[num], ListA0[num], ListA0[num]}]]

ListAll[num_] := Union[
    ListU4[num], ListU5[num], ListU6[num], ListAOT3[num], ListA0A0A0[num]
];

ParallelMap[
Put[ListAll[#], ToFileName[{TempDirName}, "ListAll"<>ToString[#]]]&,
    Range[$Lamp] ];

ampptest[func_, m_] := func*Plus@@ParallelMap[
    FactorSquareFree[
    Coefficient[ #, func] //. stopmixing //. USFchanges //. stopmixingB]&,
    Amplitude[m] ]

Table[
MapThread[
If[!FileExistsQ[FileNameJoin[{TempDirName, "Amptest"<>ToString[#2]}]] ,
Print["Amptest_"<>ToString[#2]]
Put[ampptest[#1, m], ToFileName[{TempDirName},
                               "Amptest"<>ToString[m]<>ToString[#2]}]]&,
{ ListAll[m], Range[Length[ListAll[m]]] } ], {m, 1, $Lamp} ];

(*****
*** Laurent expansion around d = 4 in terms of $eps = (4-d)/2 ***
*****)

funcexpans = {
A0[a_]*A0[b_]*A0[c_] :=> Sum[ A0[a, b, c, j]*$eps^(j), {j, -3, 2}],
A0[a_]^2*A0[c_] :=> Sum[ A0[a, a, c, j]*$eps^(j), {j, -3, 2}],
A0[c_]^3 :=> Sum[ A0[c, c, c, j]*$eps^(j), {j, -3, 2}],
A0[a_]*T3[b_, c_, d_] :=> Sum[ AT[a, b, c, d, j]*$eps^(j), {j, -3, 2}],
U4[a_, b_, c_, d_] :=> Sum[ U4[a, b, c, d, j]*$eps^(j), {j, -3, 2}],
U5[a_, b_, c_, d_, e_] :=> Sum[ U5[a, b, c, d, e, j]*$eps^(j), {j, -3, 2}],
U6[a_, b_, c_, d_, e_, f_] :=> Sum[ U6[a, b, c, d, e, f, j]*$eps^(j), {j, -3, 2} ];

DistributeDefinitions[funcexpans];

```

```

AmpSimp[m_,k_] := Get["Ampptest"<>ToString[m]<>ToString[k],
                    Path->{ToFileName[{TempDirName}]}];

AmpLexp[num_,i_] := Sum[ $eps^(-m)*Coefficient[
    Collect[
    ListAll[num][[i]]*Collect[
    Numerator[Coefficient[AmpSimp[num,i],ListAll[num][[i]]],{eps}]
    / Denominator[AmpSimp[num,i]] /. funcexpans, {eps}], $eps, -m],
    {m, 0, 3}]

coeffeps[num_,j,l_] := Coefficient[ AmpLexp[num,l], $eps, -j]

ampeps[num_,m_] := $eps^(-m)*(Plus@@Table[coeffeps[num,m,l],{l,1,Length[ListAll[num]}])

epsamps = Flatten[
    ParallelTable[
    ameps[num,j], {num, 1, $Lamp},{j, 0, 3}]
];

(*****
*** Explicit evaluation of the divergent and the finite part of the amplitudes ***
*** in terms of special functions, log(), Polylog(), etc. ***
*****)

i3changes = {
A0[a_,b_,c_,x_] :=> PrepIntMod[ A0[a]*A0[b]*A0[c], x],
AT[a_,b_,c_,d_,x_] :=> PrepIntMod[ A0[a]*T3[b,c,d], x],
U4[a_,b_,c_,d_,x_] :=> PrepIntMod[ U4[a,b,c,d], x],
U5[a_,b_,c_,d_,e_,x_] :=> PrepIntMod[ U5[a,b,c,d,e], x],
U6[a_,b_,c_,d_,e_,f_,x_] :=> PrepIntMod[ U6[a,b,c,d,e,f], x] };

DistributeDefinitions[i3changes];

coeffepsi3[j_,l_] := Part[
    Coefficient[$eps^(-1)*epsamps, $eps^(-j)], 1] /. i3changes;

ampepsi3[m_] := $eps^(1-m)*(Plus @@ Table[ coeffepsi3[m,l],
    {l, 1, Length[epsamps] }])

epsamps_i3 = Flatten[ParallelMap[ampepsi3[#]&, Range[4]]];
Print["epsamps_i3 Loaded!"]
Put[ epsamps_i3, ToFileName[{TempDirName}, "i3AmpsEps"]];

CloseKernels[];

Quit[];

```

I. Divergent Parts of the Three-loop Master Integrals

In this appendix we present the analytical results for the divergent part of the three-loop master integral basis depicted in Figure 3-2. For the vacuum function $U4$, we have:

$$\begin{aligned}
 U4_{div}(m_1^2, m_2^2, m_3^2, m_4^2) &= \frac{1}{\epsilon^3} \sum_{i=2}^4 \frac{m_i^2}{3} + \frac{1}{\epsilon^2} \left[-\frac{m_1^2}{6} + \sum_{i=2}^4 m_i^2 \left(\frac{5}{6} - \frac{\log m_i^2}{2} - \frac{\log m_1^2}{2} \right) \right] \\
 &+ \frac{1}{\epsilon} \left[m_1^2 \left(-1 + \frac{\log m_1^2}{2} \right) + \sum_{i=2}^4 m_i^2 \left(\frac{4}{3} + \frac{\pi^2}{12} - \log m_i^2 - \frac{3}{2} \log m_1^2 \right. \right. \\
 &\quad \left. \left. + \frac{1}{4} \log^2 m_i^2 + \frac{1}{4} \log^2 m_1^2 + \log m_i^2 \log m_1^2 \right) \right]. \tag{I-1}
 \end{aligned}$$

$$\begin{aligned}
 U4_{div}(0, m_2^2, m_3^2, m_4^2) &= -\frac{1}{\epsilon^3} \sum_{i=2}^4 \frac{m_i^2}{6} + \frac{1}{\epsilon^2} \sum_{i=2}^4 m_i^2 \left(-\frac{2}{3} + \frac{\log m_i^2}{2} \right) \\
 &+ \frac{1}{\epsilon} \left[\sum_{i=2}^4 m_i^2 \left(\frac{4}{3} + \frac{\pi^2}{24} - \log m_i^2 + \frac{1}{4} \log^2 m_i^2 \right) - T3_{fin}(m_2^2, m_3^2, m_4^2) \right]. \tag{I-2}
 \end{aligned}$$

For the $U5$ three-loop function we have:

$$\begin{aligned}
 U5_{div}(m_1^2, m_2^2, m_3^2, m_4^2, m_5^2) &= \frac{1}{\epsilon^3} \left[\sum_{i=1}^4 \frac{m_i^2}{6} + \frac{m_5^2}{3} \right] \\
 &+ \frac{1}{\epsilon^2} \left[\sum_{i=1}^4 m_i^2 \left(1 - \frac{\log m_i^2}{2} \right) + m_5^2 \left(\frac{5}{3} - \log m_5^2 \right) \right] \\
 &+ \frac{1}{\epsilon} \left[\sum_{i=1}^4 m_i^2 \left(\frac{25}{6} + \frac{\pi^2}{24} - 3 \log m_i^2 + \frac{1}{4} \log^2 m_i^2 \right) \right. \\
 &\quad \left. + m_5^2 \left(\frac{17}{3} + \frac{\pi^2}{12} - 5 \log m_5^2 + \frac{1}{2} \log^2 m_5^2 \right) \right]
 \end{aligned}$$

$$\begin{aligned}
& + \frac{1}{2} \left((m_1^2 + m_2^2 - m_5^2) \log m_1^2 \log m_2^2 + \text{cycl}(125) \right) \\
& + \frac{1}{2} \left((m_3^2 + m_4^2 - m_5^2) \log m_3^2 \log m_4^2 + \text{cycl}(345) \right) \\
& + \lambda_{125} \left(\frac{\pi^2}{6} - \frac{1}{2} \log \frac{m_1^2}{m_5^2} \log \frac{m_2^2}{m_5^2} + \log u_{125} \log v_{125} - \text{Li}_2 u_{125} - \text{Li}_2 v_{125} \right) \\
& + \lambda_{345} \left(\frac{\pi^2}{6} - \frac{1}{2} \log \frac{m_3^2}{m_5^2} \log \frac{m_4^2}{m_5^2} + \log u_{345} \log v_{345} - \text{Li}_2 u_{345} - \text{Li}_2 v_{345} \right) \Big]. \quad (\text{I-3})
\end{aligned}$$

where the function $\text{cycl}(ijk)$ refers to the cyclic permutations of the set $\{m_i, m_j, m_k\}$ and

$$\lambda_{ijk} = \sqrt{m_i^4 + m_j^4 + m_k^4 - 2(m_i^2 m_j^2 + m_i^2 m_k^2 + m_j^2 m_k^2)} \quad (\text{I-4})$$

$$u_{ijk} = \frac{1}{2m_k^2} (m_i^2 - m_j^2 + m_k^2 - \lambda_{ijk}), \quad (\text{I-5})$$

$$v_{ijk} = \frac{1}{2m_k^2} (m_j^2 - m_i^2 + m_k^2 - \lambda_{ijk}). \quad (\text{I-6})$$

Finally, the divergent part of the $U6$ functions is independent of the particle masses and have a quite simple form,

$$U6_{div}(m_1^2, m_2^2, m_3^2, m_4^2, m_5^2, m_6^2) = \frac{1}{\epsilon} 2\zeta(3), \quad (\text{I-7})$$

where $\zeta(x)$ is the Riemann zeta function.

J. Known Analytical Expressions of Master Integrals

In this appendix we show the expressions of the master integrals involved in this work, plotted in Figures **3-2** and **3-4**, which can be computed analytically to all orders in ϵ . This includes the one-loop functions $A0$ and $B0$, the two-loop function $T3$ and some special cases of the three-loop integrals $U4$ and $U5$ with one and two independent mass scales. The one-loop Passarino-Veltman functions $A0$ and $B0$ have the Laurent expansions:

$$A0(m) = -e^{\gamma_E \epsilon} (m^2)^{1-\epsilon} \Gamma(-1 + \epsilon), \quad (\text{J-1})$$

and

$$\begin{aligned} B0(p^2, m_1, m_2) = & \\ (p^2)^{-\epsilon} \left[\frac{1}{\epsilon} + 2 - \text{Log} \left(\frac{m_1 m_2}{p^2} \right) + \frac{m_1^2 - m_2^2}{p^2} \text{Log} \left(\frac{m_2^2}{m_1^2} \right) + \lambda \left(1, \frac{m_1^2}{p^2}, \frac{m_2^2}{p^2} \right) \times \right. & (\text{J-2}) \\ \left. \left(\text{Log} \left(\frac{m_1 m_2}{p^2} \right) - \text{Log} \left(\frac{p^2 - m_1^2 - m_2^2 + \lambda(1, m_1^2/p^2, m_2^2/p^2)}{2p^2} \right) + i\pi \right) \right] + O(\epsilon), \end{aligned}$$

where $\lambda(x, y, z)$ is the Källén function. For a complex number z the logarithm is defined as $\text{Log}(z) = \ln|z| + i\phi$, where $\phi \in (-\pi, \pi]$. Using the definitions given by:

$$x = \frac{m_1^2}{m_3^2}, \quad y = \frac{m_2^2}{m_3^2}, \quad (\text{J-3})$$

$$u = \frac{1}{2} [1 + x - y + \lambda(1, x, y)], \quad (\text{J-4})$$

$$v = \frac{1}{2} [1 - x + y + \lambda(1, x, y)], \quad (\text{J-5})$$

$$w = \left(\frac{u}{x} - 1 \right) \left(\frac{v}{y} - 1 \right), \quad (\text{J-6})$$

$$U = \frac{x}{u}(1 - w), \quad V = \frac{y}{v}(1 - w), \quad (\text{J-7})$$

$$W = \frac{x}{u} + \frac{y}{v} - 1, \quad (\text{J-8})$$

the analytical expression of the two-loop vacuum integral can be written as:

$$\begin{aligned}
T3(m_1, m_2, m_3) = & e^{2\gamma_E \epsilon} (m_3^2)^{1-2\epsilon} \frac{\Gamma(1+\epsilon)^2}{2(1-\epsilon)(1-2\epsilon)} \left[\frac{1+x+y}{\epsilon^2} - \frac{2}{\epsilon} (x \log x + y \log y) \right. \\
& + (x \log^2 x + y \log^2 y - (1-x-y) \log x \log y \\
& + \lambda(1, x, y) \left(2 \log u \log v - \log x \log y - 2\text{Li}_2 u - 2\text{Li}_2 v + \frac{\pi^2}{3} \right) \\
& - \epsilon \left(\frac{x}{3} \log^3 x + \frac{y}{3} \log^3 y - \frac{1-x-y}{2} \log x \log y \log(xy) \right. \\
& + \lambda(1, x, y) \left\{ \frac{1}{2} \log x \log y \log(xy) + \frac{4}{3} \log^3(1-w) \right. \\
& + 2 \log^2(1-w) (\log(xy) - \log w) \\
& + \log(1-w) \left(\frac{2\pi^2}{3} + \log^2(xy) \right) + \frac{4}{3} \log^3 W + \frac{2\pi^2}{3} \log W \\
& - \frac{4}{3} \log^3 U + 2 \log^2 U \log \frac{v^2}{y^2} - \log U \left(\frac{2\pi^2}{3} + \log^2 y \right) \\
& - \frac{4}{3} \log^3 V + 2 \log^2 V \log \frac{u^2}{x^2} - \log V \left(\frac{2\pi^2}{3} + \log^2 x \right) \\
& - 2 \log x \text{Li}_2 \frac{u^2}{x} - 2 \log y \text{Li}_2 \frac{v^2}{y} + 2 \log(xy) \text{Li}_2 w \\
& + 2\text{Li}_3 \frac{u^2}{x} + 2\text{Li}_3 \frac{v^2}{y} - 2\text{Li}_3 w - 4\text{Li}_3(1-w) \\
& \left. \left. + 4\text{Li}_3 U + 4\text{Li}_3 V - 2\zeta(3) \right\} + \mathcal{O}(\epsilon^2) \right], \tag{J-9}
\end{aligned}$$

For the case of the three-loop integrals with one non-zero mass scale we have:

$$\begin{aligned}
U4(m, 0, 0, 0) = & (m^2)^{1-3\epsilon} e^{3\gamma_E \epsilon} 2\Gamma^2(1-\epsilon)\Gamma(-2+2\epsilon)\Gamma(-1+3\epsilon) \\
= & - (m^2)^{1-3\epsilon} \left[\frac{1}{6\epsilon^2} + \frac{1}{\epsilon} + \frac{100+5\pi^2}{24} \right] + \mathcal{O}(\epsilon), \tag{J-10}
\end{aligned}$$

and

$$\begin{aligned}
U5(0, 0, 0, 0, m) = & (m^2)^{1-3\epsilon} e^{3\gamma_E \epsilon} \frac{\Gamma^2(\epsilon)\Gamma^4(1-\epsilon)\Gamma(2-3\epsilon)\Gamma(-1+3\epsilon)}{\Gamma(2-\epsilon)\Gamma^2(2-2\epsilon)} \\
= & (m^2)^{1-3\epsilon} \left[\frac{1}{3\epsilon^3} + \frac{5}{3\epsilon^2} + \frac{1}{\epsilon} \left(\frac{17}{3} + \frac{5\pi^2}{12} \right) + \left(\frac{49}{3} + \frac{25\pi^2}{12} - \frac{5\zeta(3)}{3} \right) \right] + \mathcal{O}(\epsilon). \tag{J-11}
\end{aligned}$$

Three-loop master integrals with two independent mass scales have the expressions:

$$\begin{aligned}
U4(m_1, m_2, 0, 0) &= (m_2^2)^{1-3\epsilon} e^{3\gamma_E \epsilon} \frac{\Gamma(1-\epsilon)\Gamma^2(-1+2\epsilon)\Gamma(-2+3\epsilon)}{\Gamma(-2+4\epsilon)} \times \\
&\quad \left[\Gamma(\epsilon) c^{-\epsilon} {}_2F_1(\epsilon, -1+2\epsilon, -2+4\epsilon; 1-c) \right. \\
&\quad \left. - \frac{\Gamma(1+\epsilon)}{2-2\epsilon} c^{1-\epsilon} {}_2F_1(2\epsilon, 1+\epsilon, -1+4\epsilon; 1-c) \right] \\
&= (m_2^2)^{1-3\epsilon} \left[\frac{1}{3\epsilon^3} + \frac{1}{\epsilon^2} \left(\frac{5-c}{6} - \frac{1}{2} \log c \right) \right. \\
&\quad + \frac{1}{\epsilon} \left(\frac{16+\pi^2}{12} - c + \frac{c-3}{2} \log c + \frac{1}{4} \log^2 c \right) \\
&\quad + \left(\frac{20+5\pi^2+8\zeta(3)}{24} - \frac{100+\pi^2}{24} c + \frac{72c-84-11\pi^2}{24} \log c \right. \\
&\quad + \frac{3-c+4\log(1-c)}{4} \log^2 c - \frac{1}{12} \log^3 c \\
&\quad \left. + (c-1+\log c) \text{Li}_2(1-c) + 2\text{Li}_3(c) \right] + O(\epsilon), \tag{J-12}
\end{aligned}$$

$$\begin{aligned}
U4(0, 0, m_1, m_2) &= - (m_2^2)^{1-3\epsilon} e^{3\gamma_E \epsilon} \frac{\Gamma(1-\epsilon)\Gamma(-\epsilon)\Gamma(1+\epsilon)\Gamma^2(2\epsilon)\Gamma(-1+3\epsilon)}{\Gamma(2-\epsilon)\Gamma(4\epsilon)} \\
&\quad \times c^{1-\epsilon} {}_2F_1(1+\epsilon, 2\epsilon, 4\epsilon; 1-c) \\
&= - (m_2^2)^{1-3\epsilon} \left[\frac{1+c}{6\epsilon^3} + \frac{1}{\epsilon^2} \left(\frac{2(1+c)}{3} - \frac{c}{2} \log c \right) \right. \\
&\quad + \frac{1}{\epsilon} \left(\frac{52+\pi^2}{12} (1+c) - 2c \log c + \frac{c}{4} \log^2 c + (1-c) \text{Li}_2(1-c) \right) \\
&\quad + \left(\frac{40+\pi^2}{6} (1+c) + \frac{\zeta(3)}{6} (13-11c) - \frac{156c-4\pi^2+15\pi^2 c}{24} \log c \right. \\
&\quad + \frac{2c-(1-3c)\log(1-c)}{2} \log^2 c - \frac{c}{12} \log^3 c \\
&\quad + [4(1-c) - (1-2c)\log c] \text{Li}_2(1-c) \\
&\quad \left. - 4(1-c) \text{Li}_3(1-c) - (1-3c) \text{Li}_3(c) \right] + O(\epsilon), \tag{J-13}
\end{aligned}$$

$$\begin{aligned}
U5(m_1, m_2, 0, 0, 0) &= - (m_2^2)^{1-3\epsilon} e^{3\gamma_E \epsilon} \frac{\Gamma(\epsilon)\Gamma(1-\epsilon)\Gamma^2(2\epsilon)\Gamma(-1+3\epsilon)}{(1-\epsilon)(1-2\epsilon)\Gamma(4\epsilon)} \\
&\quad \times c^{1-\epsilon} {}_2F_1(1+\epsilon, 2\epsilon, 4\epsilon; 1-c)
\end{aligned}$$

$$\begin{aligned}
&= (m_2^2)^{1-3\epsilon} \left[\frac{1+c}{6\epsilon^3} + \frac{1}{\epsilon^2} \left(1+c - \frac{c}{2} \log c \right) \right. \\
&+ \frac{1}{\epsilon} \left(\frac{100+\pi^2}{24} (1+c) - 3c \log c + \frac{c}{4} \log^2 c + (1-c) \text{Li}_2(1-c) \right) \\
&+ \left(\frac{60+\pi^2}{4} (1+c) + \frac{\zeta(3)}{6} (13-11c) - \frac{300c-4\pi^2+15\pi^2c}{24} \log c \right. \\
&+ \frac{3c-(1-3c)\log(1-c)}{2} \log^2 c - \frac{c}{12} \log^3 c \\
&+ [6(1-c) - (1-2c)\log c] \text{Li}_2(1-c) \\
&\left. - 4(1-c) \text{Li}_3(1-c) - (1-3c) \text{Li}_3(c) \right] + O(\epsilon), \tag{J-14}
\end{aligned}$$

where we have defined

$$c = \frac{m_1^2}{m_2^2}. \tag{J-15}$$

Further analytical expressions with at most two independent mass scales and including just terms up to $O(\epsilon^0)$ can be consulted in [166, 182] and references therein. The analytical unknown three-loop master integrals, which contain at least three independent mass scales, are numerically evaluated with the program TVID [167, 168] based on the dispersion method.

K. Amplitudes of the Counter-term Diagrams

The insertion of the SQCD mass renormalization constants into the counter-term diagrams (one- and two-loop Higgs self-energies and tadpoles) responsible for the removal of the non-local sub-divergences are performed with the code presented below. The code takes each DRED regularized amplitude of a counter-term diagram, written in the FeynCalc notation, and inserts the mass renormalization constants listed in Appendix B. Additionally, it performs a Laurent expansion of the resulting amplitude, keeping terms up to $O(\epsilon^0)$ and putting the coefficient of the poles ϵ^{-n} in a list.

```
(* You must call the next packages in order to run this code: *)

PrependTo[$Path, ToFileName[{"path","to","SimplificationDefinitions"}]];
<< SimplificationDefinitions';

PrependTo[$Path, ToFileName[{"path","to","tvid"}]]; (* A. Freitas program*)
Get["i3.m"];
$Directory = ToFileName[{"path", "to","tvid"}];

$LoadTARCER = True; (* This is to call TARCER from FeynCalc*)
PrependTo[$Path, ToFileName[{"path","to","FeynCalc901","FeynCalc"}]];
Get["FeynCalc"];

(*****)
(** Functions devoted to perform the reduction in terms of TARCER master integrlas, **)
(** and also to take the gaugeless limit over the SQCD vertices at the desired order. **)
(*****)

changesmom = { Momentum[a_] :> Momentum[a, D],
              FAScalarProduct[a_,b_] :> Pair[ Momentum[a,D], Momentum[b,D]]};

Reduonetwol[amp_] := Block[ {amptfi,listA,listB,listrules},

amptfi = ToTFI[amp //. changesmom, q1, q2, p];
listA = Union@Cases[amptfi, (TAI | TBI | TJI | TFI)[_], Infinity];
listB = TarcercRecurse[listA];
listrules = Map[ listA[[#]] -> listB[[#]] &, Range[Length[listA]]];

Return[ MagicSimplify[ amptfi /. listrules , Feedback->False] ]; ];
```

```

Gaugeless[amp_] := Sum[ SeriesCoefficient[ amp, {MW, 0, -j}*(ht/MT)^(j),
                                     {j,0,4}] /. ht -> ht Sqrt[2] SB SW/EL

(*****
(** Call a list of DRED regularized amplitudes. Here the color and the Dirac   **)
(** algebra should have been already performed. Then apply the TARCER reduction **)
(** and the gaugeless limit over each amplitude.                               **)
(*****

Amplitudes = Get["Regularized"<>"Amplitudes"<>"Path"];

TempDirName = ToFileName[{"path", "to", "save", "your", "outputs"}];

ParallelTable[

If[ FreeQ[Amplitudes[[1]],Gstrong] ,

Print["Top1L_"<>ToString[1]];
Put[ ht^2* Reduonetwol[
    Reduonetwol[ Coefficient[Collect[ Gaugeless[ Amplitudes[[1]] ],{ht}],ht^2]],
    ToFileName[{TempDirName}, "Reduamp_"<>ToString[1]] ]; ,

Print["Top2L_"<>ToString[1]];
Put[ ht^2*Gstrong^2* Reduonetwol[
    Reduonetwol[ Coefficient[Collect[ Gaugeless[ Amplitudes[[1]] ],
    {ht,Gstrong}], Gstrong^2*ht^2 ]],
    ToFileName[{TempDirName}, "Reduamp_"<>ToString[1]]];
    ],
    {1,1,Length[Amplitudes]};

Reduampse[n_] := Get["Reduamp_"<>ToString[n], Path->{ToFileName[{TempDirName]}]];
reduamps = DeleteCases[ ParallelMap[ Reduampse[#]&, Range[Length[Amplitudes]]], 0, 1];

Put[reduamps, ToFileName[{TempDirName}, "ReduAmps" ] ]; (*save a backup!*)

(*****
(** The next functions perform an epsilon-expansion over the amplitudes. Here the **)
(** insertion of the mass counter-terms is still missing.                               **)
(*****

i3CTbasis[amp_] := Block[ {m, m1, m2, m3, $factor1L, $factor2L},

(* Q[L] = (4 Pi E^(-EulerGamma) mu^2)^(L $seps) *)

$factor1L = I*Pi^2 ;
$factor2L = -Pi^4 ;

```

```

i3basisfunc = {

BO[0,m1_,m2_] := (A0[m1]-A0[m2])/(m1 - m2) /; !(m1===m2) && !(m1===0) && !(m2===0) ,
BO[0,m_,m_] := (D-2)*A0[m]/(2*m) /; !(m===0) ,
BO[0,0,m_] := A0[m]/m /; !(m===0) ,
BO[0,m_,0] := BO[0,0,m] /; !(m===0) ,
BO[0,0,0] -> 0 ,
CO[0,0,0,m1_,m2_,m3_] := (1/(m1 - m2))*(((A0[m1]-A0[m3])/(m1-m3)) -
((A0[m2]-A0[m3])/(m2 - m3))) /; !(m1===m2) && !(m2===m3)
&& !PossibleZeroQ[m1*m2*m3] ,
CO[0,0,0,m_,m_,m_] := (D-4)*(D-2)A0[m]/(8*m^2) /; !(m===0) ,
CO[0,0,0,m1_,m1_,m2_] := ( (1/(m1 - m2))*((D-2)*A0[m1]/(2*m1)) +
(1/(m1 - m2)^2)*(A0[m2]-A0[m1])) ; !PossibleZeroQ[m1*m2]
&& !(m1===m2) ,
CO[0,0,0,m1_,m2_,m2_] := CO[0,0,0,m2,m2,m1] /; !PossibleZeroQ[m1*m2] && !(m1===m2) ,
CO[0,0,0,m1_,m2_,m1_] := CO[0,0,0,m1,m1,m2] /; !PossibleZeroQ[m1*m2] && !(m1===m2) ,
CO[0,0,0,m1_,m2_,0] := (1/(m1-m2))*(A0[m1]/m1-A0[m2]/m2)
/; !PossibleZeroQ[m1*m2]&&!(m1===m2) ,
CO[0,0,0,0,m1_,m2_] := CO[0,0,0,m1,m2,0] /; !PossibleZeroQ[m1*m2] && !(m1===m2) ,
CO[0,0,0,m1_,0,m2_] := CO[0,0,0,m1,m2,0] /; !PossibleZeroQ[m1*m2] && !(m1===m2) ,
CO[0,0,0,m_,m_,0] := (A0[m]/(2*m^2))*(D-4) /; !(m===0) ,
CO[0,0,0,0,m_,m_] := CO[0,0,0,m,m,0] /; !(m===0) ,
CO[0,0,0,m_,0,m_] := CO[0,0,0,m,m,0] /; !(m===0) ,
CO[0,0,0,0,0,m_] := (A0[m]/m^2) /; !(m===0) ,
CO[0,0,0,m_,0,0] := CO[0,0,0,0,0,m] /; !(m===0) ,
CO[0,0,0,0,m_,0] := CO[0,0,0,0,0,m] /; !(m===0) ,
CO[0,0,0,0,0,0] -> 0,

TAI[D, 0, {{1, m_}}] := $factor1L*A0[m^2] ,
TBI[D, 0, {{1, m1_}, {1, m2_}}] := (I*Pi^2)*BO[0,m1^2,m2^2] ,
TJI[D, 0, {{1, m1_}, {1, m2_}, {1, m3_}}] := $factor2L*T3[m1^2,m3^2,m2^2],

A0[m1_] := A0div[m1]/$eps + A0fin[m1] + A0evn[m1]*$eps + A0evn2[m1]*$eps^2,
BO[p_,m1_,m2_] := B0div[p,m1,m2]/$eps + B0fin[p,m1,m2] + B0evn1[p,m1,m2]*$eps
+ B0evn2[p,m1,m2]*$eps^2,
T3[m1_,m2_,m3_] := T3div2[m1,m2,m3]/($eps^2) + T3div1[m1,m2,m3]/$eps
+ T3fin[m1,m2,m3] + T3evn[m1,m2,m3]*$eps
};

Return[ amp //. i3basisfunc ];

];

(* This is a function of TVID *)

PrepIntMod[expr_,n_] := Module[{expre},
expre = expr /. usort //. urepl2 /. urepl /. usort //. urepl2 /. urepl
//. trepl /. $D -> 4-2*$eps;

```

```

expre = Map[Simplify, expre];
Return[SeriesCoefficient[expre, {$eps,0,n}]]
];

epsexpans[amp_, o_] := PrepIntMod[ Collect[
      i3CTbasis[amp] /. {D -> 4 - 2*$eps, SUNIndex[a_]:>a,
      SUNFIndex[b_]:>b}, {$eps}], o]

(* Performing the expansion *)

ParallelMap[

If[ FreeQ[reduamps[[#]], Gstrong],

Print["ampexp1l_"<>ToString[#]]
Put[Sum[ $eps^(j)*epsexpans[reduamps[[#]],j], {j,-1,2}],
      ToFileName[{TempDirName}, "epsamp_"<>ToString[#]] ],

Print["ampexp2l_"<>ToString[#]]
Put[Sum[ $eps^(j)*epsexpans[reduamps[[#]],j], {j,-2,1}],
      ToFileName[{TempDirName}, "epsamp_"<>ToString[#]] ] ]&,

      Range[Length[reduamps]] ];

epsampse[n_] := Get["epsamp_"<>ToString[n],Path->{ToFileName[{TempDirName}]}];
epsamps = ParallelMap[ epsampse[#]&, Range[Length[reduamps]] ];
$Lamp=Length[epsamps];

Put[epsamps, ToFileName[{TempDirName}, "EpsAmps" ] ]; (* Save a backup! *)

(*****
(** Now we define the mass counter-terms and perform the corresponding **)
(** insertions over the counter-term diagrams. An additional **)
(** eps-expansion up to O(eps^0) is performed. **)
(*****)

T[n_] := n*(1/2) ;

DRRenConst[const_] := Block[ {s1,s2,ji,j2,o1,o2,g1,g2},

(* Notation of the counter-terms are the same of the MSSMCT.mod file of FeynArts *)

changesDRbar={
d1tteA->0, d1tteB->0, d2tteA->0, d2tteB->0, d1bbeA->0, d1bbeB->0, d2bbeA->0, d2bbeB->0,
d1ggeA->0, d2ggeA->0, d1ggeB->0, d2ggeB->0, d1susuee->0, d2susuee->0, d1sdsdee->0,
d2sdsdee->0, d1ttAA -> 0, d2ttAA -> 0, d1ttAB -> 0, d2ttAB -> 0, d1ttHA -> 0, d2ttHA -> 0,

```

```

d1ttHB -> 0, d2ttHB -> 0, d1Asusu -> 0, d2Asusu -> 0, d1hsusu -> 0, d2hsusu -> 0,
d1Hsusu -> 0, d2Hsusu -> 0, d1sdsdsusu -> 0, disusususu -> 0, d1ttgA -> 0, d1ttgB -> 0,
d1susug -> 0, d1glstA -> 0, d1glstB -> 0, d1glstcgA -> 0, d1glstcgB -> 0,
d1ststglgl -> 0, d1tthA -> 0, d2tthA -> 0, d1tthB -> 0, d2tthB -> 0, d1AAsusu[___]->0,
d2AAsusu[___]->0, d1hhsusu[___]->0, d2hhsusu[___]->0
};

```

```
expression = {
```

```
(*----- gluino - gluino -----*)
```

```

dZG1A[g1_,g2_] :> 0,
dZG1B[g1_,g2_] :> 0,
dZG1C[g1_,g2_] :>(-I/2)*SUNDelta[g1, g2]*(Gstrong^2/(16*Pi^2))*( -3 )*MGl/$eps,
dZG1D[g1_,g2_] :> (-I/2)*SUNDelta[g1, g2]*(Gstrong^2/(16*Pi^2))*( -3 )*MGl/$eps,

```

```
(*----- squark down - squark down -----*)
```

```

dZsdA[s1_,s2_,j1_,j2_,o1_,o2_] :> 0,
dZsdB[s1_,s1_,j1_,j2_,o1_,o2_] :> (-I)*(Gstrong^2/(12*Pi^2))*SUNFDelta[o1, o2]
                                         *(-4*MGl^2)*(1/$eps),
dZsdB[ 1, 2, j1_,j2_,o1_,o2_] :> 0,
dZsdB[ 2, 1, j1_,j2_,o1_,o2_] :> 0,

```

```
(*----- squark up - squark up -----*)
```

```

dZsuA1[s1_,s2_,j1_,j2_,o1_,o2_] :> 0,
dZsuA2[s1_,s2_,j1_,j2_,o1_,o2_] :> 0,
dZsuB1[s1_, s1_, 1, j2_, o1_, o2_] :> (-I)*(Gstrong^2/(12*Pi^2))*SUNFDelta[o1, o2]
                                         *(-4*MGl^2)*(1/$eps) ,
dZsuB1[1, 2, 1, j2_, o1_, o2_] :> 0,
dZsuB1[2, 1, 1, j2_, o1_, o2_] :> 0,
dZsuB1[s1_, s1_, 2, j2_, o1_, o2_] :> (-I)*(Gstrong^2/(12*Pi^2))*SUNFDelta[o1, o2]
                                         *(-4*MGl^2)*(1/$eps) ,
dZsuB1[1, 2, 2, 2, o1_, o2_] :> 0,
dZsuB1[2, 1, 2, 2, o1_, o2_] :> 0,
dZsuB1[s1_, s1_, 3, 1, o1_, o2_] :> (-I)*(Gstrong^2/(12*Pi^2))*SUNFDelta[o1, o2]
                                         *(-4*MGl^2)*(1/$eps) ,
dZsuB1[s1_, s1_, 3, 2, o1_, o2_] :> (-I)*(Gstrong^2/(12*Pi^2))*SUNFDelta[o1, o2]
                                         *(-4*MGl^2)*(1/$eps) ,
dZsuB1[1, 2, 3, 1, o1_, o2_] :> 0,
dZsuB1[2, 1, 3, 1, o1_, o2_] :> 0,
dZsuB1[1, 2, 3, 2, o1_, o2_] :> 0,
dZsuB1[2, 1, 3, 2, o1_, o2_] :> 0,
dZsuB1[1, 1, 3, 3, o1_, o2_] :> (-I)*(Gstrong^2/(4*Pi^2))*SUNFDelta[o1, o2]*
                                         CF*(-MGl^2 - MT^2 + MGl*MT*Sin[2*ttht]

```


$$+ \text{Sin}[2*\text{tght}]^2*(\text{MSf}[2, 3, 3]^2 - \text{MSf}[1, 3, 3]^2)/4) * 1/\$eps,$$

$$\text{dZsuB1}[2, 2, 3, 3, \text{o1}_-, \text{o2}_-] \text{ :> } (-I)*(G\text{strong}^2/(4*\text{Pi}^2))*\text{SUNFDelta}[\text{o1}, \text{o2}] * \\ \text{CF}*(-\text{MGl}^2 - \text{MT}^2 - \text{MGl}*\text{MT}*\text{Sin}[2*\text{tght}] \\ + \text{Sin}[2*\text{tght}]^2*(\text{MSf}[1, 3, 3]^2 - \text{MSf}[2, 3, 3]^2)/4) * 1/\$eps,$$

$$\text{dZsuB1}[1, 2, 3, 3, \text{o1}_-, \text{o2}_-] \text{ :> } (-I)*(G\text{strong}^2/(4*\text{Pi}^2))*\text{SUNFDelta}[\text{o1}, \text{o2}] * \\ \text{CF}*\text{Cos}[2*\text{tght}]*(\text{MGl}*\text{MT} \\ - \text{Sin}[2*\text{tght}]*(\text{MSf}[1, 3, 3]^2 - \text{MSf}[2, 3, 3]^2)/4) * 1/\$eps,$$

$$\text{dZsuB1}[2, 1, 3, 3, \text{o1}_-, \text{o2}_-] \text{ :> } \text{dZsuB1}[1, 2, 3, 3, \text{o1}, \text{o2}],$$

$$\text{dZsuB2}[1, 1, 3, 3, \text{o1}_-, \text{o2}_-] \text{ :> } (-I)*((G\text{strong}^2/(4*\text{Pi}^2))^2*\text{SUNFDelta}[\text{o1}, \text{o2}] * \\ (\text{CF}^2*(\text{Cos}[2*\text{tght}]^2*\text{MGl}^2*\text{MT}^2/(\text{MSf}[1, 3, 3]^2 - \text{MSf}[2, 3, 3]^2) \\ + ((1+\text{Cos}[2*\text{tght}]^2)*\text{Sin}[2*\text{tght}]^2*(\text{MSf}[1, 3, 3]^2 - \text{MSf}[2, 3, 3]^2) \\ + 8*\text{MT}^2)/16 - (1+\text{Cos}[2*\text{tght}]^2)*\text{MGl}*\text{MT}*\text{Sin}[2*\text{tght}]/2) \\ + \text{CA}*\text{CF}*(9*\text{MGl}^2/8 + 3*(\text{Sin}[2*\text{tght}]^2*(\text{MSf}[1, 3, 3]^2 - \text{MSf}[2, 3, 3]^2) \\ + 4*\text{MT}^2)/32 - 3*\text{MGl}*\text{MT}*\text{Sin}[2*\text{tght}]/4) \\ + \text{CF}*\text{T}[6]*(-3*\text{MGl}^2/4 - (\text{Sin}[2*\text{tght}]^2*(\text{MSf}[1, 3, 3]^2 - \text{MSf}[2, 3, 3]^2) \\ + 4*\text{MT}^2)/16 + \text{MGl}*\text{MT}*\text{Sin}[2*\text{tght}]/2))*(1/\$eps^2) \\ + (G\text{strong}^2/(4*\text{Pi}^2))^2*\text{SUNFDelta}[\text{o1}, \text{o2}]*(\text{CF}^2*(3*\text{MGl}^2/4 \\ + (\text{Sin}[2*\text{tght}]^2*(\text{MSf}[1, 3, 3]^2 - \text{MSf}[2, 3, 3]^2) + 4*\text{MT}^2)/16 \\ - \text{MGl}*\text{MT}*\text{Sin}[2*\text{tght}]/2) \\ + \text{CA}*\text{CF}*(-11*\text{MGl}^2/8 - 3*(\text{Sin}[2*\text{tght}]^2*(\text{MSf}[1, 3, 3]^2 - \text{MSf}[2, 3, 3]^2) \\ + 4*\text{MT}^2)/32 + 3*\text{MGl}*\text{MT}*\text{Sin}[2*\text{tght}]/4) \\ + \text{CF}*\text{T}[5]*(3*\text{MGl}^2/4 + (\text{Sin}[2*\text{tght}]^2*(\text{MSf}[1, 3, 3]^2 - \text{MSf}[2, 3, 3]^2) \\ + 4*\text{MT}^2 + 8*\text{MSq}^2)/16 - \text{MGl}*\text{MT}*\text{Sin}[2*\text{tght}]/2) \\ + \text{CF}*\text{T}[1]*(3*\text{MGl}^2/4 + (\text{Sin}[2*\text{tght}]^2*(\text{MSf}[1, 3, 3]^2 - \text{MSf}[2, 3, 3]^2) \\ - 4*\text{MT}^2 + 4*\text{MSf}[1, 3, 3]^2 + 4*\text{MSf}[2, 3, 3]^2)/16 - \text{MGl}*\text{MT}*\text{Sin}[2*\text{tght}]/2) \\)*(1/\$eps) + (G\text{strong}^2/(4*\text{Pi}^2))^2*\text{SUNFDelta}[\text{o1}, \text{o2}] * \\ \text{Meps}^2*(- \text{CA}*\text{CF}*3/8 + \text{CF}*\text{T}[6]*1/4)*(1/\$eps) \\ - (G\text{strong}^2/(4*\text{Pi}^2))^2*\text{SUNFDelta}[\text{o1}, \text{o2}]*(\text{MSf}[1, 3, 3]^2 \\ - \text{MSf}[2, 3, 3]^2)^{-1}*\text{CF}^2*\text{Cos}[2*\text{tght}]^2*(\text{MGl}*\text{MT} - \\ \text{Sin}[2*\text{tght}]*(\text{MSf}[1, 3, 3]^2 - \text{MSf}[2, 3, 3]^2)/4)^2*(1/\$eps^2)),$$

$$\text{dZsuB2}[2, 2, 3, 3, \text{o1}_-, \text{o2}_-] \text{ :> } (-I)*((G\text{strong}^2/(4*\text{Pi}^2))^2*\text{SUNFDelta}[\text{o1}, \text{o2}]*(\\ \text{CF}^2*(\text{Cos}[2*\text{tght}]^2*\text{MGl}^2*\text{MT}^2/(\text{MSf}[2, 3, 3]^2 - \text{MSf}[1, 3, 3]^2) \\ + ((1+\text{Cos}[2*\text{tght}]^2)*\text{Sin}[2*\text{tght}]^2*(\text{MSf}[2, 3, 3]^2 - \text{MSf}[1, 3, 3]^2) + 8*\text{MT}^2)/16 \\ + (1+\text{Cos}[2*\text{tght}]^2)*\text{MGl}*\text{MT}*\text{Sin}[2*\text{tght}]/2) \\ + \text{CA}*\text{CF}*(9*\text{MGl}^2/8 + 3*(\text{Sin}[2*\text{tght}]^2*(\text{MSf}[2, 3, 3]^2 - \text{MSf}[1, 3, 3]^2) \\ + 4*\text{MT}^2)/32 + 3*\text{MGl}*\text{MT}*\text{Sin}[2*\text{tght}]/4) \\ + \text{CF}*\text{T}[6]*(-3*\text{MGl}^2/4 - (\text{Sin}[2*\text{tght}]^2*(\text{MSf}[2, 3, 3]^2 \\ - \text{MSf}[1, 3, 3]^2) + 4*\text{MT}^2)/16 - \text{MGl}*\text{MT}*\text{Sin}[2*\text{tght}]/2))*(1/\$eps^2) \\ + (G\text{strong}^2/(4*\text{Pi}^2))^2*\text{SUNFDelta}[\text{o1}, \text{o2}]*(\text{CF}^2*(3*\text{MGl}^2/4 \\ + (\text{Sin}[2*\text{tght}]^2*(\text{MSf}[2, 3, 3]^2 - \text{MSf}[1, 3, 3]^2) + 4*\text{MT}^2)/16 \\ + \text{MGl}*\text{MT}*\text{Sin}[2*\text{tght}]/2) \\ + \text{CA}*\text{CF}*(-11*\text{MGl}^2/8 - 3*(\text{Sin}[2*\text{tght}]^2*(\text{MSf}[2, 3, 3]^2 \\ - \text{MSf}[1, 3, 3]^2) + 4*\text{MT}^2)/32 - 3*\text{MGl}*\text{MT}*\text{Sin}[2*\text{tght}]/4)$$

$$\begin{aligned}
& + CF*T[5]*(3*MGl^2/4 + (\text{Sin}[2*tht]^2*(MSf[2, 3, 3]^2 - MSf[1, 3, 3]^2) \\
& + 4*MT^2 + 8*MSq^2)/16 + MGl*MT*\text{Sin}[2*tht])/2) \\
& + CF*T[1]*(3*MGl^2/4 + (\text{Sin}[2*tht]^2*(MSf[2, 3, 3]^2 - MSf[1, 3, 3]^2) \\
& - 4*MT^2 + 4*MSf[2, 3, 3]^2 + 4*MSf[1, 3, 3]^2)/16 + MGl*MT*\text{Sin}[2*tht])/2) \\
&)*(1/\$eps) + (Gstrong^2/(4*Pi^2))^2*SUNFDelta[o1, o2]*Meps^2*(-CA*CF*3/8 \\
& + CF*T[6]*1/4)*(1/\$eps) \\
& + (Gstrong^2/(4*Pi^2))^2*SUNFDelta[o1, o2]*(MSf[1, 3, 3]^2 \\
& - MSf[2, 3, 3]^2)^{-1}*CF^2*\text{Cos}[2*tht]^2*(MGl*MT - \\
& \text{Sin}[2*tht]*(MSf[1, 3, 3]^2 - MSf[2, 3, 3]^2)/4)^2*(1/\$eps^2)),
\end{aligned}$$

$$\begin{aligned}
dZsuB2[1, 2, 3, 3, o1_, o2_] & :> (-I)*(Gstrong^2/(4*Pi^2))^2*SUNFDelta[o1, o2]*(\\
& CF^2*\text{Cos}[2*tht]*((\text{Sin}[2*tht]^2 - \text{Cos}[2*tht]^2)*(MGl*MT/2 \\
& - \text{Sin}[2*tht]*(MSf[1, 3, 3]^2 - MSf[2, 3, 3]^2)/16) \\
& - 2*\text{Sin}[2*tht]*MGl^2*MT^2*(MSf[1, 3, 3]^2 - MSf[2, 3, 3]^2)^{-1}) \\
& + CF*CA*\text{Cos}[2*tht]*(-3*MGl*MT/4 + 3*\text{Sin}[2*tht]*(MSf[1, 3, 3]^2 \\
& - MSf[2, 3, 3]^2)/32) \\
& + CF*T[6]*\text{Cos}[2*tht]*(MGl*MT/2 - \text{Sin}[2*tht]*(MSf[1, 3, 3]^2 \\
& - MSf[2, 3, 3]^2)/16))*(1/\$eps^2) \\
& + (Gstrong^2/(4*Pi^2))^2*SUNFDelta[o1, o2]*(CF^2*\text{Cos}[2*tht]*(-MGl*MT/2 \\
& + \text{Sin}[2*tht]*(MSf[1, 3, 3]^2 - MSf[2, 3, 3]^2)/16) \\
& + CF*CA*\text{Cos}[2*tht]*(3*MGl*MT/4 - 3*\text{Sin}[2*tht]*(MSf[1, 3, 3]^2 \\
& - MSf[2, 3, 3]^2)/32) \\
& + CF*T[6]*\text{Cos}[2*tht]*(-MGl*MT/2 + \text{Sin}[2*tht]*(MSf[1, 3, 3]^2 \\
& - MSf[2, 3, 3]^2)/16))*(1/\$eps) \\
& + (Gstrong^2/(4*Pi^2))^2*SUNFDelta[o1, o2]*(MSf[1, 3, 3]^2 \\
& - MSf[2, 3, 3]^2)^{-1}*CF*\text{Cos}[2*tht]*(MGl*MT - \\
& \text{Sin}[2*tht]*(MSf[1, 3, 3]^2 - MSf[2, 3, 3]^2)/4)*(CF*(-MGl^2 - MT^2 \\
& + MGl*MT*\text{Sin}[2*tht] + \text{Sin}[2*tht]^2*(MSf[2, 3, 3]^2 - MSf[1, 3, 3]^2)/4) \\
& - CF*(-MGl^2 - MT^2 - MGl*MT*\text{Sin}[2*tht] + \text{Sin}[2*tht]^2*(MSf[1, 3, 3]^2 \\
& - MSf[2, 3, 3]^2)/4))*(1/\$eps^2)),
\end{aligned}$$

$$dZsuB2[2, 1, 3, 3, o1_, o2_] :> dZsuB2[1, 2, 3, 3, o1, o2],$$

(*----- quark up - quark up -----*)

$$\begin{aligned}
dZquA1[j1_, j2_, o1_, o2_] & :> 0, \\
dZquB1[j1_, j2_, o1_, o2_] & :> 0, \\
dZquC1[3, 3, o1_, o2_] & :> (-I/2)*(-(Gstrong^2/(4*Pi^2)) \\
& *SUNFDelta[o1, o2]*(2*CF*MT)*(1/\$eps)), \\
dZquD1[3, 3, o1_, o2_] & :> (-I/2)*(-(Gstrong^2/(4*Pi^2)) \\
& *SUNFDelta[o1, o2]*(2*CF*MT)*(1/\$eps)), \\
dZquA2[j1_, j2_, o1_, o2_] & :> 0, \\
dZquB2[j1_, j2_, o1_, o2_] & :> 0, \\
dZquC2[3, 3, o1_, o2_] & :> (-I/2)*(Gstrong^2/(4*Pi^2))^2*SUNFDelta[o1, o2] \\
& *(((1/\$eps^2)*(3*CA*CF + 2*CF^2 - 2*CF*T[6]) + (1/\$eps)*(-3*CA*CF + 2*CF^2 + 2*CF*T[6]))*MT), \\
dZquD2[3, 3, o1_, o2_] & :> (-I/2)*(Gstrong^2/(4*Pi^2))^2*SUNFDelta[o1, o2] \\
& *(((1/\$eps^2)*(3*CA*CF + 2*CF^2 - 2*CF*T[6]) + (1/\$eps)*(-3*CA*CF + 2*CF^2 + 2*CF*T[6]))*MT),
\end{aligned}$$

```

(*----- gluon - gluon -----*)

dZGG1 -> 0

};

Return[ MagicSimplify[const /. changesDRbar //. expression, Feedback->False] ];

];

(* Inserting the mass counter-terms and expanding in epsilon *)

coeffeps[j_,l_] := Coefficient[ DRRenConst[epsampse[l]], $eps, -j]
ampepsB[m_] := $eps^(1-m)*(Plus @@ ParallelTable[ coeffeps[m-1,l], {1,1,$Lamp}])

ampLexp = Map[ampepsB[#]&, Range[6]];
Put[ampLexp, ToFileName[{TempDirName}, "AmpLexp"]]; (* Save a backup! *)

Clear[ampLexp, epsamps, reduamps];

ParallelEvaluate[
Clear[ampLexp, epsamps, reduamps];
];

Print["The End!"]

CloseKernels[];

Quit[];

```

L. EFT loop functions

This appendix contains a list of loop-functions that appears in the stop and the gaugino-higgsino contributions to the threshold corrections of the Higgs quartic coupling λ [121] introduced in the vacuum stability analysis described in Section 4.4.

$$F_1(x) = \frac{x \ln x^2}{x^2 - 1}, \quad (\text{L-1})$$

$$F_2(x) = \frac{6x^2 [2 - 2x^2 + (1 + x^2) \ln x^2]}{(x^2 - 1)^3}, \quad (\text{L-2})$$

$$F_3(x) = \frac{2x [5(1 - x^2) + (1 + 4x^2) \ln x^2]}{3(x^2 - 1)^2}, \quad (\text{L-3})$$

$$F_4(x) = \frac{2x(x^2 - 1 - \ln x^2)}{(x^2 - 1)^2}, \quad (\text{L-4})$$

$$F_5(x) = \frac{3x(1 - x^4 + 2x^2 \ln x^2)}{(1 - x^2)^3}. \quad (\text{L-5})$$

$$F_6(x) = \frac{x^2 - 3}{4(1 - x^2)} + \frac{x^2(x^2 - 2)}{2(1 - x^2)^2} \ln x^2, \quad (\text{L-6})$$

$$F_7(x) = \frac{-3(x^4 - 6x^2 + 1)}{2(x^2 - 1)^2} + \frac{3x^4(x^2 - 3)}{(x^2 - 1)^3} \ln x^2, \quad (\text{L-7})$$

$$F_8(x_1, x_2) = -2 + \frac{2}{x_1^2 - x_2^2} \left(\frac{x_1^4}{x_1^2 - 1} \ln x_1^2 - \frac{x_2^4}{x_2^2 - 1} \ln x_2^2 \right), \quad (\text{L-8})$$

$$F_9(x_1, x_2) = \frac{2}{x_1^2 - x_2^2} \left(\frac{x_1^2}{x_1^2 - 1} \ln x_1^2 - \frac{x_2^2}{x_2^2 - 1} \ln x_2^2 \right). \quad (\text{L-9})$$

$$f(r) = F_5(r), \quad G(r) = F_7(r), \quad (\text{L-10})$$

$$f_1(r) = \frac{6(r^2 + 3)r^2}{7(r^2 - 1)^2} + \frac{6(r^2 - 5)r^4 \ln r^2}{7(r^2 - 1)^3}, \quad (\text{L-11})$$

$$f_2(r) = \frac{2(r^2 + 11)r^2}{9(r^2 - 1)^2} + \frac{2(5r^2 - 17)r^4 \ln r^2}{9(r^2 - 1)^3}, \quad (\text{L-12})$$

$$f_3(r) = \frac{2(r^4 + 9r^2 + 2)}{3(r^2 - 1)^2} + \frac{2(r^4 - 7r^2 - 6)r^2 \ln r^2}{3(r^2 - 1)^3}, \quad (\text{L-13})$$

$$f_4(r) = \frac{2(5r^4 + 25r^2 + 6)}{7(r^2 - 1)^2} + \frac{2(r^4 - 19r^2 - 18)r^2 \ln r^2}{7(r^2 - 1)^3}, \quad (\text{L-14})$$

$$\frac{4}{3}f_5(r_1, r_2) = \frac{1 + (r_1 + r_2)^2 - r_1^2 r_2^2}{(r_1^2 - 1)(r_2^2 - 1)} + \frac{r_1^3 (r_1^2 + 1) \ln r_1^2}{(r_1^2 - 1)^2 (r_1 - r_2)} - \frac{r_2^3 (r_2^2 + 1) \ln r_2^2}{(r_1 - r_2)(r_2^2 - 1)^2}, \quad (\text{L-15})$$

$$\frac{7}{6}f_6(r_1, r_2) = \frac{r_1^2 + r_2^2 + r_1 r_2 - r_1^2 r_2^2}{(r_1^2 - 1)(r_2^2 - 1)} + \frac{r_1^5 \ln r_1^2}{(r_1^2 - 1)^2 (r_1 - r_2)} - \frac{r_2^5 \ln r_2^2}{(r_1 - r_2)(r_2^2 - 1)^2}, \quad (\text{L-16})$$

$$\frac{1}{6}f_7(r_1, r_2) = \frac{1 + r_1 r_2}{(r_1^2 - 1)(r_2^2 - 1)} + \frac{r_1^3 \ln r_1^2}{(r_1^2 - 1)^2 (r_1 - r_2)} - \frac{r_2^3 \ln r_2^2}{(r_1 - r_2)(r_2^2 - 1)^2}, \quad (\text{L-17})$$

$$\frac{2}{3}f_8(r_1, r_2) = \frac{r_1 + r_2}{(r_1^2 - 1)(r_2^2 - 1)} + \frac{r_1^4 \ln r_1^2}{(r_1^2 - 1)^2 (r_1 - r_2)} - \frac{r_2^4 \ln r_2^2}{(r_1 - r_2)(r_2^2 - 1)^2}. \quad (\text{L-18})$$

All the above functions are equal to 1 when their arguments approach to unity, with the exception of F_6 which tends to 0.

Bibliografía

- [1] E. A. Reyes R., A. R. Fazio, EPJ Web Conf. **192**, 00033 (2018).
- [2] A. R. Fazio and E. A. Reyes R., Nucl. Phys. B **942**, 164-183 (2019). [arXiv:1901.03651 [hep-ph]].
- [3] E.A. Reyes R., A.R. Fazio, Phys. Rev. D **100**, no.11, 115017 (2019). [arXiv:1908.00693 [hep-ph]].
- [4] ATLAS Collaboration, G. Aad et al., Phys. Lett. B **716**, 1 - 29 (2012). [arXiv:1207.7214 [hep-ex]].
- [5] CMS Collaboration, S. Chatrchyan et al., Phys. Lett. B **716**, 30 - 61 (2012). [arXiv:1207.7235 [hep-ex]].
- [6] ATLAS, CMS collaboration, G. Aad et al., Phys. Rev. Lett. **114**, 191803 (2015). [arXiv:1503.07589 [hep-ex]].
- [7] CMS Collaboration, JHEP **1711**, 047 (2017). [arXiv:1706.09936 [hep-ex]].
- [8] ATLAS Collaboration, Phys. Lett. B **784**, 345-366 (2018). [arXiv:1806.00242 [hep-ex]].
- [9] L. D. Landau, A. A. Abrikosov, and I. M. Khalatnikov, Dokl. Akad. Nauk SSSR **95**, 497, 773, 1177 (1954).
- [10] G. Degrassi, S. Di Vita, J. Elias-Miró, J. R. Espinosa, G. F. Giudice, G. Isidori, A. Strumia, JHEP **1208**, 098 (2012). [arXiv:1205.6497 [hep-ph]].
- [11] F. Bezrukov, M. Yu. Kalmykov, B. A. Kniehl, M. Shaposhnikov, JHEP **1210**, 140 (2012). [arXiv:1205.2893 [hep-ph]].
- [12] D. Buttazzo, G. Degrassi, P. P. Giardino, G. Giudice, F. Sala, A. Salvio and A. Strumia, JHEP **1312**, 089 (2013). [arXiv:1307.3536 [hep-ph]].
- [13] B. A. Kniehl and O. L. Veretin, Nucl. Phys. B **885**, 459 (2014). [Erratum:Nucl. Phys. B **894**, 56 (2015)]. [arXiv:1401.1844 [hep-ph]].
- [14] B. A. Kniehl, A. F. Pikelner and O. L. Veretin, Nucl. Phys. B **896**, 19 (2015). [arXiv:1503.02138 [hep-ph]].
- [15] A. V. Bednyakov, B. A. Kniehl, A. F. Pikelner, O. L. Veretin, Phys. Rev. Lett. **115**, no.20, 201802 (2015). [arXiv:1507.08833 [hep-ph]].
- [16] K. G. Wilson, Phys. Rev. D **3**, 1818 (1971).
- [17] E. Gildener and S. Weinberg, Phys. Rev. D **13**, 3333 (1976).
- [18] G. 't Hooft, NATO Adv. Study Inst. Ser. B Phys. **59**, 135 (1980).
- [19] J. D. Bjorken, S. Pakvasa, S. F. Tuan, Phys. Rev. D **66**, 053008 (2002).

- [20] F. Jegerlehner, M. Yu. Kalmykov, B. A. Kniehl, *J. Phys. Conf. Ser.*, **608**, no.1, 012074 (2015). [arXiv:1412.4215 [hep-ph]].
- [21] G. Giudice and R. Rattazzi, *Nucl. Phys. B* **757**, 19 (2006). [hep-ph/0606105].
- [22] T. Barklow, J. Brau, K. Fujii, J. Gao, J. List, N. Walker and K. Yokoya, [arXiv:1506.07830 [hep-ex]] (2015).
- [23] M. Bicer, et al., *JHEP* **1401**, 164 (2014). <https://fcc.web.cern.ch>. [arXiv:1308.6176 [hep-ex]].
- [24] P. Fayet and S. Ferrara, *Phys. Rep.* **32**, 249 (1977).
- [25] H. P. Nilles, *Phys. Rept.* **110**, 1 (1984).
- [26] H. E. Haber, G. L. Kane, *Phys. Rept.* **117**, 75–263 (1985).
- [27] M. Drees, R. Godbole, and P. Roy, *Theory and Phenomenology of Sparticles*, World Scientific, Singapore, (2005).
- [28] M. Kuroda, [hep-ph/9902340] (2005).
- [29] J. Terning, *Modern Supersymmetry - Dynamics and Duality*, CLARENDON PRESS - Oxford, (2006).
- [30] H. Baer and X. Tata, *Weak Scale Supersymmetry: from Superfields to Scattering Events*, Cambridge University Press, Cambridge, UK, (2006).
- [31] I.J.R. Aitchison, *Supersymmetry in Particle Physics: an elementary introduction*, Cambridge University Press, Cambridge, UK, (2007).
- [32] N. Sakai, *Z. Phys. C* **11**, 153 (1981).
- [33] R. K. Kaul, *Phys. Lett. B* **109**, 19 (1982).
- [34] R. K. Kaul and M. Parthasarathi, *Nucl. Phys. B* **199**, 36 (1982).
- [35] L. Susskind, *Phys. Reports* **104**, 181 (1984).
- [36] S. Heinemeyer, O. Stål, G. Weiglein, *Phys. Lett. B* **710**, 201-206 (2012). [arXiv:1112.3026 [hep-ph]].
- [37] M. Carena, S. Heinemeyer, O. Stål, C.E.M. Wagner, G. Weiglein, *Eur. Phys. J.* **C73**, no.9, 2552 (2013). [arXiv:1302.7033 [hep-ph]].
- [38] E. Bagnaschi, et al. *Eur. Phys. J.* **C79**, no.7, 617 (2019). [arXiv:1808.07542 [hep-ph]].
- [39] H. Bahl, S. Liebler, T. Stefaniak, *Eur. Phys. J.* **C79**, no.3, 279 (2019). [arXiv:1901.05933 [hep-ph]].
- [40] P. Athron, J.h. Park, T. Steudtner, D. Stöckinger, A. Voigt, *JHEP* **1701**, 079 (2017). [arXiv:1609.00371 [hep-ph]].
- [41] B.C. Allanach, A. Voigt, *Eur. Phys. J.* **C78**, no.7, 573 (2018). [arXiv:1804.09410 [hep-ph]].
- [42] CERN Report No. CERN-LHCC-2006-021; CMS-TDR-008-2, (2006). <http://cmsdoc.cern.ch/cms/cpt/tdr/>.

-
- [43] J. A. Aguilar-Saavedra et al. [ECFA/DESY LC Physics Working Group]. [arXiv:0106315 [hep-ph]].
- [44] W. Siegel, Phys. Lett. B **84**, 193 (1979).
- [45] D. M. Capper, D. R. T. Jones and P. van Nieuwenhuizen, Nucl. Phys. B **167**, 479 (1980).
- [46] I. Jack, D. R. T. Jones, S. P. Martin, M. T. Vaughn and Y. Yamada, Phys. Rev. D **50**, 5481 (1994). [hep-ph/9407291].
- [47] C. Gnendiger et al., Eur. Phys. J. C **77**, no.7, 471 (2017). [arXiv:1705.01827 [hep-ph]].
- [48] R. D. L. Kronig, J. Opt. Soc. Am. **12**, 547-556 (1926).
- [49] J. Bjorken and S. Drell, Relativistic quantum mechanics. International series in pure and applied physics. McGraw-Hill, 1964.
- [50] Z. Bern, L. J. Dixon, D. C. Dunbar and D. A. Kosower, Nucl.Phys. B **425**, 217-260 (1994). [hep-ph/9403226].
- [51] Z. Bern, L. J. Dixon, D. C. Dunbar and D. A. Kosower, Nucl.Phys. B **435**, 59-101 (1995). [hep-ph/9409265].
- [52] S. Bauberger, F. A. Berends, M. Boehm, M. Buza, Nucl.Phys. B **434**, 383-407 (1995). [hep-ph/9409388].
- [53] S. Bauberger, M. Boehm, Nucl.Phys. B **445**, 25-48 (1995). [hep-ph/9501201].
- [54] Z. Bern, L. J. Dixon and D. A. Kosower, Annals Phys. **322**, 1587-1634 (2007). [arXiv:0704.2798 [hep-ph]].
- [55] R. V. Harlander, J. Klappert, A. Voigt, Eur. Phys. J. C **77**, no.12, 814 (2017). [arXiv:1708.05720 [hep-ph]].
- [56] H. Bahl, T. Hahn, S. Heinemeyer, W. Hollik, S. Paßehr, H. Rzehak, G. Weiglein, (2018). [arXiv:1811.09073 [hep-ph]].
- [57] R. Haag, J. T. Lopuszanski and M. Sohnius, Nucl. Phys. B **88**, 257 (1975).
- [58] S. R. Coleman and J. Mandula, Phys. Rev. **159**, 1251 (1967).
- [59] P. Langacker, The Standard Model and Beyond, CRC Press, Boca Raton, FL, (2010).
- [60] E. Witten, Nucl. Phys. B **188** 513 (1981).
- [61] S. Dimopoulos, H. Georgi, Nucl.Phys. B **193**, 150 (1981).
- [62] L. Girardello, M. T. Grisaru, Nucl.Phys. B **194**, 65 (1982).
- [63] R. Barbieri, M. Frigeni and F. Caravaglios, Phys. Lett. B **258**, 167 - 170 (1991).
- [64] C. Bollini, J. Giambiagi, Nuovo Cim. B **12**, 20 (1972).
- [65] J. Ashmore, Nuovo Cim. Lett. **4**, 289 (1972).

- [66] G. 't Hooft, M. Veltman, Nucl. Phys. B **44**, 189 (1972).
- [67] R. V. Harlander, L. Mihaila, M. Steinhauser, Eur. Phys. J. C **63**, 383-390 (2009). [arXiv:0905.4807 [hep-ph]].
- [68] D. Stöckinger, J. Unger, Nucl.Phys. B **935**, 1-16 (2018). [arXiv:1804.05619 [hep-ph]].
- [69] G. 't Hooft, Nucl. Phys. B **61**, 455 (1973).
- [70] W. A. Bardeen, A. J. Buras, D. W. Duke, T. Muta, Phys. Rev. D **18**, 3998 (1978).
- [71] A. J. Buras, Rev. Mod. Phys. **52**, 199 (1980).
- [72] G. Passarino, M. Veltman, Phys. Lett. C **237**, 537 (1990).
- [73] W. J. Marciano, A. Sirlin, Phys. Rev. Lett. **46**, 163 (1981).
- [74] A. Sirlin, Phys. Lett. B **232**, 123 (1989).
- [75] S. P. Martin, Phys. Rev. D **65**, 116003 (2002). [arXiv:hep-ph/0111209].
- [76] M. Böhm, W. Hollik, H. Spiesberger, Fortschr. Phys. **34**, 687 (1986).
- [77] A. Denner, Fortschr. Phys. **41**, 307 (1993).
- [78] A. Freitas, D. Stöckinger, Phys. Rev. D **66**, 095014 (2002). [hep-ph/0205281].
- [79] D. R. T. Jones and L. Mezincescu, Phys. Lett. B **136**, 242 (1984); Ibid. **138**, 293 (1984).
- [80] A. J. Parkes and P. C. West, Nucl. Phys. B **256**, 340 (1985).
- [81] The ATLAS, CDF, CMS and D0 Collaborations, (2014). [arXiv:1403.4427 [hep-ph]].
- [82] M. Beneke, V. M. Braun, Nucl.Phys. B **426**, 301-343 (1994). [hep-ph/9402364].
- [83] 't Hooft G., Nuclear Physics B. **61**, 455 (1973).
- [84] S. Alekhin, A. Djouadi and S. Moch, Phys. Lett. B, **716**, 214 (2012). [arXiv:1207.0980 [hep-ph]].
- [85] F. Jegerlehner, M. Y. Kalmykov and B. A. Kniehl, Phys. Lett. B **722**, 123 (2013). [arXiv:1212.4319 [hep-ph]].
- [86] R. Tarrach, Nucl. Phys. B **183**, 384 (1981).
- [87] N. Gray, D. J. Broadhurst, W. Grafe and K. Schilcher, Z. Phys. C **48**, 673 (1990).
- [88] L. V. Avdeev and M. Y. Kalmykov, Nucl. Phys. B **502**, 419 (1997). [hep-ph/9701308].
- [89] J. Fleischer, F. Jegerlehner, O. V. Tarasov and O. L. Veretin, Nucl. Phys. B **539**, 671 (1999). [Erratum:Nucl. Phys. B **571**, 511 (2000)]. [hep-ph/9803493].
- [90] K. Melnikov and T. V. Ritbergen, Phys. Lett. B **482**, 99 (2000). [hep-ph/9912391].
- [91] P. Marquard, A. V. Smirnov, V. A. Smirnov and M. Steinhauser, Phys. Rev. Lett. **114**, no. 14, 142002 (2015).

- [92] M. Bohm, H. Spiesberger and W. Hollik, *Fortsch. Phys.* **34**, 687 (1986).
- [93] R. Hempfling and B. A. Kniehl, *Phys. Rev. D* **51**, 1386 (1995). [hep-ph/9408313].
- [94] F. Jegerlehner, M. Y. Kalmykov and O. Veretin, *Nucl. Phys. B* **658**, 49 (2003). [hep-ph/0212319].
- [95] F. Jegerlehner and M. Y. Kalmykov, *Nucl. Phys. B* **676**, 365 (2004). [hep-ph/0308216].
- [96] B. A. Kniehl, A. F. Pikelner, O. L. Veretin, *Comput. Phys. Commun.* **206**, 84-96 (2016). [arXiv:1601.08143 [hep-ph]].
- [97] S. P. Martin, D. G. Robertson, *Phys. Rev. D* **90**, no.7, 073010 (2014). [arXiv:1407.4336 [hep-ph]].
- [98] S. P. Martin, *Phys. Rev. D* **93**, no.9, 094017 (2016). [arXiv:1604.01134 [hep-ph]].
- [99] S. P. Martin, D. G. Robertson, *Phys. Rev. D* **100**, no.7, 073004 (2019). [arXiv:1907.02500 [hep-ph]].
- [100] M. Beneke, *Phys. Lett. B* **434**, 115 (1998). [hep-ph/9804241].
- [101] A. Pineda and F. J. Yndurain, *Phys. Rev. D* **58**, 094022 (1998).
- [102] A. H. Hoang and T. Teubner, *Phys. Rev. D* **60**, 114027 (1999). [hep-ph/9904468].
- [103] A. H. Hoang, A. Jain, I. Scimemi and I. W. Stewart, *Phys. Rev. Lett.* **101**, 151602 (2008). [arXiv:0803.4214 [hep-ph]].
- [104] P. H. Chankowski, S. Pokorski and J. Rosiek, *Nucl. Phys. B* **423**, 437 - 496 (1994). [hep-ph/9303309].
- [105] A. Dabelstein, *Nucl. Phys. B* **456**, 25 (1995). [hep-ph/9503443].
- [106] D. M. Pierce, J. A. Bagger, K. T. Matchev and R.J. Zhang, *Nucl. Phys. B* **491**, 3 - 67 (1997). [hep-ph/9606211].
- [107] M. Frank, T. Hahn, S. Heinemeyer, W. Hollik, H. Rzehak and G. Weiglein, *JHEP* **0702**, 047 (2007). [hep-ph/0611326].
- [108] S. Heinemeyer, W. Hollik and G. Weiglein, *Eur. Phys. J. C* **9**, 343 (1999). [hep-ph/9812472].
- [109] S. Heinemeyer, W. Hollik, H. Rzehak and G. Weiglein, *Eur. Phys. J. C* **39**, 465 (2005). [hep-ph/0411114].
- [110] S. Heinemeyer, W. Hollik, H. Rzehak, G. Weiglein, *Phys. Lett. B* **652**, 300-309 (2007). [arXiv:0705.0746 [hep-ph]].
- [111] M. Carena, M. Quiros and C. Wagner, *Nucl. Phys. B* **461**, 407 (1996). [hep-ph/9508343].
- [112] M. Carena, H. Haber, S. Heinemeyer, W. Hollik, C. Wagner, and G. Weiglein, *Nucl. Phys. B* **580**, 29 (2000). [hep-ph/0001002].
- [113] S. Martin, *Phys. Rev.* **D71**, 016012 (2005). [hep-ph/0405022].
- [114] S. Borowka, T. Hahn, S. Heinemeyer, G. Heinrich and W. Hollik, *Eur. Phys. J.* **C74**, no.8, 2994 (2014). [arXiv:1404.7074 [hep-ph]].

- [115] G. Degrossi, S. Di Vita and P. Slavich, *Eur. Phys. J.* **C75**, no.2, 61 (2015). [arXiv:1410.3432 [hep-ph]].
- [116] S. Borowka, S. Paßehr, G. Weiglein, *Eur. Phys. J.* **C78**, no.7, 576 (2018). [arXiv:1802.09886 [hep-ph]].
- [117] R. Harlander, P. Kant, L. Mihaila and M. Steinhauser, *Phys. Rev. Lett.* **100**, 191602 (2008). *Phys. Rev. Lett.* **101**, 039901 (2008). [arXiv:0803.0672 [hep-ph]].
- [118] R. Harlander, P. Kant, L. Mihaila and M. Steinhauser, *JHEP* **1008**, 104 (2010). [arXiv:1005.5709 [hep-ph]].
- [119] J. L. Feng, P. Kant, S. Profumo, D. Sanford, *Phys. Rev. Lett.* **111**, 131802 (2013). [arXiv:1306.2318 [hep-ph]].
- [120] T. Hahn, S. Heinemeyer, W. Hollik, H. Rzehak, and G. Weiglein, *Phys. Rev. Lett.* **112**, no. 14, 141801 (2014). [arXiv:1312.4937 [hep-ph]].
- [121] E. Bagnaschi, G. F. Giudice, P. Slavich, and A. Strumia, *JHEP* **1409**, 092 (2014). [arXiv:1407.4081 [hep-ph]].
- [122] P. Draper, G. Lee, C. E. M. Wagner, *Phys. Rev.* **D89**, no.5, 055023 (2014). [arXiv:1312.5743 [hep-ph]].
- [123] G. Lee and C. E. M. Wagner, *Phys. Rev.* **D92**, 075032 (2015). [arXiv:1508.00576 [hep-ph]].
- [124] J. Pardo Vega and G. Villadoro, *JHEP* **1507**, 159 (2015). [arXiv:1504.05200 [hep-ph]].
- [125] E. Bagnaschi, J. Pardo Vega, P. Slavich, *Eur. Phys. J.* **C77**, no.5, 334 (2017). [arXiv:1703.08166 [hep-ph]].
- [126] H. Bahl, *JHEP* **1902**, 121 (2019). [arXiv:1812.06452 [hep-ph]].
- [127] E. Bagnaschi, F. Brümmer, W. Buchmüller, A. Voigt, and G. Weiglein, *JHEP* **1603**, 158 (2016). [arXiv:1512.07761 [hep-ph]].
- [128] H. Bahl, W. Hollik, *JHEP* **1807**, 182 (2018). [arXiv:1805.00867 [hep-ph]].
- [129] N. Murphy, H. Rzehak, (2019) [arXiv:1909.00726 [hep-ph]].
- [130] E. Bagnaschi, G. Degrossi, S. Paßehr, P. Slavich, (2019). [arXiv:1908.01670 [hep-ph]].
- [131] L. N. Mihaila, J. Salomon, and M. Steinhauser, *Phys. Rev. Lett.* **108**, 151602 (2012). [arXiv:1201.5868 [hep-ph]].
- [132] L. N. Mihaila, J. Salomon, and M. Steinhauser, *Phys. Rev. D* **86**, 096008 (2012). [arXiv:1208.3357 [hep-ph]].
- [133] K. G. Chetyrkin and M. F. Zoller, *JHEP* **1206**, 033 (2012). [arXiv:1205.2892 [hep-ph]].
- [134] A. V. Bednyakov, A. F. Pikelner, and V. N. Velizhanin, *Phys. Lett. B* **722**, 336–340 (2013). [arXiv:1212.6829 [hep-ph]].
- [135] K. G. Chetyrkin and M. F. Zoller, *JHEP* **1304**, 091 (2013). [Erratum: *JHEP* **1309**, 155 (2013)]. [arXiv:1303.2890 [hep-ph]].

- [136] A. V. Bednyakov, A. F. Pikelner, and V. N. Velizhanin, Nucl. Phys. B **875**, 552–565 (2013). [arXiv:1303.4364 [hep-ph]].
- [137] S. P. Martin and D. G. Robertson, Phys. Rev. D **100**, no.7, 073004 (2019). [arXiv:1907.02500 [hep-ph]].
- [138] R.V. Harlander, J. Klappert, A. Voigt. (2019) [arXiv:1910.03595 [hep-ph]].
- [139] B. Allanach, Comput. Phys. Commun. **143**, 305 - 331 (2002). [hep-ph/0104145].
- [140] A. Djouadi, J.-L. Kneur and G. Moultaka, Comput. Phys. Commun. **176**, 426–455 (2007). [hep-ph/0211331].
- [141] J. S. Lee, M. Carena, J. Ellis, A. Pilaftsis and C. E. M. Wagner, Comput. Phys. Commun. **180**, 312 - 331 (2009). [arXiv:0712.2360 [hep-ph]].
- [142] R. V. Harlander, J. Klappert, A. Voigt, Eur. Phys. J. **C77**, no.12, 814 (2017). [arXiv:1708.05720 [hep-ph]].
- [143] R.V. Harlander, J. Klappert, A.D. Ochoa, A. Voigt, Eur. Phys. J. **C78**, no.10, 874 (2018). [arXiv:1807.03509 [hep-ph]].
- [144] P. Athron, M. Bach, D. Harries, T. Kwasnitza, J. Park, D. Stöckinger, A. Voigt, J. Ziebell, Comput. Phys. Commun. **230**, 145-217 (2018). [arXiv:1710.03760 [hep-ph]].
- [145] P. Athron, M. Bach, D. Harries, W. Kotlarski, T. Kwasnitza, J. Park, T. Steudtner, D. Stöckinger, A. Voigt, J. Ziebell, [arXiv:1810.05371 [hep-ph]] (2018).
- [146] G. Lee and C. Wagner, MhEFT package, <http://gabrlee.com/code> (2016).
- [147] H. Bahl and W. Hollik, Eur. Phys. J. C **76**, no. 9, 499 (2016). [arXiv:1608.01880 [hep-ph]].
- [148] P. Athron, J. Park, D. Stöckinger and A. Voigt, Comput. Phys. Commun. **190**, 139 - 172 (2015). [arXiv:1406.2319 [hep-ph]].
- [149] F. Staub, Comput. Phys. Commun. **181**, 1077-1086 (2010). [arXiv:0909.2863 [hep-ph]].
- [150] F. Staub, Comput. Phys. Commun. **182**, 808-833 (2011). [arXiv:1002.0840 [hep-ph]].
- [151] F. Staub, Comput. Phys. Commun. **184**, 1792-1809 (2013). [arXiv:1207.0906 [hep-ph]].
- [152] F. Staub, Comput. Phys. Commun. **185**, 1773 - 1790 (2014). [arXiv:1309.7223 [hep-ph]].
- [153] W. Porod and F. Staub, Comput. Phys. Commun. **183**, 2458 - 2469 (2012). [arXiv:1104.1573 [hep-ph]].
- [154] F. Staub and W. Porod, Eur. Phys. J. **C77**, 338 (2017). [arXiv:1703.03267 [hep-ph]].
- [155] S. Heinemeyer, W. Hollik and G. Weiglein, Comput. Phys. Commun. **124**, 76 - 89 (2000). [hep-ph/9812320].
- [156] T. Hahn, S. Heinemeyer, W. Hollik, H. Rzehak and G. Weiglein, Comput. Phys. Commun. **180**, 1426 - 1427 (2009).
- [157] H. Bahl, S. Heinemeyer, W. Hollik and G. Weiglein, Eur. Phys. J. **C78**, no.1, 57 (2018). [arXiv:1706.00346 [hep-ph]].

- [158] T. Hahn, *Comput. Phys. Commun.* **140**, 418 (2001). [[hep-ph/0012260](#)].
- [159] V. Shtabovenko, R. Mertig, F. Orellana, *Comput. Phys. Commun.* **207**, 432-444 (2016). [[arXiv:1601.01167](#) [[hep-ph](#)]].
- [160] D. Stockinger, *JHEP* **0503**, 076 (2005). [[hep-ph/0503129](#)].
- [161] C. Gnedinger et al., *Eur. Phys. J.* **C77**, no.7, 471 (2017). [[arXiv:1705.01827](#) [[hep-ph](#)]].
- [162] L. V. Avdeev, G. A. Chochia and A. A. Vladimirov, *Phys. Lett. B* **105**, 272 (1981).
- [163] L. V. Avdeev and A. A. Vladimirov, *Nucl. Phys. B* **219**, 262 (1983).
- [164] F. Jegerlehner, *Eur. Phys. J.* **C18**, 673-679 (2001). [[hep-th/0005255](#)].
- [165] C. Studerus, *Comput. Phys. Commun.* **181**, 1293-1300 (2010). [[arXiv:0912.2546](#) [[physics.comp-ph](#)]].
- [166] A. Freitas, *JHEP* **1611**, 145 (2016) [[arXiv:1609.09159](#) [[hep-ph](#)]].
- [167] S. Bauberger, A. Freitas, [[arXiv:1702.02996](#) [[hep-ph](#)]] (2017).
- [168] S. Bauberger, A. Freitas, D. Wiegand, *JHEP* **2001**, 024 (2020). [[arXiv:1908.09887](#) [[hep-ph](#)]].
- [169] R. Piessens, E. de Doncker-Kapenga, C. W. Überhuber, D. K. Kahanger, *Quadpack*, Springer-Verlag Berlin Heidelberg (1983).
- [170] K. Briggs, doubledouble version 2.2, [boutell.com/fracster-src/doubledouble/doubledouble.html](#).
- [171] S. Borowka, G. Heinrich, S. P. Jones, M. Kerner, J. Schlenk, T. Zirke, *Comput. Phys. Comm.* **196**, 470-491 (2015). [[arXiv:1502.06595](#) [[hep-ph](#)]].
- [172] O. V. Tarasov, *Nucl. Phys. B* **502**, 455-482 (1997). [[hep-ph/9703319](#)].
- [173] R. Mertig and R. Scharf, *Comput. Phys. Commun.* **111**, 265-273 (1998). [[hep-ph/9801383](#)].
- [174] L. Mihaila, *Adv. High Energy Phys.* **2013**, 607807 (2013). [[arXiv:1310.6178](#) [[hep-ph](#)]].
- [175] D. J. Broadhurst, *Z. Phys. C* **54**, 599 (1992).
- [176] J. Fleischer and M. Y. Kalmykov, *Phys. Lett. B* **470**, 168 (1999). [[hep-ph/9910223](#)].
- [177] D. J. Broadhurst, *Eur. Phys. J. C* **8**, 311 (1999). [[hep-th/9803091](#)].
- [178] A. I. Davydychev and M. Y. Kalmykov, *Nucl. Phys. B* **699**, 3 (2004). [[hep-th/0303162](#)].
- [179] M. Y. Kalmykov, *Nucl. Phys. B* **718**, 276 (2005). [[hep-ph/0503070](#)].
- [180] M. Y. Kalmykov, *JHEP* **0604**, 056 (2006). [[hep-th/0602028](#)].
- [181] V. V. Bytev, M. Y. Kalmykov and B. A. Kniehl, *Nucl. Phys. B* **836**, 129 (2010). [[0904.0214](#)].
- [182] S. P. Martin, D. G. Robertson, *Phys. Rev.* **D95**, no.1, 016008 (2017). [[arXiv:1610.07720](#) [[hep-ph](#)]].
- [183] P. Marquard, N. Zerf, *Comput. Phys. Commun.* **185**, 1153-1171 (2014). [[arXiv:1309.1731](#) [[hep-ph](#)]].

- [184] P. Marquard, L. Mihaila, J.H. Piclum, M. Steinhauser, Nucl. Phys. B **773**, 1-18 (2007). [hep-ph/0702185].
- [185] P. Draper, H. Rzehak Phys. Rept. **619**, 1-24 (2016). [arXiv:1601.01890 [hep-ph]].
- [186] <http://www.feynhiggs.de/cgi-bin/fhman.cgi?man=FHSetFlags>
- [187] K. G. Chetyrkin, J. H. Kuehn, M. Steinhauser, Comput. Phys. Commun. **133**, 43-65 (2000). [arXiv:0004189 [hep-ph]].
- [188] B. Schmidt, M. Steinhauser, (2012). [arXiv:1201.6149 [hep-ph]].
- [189] F. Herren, M. Steinhauser, Comput. Phys. Commun. **224**, 333-345 (2018). [arXiv:1703.03751 [hep-ph]].
- [190] N. K. Nielsen, Nucl. Phys. B **101**, 173 (1975).
- [191] C. Ford, I. Jack and D. R. T. Jones, Nucl. Phys. B **387**, 373 (1992). [Erratum-ibid. B **504**, 551 (1997)]. [hep-ph/0111190].
- [192] S. P. Martin, Phys. Rev. D **89**, 013003 (2014). [arXiv:1310.7553 [hep-ph]].
- [193] S. P. Martin, Phys. Rev. D **92**, no. 5, 054029 (2015). [arXiv:1508.00912 [hep-ph]].
- [194] R. A. Flores and M. Sher, Phys. Rev. D **27**, 1679 (1983).
- [195] B. Kastening, Phys. Lett. B **283**, 287-292 (1992).
- [196] M. Bando, T. Kugo, N. Maekawa, H. Nakano, Phys. Lett. B **301**, 83-89 (1993). [hep-ph/9210228].
- [197] G. Isidori, G. Ridolfi and A. Strumia, Nucl. Phys. B, **609**, 387 (2001). [hep-ph/0104016].
- [198] J. R. Espinosa and R. -J. Zhang, JHEP **0003**, 026 (2000). [arXiv:9912236 [hep-ph]].